universität wien

DISSERTATION

Titel der Dissertation

„Kinetic properties of Polycomb Group Proteins during differentiation and mitosis in live *Drosophila*“

1 von 1

Verfasser

João Pedro Fonseca

angestrebter akademischer Grad

Doktor der Naturwissenschaften (Dr. rer. nat.)

Wien, 2012

Studienkennzahl lt. Studienblatt:	A 091 490
Dissertationsgebiet lt. Studienblatt:	Dr.-Studium der Naturwissenschaften Molekulare Biologie UniStG
Betreuerin	Dr. Leonie Ringrose

Abstract

Epigenetic memory mediated by Polycomb group (PcG) proteins must be maintained during cell division, but must also be flexible to allow cell fate transitions. Furthermore, it is important to study these cell fate transitions *in vivo*, in well defined lineages, as they can provide the best understanding of PcG memory and plasticity abilities. Here I quantify endogenous concentrations and dynamic chromatin binding properties of PH::GFP, PC::GFP, GFP::DSP1, GFP::PHO, and GFP::E(Z) in living Drosophila in two cell types that undergo defined differentiation and mitosis events. Quantitative FRAP analysis demonstrates that PcG binding has a higher plasticity in stem cells than in more determined cells, and identifies a fraction of PRC1 proteins that binds mitotic chromatin with up to 300 fold longer residence times than in interphase. Mathematical modeling examines which parameters best distinguish stem cells from differentiated cells and predicts an accelerated dissociation of Polycomb from mitotic chromatin in SOPs compared to neuroblasts. I identify mitotic phosphorylation of histone H3 at serine 28 as a potential mechanism that provides a cell-type specific acceleration of the extent and rate of mitotic Polycomb dissociation. Moreover, I identify Absent, Small or Homeotic discs 1 (ASH1) and the tandem kinase JIL-1 as modifiers of Polycomb kinetic properties in larval neuroblasts.

In summary these findings suggest that the regulation of the kinetic properties of PcG-chromatin binding is an essential factor in the choice between stability and flexibility in the establishment of cell identities.

Zusammenfassung

Proteine der Polycomb Gruppe (PcG) vermitteln ein epigenetisches Gedächtnis, welches bei der Zellteilung aufrechterhalten werden muss. Andererseits muss es flexibel sein, um bei der Differenzierung den Übergang zwischen unterschiedlichen Zelltypen zu ermöglichen. Es ist von großer Bedeutung, diese Übergänge in definierten Zelltypen und *in vivo* zu analysieren, um so sowohl ein besseres Verständnis des durch PcG Proteine vermittelten Gedächtnisses, als auch der Plastizität zu erlangen. In der vorliegenden Studie habe ich endogene Konzentrationen und Eigenschaften der dynamischen Bindung an Chromatin von PH::GFP, PC::GFP, GFP::DSP1, GFP::PHO und GFP::E(Z) quantifiziert. Die Untersuchungen wurden in zwei unterschiedlichen Zelltypen lebender Fruchtfliegen durchgeführt, welche exakt definierte Differenzierungs- und Zellteilungsprozesse durchlaufen. Quantitative Analysen mittels FRAP demonstrieren, dass die Bindung von PcG Proteinen eine höhere Plastizität in Stammzellen gegenüber stärker determinierten Zellen aufweist und identifizieren darüber hinaus eine Fraktion von PRC1, welche während der Mitose mit einer 300-fach längeren Residenzzeit an Chromatin bindet als in Interphase. Untersuchungen mittels mathematischer Modellierung zeigen, welche Parameter Stammzellen am besten von differenzierten Zellen unterscheiden und sagen eine schnellere Dissoziation von Polycomb von mitotischem Chromatin in SOPs als in Neuroblasten vorher. Ich identifiziere die Phosphorylierung von Serin 28 in Histon H3 während der Mitose als einen möglichen Mechanismus für das zellspezifische Ausmaßund die Geschwindigkeit der Dissoziation von Polycomb während der Mitose. Darüber hinaus zeige ich, dass Absent, Small or Homeotic discs 1 (ASH1) und die Tandemkinase JIL-1 die kinetischen Eigenschaften von Polycomb in larvalen Neuroblasten entscheidend beeinflussen.
Zusammengefasst lassen die hier beschriebenen Ergebnisse die Hypothese zu, dass bei der Etablierung von Zellidentitäten die Regulation der kinetischen Eigenschaften der Bindung von PcG Proteinen an Chromatin ein essenzieller Faktor für die Entscheidung zwischen Stabilität und Flexibilität ist.

Contents

List of Figures

List of Tables

1

Introduction

Epigenetic phenomena are changes in gene expression that are heritable through cell division, that do not depend on changes in DNA sequence and that occur in the absence of the transcription factors that initially set the expression state [1]. The Polycomb (PcG) and Trithorax Group (TrxG) proteins, which maintain the transcriptional inactive and active states of gene expression, are main epigenetic actors in fundamental processes, such as signaling, differentiation and proliferation, that provide cellular memory and flexibility during development [2].

1.1 PcG proteins as elements of stability and flexibility

1.1.1 History of Polycomb research

Polycomb Group (PcG) proteins were first identified in the 1940s, when mutations of these proteins were shown to lead to the development of ectopic sex combs on the 2nd and 3rd leg of *Drosophila melanogaster* (reviewed in [3]). Later, these mutations were mapped to the genes *Polycomb* (*Pc*) and *extra sex combs* (*esc*) and the extra sex combs phenotype was linked to a derepression of Hox genes [4]. In the 1980s, a group of counteracting proteins, named Trithorax group proteins (TrxG) was discovered. Mutations in these proteins were able to abolish the extra sex combs phenotype caused by polycomb mutations, due to a down regulation of Hox gene activity (reviewed in [3]). In the following years many proteins have been uncovered as belonging to one or both of these groups, and revealed the PcG/TrxG proteins as an evolutionarily conserved group of transcriptional regulators present across the eukaryotic domain (reviewed in [2, 5]).

1.1.2 PcG protein complexes

PcG and TrxG proteins are well conserved between flies and mammals, where it is usual to find more than one homolog for each PcG protein (reviewed in [2, 5]). Furthermore, the complexes in which these proteins are organised, are also conserved. PcG protein complexes are listed in Table 1.1. In the following paragraphs I give a brief description of the biochemical properties of the PcG complex members found in flies and in mammals.

Polycomb Repressive Complex 1 (PRC1)

Polycomb Repressive Complex 1 (PRC1) was first identified by biochemical purification in *Drosophila* S2 cells and in human HeLa cells as a 1–2MDa protein complex that encompasses four main proteins (indicated with their fly names): Polycomb (PC), Polyhomeotic (PH), Posterior Sex Combs (PSC), and Sex Combs Extra (SCE or dRING) [6, 7]. Other proteins have been listed as associated with these main PRC1 components [6, 8]. Moreover, there are recent reports that, in mammals, there are six different PRC1.x complexes which have different components and individual functions [9].
Polycomb is a chromodomain-containing protein, which is able to bind to the tri-methylated lysine 27 of histone H3 (H3K27me3) with an *in vitro* affinity of 5μM [10]. This measured affinity is rather low when compared to nM range of transcription factor affinities for their consensus sequence [11]. Nevertheless, when compared to the affinity of the PC chromodomain to other chromatin marks, it uncovers a specifity for H3K27me3 [10]. This specificity suggests that PC is targeted to chromatin that has the H3K27me3 modification. However, this model has been questioned by the observation that a recombinant HP1, whose chromodomain has been replaced by the PC chromodomain, can be targeted to ectopic loci that colocalise with PC loci in polytene chromosomes [12, 2]. However, also in polytene chromosomes, the colocalization of PC with H3K27me3 is not complete, suggesting that PC has other targeting strategies [13]. In mammals, there are 5 homologs of PC (CBX2, CBX4, CBX6, CBX7 and CBX8). Although they share a conserved chromodomain, the chromodomain of each of these proteins has a different specificity [14]. CBX7 and CBX2 bind with similar affinity H3K9me3 and H3K27me3 peptides, while CBX4 prefers the H3K9me3 peptide. CBX6 and CBX8 have low affinity (*Kd*) for both marks, which suggests a different role for these proteins [14]. It has been shown that both of these proteins do not form PRC1 complexes in embryonic stem (ES) cells [15]. In addition to histone methylation recognition, the PC homolog CBX4 has a SUMO E3-ligase activity, which targets, among other proteins, E2F1 thereby regulating

cell proliferation [16].
In the fly, the *polyhomeotic* gene is expressed as two isoforms: *polyhomeotic distal* (*ph-d*) and *polyhomeotic proximal* (*ph-p*) [17]. PH is characterized by the presence of a SAM domain which is involved in the formation of homotypic and heterotypic interactions with Sex Combs on Midleg (SCM) [18, 19]. Furthermore, it has been shown that PH can be glycosylated by SXC/OGT (*Super Sex Combs/ O-linked N-acetylGlucosamine Transferase*) [20]. Recently, it as been reported that PH is able to inhibit chromatin remodeling due to its overall positive charge [21].
The *Drosophila* Posterior Sex Combs protein was identified as the main chromatin compactor and remodeling inhibitor of PRC1 [22]. It has a functional homolog, Su(Z)2 [23]. dRING contains a RING finger domain which is responsible for histone H2AK119 monoubiquitination [24].
Other PRC1-associated proteins found are Zeste and SCM [6, 8]. SCM has been described to interact with PH through its SAM domain and to be necessary for PRC2 recruitment to the *bxd* genetic element [18, 19, 25]. Zeste is a DNA binding factor and it is thought that it adds sequence specificity to PRC1 targeting [26].
CRASCH (Chromatin Associated Silencing Complex for Homeotics), a variant of PRC1, has been identified in S2 cells. Besides PC and PH, it is composed of the Histone DeAcetylase HDAC1 and the DNA binding protein Pipsqueak (PSQ)[27, 28].

Polycomb Repressive Complex 2 (PRC2)

A second complex of PcG proteins named Polycomb Repressive Complex 2 (PRC2) has been identified in flies and human cells [29, 30, 31, 32, 33, 34]. In flies, PRC2 has a size of $\sim$600KDa to 1MDa, and is composed of Enhancer of Zeste (E(Z)), Extra Sex Combs (ESC) and Supressor of Zeste 12 (Su(Z)12) [29, 30, 31, 34]. As for PRC1, additional PRC2 components have been described [29, 34]. Enhancer of Zeste is mostly defined by the presence of a SET domain, responsible for the methylation of H3K27 [30, 31]. It has been recently shown that the mammalian homolog, E(Z)H2, is able to methylate non-histone targets [35]. E(Z) interacts via its N-terminal domain with the WD motif of the ESC protein [36, 37]. The interaction between ESC and Su(Z)12 has been reported to increase the ability of E(Z) to methylate H3K27 [30, 38].
Other proteins that have been identified as part of PRC2 complexes are the histone binding protein p55, Polycomb-like (PCL) and RPD3 [29, 34].

Table 1.1: Polycomb Group Proteins complexes. Known PcG protein complexes in *Drosophila* and in mammals are described with each component in addition to known enzymatic activities of each complex.

Complex	*Drosophila*	Mammals	Activities
Polycomb Repressive Complex 1 (PRC1)	PC PH PSC dRING	CBX2, 4, 6, 7, 8 PHC1 to 3 PCGF1 to 6 RING1A, RING1B	Binding of H3K27me3; Ubiquitination of H2A; Inhibition of chromatin remodeling
Polycomb Repressive Complex 2 (PRC2)	E(Z) SU(Z)12 ESC PCL p55	E(Z)H1 and E(Z)H2 SU(Z)12 EED1 to 4 PCL1 to 3 RBBP4, RBBP7	Methylation of H3K27me3; Binding to H3K27me3
dRING Associated Factors (dRAF)	PSC dRING KDM2	PCGF1 to 6 RING1A, RING1B KDM2B	Ubiquitination of H2A; H3K36 and K4 demethylation
PHO Repressive Complex (PhoRC)	PHO dSFMBT	YY1 SFMBT	DNA binding; H3-methyl binding
Polycomb Repressive Deubiquitinase (PR-DUB)	Calypso ASX	BAP1 ASXL1	Histone deubiquitination

Other PcG complexes

Several other complexes, namely PhoRC, dRAF and PR-DUB, have been described only in flies, although their components have mammalian homologs. PhoRC, identified in embryonic extracts, is composed of Pleiohomeotic (PHO) and Scm-related gene containing four MBT domains (dSFMBT) [39, 40]. Both dSFMBT and its human homolog SFMBT recognise specifically mono- and dimethylated histones H3K9 and H4K20 their MBT repeats [41, 42]. PHO is a DNA binding protein, which in addition to its interaction to dSFMBT has been reported to interact with PRC2 component E(Z) and PRC1 component PC [43] and with the Trithorax Group protein Brahma [44].
dRAF (RING-Associated Factors) has PSC, SCE and Lysine (K)-specific demethylase 2 (KDM2) as its core components [45]. It has been shown that KDM2 is responsible for H3K36 demethylation and also essential for histone ubiquitination and gene silencing [45].
The more recently discovered PR-DUB is composed of Calypso and Additional Sex Combs (ASX) [46]. The reported activity of this complex is the deubiquitination of H2A [46]. Unexpectedly, the removal of this complex from *Drosophila* tissues led to ectopic activation of Hox genes [46].

Trithorax Group proteins

TrxG proteins identified to date have been found mainly involved in general transcription regulation processes (reviewed in [47]). In flies, the few proteins identified with specific polycomb-related roles are the Trithorax (TRX), Absent, Small or Homeotic discs 1 and 2 (ASH1 and ASH2) proteins [48]. All these proteins are essential for H3K4me3 and H3K36me3 (TRX and ASH1 are histone methyltransferases, and ASH2 mutants have reduced amounts of H3K4me3 in the genome), which are chromatin hallmarks of active transcription [49, 50, 51, 52, 53, 54].
There are many TrxG protein complexes identified. These complexes share two main functions: histone modification and ATP-dependent chromatin remodeling (reviewed in [47]).

Summary

In summary, the biochemical identification of PcG and TrxG protein complexes elucidates the complex interactions that exist between different PcG and TrxG proteins. Moreover, it helps to understand how the different biochemical activities associated with each protein might work together. However, the PcG and TrxG complexes identified have unique compositions that might depend on the cell or fly tissue from which they were isolated as well on the techniques used for the identification of their components. Therefore, the biochemical characterization of PcG complexes only gives a glimpse of the function of its components *in vivo*, as the associations that these make in specific cell types might have an impact in the balance of the PcG system.

1.1.3 Roles of PcG proteins in development

PcG proteins are essential in distinct stages of development of animals and plants (reviewed in [55, 56]). In *Drosophila* null mutations of PcG proteins lead to early death in embryogenesis (reviewed in [3]). A closer look at different roles in single tissues of flies has shown that neuroblasts of the central nervous system need PcG proteins for normal survival and that neuroblast lineage competence is restricted by the action of PcG proteins [57, 58, 59]. Moreover, in bristle sensory organs, the tight regulation of PcG gene levels is important for the normal development [60, 61]. In many other tissues, such as the eye, PcG proteins are essential for the regulation of several genes and normal tissue development, demonstrating the need for the study of these proteins in *in vivo* scenarios [62, 63, 64].

1.1.4 Mechanisms of action

The Hox genes have so far provided paradigms for understanding PcG and TrxG function. Here, the two groups of proteins act antagonistically, with PcG proteins responsible for the maintenance of the silent state of the target genes, and TrxG proteins mediating mechanisms important for the active state. Importantly, they are able to perform these actions stably across cell generations in the absence of the initiating transcription factors that initially set the target gene transcription state (reviewed in [65]).

Recruitment of PcG proteins to target sites

PcG and TrxG proteins regulate their target genes via cis-regulatory DNA elements that are termed Polycomb/Trithorax Response Elements (PRE/TREs) (reviewed in [65]). The first identified PREs were found in the Bithorax complex locus (BX-C). In a reporter construct, these elements are able to provide silencing activity in a heritable fashion that depends on PcG and TrxG proteins [66, 67, 68].
PREs are not defined by a common consensus sequence but by a combination of multiple binding sites for various proteins [69]. These include the previously mentioned PHO, Zeste and PSQ, but also GAGA factor (GAF), Grainyhead (Grh), Sp1/KLF and Dorsal switch Protein 1 (DSP1) (reviewed in [65, 70]). Recruitment of vertebrate PcG proteins by DNA binding proteins is under debate because only GAF and PHO have known homologues and their implication in PcG function is still under debate [71, 72, 73]. Other proteins have been implicated in the global recruitment of PcG proteins such as the JARID2 protein [74, 75, 76], REST [77], and core binding transcription factors [78].
Other models of recruitment of PcG proteins have been brought forward. Currently one the most favored hypotheses is the recruitment through histone modifications. As stated above PC and several CBX proteins can recognise specifically the H3K27me3 mark, thereby recruiting PRC1 as a whole [10]. It has also been shown that PcG proteins overlap extensively with this mark in polytene chromosomes [13] and ChIP experiments [79, 80, 81]. Furthermore, in mammals, it has been reported that PRC2, which contains the histone methyltransferase E(Z)H2, can recognize the histone methyl mark H3K27me3 via interaction of EED (ESC homolog) with modified chromatin during replication [82, 83, 84].
Another mechanism for recruitment of PcG and TrxG proteins proposed the interaction of these proteins with non coding RNAs (ncRNAs) (reviewed in [85]. It has been reported that ncRNAs arising from PREs can interact with TrxG

proteins and PcG proteins, both in mammals and flies [86, 87, 88]. How this specificity is defined is largely unknown.
Alternatively, the enrichment of CpG dinucleotides has been reported as possible mechanism to mark sites of PcG recruitment to mammalian chromatin [73, 89], and this enrichment has been recently used to increase the prediction accuracy of PREs in flies [90].

Silencing of genes by PcG proteins

How PcG proteins promote the silencing of the same genes to which they are recruited remains an open question. Various models have been put forward, but the most prominent ones include chromatin compaction, transcriptional pausing, histone modification and reduced histone turnover.
Inhibition of chromatin remodeling and chromatin compaction have been shown to be properties, *in vitro* and *in vivo*, of several PcG proteins [21, 22, 91, 92]. This might occlude binding sites or reduce the affinity of transcription factors to PcG regulated genes. However, since general transcription factors have been shown to bind to PcG silenced promoters, it is not possible to exclude that other mechanisms are used for PcG-mediated repression [93, 94].
PcG protein occupancy has been shown to correlate with RNA polymerase II pausing or stalling [95, 96]. However, it is not clear if PcG proteins inhibit RNA polymerase pausing [97] or if they are recruited by the small RNAs that arise from these promotors [98]. It has been proposed that H2A ubiquitination by RING1B inhibits transcription elongation, however it is not clear what is the mechanism behind the polymerase perturbation [99, 100, 101]. One of the models put forward is based on the reduction of the affinity of the chromatin remodeling complex FACT for the H2A/H2B dimer, if H2A is ubiquitinated [101]. This model is inconsistent with other observations that *Hox* loci in mouse ES cells are able to be compacted and repressed by an enzymatically inactive RING1B mutant, albeit in the absence of detectable H2A ubiquitination [91]. This report excludes the possibility that promoter stalling or inhibition of chromatin displacement by H2A ubiquitination is the sole mechanism responsible for PcG silencing.
A longer standing idea is that histone modifications, like H3K27me3 which correlate with a silenced state of a gene and H3K27 acetylation (H3K27ac), H3K4me3 and H3K36me3 which correlate with the active state of a gene, are responsible for the silencing or activating properties of PcG and TrxG proteins [102]. While it is true that these modifications might regulate the recruitment of PcG and TrxG proteins to target sites, it is still unclear how they can promote

repression or activation. Moreover, it is becoming clearer that the proteins that promote these histone modifications are acting also on non-histone proteins, as it has been recently shown for E(Z)H2, which is able to promote silencing of several genes through methylation of the cardiac transcription factor GATA4 [35]. It is possible that the biochemical activities that PcG proteins possess are not directed towards histones, but instead towards transcription factors and polymerase associated factors, which have a direct role on the regulation of the efficiency of transcription.
Another attractive model of transcriptional repression is the reduction of histone turnover in sites where PcG proteins bind compared to TrxG sites [103]. These slower dynamics might occlude more efficiently active DNA elements that are covered by PcG proteins. It has been recently shown that a similar mechanism is present during *Drosophila* heat shock, whereby repression of transcriptional elongation is accompanied by a reduction in histone turnover [104].

1.1.5 Epigenetic action of PcG proteins

PcG proteins as described above are silencers of gene expression. However, they differentiate from other proteins with the same role as they are able to promote this silencing across several cell generations, in the absence of the initial silencing signal, in what is described as epigenetic memory [66, 67, 68].
This was first described for their action upon the Bithorax complex (BX-C) PREs, where it has been shown that these DNA elements were able to maintain the transcription level established by transcription factors at the gene promoter, well after these transcription factors were no longer present [105, 106, 107]. Outside the Hox complexes, many other PREs have been identified in the *Drosophila* genome [69, 108, 109, 110, 111, 112]. These DNA elements were able to repress a reporter construct through the fly development, in a Polycomb-dependent manner. Taken together, these results show that PcG proteins are responsible for the stability of the transcriptional state of several genes, through their action on PREs.
Further genome-wide studies have reported that PcG targets are not just a handful, but are present in the range of hundreds targets in both flies [79, 80, 81] and mammals [113, 114, 115]. These studies identified that many of the additional PcG target genes regulate differentiation, signaling and transcription. These suggested that PcG proteins regulate several differentiation pathways, where they assure that several pro-differentiation genes are kept silenced in undifferentiated cells. Upon differentiation, these genes would lose PcG silencing and proliferation genes would gain PcG binding and become silenced. This

model has been validated for several genes, as PcG targets are gained and lost upon neuronal differentiation of NT2/D1 [113] and ES cells [116].
Plasticity of PcG protein action has also been reported for flies. It has been shown that PcG induced stability of transcription of the *Hox* genes can be modified. Silenced reporter genes carrying a PRE can be switched on in early development, upon exogenous induction of transcription through the PRE, and this altered state can then be memorized through several generations [106, 107]. Furthermore, genome-wide localisation of PcG proteins change during development, providing a glimpse that PcG proteins do not always stably repress their target genes [40, 117, 118, 119]. Taken together, these experiments show that PcG proteins are able to maintain stability and flexibility of gene expression.
These observations lead to interesting questions of how PcG proteins are regulated during differentiation, where flexibility of PcG action is vital, but also during replication and cell division, where stability of transcriptional states have to be maintained.
The behaviour of PcG proteins during replication has been studied *in vivo* and *in vitro*. *In vitro* studies showed a remarkable tight association of the PRC1 complex to chromatin or DNA, suggesting that memory of a silenced state can be directly transmitted by the PcG proteins [120]. Furthermore, *in vivo* studies, showed that PcG proteins associate during or immediately after replication with chromatin [121]. In addition, the authors suggest that PcG proteins as well as the histone mark H3K27me3 are deposited at the BX-C PREs during early replication to ensure the transmission of epigenetic memory [121]. Additional *in vivo* studies have been performed to study the transmission of H3K27me3 by PRC2. In human cells, it has been shown that PRC2 is able to bind the H3K27me3 mark, and that EZ(H)2 colocalises with newly replicated chromatin [82]. These findings suggest that upon replication and addition of new, unmarked nucleosomes, PRC2 is able to bind neighbouring marked histones and methylate the new histones assuring the transmission of the H3K27me3 mark [82, 83].
A detailed description of how stability and flexibility is achieved through PcG proteins during differentiation and mitosis will be addressed in the next sections.

1.2 PcG protein regulation during differentiation

The regulation of PcG proteins during differentiation occurs at different levels. PcG proteins are responsible for the regulation of different genes in several differentiation pathways and the mechanism to achieve this regulation encompass the action through different PcG protein complexes and also post-translational regulation of single PcG proteins.

1.2.1 Genome-wide targeting of PcG proteins during differentiation

In order to study PcG regulation during differentiation, several authors have addressed the genome-wide positioning of several PcG proteins.
Comparison of *Drosophila* PcG protein binding sites in embryonic stages and in larval stages has been performed both in flies and in cell culture, suggesting that PcG proteins have an inherent flexibility for their target sites [40, 117, 118, 119]. Moreover, similar mammalian studies have been performed and have also shown that PcG targets change during embryonic stem (ES) cell differentiation to neuronal lineages [113, 114, 115, 116, 122]. In addition, it has been shown that there is an increase in the number of PcG targets during differentiation, also accompanied by DNA methylation [116].
How these changes happen has been addressed to a smaller extent. Differentiation of skeletal muscle precursors and neuronal differentiation of human embryonic terato-carcinoma cells, with the consequent alteration of PcG targets, requires the action of the MSK1 kinase [123, 124]. MSK1 is required for the phosphorylation of H3S28 (H3S28p) [123, 125]. Upon phosphorylation of this residue, PRC2 components, and to a lesser extent also the Polycomb homolog CBX8, are displaced from chromatin [123, 125]. The use of a phospho-switch to activate displacement appears to be a common mode of regulating binding events of transcription regulators such as HP1 and TAF3 [126, 127, 128].
Although it is probable that chromatin post-translational modifications affect the specifity and affinity of the interaction of PcG proteins with their target sites, there is also evidence that this regulation occurs at the level of the PcG proteins themselves and the complexes they form.

1.2.2 Different polycomb complexes in development

In addition to the core Polycomb Repressive complexes described in subsection 1.1.2, several additional proteins have been identified to contribute to the

function of these complexes, thereby adding to the intricate regulation of PcG proteins and their target genes.
The presence of the functional homologs of PSC, ESC and PHO in *Drosophila*, as well as the large number of PcG protein homologs found in mammalian genomes, already emphasizes the diversity that PcG complexes can have [23, 129, 130]. Moreover, by ChIP analysis, it has been shown that there is not a complete overlap of all PcG proteins of each main complex at each binding site, underlining the presence of sub-complexes with probable individual functions [80, 81, 131, 132]. In addition, the diverse phenotypes of PcG mutations in flies and mammals also suggest the existence of PcG regulation through Polycomb complex diversity [64, 133, 134, 135].
Notable examples of this type of regulation are the switch between a PRC2 containing E(Z)H2 (PRC2-E(Z)H2) to a E(Z)H1 containing PRC2 (PRC2-E(Z)H1) that is essential for normal skeletal muscle differentiation [124, 136]. Remarkably, the presence of a PRC2-E(Z)H1 complex can lead to the enhancement of transcription elongation [136]. This result comes as a further surprise as PRC2-E(Z)H1 had previously been shown to have overlapping repressive functions with PRC2-E(Z)H2 in ESC [137, 138]. On the other hand, these authors reported that the contribution of PRC2-E(Z)H1 to H3K27 methylation was small and that PRC2-E(Z)H1 is able to promote chromatin condensation without its active SET domain. Another example is the report of the different *in vitro* affinities for histone methylation by PRC2, due to the incorporation of four different EED isoforms [139, 140]. Interestingly, these isoforms are differentially expressed during induced differentiation of ES cells [140]. In flies, studies of PRC2 report complex diversity as ESC and ESC-like (ESCL) proteins are differently used during *Drosophila* development [130, 141, 142]. It has been reported that ESC was the main component of a functional PRC2 in embryonic tissues and ESCL enlarges its role later in development [141, 142].
Recently complex diversity and complexity has been reported for PRC1 [9]. This comprehensive study of PRC1-like complexes in human cells, identified six classes of PRC1 components that have in common the presence of RING1A or RING1B and are distinguished by the presence of CBX proteins or RYBP (RING1/YY1 Binding Protein) and the presence of one RING finger containing protein (six paralogs, from which Bmi1 and Mel18 are the most known examples) [9]. These different complexes have different targets in the same cells in addition to different H2A ubiquitination efficiencies [9]. In addition, it has been reported that ES cells use only a subset of CBX proteins on PRC1 complexes and that these are substituted upon ES cell differentiation [15].
Taken together, these results suggest that Polycomb complex diversity is a pow-

erful mechanism of PcG regulation, due to its ability to influence targeting and enzymatic properties.

1.2.3 Modification of PcG protein interactions

An additional layer of regulation for the action of PcG proteins arises from post-translational modifications (PTMs) that these proteins are subject to. These modifications can modify activity, stability and localization of PcG proteins.
It has been reported that stability of PRC2 can be enhanced by phosphorylation of its component ESC [143, 144]. Furthermore, a wide variety of PTMs has been linked to changes in PcG protein activity. One report has linked the addition of N-acetylglucoseamine (GlcNAc) by the *super sex comb* encoded protein Ogt to PH. This modification reduced the repression of PcG target genes without changing the binding of these loci [20]. Recently, methylation of CBX4 by suv39h has been shown to modulate interaction of CBX4 with different ncRNAs and induce the intranuclear relocalisation and transcriptional regulation of several target genes [35]. A common PTM encountered in regulation of PcG proteins is phosphorylation. CBX2 has been reported to have an increased affinity for H3K27me3 upon chromodomain residue phosphorylation, with a concomitant reduction in H3K9me3 affinity [145]. An additional example of the complex effect that phosphorylation can have on one protein is E(Z)H2 (reviewed in [146]). Phosphorylation of E(Z)H2 by CDK1/2 kinases is cell cycle regulated and can modify the ability of E(Z)H2 to interact with RNAs [147] in addition to the recruitment to target sites, maintenance of H3K27me3 levels and PRC2 stability [148, 149]. Moreover, extrinsic signals can lead to phosphorylation of E(Z)H2 by AKT, which results in reduced methyltransferase activity due to a lower affinity of E(Z)H2 for histone H3 [150]. Furthermore, p38 is able to phosphorylate E(Z)H2 in satellite cells, thereby enhancing the interaction of E(Z)H2 with YY1 in order to repress the *pax7* locus [151]. A different protein whose activity is also regulated by phosphorylation is Bmi1, in which the addition of a phospho group correlates with displacement from chromatin [152, 153]. Furthermore, MEL18 can be phosphorylated by JNK kinases and directs RING1B substrate specific [154]. Moreover, phosphorylation of the PHO homolog, YY1, regulates its intracellular localisation in human cells. It has been reported that PHO is able to shuttle to the cytoplasm during replication [155].
In addition to PHO, the localization of other PcG proteins has been reported to be dynamically regulated through cell cycle or differentiation. It has been reported that CBX2 is differently phosphorylated in mouse liver. The phosphorylated form is associated with nuclear localization, and with actively prolifer-

ating cells after liver regeneration, while the non-phosphorylated form of CBX2 was only found in the cytoplasm of non-proliferating cells [156]. Additional evidence for the regulation of PRC1 proteins has been found in the testis of flies. There the localization to the nucleolar region depended on the expression of testis-specific TATA-Binding-Protein Associated Factors during sperm maturation [157]. A more recent work also reported a striking nuclear reorganization of E(Z)H2 and H3K27me3-marked chromatin to the nuclear periphery in C2C12 cells and primary mouse myoblasts, which is dependent of the homeoprotein MSX1, and is necessary for efficient target gene silencing [158].
In summary, the analysis of PcG protein PTMs and intracellular localization has made clear that PcG proteins are dynamically regulated proteins and that the regulation of their interaction with other proteins and chromatin deserves a closer look.

1.2.4 Dynamic interaction of PcG proteins with chromatin during development

The dynamic interaction with chromatin has been reported for several nuclear proteins [159, 160]. Furthermore, this dynamic interaction is regulated through differentiation, since histone H1 and HP1α in stem cells have a looser interaction with chromatin than in differentiated cells [161]. In addition, a reduction in the plasticity of binding of TFIIH has been detected in the differentiation *in vivo* and *in vitro* of different mouse tissues [162]. Examples of this type of regulation for PcG proteins, though not abundant, are present in the literature (Figure 1.1). The first report of PcG dynamic interactions was shown for PC, which is able to be competed out of salivary gland chromatin by H3K9me3 and H3K27me3 peptides [13]. Interestingly, the ability of PC to be removed from chromatin was not equal for all binding sites and it correlated with the level of transcription of the binding site. Using GFP-fusions in *Drosophila*, it has been shown that PC and PH are able to interact dynamically with chromatin, with residence times between two and six minutes [163]. Remarkably this interaction is also developmentally regulated as PcG interaction with chromatin in larval tissues is tighter than in embryonic cells [163]. A study of PC and PH mobility during embryogenesis has been recently reported, showing that movement of highly concentrated binding sites for PC and Ph, called Polycomb bodies (PC bodies), is also developmentally regulated [164]. Through the analysis of mean displacement of these structures, the authors documented that PC bodies have a faster constrained movement, and a slower, chromatin-driven movement, both of which become progressively slower through embryogenesis [164]. In mam-

malian cells, CBX proteins and BMI-1 have been also subject of study. It has been reported that in synchronized U2OS cells, BMI-1 shows different kinetics between G1 and G2. In both cell cycle stages BMI-1 has a dynamic interaction with chromatin, however in G1 the authors report a larger immobile fraction than in G2, during which BMI-1 has a longer residence time [165]. A different study addressed differences in CBX binding to chromatin during ES cell differentiation upon removal of LIF and addition of trans-retinoic acid (RA). In this study, it was shown that most CBX proteins bind more tightly to chromatin and have larger immobile fractions through the differentiation process [166].
While these studies have started to shed light upon the dynamic interaction of PcG proteins with chromatin during development and differentiation, a detailed quantitative analysis of the behaviour of PcG proteins in living animals in a single cell system with defined differentiation processes is lacking. It is essential that these studies are performed *in vivo*, since it has been reported that the interactions of nuclear proteins with chromatin can have different properties depending if the differentiation occurs in the animal or *in vitro* [162].

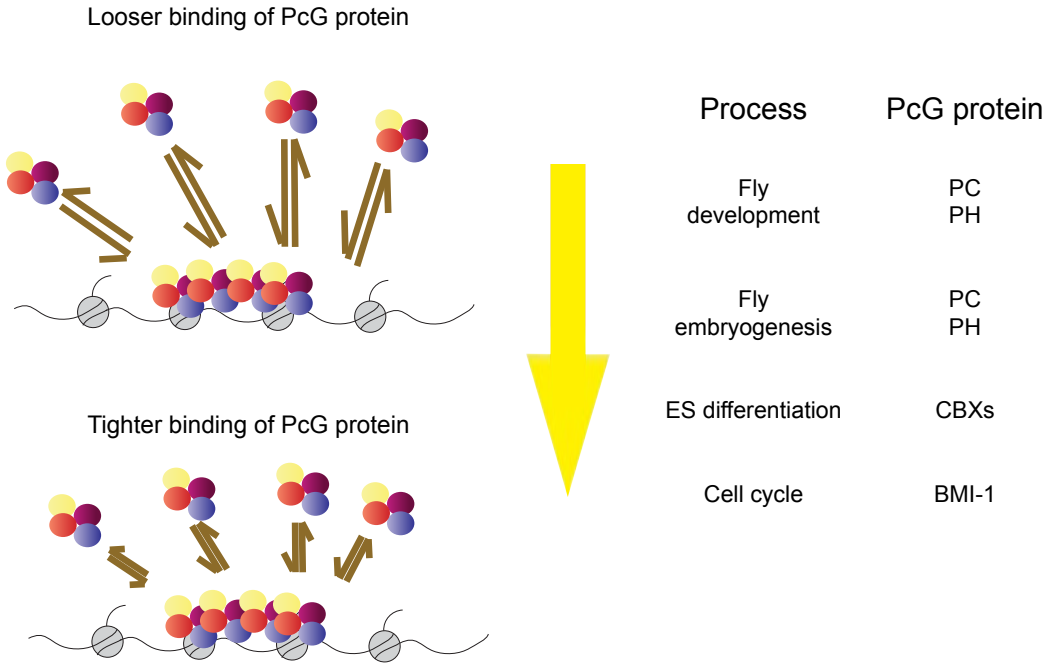

Figure 1.1: Dynamic interaction of PcG proteins with chromatin during differentiation. Several studies in flies and mammals have reported that in different developmental processes, differentiation pathways and during cell cycle, the interaction of PcG proteins with chromatin changes from a looser to a tighter binding state. Details for each of the examples shown are given in text.

1.3 PcG protein behaviour in mitosis

Cell division is a vital moment for the action of PcG proteins. The vast majority of chromatin binding proteins dissociates from mitotic chromatin and there is a global transcriptional shutdown [167, 168, 169]. However, for the PcG target genes, it is through mitosis that the memory of transcriptional status must be maintained and it is also during mitosis that an opportunity for flexibility in PcG target status exists, enabling changes of cell identity during differentiation. Thus, to better understand epigenetic memory, it is essential to study the behaviour of PcG proteins during mitosis.

1.3.1 Mitosis and transmission of epigenetic memory

The mechanisms behind PcG memory remain largely unknown, though hypotheses have been put forward (Figure 1.2, reviewed in [65]). The fact that several PcG proteins have enzymatic activities towards histones, has led to the idea that modified histones function as beacons to recruit PcG proteins after cell division [170]. It is unclear if this model is correct, as histone modifications do correlate with gene activity but there is no strong evidence of causality (reviewed in [2, 171]). Although histone marks that interact with PcG proteins (H3K27me3) are present during mitosis, there is evidence that after replication there is a dilution of H3K27me3, which is not restored until late G1 of the next cell cycle [172]. It is unclear if this dilution affects PcG targeting. Moreover there is clear data that at least for some PcG targets the presence of DNA binding proteins is essential for PRC2 and PRC1 recruitment [173].
Another possible mechanism is the transmission of epigenetic memory through ncRNAs. ncRNAs have been shown to be transcribed from PREs in flies [96, 107, 109] and from Polycomb binding sites in mammalian cells [122, 174, 175], and to interact with PcG and TrxG proteins [86, 87, 88, 176]. In addition, it has been shown that PRE transcription can be maintained through development and, in a transgenic assay, that this transcription has to be maintained through embryogenesis for the memory of an active state [109]. The authors suggest a model in which PcG targets are silenced by default and only an active state requires to be remembered. Further evidence for this model has also been reported in *Drosophila*, where PREs can silence indiscriminately any gene if PcG proteins are present [177] and TrxG proteins act as anti-repressors that inhibit ectopic PcG gene silencing [48].
Other mechanisms, in addition to ncRNAs, that could promote the memory of active states are deposition of active histone marks, like H3.3 [178, 179],

H3K4me2/3, which can be recognized by the Trithorax homolog MLL1 [180], and H4K5ac [181], which is recognized by the BRD4 protein and allows rapid reactivation of bookmarked genes. Though interesting, these findings have the same limitations that are true for silencing marks, such as the transmission of memory through replication and the targeting specificity.
An additional model for gene transcription memory could be the binding of proteins to mitotic chromatin, which will be discussed in the next section.

1.3.2 Interaction of PcG proteins with mitotic chromatin

Most transcription factors are displaced from chromatin upon entry into mitosis. However, there are many examples of proteins that are able to bind mitotic chromatin and that this binding is essential for normal development and tightly regulated.
TATA-Binding Protein has been shown to be remarkably stably associated with mitotic chromatin [182], as well as RNA polymerase I transcription factors and histone H1, which have longer residence times in mitotic chromatin than in interphase [183]. Interestingly, even during mitosis this binding is modulated, as specific isotypes of H1 are phosphorylated during mitosis in order to increase their residence times [184, 185]. An additional example of this type of regulation has been reported for HMG1A, whose interaction with chromatin is

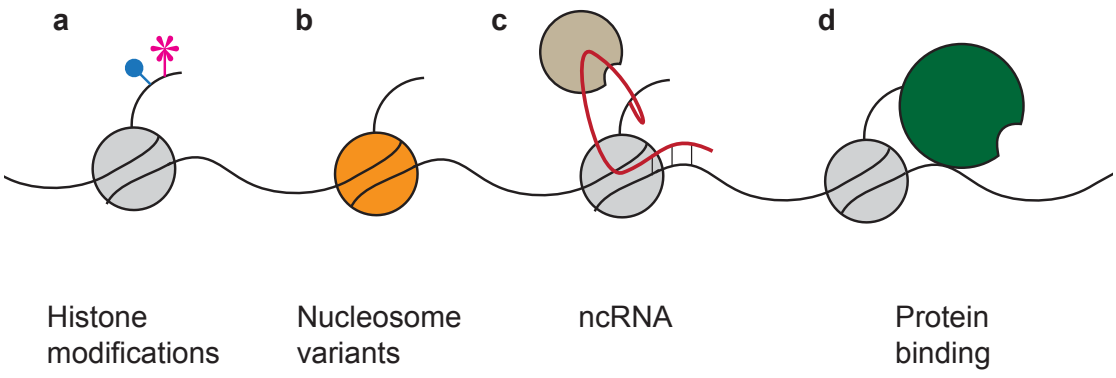

Figure 1.2: Models of mitotic inheritance of epigenetic memory. Transcriptional states that are regulated by PcG and TrxG proteins have been envisioned to be maintained through cell division by deposition of histone marks (a) or histone variants (b) that are recognized and target PcG and TrxG proteins to their targets in the following interphase. An additional hypothesis is the presence of ncRNAs, which are able to specifically recognise a DNA sequence and recruit PcG or TrxG proteins during interphase or early in interphase (c). A simpler model requires the direct binding of PcG or TrxG proteins to their targets in a manner that these genes are further silenced or activated in the next cell cycle (d). Experimental evidence for these hypotheses are given in the text.

dependent on its 3 AT-hooks, and is phosphorylated in mitosis [186]. This phosphorylation leads to a reduced mobility of HMG1A [186]. In contrast, phosphorylation of Regulator of Chromatin Condensation 1 (RCC1) is necessary for its higher mobility recorded during cell division [187]. Interestingly, this change in dynamics is necessary for mammalian spindle assembly and high RanGTP concentration on chromatin [187].
Studies on PcG protein interaction with chromatin during mitosis are not common and mostly rely on immunofluorescence analysis (Figure 1.3). There are contrasting data that show binding of several PcG and TrxG proteins to larval neuroblast chromosomes [188] and complete dissociation of PC, PH and PSC in embryo mitosis [189]. These divergent results may result from artifacts derived from fixing protocols or may be cell type specific interactions of PcG proteins with mitotic chromatin. Interestingly, the reassociation timing of PcG proteins after mitosis was shown to be different for each PC, PH and PSC [189]. Similar analysis in mammalian cells has also proved inconclusive as there are reports that PRC1 components BMI-1, PH1 and RING1B do not colocalise with mitotic chromatin [152, 190], while CBX2 and CBX6 interact with histones during mitosis [191]. A detailed study was performed for MLL1 in HeLa cells, where binding of this TrxG protein was verified by immunofluorescence and ChIP [192]. Interestingly, the binding sites for MLL1 were largely changed from interphase to mitosis, revealing different affinities during cell cycle progression of TrxG proteins for their binding sites [192].
Analysis of PcG-chromatin interactions during mitosis in live cells has been reported for PC in flies. Analysis in embryo and larval neuroblast cell divisions revealed that most of the PC proteins dissociate from chromatin, though it was not possible to determine to what extent the dissociation occurred [193].
Another area of interest is the interaction of DNA binding proteins with mitotic chromatin as they can serve as binding platforms for other PcG and TrxG proteins. There is evidence that PHO, GAGA, PSQ and RUNX2, which is a paralog of RUNX1, a protein recently shown to interact and recruit PRC1 to target loci, are able to interact with mitotic chromatin [78, 188, 194, 195], thus potentially providing a platform for recruitment of additional PcG proteins during mitosis and/or early interphase. It will be essential in the future to study in detail the interaction of PcG proteins with mitotic chromatin. To what extent are PcG proteins binding chromatin and how cell type specific these interactions are is of great interest, not only for general PRC1 and PRC2 components but also for DNA binding proteins. Moreover, due to the large number of proteins involved in PcG regulation and the specific regulation of binding properties through the cell cycle, it would be vital to integrate data in meaningful quantitative models.

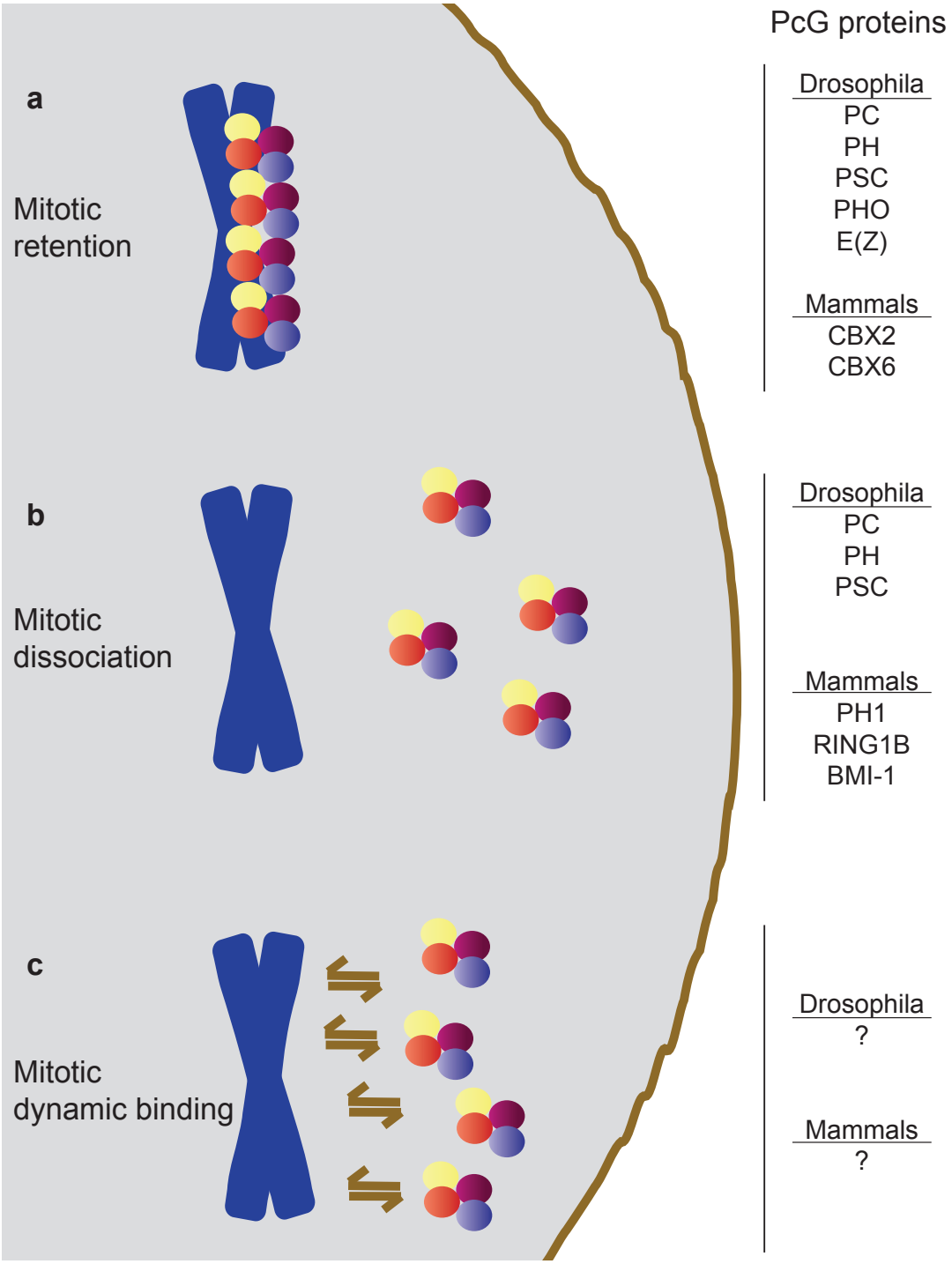

Figure 1.3: Binding of PcG proteins to mitotic chromatin. Summary of PcG proteins in flies and mammals that have been reported to bind (a) or dissociate from mitotic chromatin (b). The presence of the same protein in these two exclusive categories indicates contradictory data present in the literature that requires further reexamination. To my knowledge, studies of dynamic binding of PcG proteins to chromatin during cell division have not been reported (c). Details of the experimental evidence for the examples show are given in the text.

1.4 Quantification and modeling of epigenetic systems

When analyzing large-scale systems, sometimes results can be unexpected and counterintuitive. However, this does not mean these results cannot be predicted, for the use of mathematical modeling can provide a way to understand these systems [196].
Biological systems are inherently heterogeneous and redundant which makes them hard to model. However, as large amounts of complex data are made available everyday, one is required to use mathematical modeling not only to integrate such amounts of data but also to understand biological phenomena and to generate hypotheses for further studies [197, 198, 199]. Even simple mathematical models will allow to understand if all components in the studied system have been found (when the model fits the data), or if some are missing (when models do not fit the data), as well as if some of these components or parameters are superfluous for the understanding of the biological system [196].
Mathematical modeling of biological systems can be addressed from two opposing strategies. The first one, a top-down strategy, starts with large data sets and uses statistical methods for determining correlations between components of the system and allows the generation of predictions based on system organization [200]. The second, a bottom-up approach, is based on the mathematical description of a hypothetical mechanism through the use of kinetic, deterministic or stochastic models. These mathematical descriptions are used to run simulations which allow the generation of predictions about the system. These predictions can be tested *in vivo*, leading to an iterative cycle between experiments and development of the mathematical model. [200]
Most mathematical models of epigenetic systems described to date have used a bottom-up strategy and a description of the advances made in this field will be described below.

1.4.1 Modeling of epigenetic systems

Due to its smaller complexity and extensive studies, yeast has been the preferred organism for modeling of epigenetic phenomena. Cheutin and colleagues have used a kinetic model to describe Swi6 behaviour in *S. pombe* [201]. Swi6 is the yeast homolog of HP1 known to interact with methylated H3K9 [202]. This model predicted that there are at least two kinetically distinct populations of Swi6 bound to methylated chromatin. Several predictions of the kinetic behaviour of the protein were tested by Fluorescence Recovery After

Photobleaching (FRAP) analysis in mutant backgrounds [201]. A theoretical approach to the maintenance of histone modifications has also been reported [203, 204]. In these mathematical models, the mating-type locus of *S. pombe* was modeled using stochastic simulations of nucleosome replacement and modification through the cell cycle. The assumptions of these models were that nucleosomes can have three (active, unmodified, inactive) [203] or two states (active, inactive) [204], that nucleosome replacement during replication is random and that there is a inherent noise in system due to unspecific action of histone modifying enzymes. The remarkable predictions of these models were three-fold. First, bistability of nucleosomal states can be obtained in systems where the specific histone modification to noise ratio of the modifying enzymes is low (2-4 fold). Second, that this bistabilty of states requires cooperativity. While this had been shown in other systems of signal transduction, it was the first time that such phenomena has been reported in epigenetic systems. Moreover, this cooperativity can be either explicit, through the action of two non-adjacent nucleosomes on the modification of another nucleosome, or implicit, as the action of both pre-established nucleosome modifications and the histone modifying enzymes. The third prediction relates to the size of the region. With the increase in the number of nucleosomes in the studied region, the more stable this region becomes to changes in nucleosomal states. Interestingly, the authors also suggest that the cell cycle speed might also be important for stability of nucleosomal states, and that this might be a widespread phenomenon, also present in induced pluripotent stem cell generation [204].

Another approach to mathematical modeling of histone modifications has been performed to describe the levels of H3K79 methylation in single cells and populations of yeast [205]. These models and the experimental validation that accompanied them, provided new insights into the accumulation of this histone modifications in old histones and propose that this type of slow accumulating marks can function as cell cycle timers.

Epigenetic modeling has also been applied in plants, as a similar modeling approach to the one reported by [203] has been used in the study of vernalisation in *A. thaliana* [206]. This stochastic model of methylation of nucleosomes in the *FLC* locus predicted a bistable *FLC* expression that depended quantitatively of the number of days in cold that plants experienced. Furthermore, the predictions that bistability was cell autonomous and that methylation levels would need to be upregulated fast after switch into cold temperatures, were tested and validated experimentally [206].

In addition to histone methylation, histone ubiquitination by Ring1B and BMI-1 has also been modeled [207]. In this deterministic model, RING1B and BMI-1

associate and are responsible for histone and self-ubiquitination. The prediction of this model is that histone ubuitination can be controlled by the levels of BMI-1 expression. Moreover, the system, depending on the quantities and kinetic parameters of its components, can give rise to a wide range to behaviours that include oscillations, stability of ubiquitination that shows hysteresis and excitable overshoots of ubiquitination activity upon perturbation of the system [207].
Modeling of PcG protein behaviour has been performed for the interaction of PC with histones and DNA binding proteins in salivary glands and SL2 cells [13]. This model reported the effect of higher-order chromatin structure (PC binding to two separate nucleosomes) in increasing the stability of PC binding, as well as the effects of methylation dependent and independent PC-chromatin binding. A recent model loosely based on the regulation of transcription by PcG and TrxG proteins through DNA and histone modifications recruitment has been proposed [208]. The results from this model are the prediction that bistability is present in regions that are bound by PcG protein complexes and that the ability to memorize states is dependent on the size of the region. Moreover, this model predicted that histone modifications were stronger attractors of PcG complexes than DNA information. Unfortunately, this model did not address the effects of cell cycle progression on PcG recruitment.
In summary, work on modeling of epigenetic systems has brought many new insights as well as introduced new hypothesis that have been validated or are still open questions. Interestingly, many of the authors report that the behaviour of these epigenetic systems depend on the quantities and kinetic rates that the components have *in vivo*, suggesting that the measurement of these values is of great importance for the correct understanding of biological phenomena [13, 205, 207].

1.4.2 Measurement of protein properties in live systems

Mathematical models of biological systems depend on the good understanding of how the biological system works. However, if they are to be meaningful, they also depend greatly on knowing the quantities and kinetic properties of the components inside the system.

Determination of protein quantities *in vivo*

Quantification of proteins or of their modifications is an invaluable resource for understanding biological phenomena. In fact, knowing the number of molecules allows for the elaboration of hypotheses due to the presence of a

small population of modified proteins [147]; to compare the ability of two transcription factors to compete for the same binding sites [209]; and also to understand disease phenomena [210].
The methods to determine protein quantities *in vivo* usually rely on the comparison of samples containing the proteins of interest with known amounts of recombinant protein, probed with specific antibodies, either after electrophoresis or through ELISA assays (reviewed in [211]). An increasing trend is to probe the number of proteins or of modified peptides through to use of quantitative mass spectrometry (reviewed in [212, 213]). However, these approaches do not question the number of molecules of the protein of interest in a single cell, addressing instead a more or less homogeneous population of cells. To answer this question, methods have been developed that require the use of fluorescently tagged proteins. This type of strategy allows for the quantification of relative levels of protein expression [197] but also of the absolute number of proteins. In yeast, Wu and colleagues have quantified the number and local concentration of 28 cytokinesis proteins in live yeast by using combination of YFP-tagged proteins analyzed by FACS and live imaging with quantitative immunoblotting [214]. A remarkable approach has also been developed which uses GFP-fused Virus-like-particles (GFP-VLP). These rotavirus-like particles have their VP2 capsid protein N-terminally fused to GFP, which allows the incorporation of 120 GFP molecules into each GFP-VLP [215]. These diffraction limited particles have been used to quantify several GFP-fusion protein in live cells [216, 217]. An additional approach, which relies on the measurement of autocorrelation levels by fluorescence correlation spectroscopy (FCS) was brought forward recently (reviewed in [218]), and it has been reported for the measurement of local concentration of Bicoid in live *Drosophila* embryos [219].

Extraction of protein kinetic parameters *in vivo*

Measurement of kinetic properties of proteins has been traditionally described by *in vitro* methods [211, 220]. However, the measurement of these properties *in vivo* might give different and more meaningful results, due to the influence of the environment on the protein and its binding target, as well as the *in vivo* concentration of the components which might be essential for the better understanding of the kinetic behaviour [220]. Most protocols for determination of kinetic properties of proteins employ fluorescently tagged proteins which are interrogated whether using photoactivation, bi-complementation assays, fluorescence correlation spectroscopy (FCS), fluorescence resonance energy transfer (FRET), or fluorescence recovery after photobleaching (FRAP) (Figure 1.4) [211].

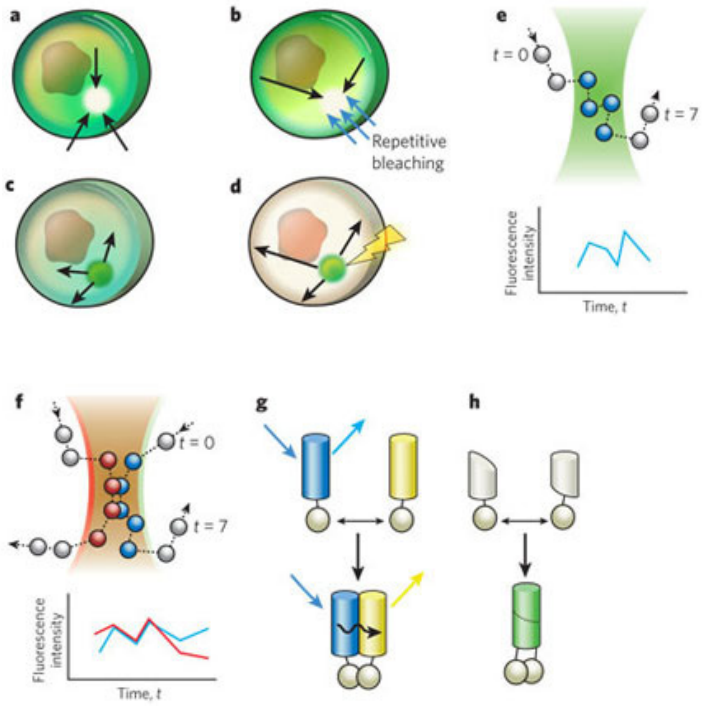

Figure 1.4: Methods for measuring molecular dynamics and protein interactions. (a) Fluorescence recovery after photobleaching (FRAP). A region of interest (white circle) is intentionally photobleached and the recovery of fluorescence by movement of fluorescent protein (black arrows) is measured over time. (b) Fluorescence loss in photobleaching (FLIP). Measurement of decay of fluorescence outside a region that is repeatedly photobleached (blue arrows) due to the movement of fluorescent proteins to this region (black arrows). (c) Inverse FRAP. The whole cell is photobleached except a region of interest (green circle), where reduction in fluorescence intensity is measured over time due to movement of fluorescent proteins outside this region (black arrows). (d) Photoactivation. In this method, a specify fluorescent protein with the ability to switch on or off or to change its emission spectrum is activated in response to light (lightning bolt) in a region of interest (green circle). Afterwards the movement of the structure or of proteins inside the photoactivated region is measured through time (black arrows). (e) Fluorescence correlation spectroscopy. This technique measures the number of fluorescent molecules and the fluctuations of fluorescence inside a defined volume of light (green region). The excitation of a single fluorescent molecules (blue molecule), leads to changes in fluorescent intensity trough time (blue line in plot). From the correlation function that is measured, the diffusion times of the fluorescently tagged proteins can be extracted, in addition to the absolute number of molecules in the confocal volume. (f) Fluorescence cross correlation spectroscopy. This is a derivative of FCS, in which fluorescent fluctuations of two or more fluorescently tagged proteins are measured in a defined volumes (green and red regions). The excitation of the fluorescent molecules (blue and red), leads to changes in total fluorescent intensities which are plotted against time (plot below). The correlation of these curves with time and to each other can be used to extract binding parameters of these molecules. (g) Fluorescence resonance energy transfer (FRET). This method measures the efficiency of the transfer of Förster's energy (black wavy line) between two fluorescently tagged proteins of interest, when in close proximity (1–10nm). (h) Bi-complementation assay. In this assay, two separate proteins are tagged with "half" domain of a fluorescent protein (white half-cilinder). When the proteins interact, the domain are reconstituted and a fluorescent signal is measured (green cylinder). Modified from [211]

The resulting data from the application of these methods has been discussed in previous sections of this introduction and a more detailed description of these methods is presented below.
Photoactivation can be used to measure fluorescence decay of the tagged protein, thereby extracting values for diffusion of proteins as well as binding properties, as has been described for Oct4 in pre-implantation mouse embryos [221].
Bi-complementation assays are based on the expression of two proteins, each tagged with half of a fluorescent protein or another reporter. The interaction of these proteins, or their close proximity, leads to an increase in reporter activity [222].
FCS techniques are based on the measurement of fluctuation of fluorescence signals of tagged proteins in a diffraction limited volume through time [223]. These fluctuations are posteriorly correlated and provide diffusion coefficients and binding properties of proteins in addition to concentration estimates. FCS can be performed in several distinct volumes across a nucleus of cell, providing a spatial map of kinetic properties of proteins (image-correlation spectroscopy). Furthermore, two color tagging of different proteins can be applied, and cross-correlation between proteins can be acquired providing information of how the proteins interact with their binding sites, as well as each other (Fluorescence Cross-Correlation Spectroscopy, FCCS) [223].
FRET techniques are based on the transfer of energy of two fluorophores, of two differently tagged proteins, when these are in close proximity (1–10nm) [224]. This energy transfer is either detected by two-channel imaging with an algorithm that corrects for excitation and emission crosstalk, acceptor photobleaching, fluorescence lifetime imaging, spectral imaging or fluorescence polarization imaging [224].
FRAP is a method that relies on the intentional photobleach of a small region of a cell or nucleus and consequent measurement of the rate at which fluoresce is gained in this region [225]. The speed at which this recovery happens includes information about the diffusion of the tagged protein as well as interaction with binding sites that reside inside the bleach region. Analysis of FRAP curves can be qualitative, thereby giving information about half-times of recovery (time required to recover 50% of final fluorescence) and also immobile fractions (fraction of fluorescence that is not recovered after photobleaching) [225]. Furthermore this analysis can be quantitative. In this type of analysis different models can be applied that take into account size of the nucleus, diffusion, binding reactions with dissociation and association rates as well as distribution of binding sites [226, 227, 228]. Variations of FRAP have been applied and they include iFRAP (whole cell area outside a small region of interest is photobleached, and

the subsequent decrease in fluorescence in this unbleached region is acquired) and FLIP (fluorescence loss in photobleaching, where a region in repeatedly photo bleached, while in a different region of interest, the decrease in fluorescence is recorded) [211].

1.5 Aim

PcG proteins play a crucial role in maintaining the repressed transcriptional states of their target genes in stem cells and differentiated cells. Nevertheless, this proteins have to demonstrate flexibility for their targets upon differentiation. Importantly, it is through cell division that the stability and flexibility properties of PcG properties are put to test, revealing that it is essential to study

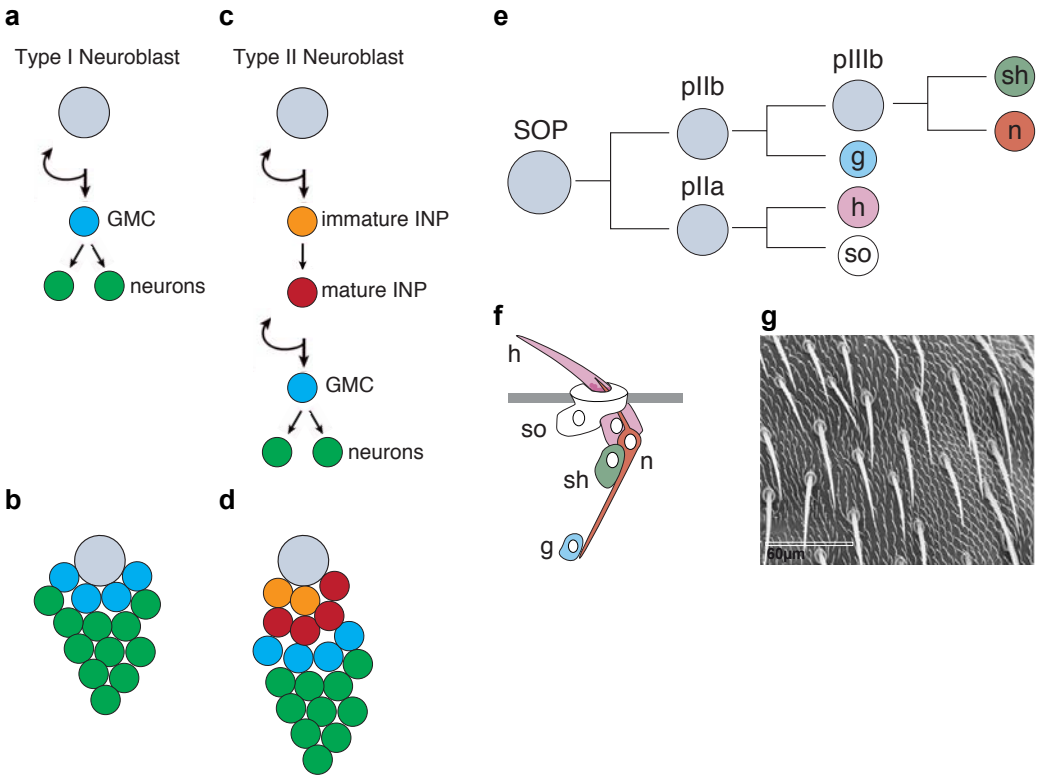

Figure 1.5: *Drosophila* neuroblast and sensory organ precursor cell lineages. (a–d) Type I (a) and type II (c) neuroblast lineage divisions with respective lineage diagrams (b, d). GMC indicates ganglion mother cell and INP intermediate neural progenitor. (e–g) Sensory Organ Precursor (SOP) cell lineage divisions (e) and external sensory organ structure (diagram in (f) and electron micrograph (g) where hair and socket cells are visible). g indicates glia cell which will undergo programmed cell death, h indicates hair cell, so indicates socket cell, sh indicates sheath cell, and n indicates a neuron. (a–d) were based on [229], (f, g) were modified from [230] and (g) was modified from [231].

the behaviour of PcG proteins during mitosis and differentiation.
My aim in this thesis is to perform a detailed quantitative analysis of the behaviour of PcG proteins in living animals in single cell systems with defined differentiation processes and mitotic activity. Moreover, I wish to measure quantitative changes in the nature of PcG binding to mitotic chromatin in different cell types of a single animal. In order to do this, I have analyzed the behaviour of GFP-fused Polyhomeotic (PH::GFP), Polycomb (PC::GFP), Pleiohomeotic (GFP::PHO), Dorsal switch Protein 1 (GFP::DSP1) and Enhancer of Zeste (GFP::E(Z)) in living *Drosophila* larval type I neuroblasts and pupal sensory organ precursor cells (SOPs).
Type I neuroblasts are stem cell neuronal progenitors that divide asymmetrically to give origin to another neuroblast and a ganglion mother cell (GMC) [232](Figure 1.5). SOPs are more determined cells that arise later in fly development and divide asymmetrically to give two well-defined daughter cells pIIa and pIIb. Further divisions of these cells lead to the development of external sensory organs in fly nota [233] (Figure 1.5).
Through the combination of quantitative live imaging and mathematical modeling I have shown that PcG protein mobilities are decreased during development and differentiation and that most PcG and DNA binding proteins have a small fraction of kinetically distinct molecules bound to mitotic chromatin. Mathematical modeling was used to identify potential mechanisms for the rapid dissociation of PC from mitotic chromatin and modifiers of PC kinetic properties were identified in neuroblasts.
In summary, I demonstrate here that the properties of the PcG proteins are not only different in different lineages, but are also profoundly altered at mitosis. I propose that this regulation of PcG properties may be essential both to the stability of determined cell identities, and to the flexibility of the stem cell state.

2

Materials and Methods

2.1 Fly strains

Fly strains used in this thesis are shown in Table 2.1

2.2 Fly husbandry and rescue experiments

All flies were maintained in standard medium at 18ºC, unless stated otherwise. Rescue experiments were performed at 25ºC, according to the scheme shown in Figure 3.1. Adult flies without balancer chromosomes were counted and registered as rescued.

For imaging of PH and PHO GFP-fusion proteins and GFPnls in neuroblasts, PH::GFP, H2A::RFP and GFP::PHO, H2A::RFP and GFPnls, H2A::RFP third instar larvae were collected and imaged without further crossing. For neuroblast lineage imaging of PC::GFP, GFP::DSP1 and GFP::E(Z), crosses between H2A::RFP and PC::GFP,H2A::RFP, GFP::DSP1 or GFP::E(Z) flies were conducted to obtain the following genotypes: $w^{1118}; +; P\{pPc-$ PC::GFP$, w^+\}, P\{pUbi-$ H2A::mRFP$, w^+\}/P\{pUbi-$ H2A::mRFP$, w^+\}$; $w^{1118}; \{pTub-$ GFP::DSP1$\}/+; P\{pUbi-$ H2A::mRFP$, w^+\}/+$; and $w^{1118}; \{pTub-$GFP::E(Z)$\}/+; P\{pUbi-$H2A::mRFP$, w^+\}/+$. These flies were collected at the third instal larval stage.

For SOP lineage imaging of PH::GFP, PC::GFP, GFP::DSP1, GFP::E(Z) and GFPnls, crosses were made between the *neuralized*-GAL4 driver (*neur* driver)and PH::GFP, PC::GFP, GFP::DSP1, GFP::E(Z)and GFPnls flies to obtain the following respective progenies: $w^{1118}; P\{Tub-GAL80ts, w^+\}/P\{UAS, pPc-$ PH::GFP$, w^+\}; P\{neur-GAL4, w^+\}, P\{UAS-$ H2A::mRFP$, w^+\}/+$; $w^{1118}; P\{Tub-GAL80ts, w^+\}/+; P\{neur-GAL4, w^+\}, P\{UAS-$ H2A::mRFP$, w^+\}/P\{pPc-$ PC::GFP$, w^+\}$; $w^{1118}; P\{Tub-GAL80ts, w^+\}/$

Table 2.1: Fly strains

Name	Genotype	Source
PH::GFP	$w^{1118}; P\{UAS, pPc-\text{PH::GFP}, w^+\}; +$	D. A.-Jovin
PH::GFP, H2A::RFP	$w^{1118}; P\{UAS, pPc-\text{PH::GFP}, w^+\}, P\{worn-GAL4, w^+\}/Cy, O; P\{pUbi-\text{H2A::mRFP}, w^+\}$	this thesis
PC::GFP	$w^{1118}; +; P\{pPc-\text{PC::GFP}, w^+\}$	R. Paro
PC::GFP (II)	$w^{1118}; P\{pPc-\text{PC::GFP}, w^+\}; +$	R. Paro
PC::GFP, H2A::RFP	$w^{1118}; +; P\{pPc-\text{PC::GFP}, w^+\}, P\{pUbi-\text{H2A::mRFP}, w^+\}$	this thesis
GFP::DSP1	$w^{1118}; \{pTub-\text{GFP::DSP1}, w^+\}; +$	L. Ringrose
GFP::PHO, H2A::RFP	$w^{1118}; \{pTub-\text{GFP::PHO}, w^+\}; P\{pUbi-\text{H2A::mRFP}, w^+\}$	this thesis
GFP::PHO, H2A::RFP (II)	$w^{1118}; \{pTub-\text{GFP::PHO}, w^+\}; P\{neur-GAL4, w^+\}, P\{UAS-\text{H2A::mRFP}, w^+\}$	this thesis
GFP::E(Z)	$w^{1118}; \{pTub-\text{GFP::E(Z)}, w^+\}; +$	L. Ringrose
GFPnls	$w^{1118}; P\{UAS-\text{GFPnls}, w^+\}; +$	B. Dickson
GFPnls, H2A::RFP	$w^{1118}; P\{UAS-\text{GFPnls}, w^+\}, P\{worn-GAL4, w^+\}/Cy, O; P\{pUbi-\text{H2A::mRFP}, w^+\}$	this thesis
H2A::RFP	$w^{1118}; +; P\{pUbi-\text{H2A::mRFP}, w^+\}$	J. Knoblich
neur driver	$w^{1118}; P\{pTub-GAL80ts, w^+\}; P\{neur-GAL4, w^+\}, P\{UAS-\text{H2A::mRFP}, w^+\}$	J. Knoblich
insc driver	$w^{1118}, P\{UAS-dcr2, w^+\}; P\{insc-GAL4, w^+\}/Cy, O; P\{pTub-GAL80ts, w^+\}$	J. Knoblich
type 2 driver	$w^{1118}, P\{UAS-dcr2, w^+\}; P\{ase-GAL80, w^+\}, P\{worn-GAL4, w^+\}; P\{UAS-\text{CD8::GFP}, w^+\}$	J. Knoblich
JIL-1 RNAi	$w^{1118}; P\{UAS-JIL-1RNAi\}; +$	VDRC #107001
ASH1 RNAi	$w^{1118}; P\{UAS-ASH1RNAi\}; +$	VDRC #108832
JIL-1 RNAi, PC::GFP	$w^{1118}; P\{UAS-JIL-1RNAi\}; P\{pPc-\text{PC::GFP}, w^+\}, P\{pUbi-\text{H2A::mRFP}, w^+\}$	this thesis
ASH1 RNAi, PC::GFP	$w^{1118}; P\{UAS-ASH1RNAi\}; P\{pPc-\text{PC::GFP}, w^+\}, P\{pUbi-\text{H2A::mRFP}, w^+\}$	this thesis
Pc^{XL5}	$w^{1118}; +; Pc^{XL5}/TM3, Ser$	L. Ringrose
Pc^3	$w^{1118}; +; In(3R)P(Pc^3), Pc^3/TM1$	DGRC #106475

$\{pTub-$GFP::DSP1$, w^+\}; P\{neur-GAL4, w^+\}, P\{UAS-$H2A::mRFP$, w^+\}/+$; $w^{1118}; P\{Tub-GAL80ts, w^+\}/\{pTub-$GFP::E(Z)$, w^+\}; P\{neur-GAL4, w^+\}$, $P\{UAS-$H2A::mRFP$, w^+\}/+$; and $w^{1118}; P\{Tub-GAL80ts, w^+\}/P\{UAS-$ GFPnls$, w^+\}; P\{neur-GAL4, w^+\}, P\{UAS-$H2A::mRFP$, w^+\}/+$. White prepupae of these crosses were switched to 25°C 15h before SOP imaging and FRAP to allow for GAL4-driven expression. For SOP lineage imaging and FRAP of GFP::PHO, GFP::PHO, H2A::RFP (II) flies were raised at 18°C until they reached white prepupal stage, when they were transfered to 25°C for 15h to allow for GAL4 expression.
Short-time knockdown of JIL-1 and ASH1 was performed by crossing *insc* driver female flies to male *JIL-1* RNAi, PC::GFP or *ASH1* RNAi, PC::GFP. Upon appearance of third-instar larvae, the progeny was switched to 29°C 24–48h before FRAP analysis to allow for GAL4 expression. H2A::RFP expressing neuroblasts were used for subsequent experiments.
Long-time knockdown of JIL-1 and ASH1 was performed by crossing type 2 driver female flies to male *JIL-1* RNAi or *JIL-1* RNAi, PC::GFP and *ASH1* RNAi or *ASH1* RNAi, PC::GFP. Upon 2 days of laying at 25°C, the parent flies were removed and the progeny switched to 29°C. GFP-marked neuroblasts were used for subsequent experiments.

2.3 Purification of Neuroblasts

Isolation and purification of neuroblasts from third instal larval brains was done in collaboration with Juergen Knoblich's group at IMBA. The protocol for this purification will be published elsewhere.

2.4 Quantitative Western Blotting

Fly extracts and Western blots were performed as described in [163] with minimal changes. Proteins were separated in NuPAGE gels (Invitrogen) and probed with antibodies as listed in Table 2.2. PC protein levels were quantified with a Typhoon scanner (GE Healthcare), used to detect chemofluorescence generated after ECL-Plus (Amersham) addition. For all other proteins, Luminata Forte Western HRP Substrate (Millipore) was used to generate chemofluorescence, which was detected in Hyperfilm ECL (Amersham) films. Films were scanned at 600dpi (Cannon) and posteriorly quantified with ImageJ (NIH). All values were normalised to a loading control.

Table 2.2: Antibodies for quantitative western blot

Protein	Gel Concentration	Primary Antibody	Secondary Antibody
Polyhomeotic	3–8%	polyclonal α-PH (gift from R. Paro)	HRP-α-rabbit (NA934 GE Healthcare)
Polycomb	4–12%	polyclonal α-PC (d-220, Santa Cruz Biotechnology)	HRP-α-rabbit (NA934 GE Healthcare)
Dorsal Switch Protein 1	4–12%	polyclonal α-DSP1 (gift from D. Locker)	HRP-α-rabbit (NA934 GE Healthcare)
Pleiohomeotic	3–8%	polyclonal α-PHO (gift from J. Kassis)	HRP-α-rabbit (NA934 GE Healthcare)
Enhancer of Zeste	3–8%	polyclonal α-E(Z) (gift from R. Jones)	HRP-α-rabbit (NA934 GE Healthcare)
Histone H3	4–12%	polyclonal α-H3 (Abcam ab1791)	HRP-α-rabbit (NA934 GE Healthcare)
Tubulin	3–8%	monoclonal α-Tub (Sigma-Aldrich T5168)	HRP-α-mouse (Sigma-Aldrich A4416)

2.5 Immunocytochemistry in larval brains and pupal nota

Immunocytochemistry experiments in larval brains were performed as described [234]. Immunocytochemistry experiments in pupal nota were performed by dissecting the pupae in 5% paraformaldehyde in phosphate-buffered saline (PBS). The total time of fixation was 20 min, and the subsequent procedure was identical to that described for larval brains. The primary antibodies used were rabbit α-Miranda (1:250) [234] and rabbit α-H3K27me3S28ph (1:2000) [235]. The secondary antibody was AlexaFluor 647 goat α-rabbit (1:500) (Invitrogen A-21245). For the images shown in Figure 3.17, GFP was imaged directly without staining.

2.6 Imaging of larval brains and adult bristles

For brain imaging, larval brains of 3rd instal larvae were dissected in a drop of PBS and immediately imaged with a Zeiss Stereomicroscope.
For bristle imaging, adult flies were anesthetised and imaged with a Zeiss Stereomicroscope.

2.7 Quantification of GFP-fusion proteins using GFP-VLP

For quantification of GFP-fused proteins, GFP-VLPs (100 ng/mL) were spread on a #1.5 coverslip and imaged under the same settings as the GFP fusion protein of interest. Images of GFP-VLPs were deconvolved with the Classic Maximum Likelihood Estimation (CMLE) method of the software Huygens Pro (SVI), and a total intensity of at least 80 particles was determined using Imaris (Bitplane). After binning of intensities, the mode of the distribution was selected as the intensity of 120 GFP molecules. Comparison of GFP fusion intensities calculated with Imaris (Bitplane) with this value allowed the estimation of GFP fusion protein quantities.

2.8 Quantification of GFP-fusion proteins using ELISA

Quantification of GFP-fused proteins with ELISA was performed by Philipp Steffen and is described in [235].

2.9 Preparation of specimens for microscopy and imaging

For SOP imaging, pupae were prepared as described in [240]. Imaging was performed at room temperature on a Zeiss LSM710 with a 633 1.4 NA oil immersion objective using an Argon laser at 488 nm for GFP imaging (collection between 485 and 563 nm) and a DPSS 561-10 laser at 561 nm for mRFP imaging (collection between 563 and 728 nm) and a pinhole equivalent to 2.45 Airy units. The voxel size was $51x51x150$nm.
For neuroblast imaging, larval brains were dissected in a Lab-Tek II Chamber #1.5 German Coverglass (Nalgene Nunc International) containing 200 mL of PBS. Imaging was performed at room temperature on a Zeiss LSM710 with a 633 1.2 NA water immersion objective using an Argon laser at 488 nm for GFP imaging (collection between 485 and 563 nm) and a DPSS 561-10 laser at 561 nm for mRFP imaging (collection between 563 and 728 nm) and a pinhole equivalent to 2.07 Airy units. The voxel size was $51x51x150$nm.

2.10 Image processing

Images in Figure 3.6, Figure 3.7, Figure 3.8 and Figure 3.17 were deconvolved using measured Point Spread Functions (PSFs) with the CMLE method of the software Huygens Pro (SVI). The measurement of the volumes occupied and the total fluorescence intensity of GFP and RFP in Figure 3.6, Figure 3.7 and Figure 3.8 were performed with the surface tool of Imaris (Bitplane). Background was subtracted from intensity measurements.
Images in Figure 3.2 (d–f and j–l) and Figure 3.19 were smoothened with ImageJ (NIH).

2.11 Fluorescence Recovery After Photobleaching

FRAP experiments were performed as described in [228] with minimal changes. FRAP was performed in a Zeiss LSM710 with the confocal pinhole set to 3 Airy units. The image size was $512x62$ pixels, with a pixel size of 45nm. Images were acquired every 20 msec for GFPnls and PC::GFP experiments, 50 msec and 100 msec for PH::GFP, and 30ms for GFP::DSP1, GFP::PHO and GFP::E(Z), setting the Acousto-Optic Tunable Filter (AOTF) to 1% (1.5% for GFP::PHO) of the 488 line of an Argon laser. The circle bleach region had a diameter of 40 pixels; it was centered on the image field and overlapped with expression of H2A::RFP. The bleach iteration number was set to 2 and 100% AOTF of the 488 line in an Argon laser. Background was measured within a region with no cells of the image and subtracted from data. All intensity measurements were performed with MatLab (Mathworks).

2.12 FRAP model fitting

FRAP modeling of recovery curves was performed according to [228] in MatLab (Mathworks) with minimal changes, and is described in detail in the Appendix B. An adaptation of the model described in [227] for evaluation of the effect of nonhomogeneous protein distribution on extracted parameters was implemented in Mathematica (Wolfram) by Dr. James Lu. Cross-validation was also performed on FRAP recovery curves measured in metaphase according to [226] using Matlab (Mathworks). The above methods are described in detail in the Appendix B).

2.13 Estimation of molecular weight

Molecular weight based on estimated Df were calculated according to [220], using the following equation: $Mw_{protein} = \frac{Mw_{GFP}}{(\frac{Df_{protein}}{Df_{GFP}})^3}$

2.14 Mathematical model of PC interaction with chromatin

A linearized ordinary differential equation system was used to model the interaction of endogenous PC proteins with chromatin in a collaboration with Dr. S. Müller. A full description of the equations and parameters of this model are given in Appendix C and Table A.4. Simulations were performed using MatLab (Mathworks).

3

Results

3.1 Expression of transgenic Polycomb Group proteins fused to GFP does not affect the development of neuroblast and sensory organ precursor cell lineages

3.1.1 Transgenic Polycomb Group proteins fulfill the functions of the endogenous proteins

To investigate the behaviour of the Polycomb Group proteins (PcG) Polyhomeotic (PH), Polycomb (PC), Dorsal switch Protein 1 (DSP1), Pleiohomeotic (PHO) and Enhancer of Zeste (E(Z)) during cell division and differentiation, I studied previously characterised GFP fusions of these proteins [163, 193, 236]. The PH::GFP, GFP::PHO and GFP::E(Z) fusion proteins fully rescue homozygote null alleles of the respective endogenous genes, and thus can replace the endogenous protein [163, 236]. The rescue of GFP::DSP1 was not performed due to the unexpected lethality of the temperature sensitive allele Dsp^1 at the permissive temperature [236]. Nevertheless it was shown that GFP::DSP1 localises correctly in polytene chromosomes [236]. The PC::GFP fusion protein has been reported to rescue homozygous alleles carrying mutations in the PC chromodomain such as Pc^{XL5}, but not homozygous null alleles such as Pc^3, or those that produce C terminally truncated protein [193]. Thus the PC::GFP fusion can partially fulfill the functions of the endogenous protein in a *Pc* homozygote mutant context. The suitability of this fusion protein for live imaging studies has been addressed by several authors, demonstrating that the PC::GFP fusion protein binds chromatin and participates in the PRC1 complex. This is supported by the banding pattern of PC::GFP on polytene chromosomes,

both in intact salivary gland nuclei [163, 193, 236], and in fixed preparations [163, 237]. Further evidence for the correct chromatin binding behaviour of PC::GFP comes from the genome-wide distribution of PC::GFP in embryos and larval disc that coincides substantially with data sets generated by Chromatin ImmunoPrecipitation (ChIP) in tissue culture for endogenous PC [118]. In addition, the timing of mitotic dissociation and reassociation measured by live imaging [193] is identical to the distribution of PC measured for the endogenous PC protein determined by immunofluorescence [189].
Nevertheless, to further characterise the PC::GFP fusion protein, we reexamined its ability to rescue transheterozygote *Pc* mutants. Previous rescue experiments have been performed in homozygote mutant backgrounds [163]. Since chromosomes carrying lethal mutations are maintained as heterozygote stocks over balancer chromosomes, they may accumulate second site mutations that lead to lethality when the chromosome is brought into the homozygote state in the rescue experiment. I did not observe rescue of transheterozygote combinations of null alleles, however this analysis showed that the transheterozygote lethal combination of Pc^{XL5}/Pc^{3} was partially rescued to adulthood by the PC::GFP transgene (Figure 3.1).
Thus, the PC::GFP transgene can rescue lethality in a more severely compromised genetic background than previously shown.

3.1.2 Expression of transgenic Polycomb Group proteins does not affect normal development of neuroblast and sensory organ precursor cell lineage

In the following experiments I examined the behaviour of the GFP fusions of PH, PC, DSP1, PHO and E(Z) in neuroblasts (NB) of 3rd instar larval brains and in sensory organ precursor cells (SOP) of pupae.
PcG expression is essential for neuroblast survival [57, 58] and for normal development of SOPs and sensory organs [60, 61]. I therefore asked whether the expression of an additional transgenic copy of these proteins would adversely affect development in these lineages. PC::GFP was expressed under the control of the ubiquitous PC promoter [193], GFP::PHO, GFP::DSP1 and GFP::E(Z) were expressed from the *tubulin* promoter [236], whereas PH::GFP was expressed conditionally from a UAS transgene [163]. It has been demonstrated that overexpression of PH transgenes leads to cell death and tissue abnormalities [64, 163]. The UAS-GAL4 expression strategy for PH::GFP was intended to circumvent this problem by expressing the transgene during a limited developmental window (see section 2.2). To drive expression of PH::GFP specifically in

the neuroblast and SOP lineages, the *worniu* and *neuralized* GAL4 drivers were used. *worniu* is active in all neuroblasts of the larval brain, but not in neuroblast progeny [238], in addition to expression in the embryonic central nervous system [239]. *neuralized* is expressed in the SOP and its progeny cells [240].
In order to test whether even this limited expression strategy would nevertheless disrupt the lineages of interest, the morphology and number of neuroblasts in larval brains, and the morphology of sensory organs in adult flies, were examined. This analysis was performed for all transgenes. Despite readily visible GFP signals, transgenic animals expressing any of the PcG proteins showed normal larval brain morphology (Figure 3.2 a–c, g–i) and no detectable change in number or morphology of neuroblasts (Figure 3.2 d–f, j–l). Likewise, in adults, no change in the number or morphology of sensory organs was detected in transgenic animals (Figure 3.3). I therefore conclude that the additional transgenic copy of any of the PcG-GFP fusions does not adversely affect the development of the neuroblast and SOP lineages.

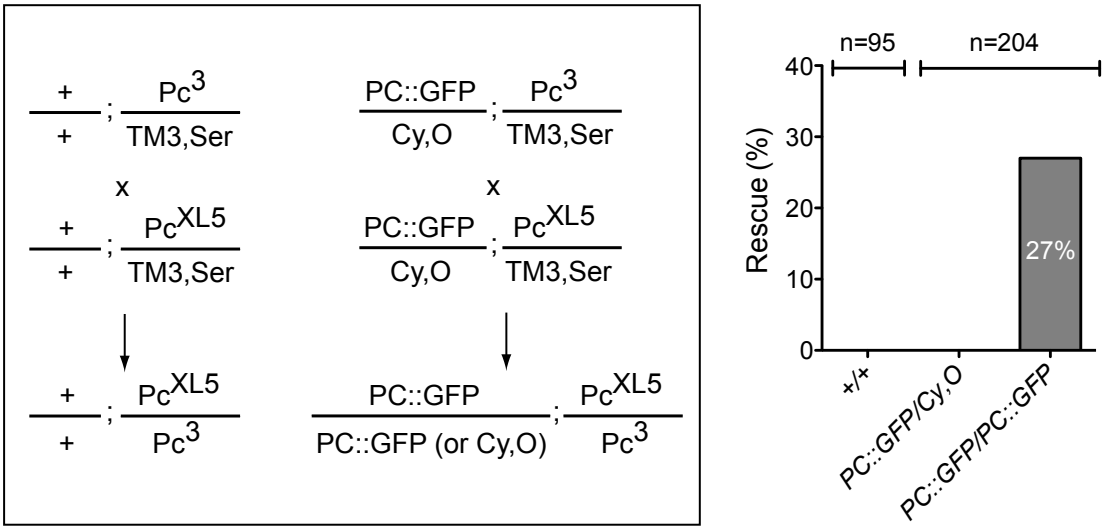

Figure 3.1: Rescue of Pc^{XL5}/Pc^{3} mutants by PC::GFP expression. Progeny of the crosses between +; $Pc^{XL5}/TM3,Sb$ and +; $Pc^{3}/TM3,Sb$, and between $Pc::GFP/CyO$; $Pc^{XL5}/TM3,Sb$ and $Pc::GFP/CyO$; $Pc^{3}/TM3,Sb$, were scored for the number of adult flies for which the third chromosome was Pc^{XL5}/Pc^{3}, and the proportion of these for which the second chromosome was heterozygous for the transgene ($PC::GFP/+$) or homozygous for the transgene ($PC::GFP/PC::GFP$) was calculated. The expected number of flies of each genotype in the event of a full rescue was calculated. % rescue indicates the percentage of this expected number that was represented by flies of that genotype. Above the plot are shown the total number of flies counted in each experiment.

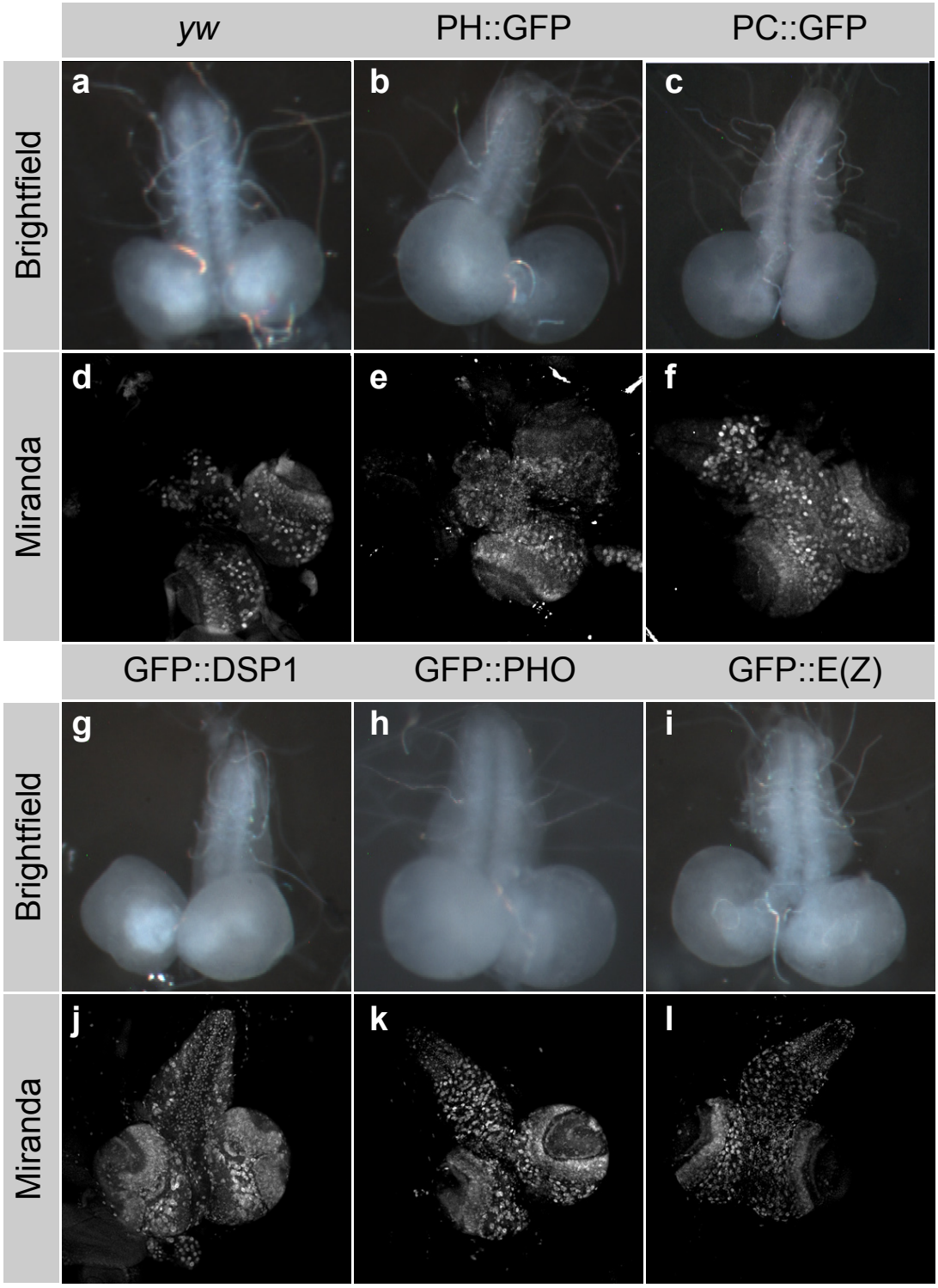

Figure 3.2: Transgenic PcG::GFP do not adversely affect the neuroblast lineage.(a–c and g–i) 3rd instar larval brains showing normal morphology in the presence of either PH::GFP (b), PC::GFP (c), GFP::DSP1 (g), GFP::PHO (h) and GFP::E(Z) (i) in comparison to control *yw* brains (a). (d–f and j–l) 3rd instar larval brains were stained with αMiranda antibody to visualise neuroblasts, showing no detectable change in neuroblast number and localisation in the presence of either transgene.

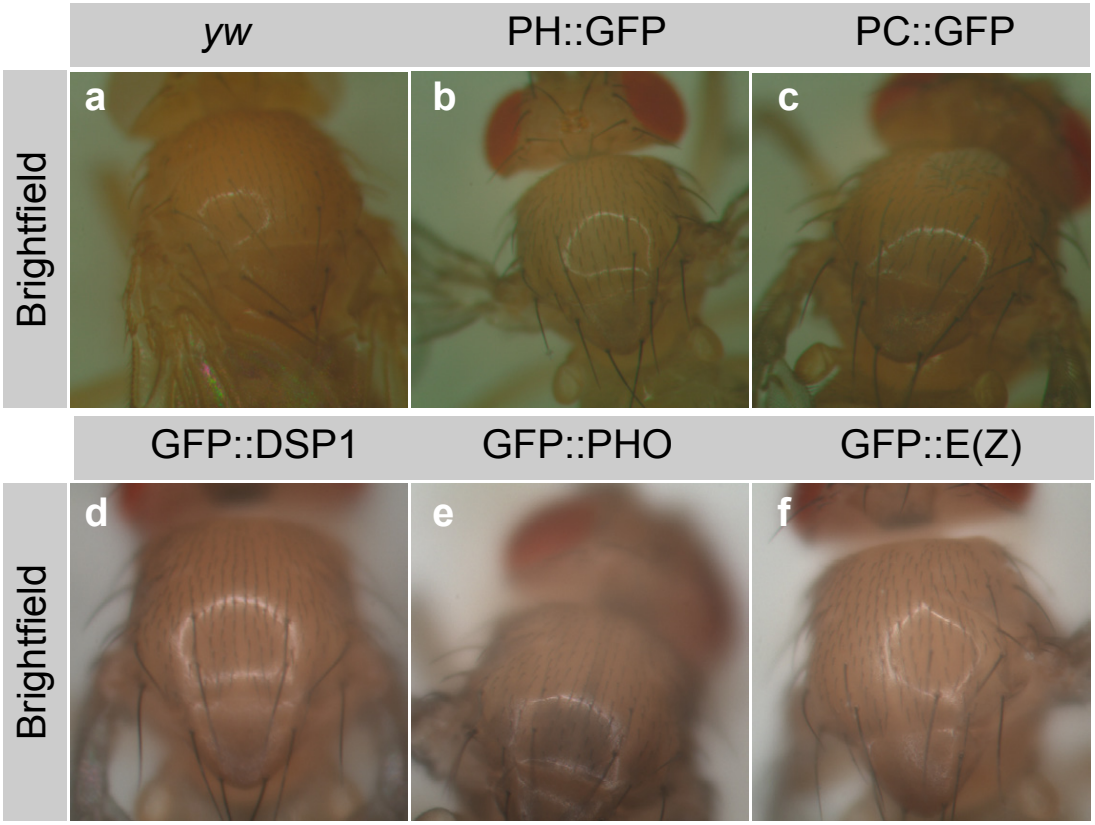

Figure 3.3: Adult nota of yw (a), PH::GFP (b), PC::GFP (c), GFP::DSP1 (d), GFP::PHO (e) and GFP::E(Z) (f) flies are shown, showing no detectable change in sensory organ number and morphology in transgenic flies.

3.1.3 Quantification of expression levels reveals near-endogenous levels for transgenic Polycomb Group proteins

To determine expression levels of transgenes I used quantitative western blotting. Due to the driver inducible neuroblast and SOP specific expression, quantification of PH::GFP required cell type specific extraction of proteins. While this was not possible in SOP, quantification in neuroblasts was performed upon neuroblasts that were isolated by fluorescence activated cell sorting (FACS) from dissociated brains. To evaluate the efficacy of neuroblast sorting, I compared extracts of sorted cells with whole brain tissue extracts, and quantified the expression levels of deadpan, a neuroblast-specific transcription factor [241]. This analysis revealed a 5-7-fold enrichment of deadpan in sorted cells (Figure 3.4), which indicated a high contribution from neuroblasts to extracts from sorted cells. Following this result, I have quantified the expression of PH::GFP in neuroblasts (Figure 3.5a, b).
In order to examine the differences in expression levels of ubiquitously expressed proteins between extracts of sorted neuroblasts and whole brain tissue

extracts, I compared the levels of expression of PC and PC::GFP. Interestingly, the ratios of endogenous and transgenic PC in extracts of sorted neuroblasts and of whole brain tissue were similar (Figure 3.4). This lead me to reason that whole tissue extracts of larval brain western blots would be informative for quantification of ubiquitously expressed PcG-GFP fusions (Figure 3.5 c, f, i, l). Whole pupae extracts were used for quantification of GFP-fusions in SOPs (Figure 3.5 d, g, j, m). Remarkably, all endogenous proteins, with the exception of DSP1 expressed in brains were downregulated in the presence of the transgenes. Similar downregulation of the endogenous proteins in the presence of PH::GFP or PC::GFP transgenes in wing discs and embryos has been reported previously [163]. The highest overexpression levels detected came from PH::GFP with a 4-fold overexpression in neuroblasts (Figure 3.5 b), and by GFP::E(Z) in brains and pupae and PC::GFP in brains with overexpressions of 2-fold. Surprisingly, GFP::DSP1, GFP::PHO and PC::GFP expressed in pupae,

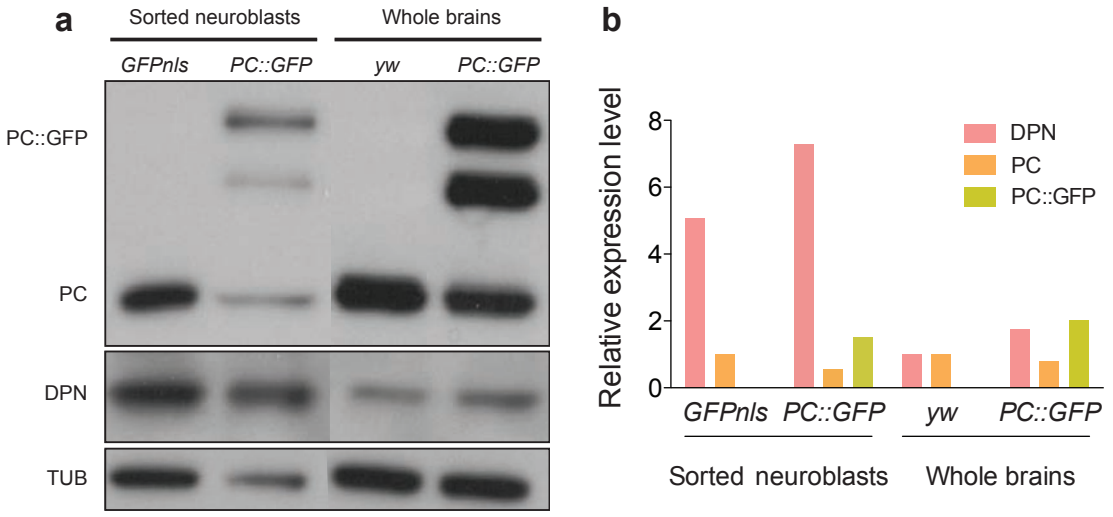

Figure 3.4: Comparison of PC::GFP expression levels between sorted neuroblasts and whole larval brains. (a) Western blots of neuroblast-specific marker, deadpan (DPN) show an enrichment of neuroblasts in the sorted neuroblasts extracts compared to whole brains. Western blots of Polycomb show similar ratios between endogenous (PC) and transgenic (PC::GFP) expression of Polycomb in extracts of sorted neuroblasts and whole brains. (b) Quantification of band intensities. Tubulin (TUB) was used as a loading control and *yw* DPN levels were set to 1, as well as *GFPnls* and *yw* PC levels.

Figure 3.5 *(following page)*: Western blots of PH(a) and PC (c, d), DSP1 (f, g), PHO (i, j) and E(Z) (l, m) used to detect endogenous and GFP-fused proteins in extracts of 3rd instar larval whole brains (c, f, i, l) or sorted neuroblasts (a) and whole pupae (d, g, j, m) of control (*yw* and *GFP*) and transgenic flies. Histone H3 (H3) and tubulin (TUB) were used as loading controls. (b, e, h, k, n) Quantification of western blots in (a, c, d, f, g, i, j, l, m) performed as described in Methods. Data show mean and standard error of at least three independent western blots.

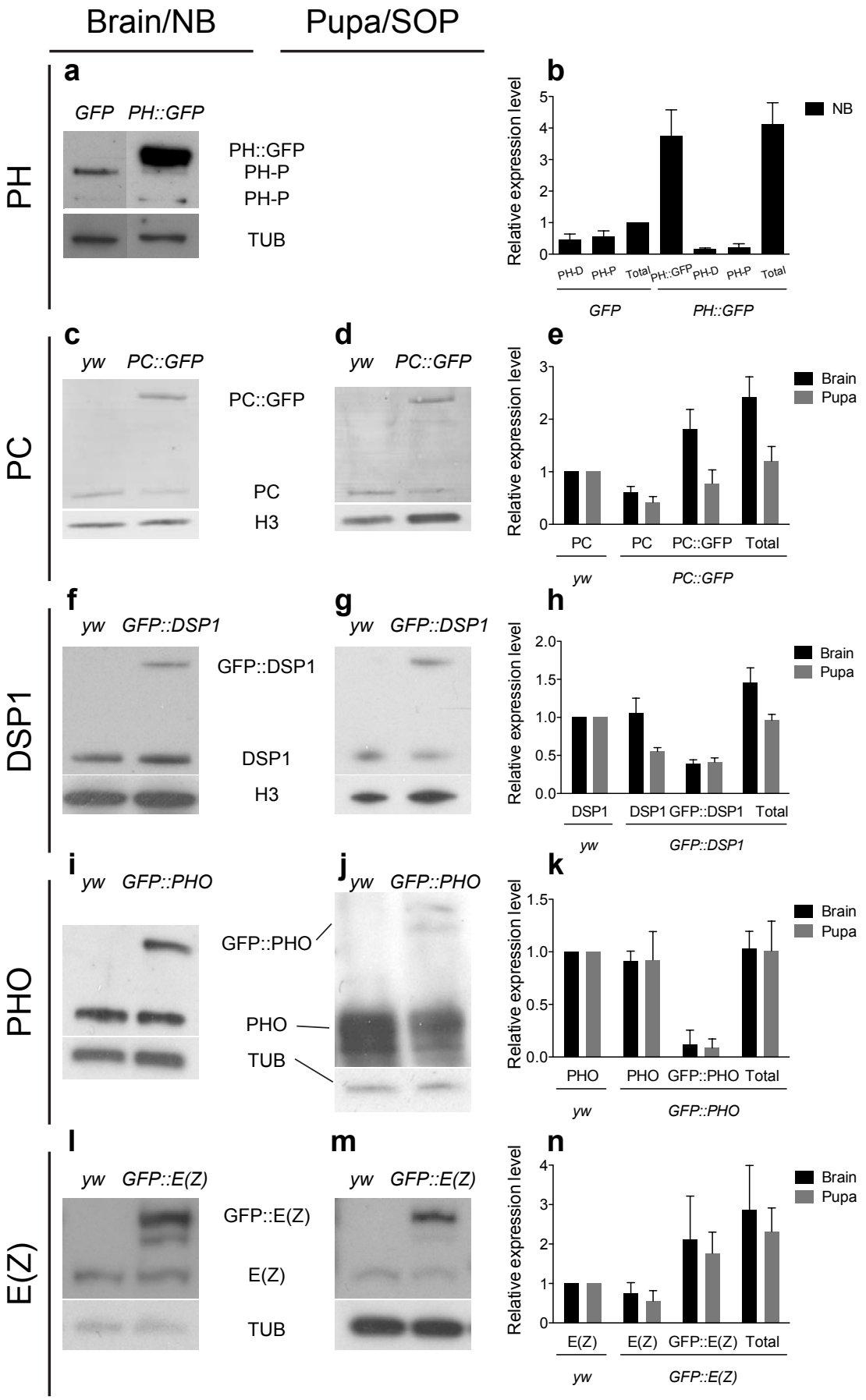
Brain/NB
Pupa/SOP
PH
PC
DSP1
PHO
E(Z)
a
GFP
PH::GFP
PH::GFP
PH-P
PH-P
TUB
b
Relative expression level
NB
PH-D
PH-P
Total
PH::GFP
PH-D
PH-P
Total
GFP
PH::GFP
c
yw
PC::GFP
PC::GFP
PC
H3
d
yw
PC::GFP
e
Relative expression level
Brain
Pupa
PC
PC
PC::GFP
Total
yw
PC::GFP
f
yw
GFP::DSP1
GFP::DSP1
DSP1
H3
g
yw
GFP::DSP1
h
Relative expression level
Brain
Pupa
DSP1
DSP1
GFP::DSP1
Total
yw
GFP::DSP1
i
yw
GFP::PHO
GFP::PHO
PHO
TUB
j
yw
GFP::PHO
k
Relative expression level
Brain
Pupa
PHO
PHO
GFP::PHO
Total
yw
GFP::PHO
l
yw
GFP::E(Z)
GFP::E(Z)
E(Z)
TUB
m
yw
GFP::E(Z)
n
Relative expression level
Brain
Pupa
E(Z)
E(Z)
GFP::E(Z)
Total
yw
GFP::E(Z)

showed a very tight regulation of the total levels of proteins in the transgenic background (endogenous + GFP-fusion) that were comparable to levels in *yw* flies (Figure 3.5 e, h, k).
Thus despite the presence of the additional transgenic copy, in the majority of transgenic lines, the total protein levels are near to endogenous levels. It can be concluded that the PcG transgenes reported in this thesis are useful reporters of endogenous protein behaviour.

3.2 Quantitative live imaging of Polycomb Group proteins in single cells of defined cell lineages reveals transitions in protein concentrations upon entry into mitosis

3.2.1 Live imaging of Polycomb Group proteins in neuroblast and SOP lineage reveals that most, but not all, proteins dissociate from mitotic chromatin

To examine the behaviour of PH::GFP, PC::GFP, GFP::DSP1, GFP::PHO and GFP::E(Z) during mitotic division in neuroblasts and SOPs, I performed live cell imaging on neuroblasts in whole larval brains (Figure 3.6) and on the SOP lineage in the pupal notum (Figure 3.7). Chromatin localisation was identified by the red fluorescently tagged histone H2A::RFP
All proteins localised in the nucleus and were distributed through several foci, in interphase neuroblasts and ganglion mother cells (GMCs) (Figure 3.6 a, i, q,

Figure 3.6 *(following page)*: Live imaging of PcG::GFP in neuroblast lineage. Deconvolved confocal laser scanning images of PH::GFP (a, e), PC::GFP (i, m), GFP::DSP1 (q, u), GFP::PHO (y, ac), GFP::E(Z) (ag, ak) and H2A::RFP (b, f, j, n, r, v, z, ad, ah, al) in neuroblast interphase (a–d, i–l, q–t, y–ab, ag–aj) and metaphase (e–h, m–p, u–x, ac–af, ak–an). Diagrams (left) identify neuroblast (NB) and ganglion mother cells (GMCs) in images. Merge panel (c, g, k, o, s, w, aa, ae, ai, am) shows PH::GFP (c,g), PC::GFP (k,o), GFP::DSP1 (s,w), GFP::PHO (aa, ae) or GFP::E(Z) (ai, am) in green and H2A::RFP in red. Mask panel (d, h, l, p, t, x, ab, af, aj, an) shows volumes occupied by PH::GFP (d,h), PC::GFP (l,p), GFP::DSP1 (t, x), GFP::PHO (ab, af) or GFP::E(Z) (aj, an) in blue and by H2A::RFP in yellow. Neuroblast lineage specific expression of PH::GFP and H2A::RFP was obtained by using a *worniu*-GAL4 driver. For PC::GFP imaging, PC::GFP was expressed under the endogenous *Pc* promoter. For GFP::DSP1, GFP::PHO and GFP::E(Z) imaging, expression was obtained using the *tubulin* promoter. H2A::RFP was expressed from the *ubiquitin* promoter (see section 2.1 for genotypes). Units in images (a–p) are μm and scale bars in images (q–an) represent 2μm.

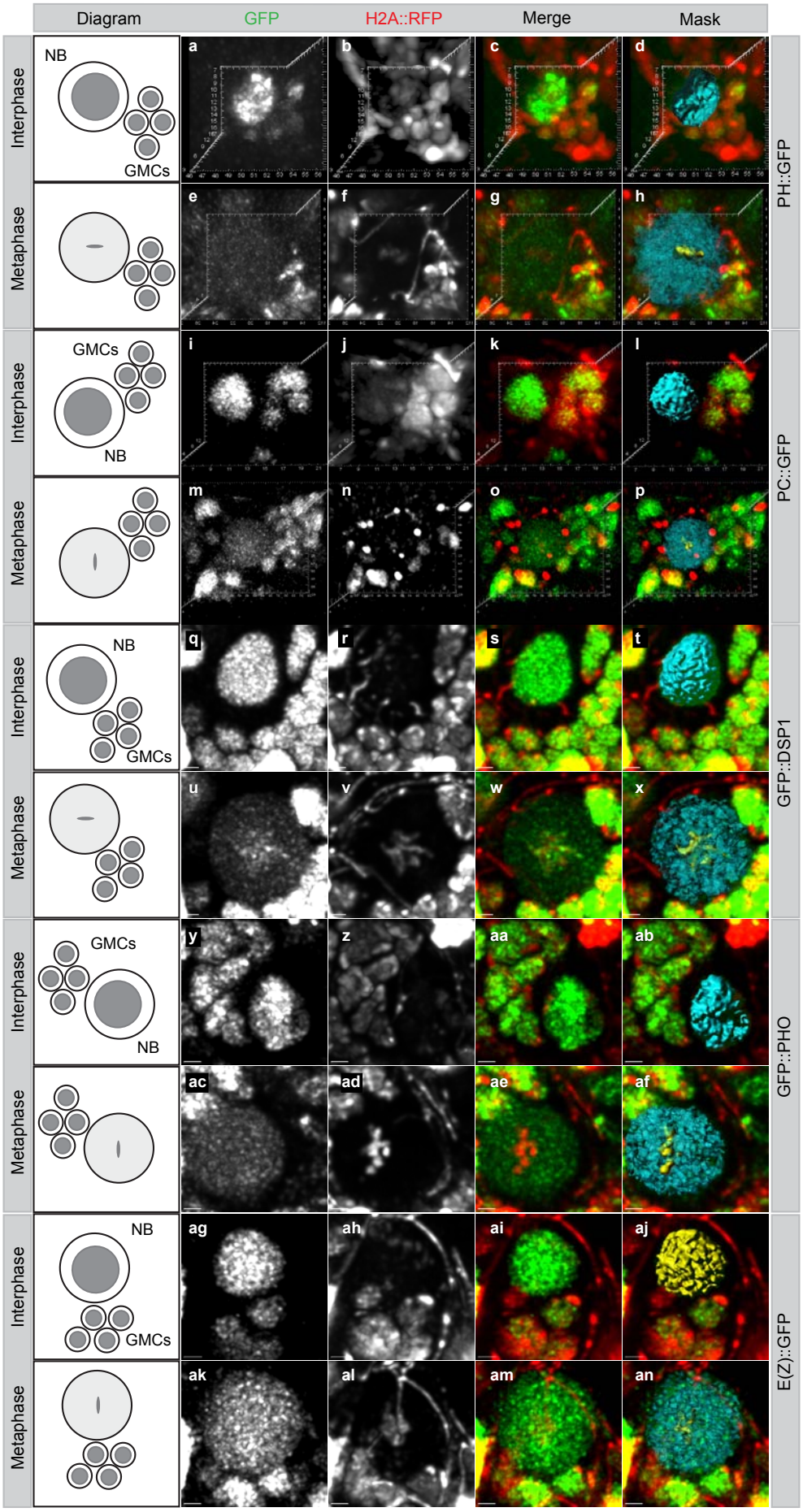
Diagram
GFP
H2A::RFP
Merge
Mask
Interphase
Metaphase
NB
GMCs
PH::GFP
PC::GFP
GFP::DSP1
GFP::PHO
E(Z)::GFP
a
b
c
d
e
f
g
h
i
j
k
l
m
n
o
p
q
r
s
t
u
v
w
x
y
z
aa
ab
ac
ad
ae
af
ag
ah
ai
aj
ak
al
am
an

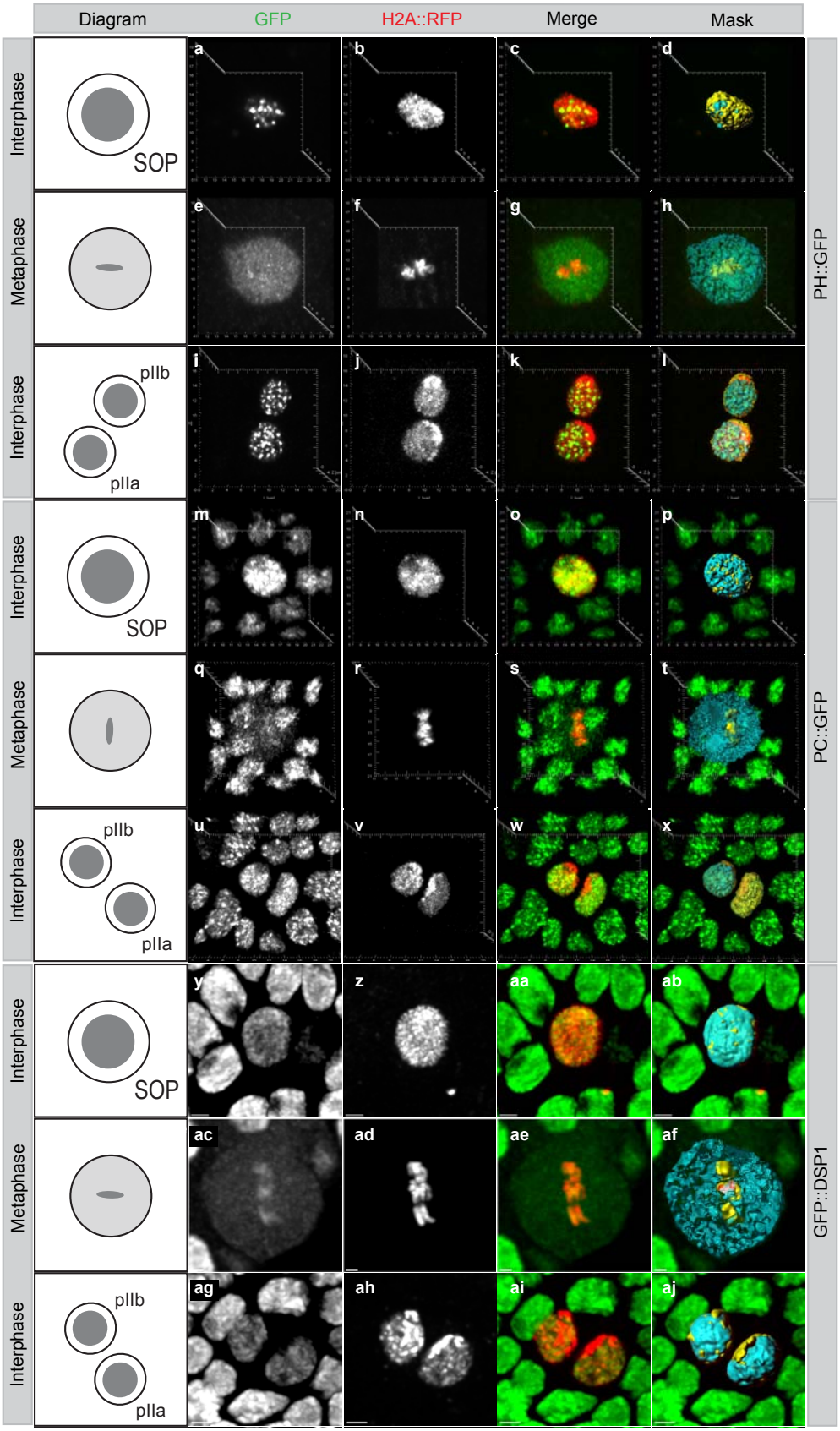
Diagram
GFP
H2A::RFP
Merge
Mask
Interphase
Metaphase
Interphase
PH::GFP
Interphase
Metaphase
Interphase
PC::GFP
Interphase
Metaphase
Interphase
GFP::DSP1
SOP
pIIb
pIIa
a
b
c
d
e
f
g
h
i
j
k
l
m
n
o
p
q
r
s
t
u
v
w
x
y
z
aa
ab
ac
ad
ae
af
ag
ah
ai
aj

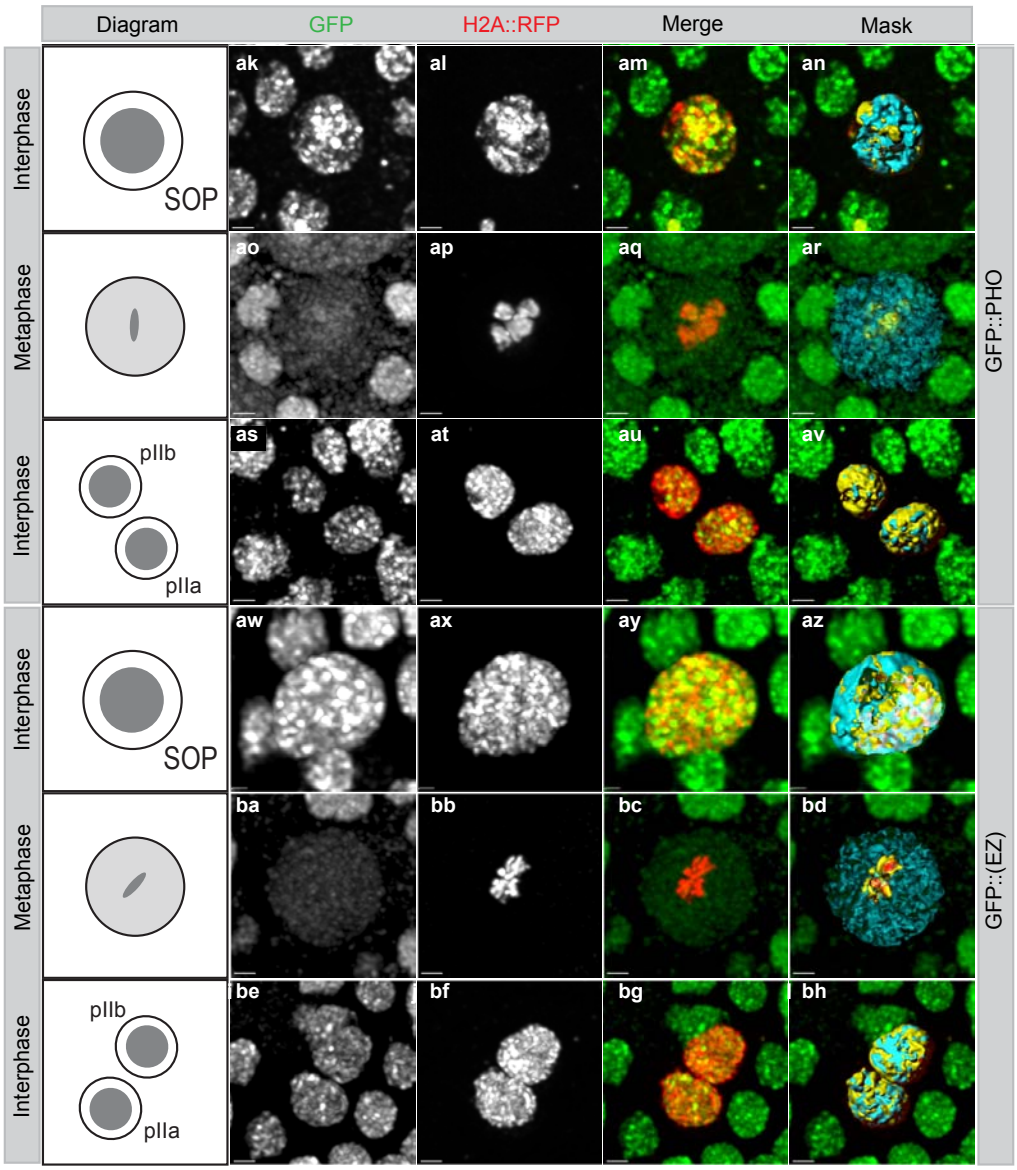

Figure 3.7: Live imaging of PcG::GFP in sensory organ precursor cell lineage. Deconvolved confocal laser scanning images of PH::GFP (a, e, i), PC::GFP (m, q, u), GFP::DSP1 (y, ac, ag), GFP::PHO (ak, ao, as), GFP::E(Z) (aw, ba, be) and H2A::RFP (b, f, j, n, r, v, z, ad, ah, al, ap, at, ax, bb, bf) in sensory organ precursor cell (SOP) interphase (a–d, m–p, y–ab, ak–an, aw–az), metaphase (e–h, q–t, ac–af, ao–ar, ba–bd) and pIIa and pIIb interphase (i–l, u–x, ag–aj, as–av, be–bh). Diagrams (left) identify SOPs and their daughter cells in images . Merge panel (c, g, k, o, s, w, aa, ae, ai, am, aq, au, ay, bc, bg) shows PH::GFP (c, g, k), PC::GFP (o, s, w), GFP::DSP1 (aa, ae, ai), GFP::PHO (am, aq, au) or GFP::E(Z) (ay, bc, bg) in green and H2A::RFP in red. Mask panel (d, h, l, p, t, x, ab, af, aj, an, ar, av, az, bf, bh) shows volume occupied by PH::GFP (d, h, l), PC::GFP (p, t, x), GFP::DSP1 (ab, af, aj), GFP::PHO (an, ar, av) or GFP::E(Z) (az, bf, bh) in blue and by H2A::RFP in yellow. SOP lineage specific expression of PH::GFP and H2A::RFP was obtained by using a *neuralized*-GAL4 driver. For PC::GFP imaging, PC::GFP was expressed under the endogenous *Pc* promoter. GFP::DSP1, GFP::PHO and GFP::E(Z) were expressed from the *tubulin* promoter (see section 2.1 for genotypes). Units in images (a–x) are µm and scale bars represent 2µm (y–ab, ag–av, aw–bh) or 1µm (ac–af, aw–az). Gamma was altered to 2 for better visualization of green channel in images ao–ar and ba–bd.

y, ag), and SOPs and their daughter cells, pIIa and pIIb (Figure 3.7 a, i, m, u, y, ag, ak, as, aw, be). PH::GFP showed the highest heterogeneity in protein distribution (Figure 3.6 a). Upon entry into mitosis, visible by chromatin compaction in the metaphase plate of both neuroblasts (Figure 3.6 f, n, v, ad, al) and SOPs (Figure 3.7 f, r, ad, ap, bb), most proteins dissociated from mitotic chromatin, as no clear visible enrichment was noted (Figure 3.6, e, m, ac, ak and Figure 3.7 e, q, ba). However, for GFP::DSP1 in neuroblasts and SOPs (Figure 3.6 w and Figure 3.7 ae) and for PC::GFP and GFP::PHO in SOPs (Figure 3.7 s, aq), a significant enrichment was visible on mitotic chromatin. An image-based quantification of mitotic binding of all transgenic proteins is shown in Table A.3.
Thus, I conclude that while most PcG proteins dissociate, if not completely, to a great extent from mitotic chromatin, the DNA-binding proteins DSP1 and PHO show a more robust association with chromatin during mitosis

3.2.2 Virus-like-particle GFP quantification provides a readout of the number of proteins in live *Drosophila* tissues

In order to quantify the number of GFP-fused molecules in single neuroblast, SOP, pIIa, and pIIb cells, I set out to calibrate live GFP numbers with GFP-virus-like-particles (GFP-VLP). GFP-VLPs are rotavirus-like-particles in which the capsid protein VP2, present 120 times, is fused to GFP [215]. This allows for the visualization of individual VLPs in confocal microscopy. While this technique has been reported to be useful in quantification of small punctate structures as the RPA40 subunit of RNA polymerase I [216] and nuclear pore

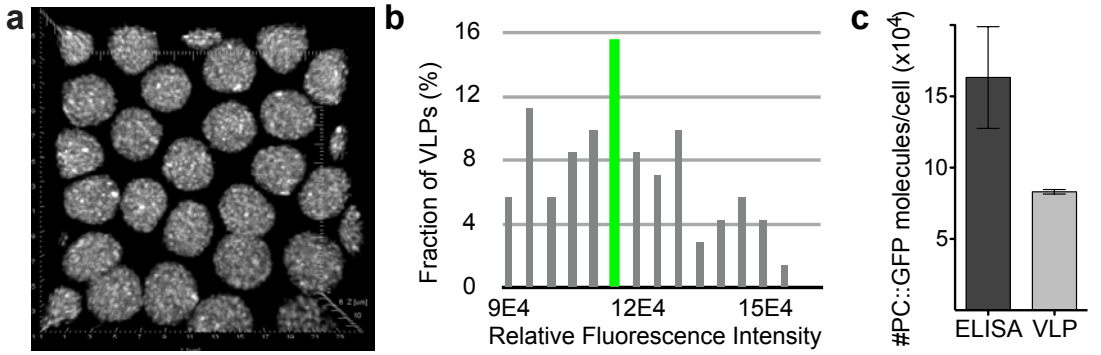

Figure 3.8: Blastoderm embryos (2-3h) expressing PC::GFP (a) were used to compare the number of estimated PC::GFP molecules per nucleus, using GFP detection by ELISA (Cell Biolabs, San Diego) in embryo extracts, or by GFP- VLP calibration in live embryos. GFP intensity distribution of GFP-VLPs was plotted and the mode of the distribution was chosen as the brightness of 120 GFP molecules (b). Data show mean and 95% confidence intervals of 10 cells for GFP-VLP measurements and 10 independent ELISA assays (c). ELISA was performed by P. Steffen.

complex components [217], it has not been reported for the quantification of nuclear-wide distributed proteins.
To evaluate the accuracy of GFP-VLP calibration, we compared this technique to GFP ELISA by applying both quantification methods to blastoderm embryos of PC::GFP expressing flies. (ELISA performed by P. Steffen; Figure 3.8 a). This analysis showed approximately 2-fold difference between the ELISA and VLP measurements (Figure 3.8 c), probably due to diffraction of GFP signal caused by the thickness of the embryo.
In conclusion, live GFP quantification by GFP-VLP calibration gives a meaningful readout of protein numbers for single cell experiments.

3.2.3 Quantification of GFP and endogenous levels of Polycomb Group proteins reveals similar interphase concentrations in different lineages

To quantify GFP signal intensities, a 3D mask of the volume occupied by the GFP fusion protein in the cell of interest was applied, and signal intensities were measured (Figure 3.6 d, h, i, p, t, x, ab, af, aj, an and Figure 3.7 d, h, i, p, t, x, ab, af, aj, an, ar, av, az, bd, bh). In order to convert signal intensities to absolute numbers of GFP fusion proteins in single cells we performed calibration using GFP-VLP [216, 217]. By performing live GFP quantification and GFP-VLP calibration for all PcG-GFP fusion proteins in each cell lineage at interphase and metaphase (Figure 3.6 and Figure 3.7) I calculated the number of GFP fusion protein molecules in each cell type (Table A.1).
Since the ratio of endogenous protein to transgenic protein had previously been determined for all GFP-fusions (Figure 3.5), the estimated number of endogenous proteins in *yw* flies could be determined (Figure 3.9 b, Table A.1). This quantification revealed that the calculated number of endogenous proteins did

Figure 3.9 *(following page)*: (a) Estimated number per cell of PH::GFP, PC::GFP, GFP::DSP1, GFP::PHO and GFP::E(Z) by GFP-VLP calibration in neuroblast interphase (NB int.) and metaphase (NB met.) and SOP interphase (SOP int.), metaphase (SOP met.) and interphase of pIIa (pIIa int.) and pIIb (pIIb int.). (b) Estimated number per cell of PH, PC, DSP1,PHO and E(Z) in neuroblast interphase (NB int.) and metaphase (NB met.) and SOP interphase (SOP int.), metaphase (SOP met.) and interphase of pIIa (pIIa int.) and pIIb (pIIb int.) of *yw* or *GFP* flies (PH). (c) Measured cell volumes of different cells in NB and SOP lineage. (d) Estimated micromolar concentrations of PH::GFP, PC::GFP, GFP::DSP1, GFP::PHO and GFP::E(Z) by GFP-VLP calibration in neuroblast interphase (NB int.) and metaphase (NB met.) and SOP interphase (SOP int.), metaphase (SOP met.) and interphase of pIIa (pIIa int.) and pIIb (pIIb int.) of *yw* or *GFP* flies (PH). Data show mean and SEM of at least 3 cells.

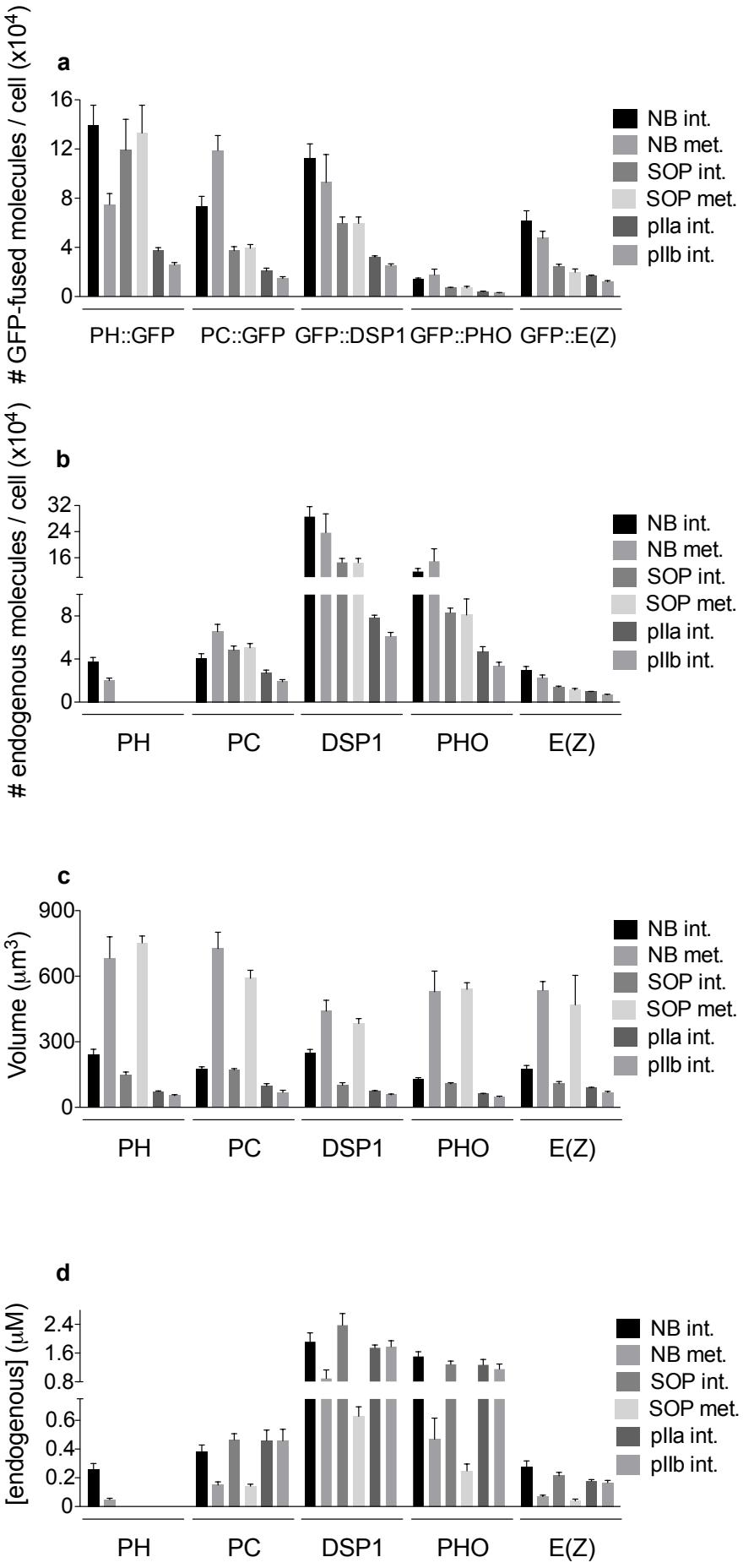
a
GFP-fused molecules / cell (x10^4)
16
12
8
4
0
PH::GFP
PC::GFP
GFP::DSP1
GFP::PHO
GFP::E(Z)
NB int.
NB met.
SOP int.
SOP met.
pIIa int.
pIIb int.
b
endogenous molecules / cell (x10^4)
32
24
16
8
4
0
PH
PC
DSP1
PHO
E(Z)
c
Volume (µm^3)
900
600
300
0
d
[endogenous] (µM)
2.4
1.6
0.8
0.6
0.4
0.2
0

not change greatly upon the transitions from interphase to metaphase of both neuroblasts and SOPs. Remarkably, the DNA-binding proteins DSP1 and PHO are present in higher numbers than the analyzed PRC1 and PRC2 components, PH, PC and E(Z), with numbers that range 3- to 9-fold in neuroblasts and 2- to 10-fold in SOPs. Furthermore, the PH, PC and (EZ) number of molecules were very similar (30000-40000) in neuroblasts and unlike all the other studied proteins, PC did not show a reduction in levels when comparing SOPs to NBs. Moreover, the calculated numbers of all endogenous proteins were reduced $\sim$2-fold upon the differentiation of SOPs into pIIa and pIIb.
Conversion to micromolar concentrations via the measured volume occupied by GFP (Figure 3.9 c) in each cell type revealed that all proteins undergo a substantial dilution (between 2 and 5-fold, Figure 3.9 d, Table A.1) upon the interphase to metaphase transition in both cell lineages due to the increase in volume upon nuclear envelope breakdown. Remarkably, besides the different numbers of molecules estimated in neuroblasts, SOPs, pIIa and pIIb cells, and due to the different nuclear volumes of these four different cell types, the calculated micromolar concentrations of PC, DSP1, PHO and E(Z) did not change considerably between lineages (Figure 3.9 d). These concentrations were approximately 0.4µM for PC, 2µM for DSP1, 1.3µM for PHO and 0.2µM for E(Z) (Table A.1).
In summary, this quantitative analysis of single defined cell lineages reveals substantial dilution of PcG proteins upon entry into mitosis, but a remarkably similar endogenous concentration at interphase in both lineages.

3.3 Fluorescence Recovery After Photobleaching analysis of Polycomb Group proteins in neuroblasts and sensory organ precursor cell lineages

3.3.1 A diffusion component is present in FRAP curves of all analysed proteins

To ask whether different PcG proteins interact differently with chromatin, and whether different cell lineages and cell cycle stages are distinguished by different chromatin binding properties of any of the proteins, Fluorescence Recovery After Photobleaching (FRAP) on all GFP fusion proteins was performed in each cell type at interphase and metaphase(Figure 3.10). Histone H2A::RFP, used to mark chromatin in both lineages (Figure 3.6 and Figure 3.7), served as a guide for bleach spot placement on metaphase chromatin.The rational behind

this approach is that FRAP is one of the few techniques that allow the *in vivo* measurement of diffusion and binding properties of proteins, therefore taking into account the influence of the cell environment on those properties, which is not possible with *in vitro* approaches [220].

Most FRAP experiments are analyzed by models that do not include a diffusion coefficient for the free protein. However it has been shown that wrongly ignoring this component can introduce large errors in the estimation of binding parameters [226, 227]. To test if diffusion influences the FRAP recovery curves of the studied PcG-GFP fusion proteins, I performed a curve smoothing test on the recovery curves of all GFP-fusion proteins in interphase, as well as the controls GFPnls (diffusing protein with no binding component in recovery curves)

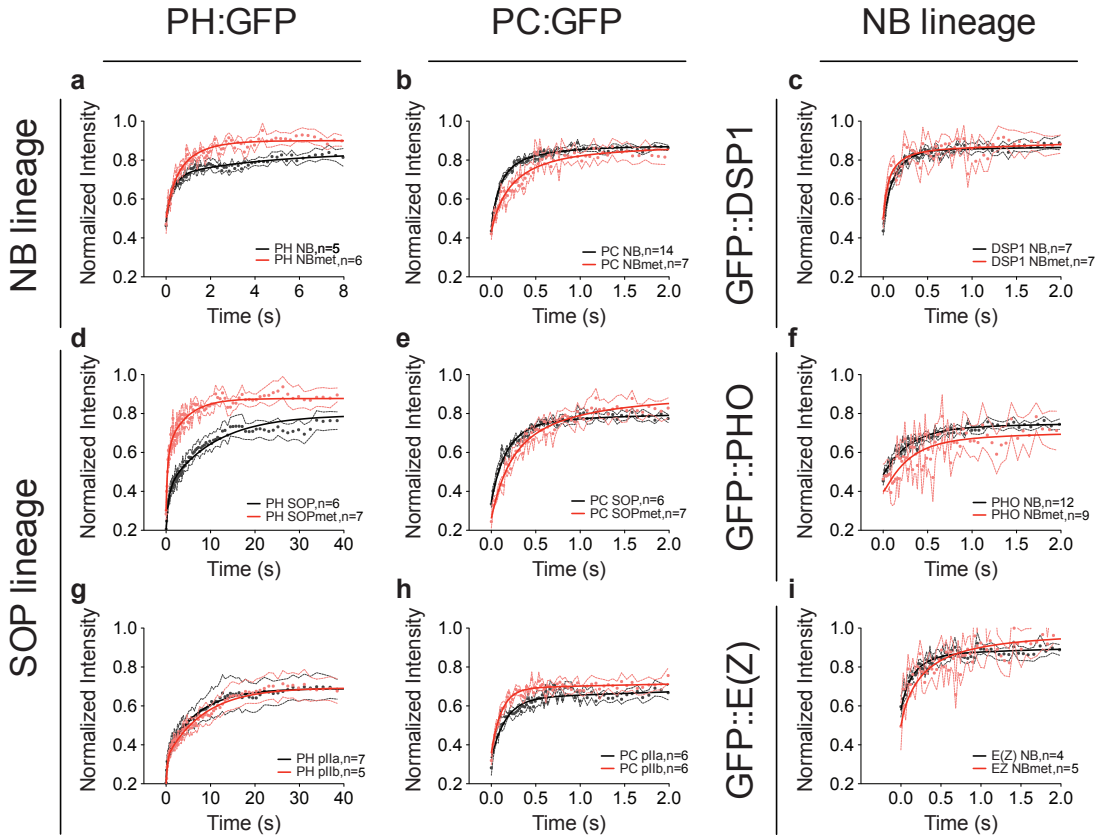

Figure 3.10: FRAP analysis of PH::GFP (a, d, g), PC::GFP (b, e, h), GFP::DSP1 (c), GFP::PHO (f) and GFP::E(Z) (i) in neuroblast (NB) (a–c, f, i) and sensory organ precursor cell (SOP) (d, e, g, h) lineages. Interphase bleach spots were placed to cover several PcG::GFP foci (see Figure 3.6 and Figure 3.7). Metaphase bleach spots were placed in the region of RFP signal (see Figure 3.6 and Figure 3.7). Symbols represent mean of experimental values and are accompanied by standard error of the mean represented by a dashed line of the same colour. Solid darker line shows fit of FRAP model to the experimental data (see section 2.12). NB and SOP (black on a–f, i) indicate neuroblast and SOP interphase; NBmet and SOPmet (red on a–f, i), indicate neuroblast and SOP metaphase. pIIa (black on b, h) and pIIb (red on b, h) indicate the interphase of the respective SOP daughter cells.

and H2A::RFP (slow exchanging protein with negligible diffusion component in recovery curves) (Figure 3.11) [227]. All GFP-fusion proteins showed a significant smoothing of the FRAP curves with time with the exception of H2A::RFP, leading to the conclusion that FRAP curves in Figure 3.10 showed contributions of diffusion.

The recovery data were analysed by fitting kinetic models ([220, 228, 242]). Comparison of different fitting procedures showed contributions of both diffusion and binding to the recovery kinetics (see Materials and Methods) of all proteins with the exception of GFP::E(Z) in neuroblast metaphase, were only diffusion was identified. Thus the reaction-diffusion model of [228] was used for all data sets of PH::GFP (Figure 3.10 a, d, g), PC::GFP(Figure 3.10 b, e, h), GFP::DSP1 (Figure 3.10 c), GFP::PHO (Figure 3.10 f), and GFP::E(Z) in neuroblast interphase (Figure 3.10 i), while a pure-diffusion model [228] was chosen for GFP::E(Z) in neuroblast metaphase, enabling values to be extracted for the pseudo first order association rate (k^*_{on}) and the dissociation rate (k_{off}) (Figure 3.12), as well as the diffusion coefficient (D_f(1), Figure 3.13 a). Extracted parameters are listed in Table A.2 and are further discussed in subsection 3.3.4 to subsection 3.3.6.

Figure 3.11 *(following page)*: Diffusion influences FRAP curves of GFPnls, PC::GFP, PH::GFP, GFP::DSP1, GFP::PHO, GFP::E(Z) and H2A::RFP. (a) Diffusion test was performed using an adaptation of the method of curve smoothing ([227]), where gaussian photobleaching profiles of FRAP experiments ([228]) were acquired at four different time points after photobleaching and the slope region was fitted using linear regression. A reduction in these slopes signifies diffusion-dependence in the FRAP curves. (b–j) Slope regions of intensity profiles are plotted (symbols) and were fitted using linear regression (solid lines) at four different time points (time in seconds is shown at the right of each plot). The grey background identifies the bleach region. (b) H2A::RFP recovery is not affected by diffusion, indicated by similar slopes of lines at all four time points. Comparison of the extracted slopes was performed using ANCOVA (p-value given on each plot represents significance of difference between slopes at the four time points). (c-j) GFP-nls, PC::GFP and PH::GFP, GFP::DSP1, GFP::PHO and GFP::E(Z) FRAP recovery shows an influence of diffusion, indicated by gradual flattening of radial profiles at later time points. (e) Comparative summary plot. For data in (b-j), the value 1/slope was calculated for each linear fit and normalised to the slope at time 0. These values are plotted for each data set for consecutive time points, showing a gradual increase in (1/slope) at later time points for all experiments with the exception of H2A::RFP (dark green) for which little change was detected.

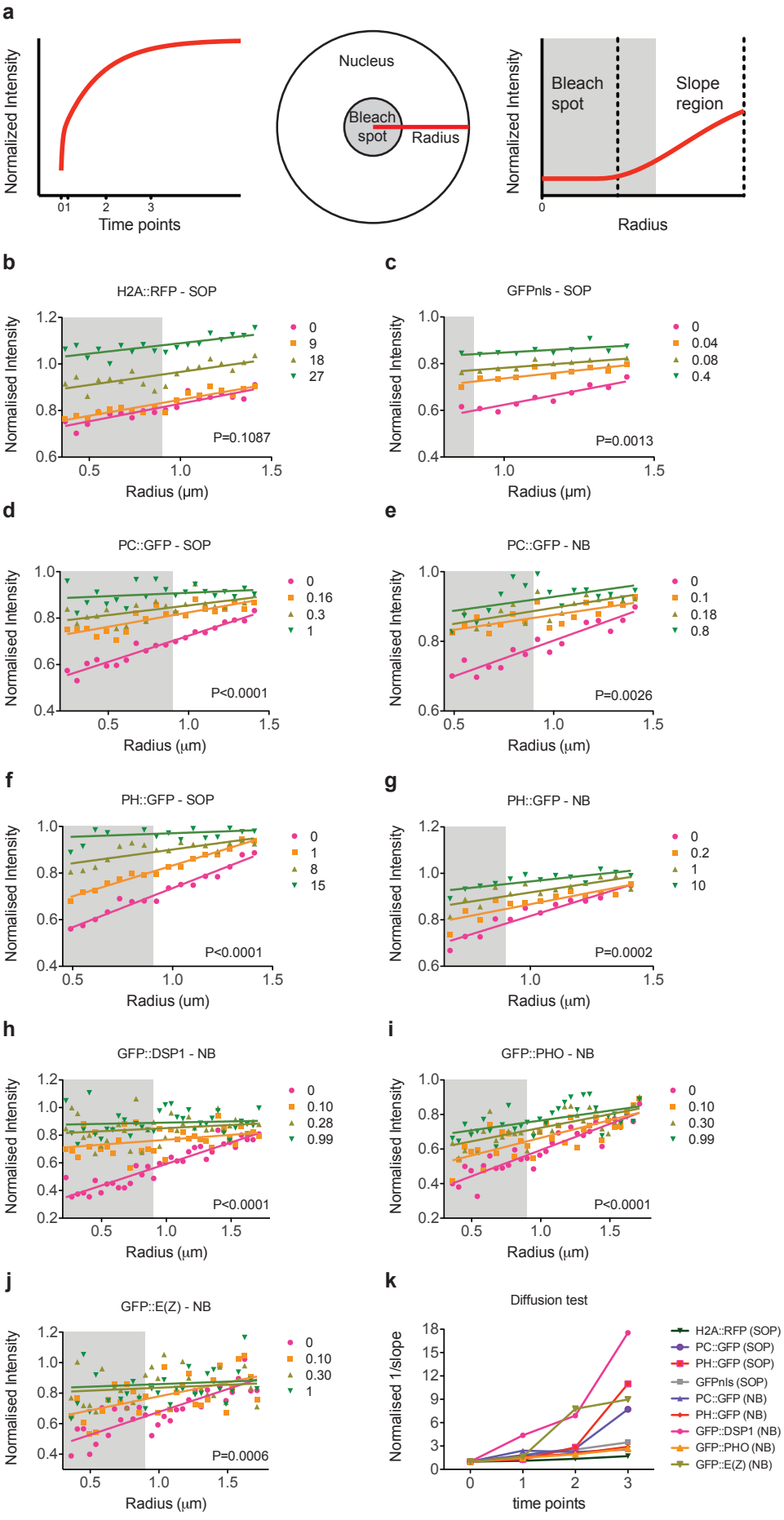
a
Normalized Intensity
Time points
Nucleus
Bleach spot
Radius
Bleach spot
Slope region
Radius
b
H2A::RFP - SOP
P=0.1087
c
GFPnls - SOP
P=0.0013
d
PC::GFP - SOP
P<0.0001
e
PC::GFP - NB
P=0.0026
f
PH::GFP - SOP
P<0.0001
g
PH::GFP - NB
P=0.0002
h
GFP::DSP1 - NB
P<0.0001
i
GFP::PHO - NB
P<0.0001
j
GFP::E(Z) - NB
P=0.0006
Normalised Intensity
Radius (µm)
k
Diffusion test
Normalised 1/slope
time points
H2A::RFP (SOP)
PC::GFP (SOP)
PH::GFP (SOP)
GFPnls (SOP)
PC::GFP (NB)
PH::GFP (NB)
GFP::DSP1 (NB)
GFP::PHO (NB)
GFP::E(Z) (NB)

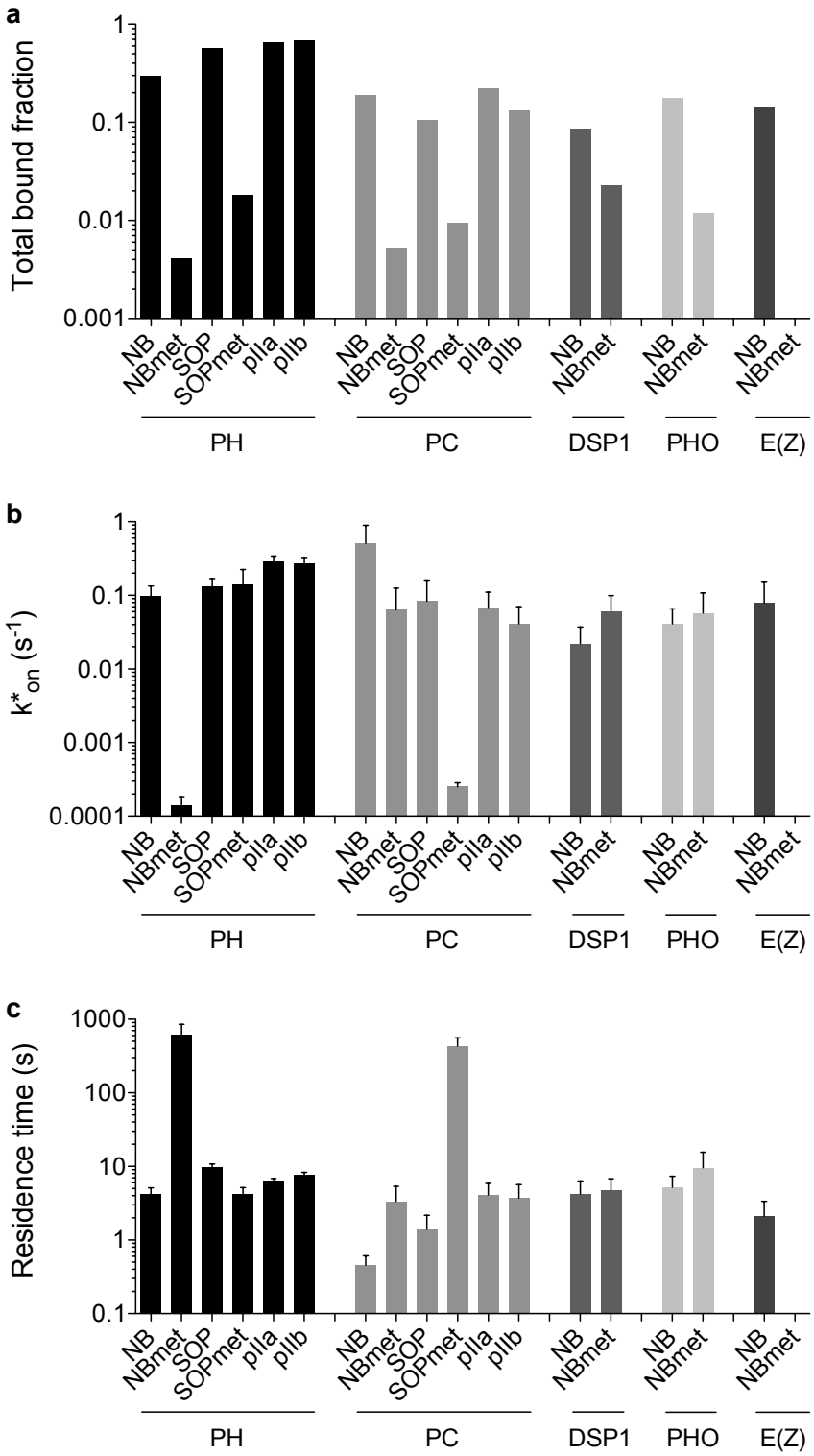

Figure 3.12: Extracted total bound fraction (a), pseudo first order association rate $k*_{on}$ (b) and Residence time (c) of PH::GFP and PC::GFP in NB and SOP lineage and of GFP::DSP1, GFP::PHO and GFP::E(Z) in NB lineage from FRAP model fit (Figure 3.10). Fraction bound in chromatin region was calculated as $(k^*_{on}/k_{off} + k^*_{on})$. For metaphase measurements, the fraction bound in chromatin region was used in combination with the quantity of free protein outside the chromatin volume, to calculate fraction of total protein bound, shown on plots (See also section 2.12, Table A.2). Residence time was calculated as $(1/k_{off})$. Error bars show 95% confidence intervals.

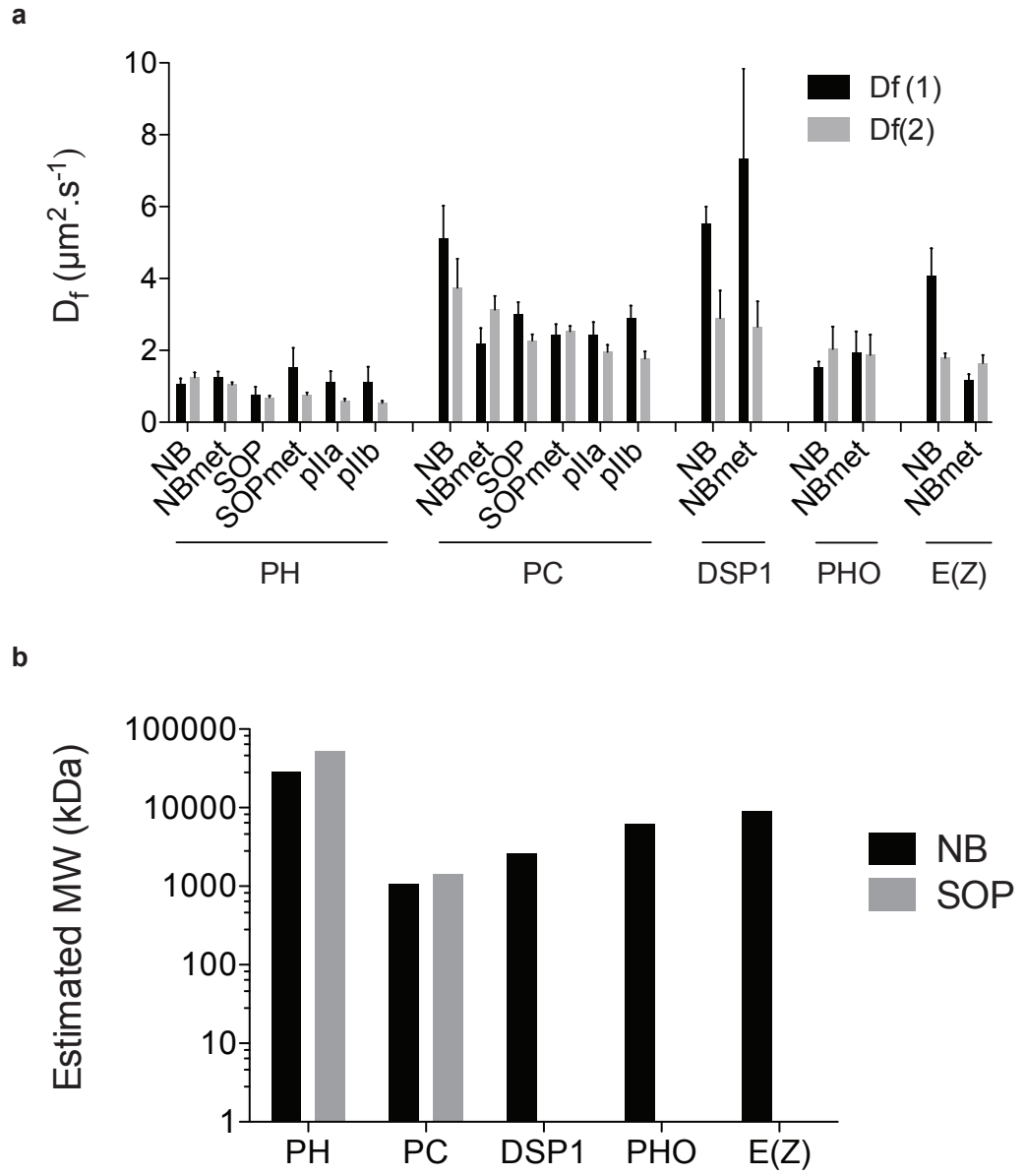

Figure 3.13: Cross validation of extracted diffusion constants by independent measurements. (a) Comparison of diffusion constants extracted from fitting 3 parameter FRAP model in all cell types (D_f(1), black) [228] to diffusion constants calculated by fitting single parameter FRAP model (diffusion only) to FRAP recovery performed on the non-chromatin volume in metaphase D_f(2), grey) [228]. For GFP::E(Z) in neuroblast metaphase (NBmet), (D_f(1) was obtained from a diffusion only FRAP model. The interphase D_f values (grey) were calculated using GFPnls for calibration as described in section 2.12. The D_f values calculated by the two procedures show good agreement. NB and SOP indicate neuroblast and SOP interphase and NBmet and SOPmet indicate neuroblast and SOP metaphase. pIIa and pIIb indicate the interphase of the respective cells. Data show mean of at least four measurements for each cell type. Error bars represent 95% confidence intervals. (b) Estimated molecular weight of PH::GFP and PC::GFP, GFP::DSP1, GFP::PHO, GFP::E(Z) in neuroblasts (black) and SOPs (grey). Estimations were based on the extracted D_f in regions outside chromatin at metaphase in neuroblasts and SOPs and calculated as described in section 2.13 [220]

.

3.3.2 Extracted diffusion constants from FRAP curves are in agreement with independent measurements

To evaluate the robustness of the extracted values for D_f from fitting the reaction-diffusion model, the D_f for each protein in each cell type was measured independently (Figure 3.13 a). This was achieved by performing FRAP on the region of the metaphase cell that is outside chromatin and fitting the pure diffusion model [228] to the recovery data, giving an independent and direct measure of D_f. Interphase values were calculated by conversion via diffusion coefficients measured for GFP by fitting the pure diffusion model to FRAP recovery curves measured in both interphase and metaphase Table A.2. The values of D_f thus measured ($D_f(2)$) agreed with those extracted from fitting the full model ($D_f(1)$), with the exception of GFP::DSP1, where $D_f(1)$ was consistently higher than $D_f(2)$ (Figure 3.13, Table A.2).
Moreover, the molecular weights of the PcG-GFP fusion proteins could be estimated from $D_f(2)$. The molecular weight estimated for PC::GFP is consistent with the predicted size of the PRC1 complex (over 600kDa [6, 8]) (Figure 3.13 b). In contrast, the molecular weights estimated for all other proteins is higher than any single protein, or known Polycomb protein complex, with PH::GFP reaching an approximately estimated weight of 15MDa (Figure 3.13 b). These high molecular weights that originate from slow diffusion coefficients are probably due to the incorporation of binding information into the diffusion coefficient which slows down the true diffusion coefficient of the protein [220]. Thus, the diffusion constants extracted for PH::GFP, GFP::DSP1, GFP::PHO and GFP::E(Z) are named effective diffusion constants [220].
Taken together, these results show that extracted diffusion constants of PcG::GFP proteins agree with an independent approach and that the extracted diffusion constant for PH::GFP, GFP::DSP1, GFP::PHO and GFP::E(Z) may comprise both the true diffusion and a binding component [220, 228].

3.3.3 Non-homogeneity of binding sites does not have a major impact on parameters extracted from FRAP curves

In order to further assess the robustness of the extracted k^*_{on} and k_{off} values (Figure 3.12), I simulated FRAP recovery curves of the reaction-diffusion model [228], where D_f was fixed and the binding rates varied in between 5 orders of magnitude (Figure 3.14). This analysis showed that for most data sets, a limited range of k^*_{on} and k_{off} values gave optimal fits to the data.
Furthermore, we examined the the effect of non-homogeneity in protein dis-

tribution observed in interphase (see Figure 3.6 and Figure 3.7). To test this effect, we adapted the model described in [227] from its original application to redistribution of photoactivatable GFP, to render it applicable to the analysis of FRAP recovery curves described here (performed in a collaboration with J. Lu). Fitting this model to interphase data for individual nuclei gave similar values for the three extracted parameters whether initial distribution was assumed to be heterogeneous or homogeneous (Figure 3.15).

3.3.4 Polycomb shows more dynamic interactions with neuroblast interphase chromatin than other PcG proteins

In order to ask if different PcG proteins interact differently with chromatin I compared the recovery kinetics and measured parameters for all GFP-fusion proteins in neuroblasts. This analysis showed that PH::GFP and PHO::GFP typically showed far slower recoveries than all the other PcG proteins (Figure 3.10). This was due in part to the slower D_f extracted for these proteins (with values that ranged from 1 to 1.5$\mu m^2.s^{-1}$) when compared to values encountered for the other proteins (from 4 to 5.5$\mu m^2.s^{-1}$, Figure 3.13). Further differences were encountered upon comparison of the bound fractions and kinetic rate constants. PH::GFP had the highest extracted bound fraction of all PcG proteins ($\sim$30%, Figure 3.12 a). However, when the estimated numbers of endogenous molecules were taken into account, it was the DNA binding proteins DSP1 and PHO that had the higher number of bound molecules ($\sim$20000 molecules) followed by the PRC1 components, PH and PC (7000 to 11000 bound molecules) and finally PRC2 component E(Z) ($\sim$4000 bound molecules, Table A.2). Moreover, the comparison of residence times, which reflect an inherent, concentration independent property of protein-chromatin binding, revealed 2-fold shorter residence times for PC::GFP when compared to GFP::E(Z), and a remarkable $\sim$10-fold difference when compared to PH::GFP, GFP::DSP1

Figure 3.14 *(following page)*: Parameter space for best fits of FRAP model to recovery data. (a, b, d, e, g, h, j, k, m, n, p–t, v, w) For each FRAP recovery data set fit with a reaction-diffusion model (Figure 3.10), simulations were performed in which D_f was fixed to the value extracted from the 3 parameter fit (Figure 3.13, grey bars; Table A.2), and k^*_{on} and k_{off} were varied between 10^{-4} and 10. For each simulation, the fit to the experimental data was evaluated as squared sum of residuals (ssrs). Ssrs for each data set are plotted as heat maps (colour scale for ssrs is shown at the bottom right of the figure.) The white or black line delineates ssrs 1.25 times larger than the minimum ssr found. (c, f, i, l, o, u) Comparison of parameter space for best fits of PH::GFP (c), PC::GFP (f), GFP::DSP1(i) and GFP::PHO(l) in neuroblast lineage (NB) and of PH::GFP (o) and PC::GFP (u) in sensory organ precursor cell (SOP) lineage (f).

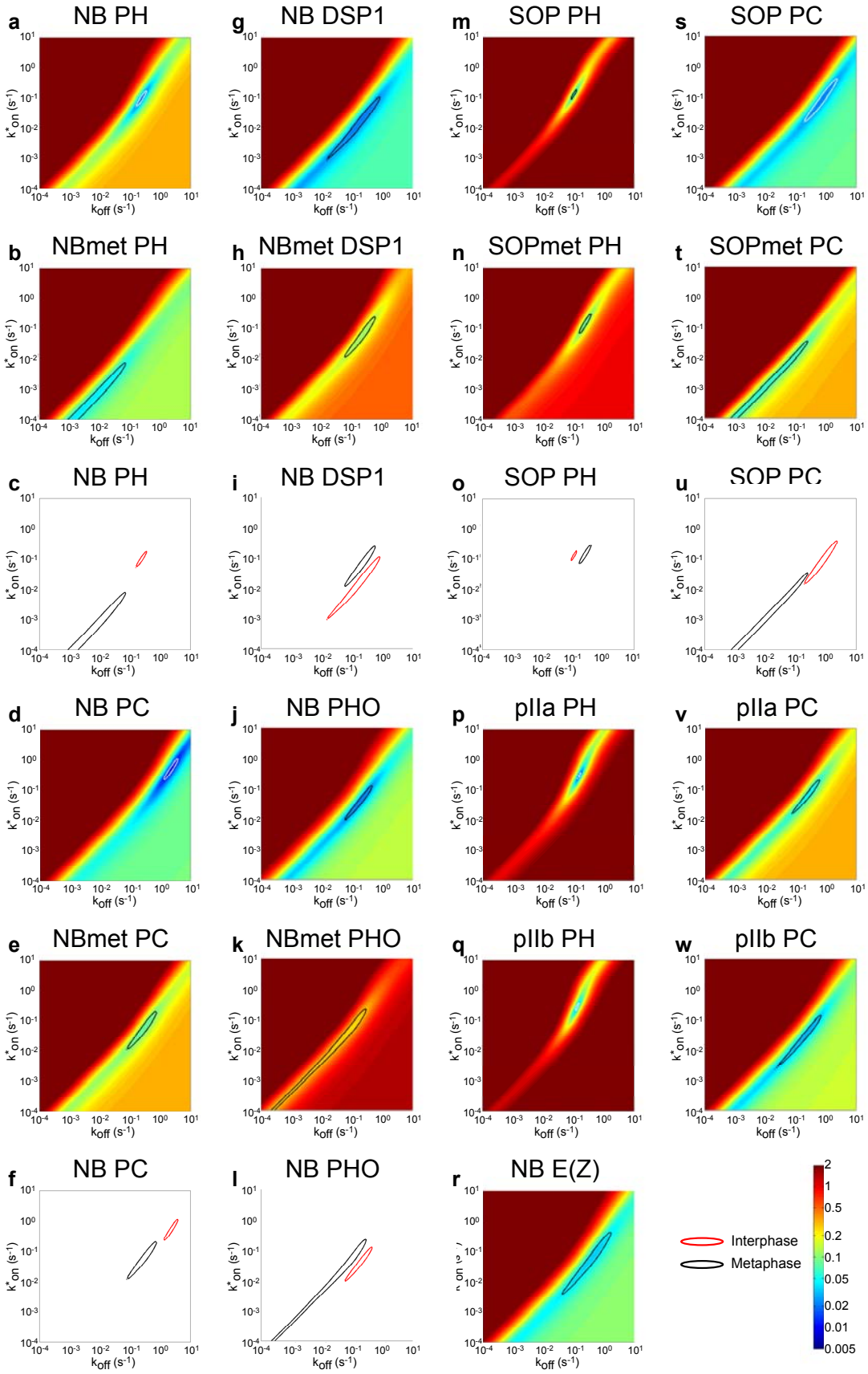
a NB PH
g NB DSP1
m SOP PH
s SOP PC
b NBmet PH
h NBmet DSP1
n SOPmet PH
t SOPmet PC
c NB PH
i NB DSP1
o SOP PH
u SOP PC
d NB PC
j NB PHO
p pIIa PH
v pIIa PC
e NBmet PC
k NBmet PHO
q pIIb PH
w pIIb PC
f NB PC
l NB PHO
r NB E(Z)
k*on (s-1)
koff (s-1)
Interphase
Metaphase
2
1
0.5
0.2
0.1
0.05
0.02
0.01
0.005

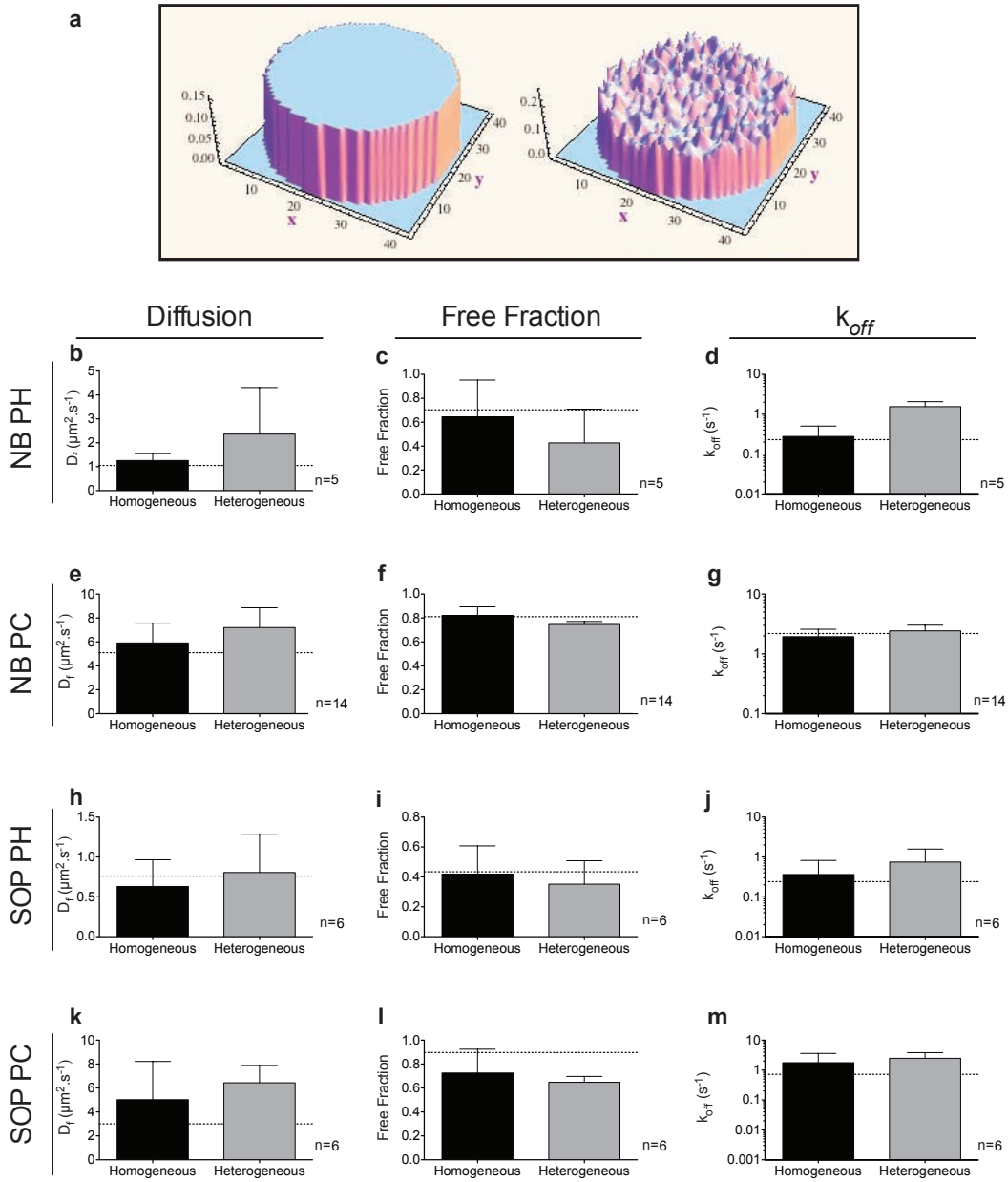

Figure 3.15: Comparison of the effects of binding site non-homogeneity on parameters extracted from FRAP experiments. (a) Depiction of two model nuclei with an homogeneous (left) and a image-based heterogeneous (right) binding site distribution. (b–m) Extracted diffusion (b, e, h, k), free fraction (c, f, i, l) and dissociation rates (k_{off}, d, g, j, m) of PH::GFP (b–d, h–j) and PC::GFP (e–g, k–m) FRAP experiments in neuroblast interphase (b–g) and sensory organ precursor cell interphase (h–m) were analysed using an adaptation of the model described in [227] (performed in a collaboration with J. Lu; see section 2.12). Black bars represent the mean and 95% confidence intervals of the extracted parameters using the same model with an initial homogeneous distribution of binding sites and grey bars represent the mean and 95% confidence intervals of the extracted parameters using the image-based heterogeneous distribution of binding sites for each nucleus. n represents number of nuclei used in each experiment. 2-tailed paired t-tests were performed for each comparison resulting in p-values > 0.05 with the exception of b (p=0.0001), c (p=0.0069), d (p=0.0282) and e (p=0.0163). Dashed lines represent parameters extracted using the FRAP model described in [228] and shown in Figure 3.12 and Table A.2.

and GFP::PHO (Figure 3.12 c).
Taken together these results demonstrate inherently different behaviours of PcG proteins in neuroblasts, in terms of both diffusion and chromatin interaction, with PC::GFP showing the highest dynamic interaction with chromatin and DNA binding proteins showing the highest number of bound molecules followed by PRC1 and PRC2 members.

3.3.5 Polycomb and Polyhomeotic have decreased mobility upon lineage commitment

Previous studies of the kinetics of PH::GFP chromatin binding in Drosophila at different developmental stages have documented an approximately 2-fold lower average dissociation rate in larval wing imaginal discs than in embryos, indicating longer residence times and thus suggesting more stable chromatin association as development proceeds [163]. To evaluate whether PcG proteins interact differently with chromatin in different cell lineages, and in the progressive commitment of a single lineage, I compared kinetic parameters of PH::GFP and PC::GFP at interphase in neuroblasts and in the SOP lineage (Figure 3.10). For PH::GFP, I measured an approximately 2-fold lower dissociation rate constant, giving a 2-fold longer residence time in SOP interphase compared to neuroblast interphase (Figure 3.12 c, Table A.2). In the more determined daughters of the SOP, (pIIa and pIIb), no further increase in residence time was detected. However the association rate constant was approximately 2-fold higher in these daughter cells, contributing to a substantial increase in the calculated bound fraction from 57% in SOP to 66-68% in the daughters (Figure 3.12 a, Table A.2). For PC::GFP, a similar trend was observed. I measured a 3- fold longer residence time at interphase in SOPs than in neuroblasts, and a further 3-fold increase in residence time in pIIa and pIIb (Figure 3.12 a, Table A.2). Taken together these results indicate that the interaction of both PC and PH with chromatin is not only more dynamic in the stem cell neuroblast than in the SOP, but also that the mobility of both proteins decreases upon increasing cell fate commitment within the SOP lineage.

3.3.6 Polycomb Group Proteins have tighter interactions with mitotic chromatin than interphase chromatin

To determine whether the nature of PcG chromatin interactions changes during the cell cycle, I examined metaphase binding. Calculation of bound fractions of PH::GFP and PC::GFP, GFP::DSP1, GFP::PHO and GFP::E(Z) from FRAP analy-

sis of metaphase chromatin of neuroblasts showed a clear reduction in binding, with no detectable binding of GFP::E(Z) and 0.5% to 0.1% of total protein remaining bound to metaphase chromosomes for the other proteins (Figure 3.12 a). Furthermore, in SOP metaphase a similar reduction was also observed for PH::GFP and PC::GFP (1.8 and 0.9% respectively). Independent calculation of metaphase bound fractions based on image quantification gave consistent results (section 2.7, Table A.3). Thus a small fraction of the majority of PcG proteins remains bound to mitotic chromatin.
To assess the kinetic properties of this fraction I examined association rates and residence times (Figure 3.12 b, c, Figure 3.14, Table A.2). Remarkably, for PH::GFP and PC::GFP, in most cases, this metaphase bound population showed profoundly different properties to that bound in interphase, both in terms of a slower association rate (Figure 3.12 b), and a longer residence time (Figure 3.12 b)(Figure 3.14 c, f, u). For each protein, the extent of kinetic changes was different in different lineages. For example, PH::GFP showed no detectable change in behaviour between interphase and metaphase in SOPs, but a profound change in neuroblasts (Figure 3.12 b, c, Table A.3). For PC::GFP, the residence time in neuroblasts increased 7.3-fold from 0.46s in interphase to 3.35s in metaphase. In contrast, in SOPs for the same protein, the increase in residence time at metaphase was over 300-fold, from 1.39s in interphase to over 5 minutes in metaphase. For proteins GFP::DSP1 and GFP::PHO, no significant difference was found between the kinetic properties of the mitotic bound fraction (Figure 3.12 b, c, Table A.3).
These protein and lineage specific differences in kinetic behaviour suggest that the changes in binding properties at metaphase are not a general effect of chromatin condensation at mitosis, but are specific to each protein in each cell type.

3.4 Modeling of Polycomb interaction with chromatin during cell cycle progression in neuroblasts and sensory organ precursor cells

3.4.1 Mathematical modeling predicts a slower timescale for mitotic dissociation of Polycomb in SOPs than in neuroblasts

In the above experiments I measured different chromatin binding properties of PcG proteins at specific points during the cell cycle, namely interphase and

metaphase. I next asked whether the changes in kinetic properties I have measured are sufficient to account for the observed reduction in binding at metaphase within the known time frame of cell division in SOPs and neuroblasts [238, 243].

To this end, mathematical modeling was used to simulate a time course of Polycomb-chromatin interactions upon cell cycle transitions (performed in a collaboration with S. Müller; Figure 3.16 a). Polycomb was the chosen molecule to be modeled due to the previous extraction of binding parameters (Figure 3.12) and endogenous protein quantification (Figure 3.9) in both neuroblast and SOP lineages. The PC-chromatin interaction was modeled using ordinary differential equations (Figure 3.16 a, Appendix C). As inputs we used the calculated numbers of endogenous PC molecules in SOPs and neuroblasts, the association and dissociation rates measured in FRAP at interphase and metaphase in each cell lineage, and the corresponding nuclear or cell volumes (Table A.4). I first asked whether a change in kinetic properties of PC is actually required for protein dissociation at metaphase or whether the simple effects of protein dilution at nuclear envelope breakdown (NEBD) would be sufficient (Figure 3.16 b,

Figure 3.16 *(following page)*: Mathematical modeling of mitotic dissociation of PC from chromatin. (a) Model for interaction of PC protein with chromatin targets. PC interacts with chromatin with the association rates k^*_{on} and dissociation rates k_{off}. The model describes three species: chromatin bound PC, free PC and free chromatin. Implementation of the model was performed as a collaboration with S. Müller and is described in Appendix C.(b,c) Modeling of endogenous PC in neuroblasts (NB, b) and sensory organ precursor cell (SOP, c) lineage of *yw* flies. Time is scaled in real time according to [238, 243]. Solid bars represent calculated numbers of bound PC molecules extracted from FRAP experiments at interphase or metaphase in each cell type as indicated. Solid lines represent bound numbers of PC molecules predicted by simulation using the model shown in (a) under different assumptions as follows: Dilution only model (black line), dilution of PC as measured (Figure 3.9 c) occurs at nuclear envelope breakdown (NEBD), but changes in binding rates are not included in the simulation, to evaluate the contribution of dilution alone to the chromatin binding properties of the system. This model predicts a substantial dissociation of PC caused by dilution alone in both cell types (b,c), which nevertheless fails to reach the measured levels of dissociation. All changes at NEBD (green). The measured dilution (Figure 3.9 c) and extracted changes in binding parameters (Figure 3.10 b, c) are included in the model, with all changes occurring simultaneously at NEBD. For NB (a), this model predicts a rapid dissociation to measured levels, whereas for SOP (b) the same model using SOP parameters predicts a gradual dissociation, which does not reach measured levels of dissociation by the onset of cytokinesis. Initial gradual change of k_{on} (red). The model assumes dilution as measured (Figure 3.9 c) at NEBD, change in k_{off} as measured (Figure 3.10 c) at NEBD, but the association rate changes gradually from extracted interphase to metaphase values (Figure 3.9 b) from prophase to NEBD. This model predicts dissociation of PC in SOPs that is close to measured levels (b).

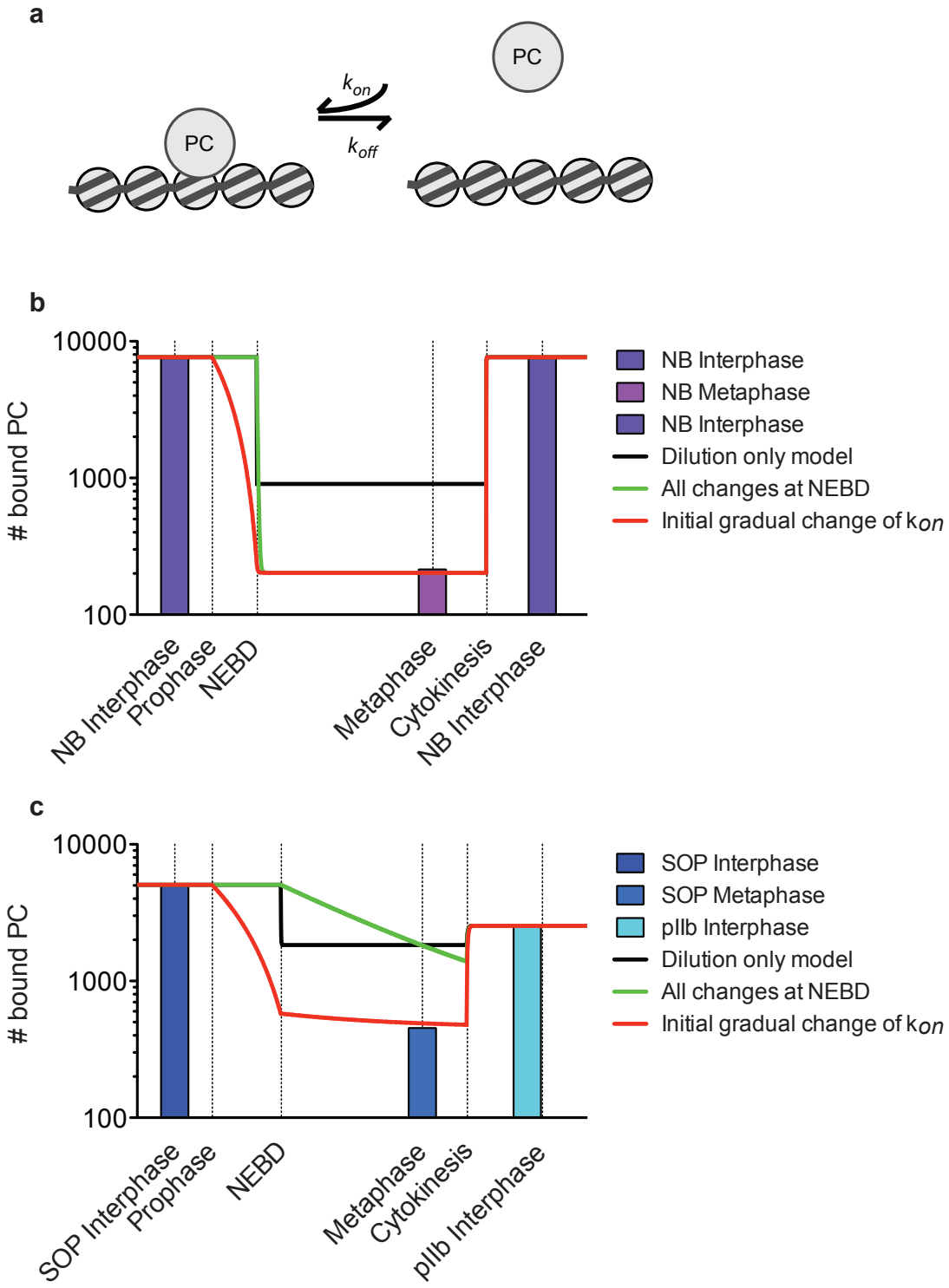
a
PC
k_{on}
k_{off}
PC
b
10000
1000
100
bound PC
NB Interphase
Prophase
NEBD
Metaphase
Cytokinesis
NB Interphase
NB Interphase
NB Metaphase
NB Interphase
Dilution only model
All changes at NEBD
Initial gradual change of k_{on}
c
10000
1000
100
bound PC
SOP Interphase
Prophase
NEBD
Metaphase
Cytokinesis
pIIb Interphase
SOP Interphase
SOP Metaphase
pIIb Interphase
Dilution only model
All changes at NEBD
Initial gradual change of k_{on}

c, black lines). These simulations predicted that although dilution alone would achieve a substantial degree of dissociation, the measured levels of metaphase binding are an order of magnitude lower still. We next asked whether the changes in kinetic rate constants we have measured would be sufficient to remove this additional protein from mitotic chromosomes within the time frame imposed by the cell cycle (Figure 3.16 b, c, green lines). For this simulation, the dilution and changes in binding properties were all effected concomitantly upon nuclear envelope breakdown. This simulation predicted a rapid dissociation to the observed levels within seconds of NEBD in neuroblasts. However the predicted dissociaton in SOPs was very slow, such that the observed levels were not reached before the cell enters cytokinesis at the end of metaphase (Figure 3.16 c). In the simulation, the system reached equilibrium after approximately 33 minutes, predicting 385 bound molecules. Further inspection of parameters revealed that this difference between the cell types was independent of diffusion (Appendix C), and was due mainly to the faster exchange of PC in neuroblast interphase and the very slow dissociation of PC in SOP metaphase. The assumption made above, that all parameters change at the same moment upon NEBD, is sufficient to explain dissociation in neuroblasts, but proved to be invalid for SOPs (Figure 3.16 c). We thus evaluated whether a changed order of events could accelerate mitotic dissociation. The moment of NEBD is well defined in our experiments, (visible as dispersal of GFP fusion proteins in Figure 3.6 and Figure 3.7). The assumption that protein dilution occurs effectively instantaneously upon NEBD is valid (Appendix C). However, the condensation and modification of chromatin begins at prophase, well before NEBD [244]. To simulate this gradual change in the nature of the chromatin template, we introduced a gradual change in the association rate k_{on}, starting at prophase (Figure 3.16 c, red line). In both neuroblasts and SOPs, this resulted in rapid dissociation of PC before NEBD, and full dissociation to the measured levels at metaphase.
In summary, this analysis predicts a slower dissociation kinetic for PC in SOPs than in neuroblasts, which can be accelerated by modeling a reduction in the association rate during prophase.

3.4.2 H3K27me3S28 phosphorylation during prophase may accelerate PC mitotic dissociation

I next asked what molecular mechanisms could account for a change in the association rate of PC to chromatin during prophase. I reasoned that phosphorylation of serine 28 on histone H3 (H3S28p) may be a good candidate.

H3S28 phosphorylation is present during interphase, and increases during mitosis [245, 246]. PcG proteins have a reduced ability to bind to the H3 tail trimethylated at lysine 27 (H3K27me3) if the adjacent H3S28 site is phosphorylated [123, 125]. I reasoned that an accumulation of H3K27me3S28p during prophase could effectively reduce the association rate of PC to chromatin, by reducing the number of sites available for binding, in a manner analogous to that reported for HP1 [126, 127]. To determine whether H3K27me3S28p accumulates during prophase in neuroblasts and SOPs, whole brain and notum of PC::GFP expressing flies were stained with an antibody that specifically recognises the double modification. Figure 3.17 shows that robust accumulation of H3K27me3S28P was indeed detectable in prophase in both neuroblasts and SOPs, before the onset of NEBD. These results are consistent with a role of this double modification in ejecting PC from chromatin during prophase.
I conclude that this modification may contribute to the reduction in association rate that we have predicted by mathematical modeling to be required before NEBD, thus accelerating mitotic dissociation of PC.

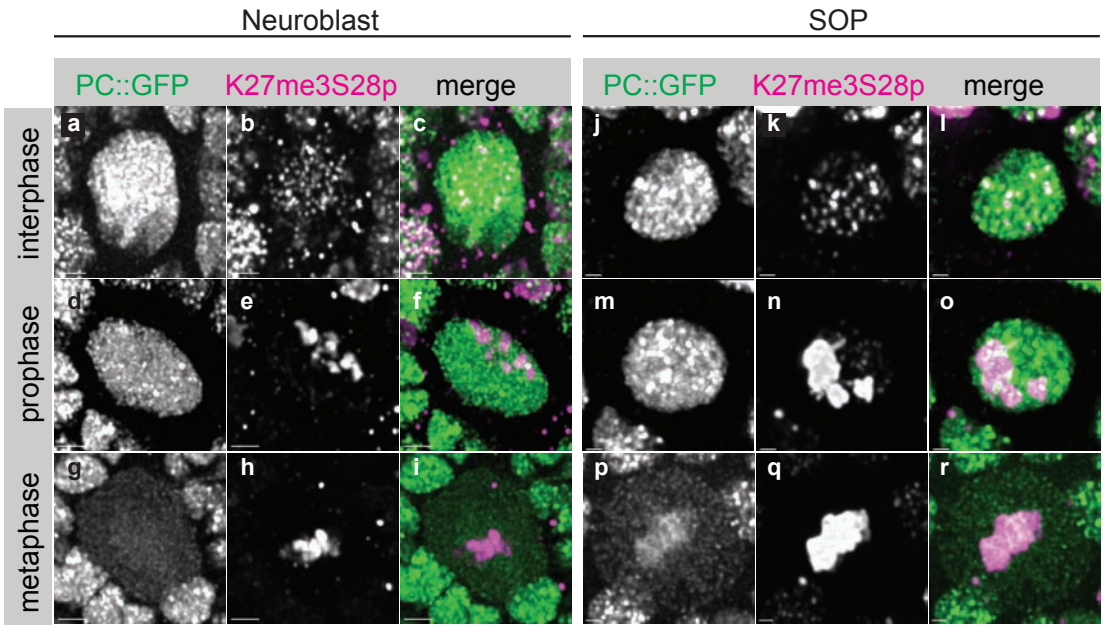

Figure 3.17: The H3K27me3S28p double mark accumulates during prophase in neuroblasts and SOPs. Neuroblasts (a–i) and SOPs (j–r) of larvae and pupae expressing PC::GFP were fixed and stained with αH3K27me3/S28p. GFP signal (a, d, g, j, m, p) reveals PC::GFP distribution and identifies cells that have not yet undergone NEBD, visible as distinct nuclear and cytoplasmic regions in (a, d, j, m). After NEBD, the PC::GFP signal is dispersed throughout the cell volume (g, p). Detection of H3K27me3/S28p reveals that the double mark is present in interphase (b, k), and accumulates during prophase, prior to NEBD (e, n). Maximum levels of double mark are detected at metaphase (h, q). Scale bars represent 2 µm in (a–i) and 1 µm in (j–r).

3.5 ASH1 and JIL-1 modulate kinetic properties of Polycomb in neuroblasts

3.5.1 Neuroblast-specific downregulation of ASH1 and JIL-1 alters Polycomb kinetics

I showed above that PC binds more strongly to differentiated cells (SOPs) than to stem cells (neuroblasts). This lead me to ask if the kinetic properties of the PC-chromatin interaction could be altered *in vivo*. To examine this possibility, I performed a neuroblast specific knockdown within a short time window (section 2.2), of interactors, and possible regulators, of Polycomb kinetics. I chose to knockdown, PHO and DSP1 as they have been reported to important for recruitment of PcG proteins [44, 247], and of the TrxG protein ASH1, as it has been shown to be an antagonistic effector and competitor of PcG proteins [48]. Since the H3K27me3S28p double mark has been reported to regulate Polycomb binding in mammalian cells [123, 125], in addition to the previous proteins, additionally I have targeted JIL-1, the *Drosophila* homolog of MSK1, the H3S28 interphase kinase. While none of knockdowns altered significantly the bound fraction of PC::GFP in neuroblast interphase (Figure 3.18 b), the reduction of ASH1 and JIL-1 levels lead to significant increase in the residence time of PC::GFP (Figure 3.18 a).

I further asked what would be the effect of these knockdowns on the mitotic kinetic properties of PC::GFP. This examination revealed that, while in control flies PC::GFP increased its residence time on mitotic chromatin, after knockdown of ASH1 and JIL-1, this alteration was abolished, and residence times were maintained from interphase to mitosis (Figure 3.18 c). Interestingly the reduction of ASH1 further lead to a small, however significant, increase in the bound fraction of PC::GFP during mitosis (Figure 3.18 d).

To exclude the possibility that these differences were simply caused by alteration of PC::GFP levels upon knockdown of interacting proteins, I next asked if the levels of PC::GFP expression were also affected by the knockdown of these proteins. Quantification of PC::GFP fluorescence levels showed no significant change in protein expression with any of the genotypes (Figure 3.18 e, f).

Taken together, these results reveal that it is possible by ASH1 and JIL-1 knockdown to alter the binding kinetics of Polycomb. ASH1 knockdown leads to an increase in the residence time of Polycomb in neuroblast interphase while abolishing the further increase registered upon the mitotic transition, in addition to an increase in the amount of Polycomb bound to mitotic chromatin. JIL-1 RNAi causes the same changes in binding kinetics as ASH1, although no significant

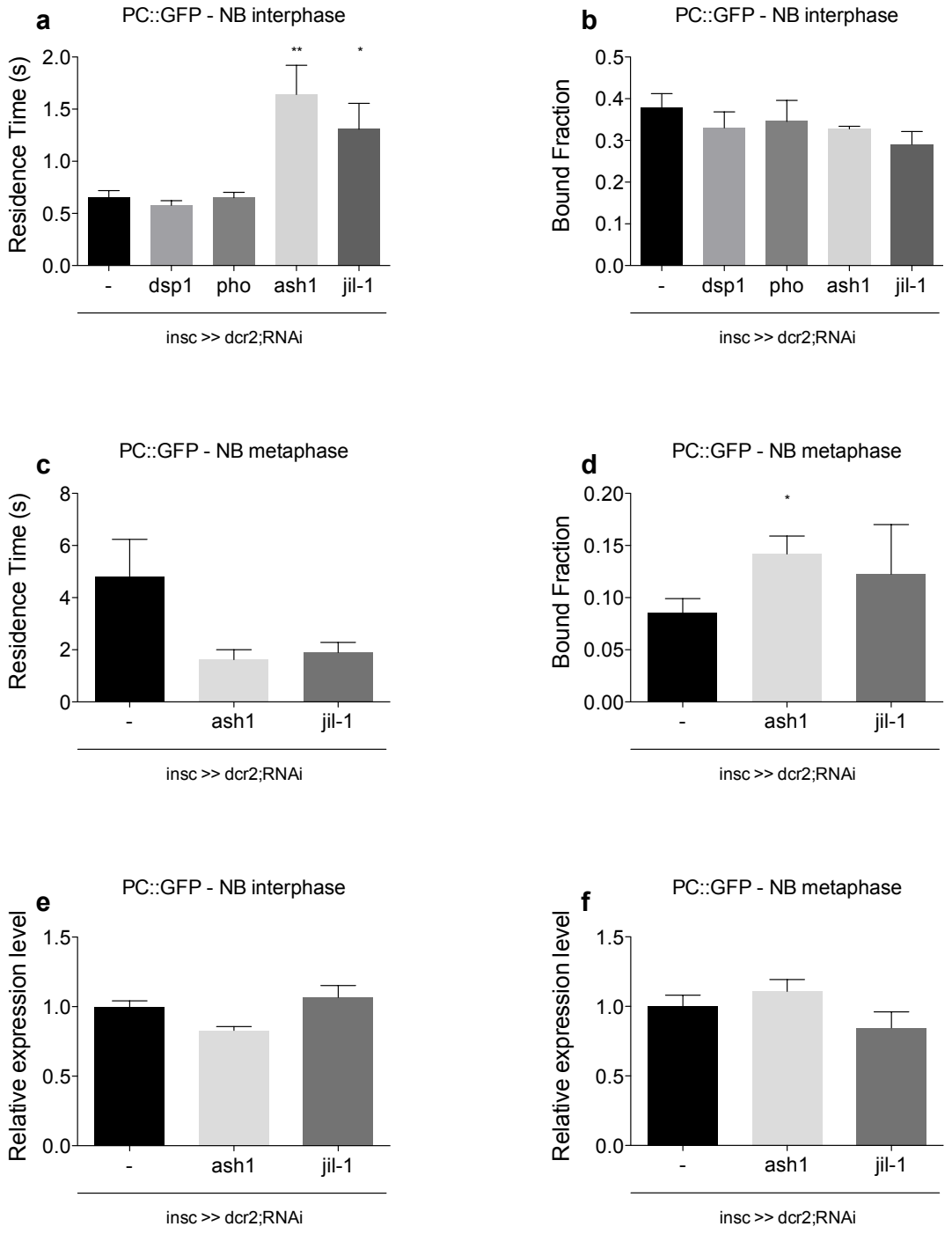

Figure 3.18: ASH1 and JIL-1modulate PC::GFP kinetics in neuroblast lineage. (a–d) Extracted residence time (a, c) and bound-fraction (b, d) of PC::GFP in neuroblast interphase (a, b) and metaphase (c, d) upon no RNAi (-) and knockdown of *dsp1* (dsp1), *pho* (pho), *ash1* (ash1) and *jil-1* (jil-1). (e, f) Quantification of GFP sum intensity in PC::GFP expressing nuclei of neuroblasts in interphase (e) and metaphase cells. Data show mean and SEM of at least 3 experiments. ANOVA tests with Dunnett's post-test (a,b) and two-tailed t-test (c,d, e, f) were performed and p-values < 0.05 (*) or < 0.01 (**) are shown.

increase in PC binding is present during cell division.

3.5.2 ASH1 level reduction leads to reduction in number of neuroblasts

To examine if the ASH1 and JIL-1 RNAi knockdown lead to phenotypic changes in neuroblasts, I performed a type II lineage neuroblast-specific knockdown within a large time window (see section 2.2). The knockdown was performed in type II lineages due to the presence of only eight neuroblasts [229], which allows for an easier determination of over and under proliferation phenotypes. This analysis revealed that while JIL-1 knockdown did not alter the number of neuroblast lineages present in each brain lobe, ASH1 RNAi lead to a striking reduction in number and size of neuroblast lineages (Figure 3.19).
In summary, these results show that the reduction of ASH1 levels leads to a reduction in the number of neuroblasts.

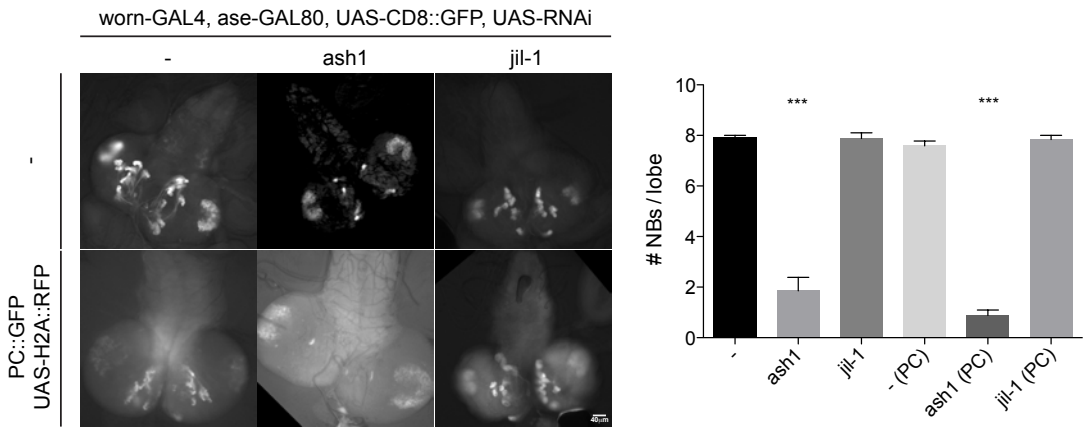

Figure 3.19: *ash1* knockdown leads to reduction in number of type-II lineage neuroblasts. (a) GFP marked type II lineage neuroblasts in fixed 3rd instal larval brains after no RNAi (-) or knockdown of *ash1* (ash1) or *jil-1* (jil-1) in the absence (-) or presence of PC::GFP and H2A::RFP (PC::GFP, UAS-H2A::RFP). Scale bar is applicable to all images. (b) Quantification of number of neuroblasts from brain images represented in (a) from at least 3 brains. (PC) indicates presence of PC::GFP and H2A::RFP transgenes. ANOVA test was performed followed by Tukey's post-test and p-values < 0.001 are shown (***)

4

Discussion

In this thesis I have used a combination of *in vivo* protein quantification and kinetic analysis, with mathematical modeling to investigate changes in the dynamic behaviour of PcG proteins upon mitosis and cell fate transitions in living *Drosophila*, giving quantitative insights into properties of the PcG proteins in stem cells and differentiated cells.

4.1 Quantification of PcG proteins

I have quantified total numbers of GFP-fused and endogenous molecules of PH, PC, DSP1, PHO and E(Z) in neuroblasts, SOPs, and the daughter cells pIIa and pIIb in live animals, using a combination of of live imaging of the GFP fusions, calibration with GFP-VLPs and quantitative western blots.
For the PH::GFP fusion protein, the use of limited tissue specific expression strategies was necessary to avoid cell death associated with PH overexpression, as has been reported previously [248, 249]. To determine the expression level of PH::GFP in neuroblasts, I FACS sorted large cells from dissociated brains, which were GFP-positive. This strategy allowed for the enrichment of neuroblasts in sorted cell extracts (Figure 3.4) and the quantification of the ratio between PH::GFP and PH (Figure 3.5). Since protocols for the isolation of GFP-marked SOPs are not currently available, the quantification of PH::GFP in SOPs was not performed. A goal of future studies will be to isolate the PH::GFP expressing cell types of interest, in order to enable relative quantification of PH::GFP and endogenous PH in the differentiated cell type. For all the other PcG::GFP fusion proteins, the transgenes were expressed under ubiquitous promoters, enabling the quantification of the relative amount of transgenic and endogenous protein from whole tissues.

The use of GFP-VLP for quantification of GFP molecule numbers showed a 2-fold lower measurement when compared to an ELISA-based method (Figure 3.8). A possible reason for this discrepancy in the measurements is the detection of GFP-VLP fluorescence intensities in a different environment (outside the embryo) from the GFP-fusion proteins. The brightness of GFP might be lower inside the embryo due to the presence of highly scattering structures inside the nucleus, such as chromatin [250]. Additionally, for fluorescence detection, the GFP protein needs to be correctly folded, which is not necessary for detection in an ELISA method, which may thereby lead to an underestimation of total number of GFP molecules through live imaging. Nevertheless, the discrepancy registered here between these two methods is similar to the estimated accuracy of GFP-VLP quantification [216]. It would be interesting in the future to compare the values calculated here with ones acquired through different methods such as FCS or quantitative mass spectrometry [217].
The values registered here for the total numbers and concentrations of endogenous molecules of the various PcG proteins (Figure 3.9 and Table A.1) agree well with the numbers of molecules of several transcription factors [11]. One example of this similarity is the 0.2μM concentration of FTZ protein in blastoderm nuclei of embryos found by comparison of embryo extracts to known amounts of recombinant protein [251].
A more direct comparison can be drawn by the numbers of endogenous PC molecules previously estimated to be present in salivary gland and S2 cell nuclei using quantitative western blotting calibrated with recombinant PC protein [13]. The values registered here of 0.4-0.5μM of Polycomb/cell are 2–3-fold lower than the extrapolated concentration of endogenous PC in salivary gland nuclei [13, 252]. Although this discrepancy might originate from the different methods used for the determination of protein quantities, or from the different cell types used in the different studies (salivary glands are polyploid and may require higher number of PC proteins), the quantities measured here show good agreement with previous quantification attempts.
Furthermore, our western blot analysis revealed that most transgenic proteins exhibited repression of endogenous protein expression (Figure 3.5). This result is in agreement with reports of transgenic down regulation of endogenous PC and PH proteins [163].
In addition to total number of molecules, in this thesis I report the number of chromatin bound endogenous molecules of PcG proteins (Table A.2). To calculate the bound fraction of molecules I have used the extracted bound fraction from FRAP experiments performed for each of the GFP-fusion proteins.
FRAP is one of the few techniques that allows for the determination of bound

fractions *in vivo* [220]. Nevertheless, it has its own limitations, as it has been reported that erroneous models or negligence of essential parameters in the FRAP model can lead to crass errors in the estimation of binding parameters [228] and, due to the photobleach step in the method, it introduces a perturbation to the system which is hard to control for [220]. I tested different models for FRAP analysis, with the main difference being the presence or absence of heterogenous concentration of binding sites (Figure 3.15, [227]). Because results were similar with both models, we have opted to use a homogeneous model [228], which enhances the previous models by taking into account the true photobleach profile, as well as the diffusion component in the recovery curves. The next step in the future will be to cross-validate the binding parameters estimated here with a different protocol, such as FCS [253].

Although precaution is always necessary when analysing *in vivo* binding parameters, we find good agreement with bound fractions estimated from images (Table A.3) and it has been shown that in FRAP analysis the bound fraction is the best estimated parameter [226, 227, 228, 253]. This is consistent with the analysis of robustness of k_{off} and k^*_{on} (Figure 3.14).

It is important to consider to what extent the partial rescue of Pc mutants by the PC::GFP transgene will affect the quantitative conclusions drawn here. By quantitative comparison with PH::GFP behaviour, it has been proposed that the PC::GFP fusion is less favoured by 4 to 5 fold in the PRC1 complex than the endogenous protein [163]. These authors concluded that the population of PRC1 is marked with PC::GFP, but the bound fraction of PC::GFP may be an underestimation of bound fraction of endogenous PC. This effect may lead to the lower bound fraction that I measure for PC::GFP in comparison to PH::GFP. It also follows from this that second order kinetic processes (on rates) will be prone to inaccuracies, but first order processes (off rates and therefore residence times) will be unaffected. I note that the accurate determination of the true on rate (k_{on}) from the pseudo first order association rate (k^*_{on}) extracted from FRAP experiments such as these, is also limited by the unknown quantity of free binding sites [220], thus at best, one can extract relative k_{on} values that allow comparisons between different cell types. This in itself allows meaningful comparisons. In summary, I conclude that the PC::GFP fusion protein is a useful reporter of specific aspects of endogenous protein behaviour: it enables the accurate determination of residence times, of absolute protein quantities (which do not rely on protein activity), and the determination of relative differences between on rates in different cell types and at different cell cycle stages.

DSP1::GFP has previously been tested for rescue of endogenous *dsp1* mutations [236]. However, these attemps failed due to the unexpected lethality of the tem-

perature sensitive allele *Dsp*^{1} at the permissive temperature [236]. It will be of interest to determine the rescue ability of this fusion protein using other mutant alleles. The unavailability of rescue experiments for the GFP::DSP1 fusion leads to the question of the validity of the results presented in this thesis for the behaviour of DSP1. It has been reported that GFP::DSP1 and its endogenous version have overlapping binding sites in polytene chromosomes of salivary glands [236]. In addition I have shown here that GFP::DSP1 dynamically binds mitotic chromatin through live imaging and FRAP experiments (Figure 3.6, Figure 3.7, and Figure 3.12). It has previously been shown that mitotic binding is an hallmark of HMGB proteins [254], which are the human homologues of DSP1. In summary, the GFP::DSP1 fusion protein is able to fulfill at least some of the binding properties that are expected for DSP1 and it allows the quantification of the endogenous levels of DSP1 and the comparison of binding properties between different cell types and during cell cycle.

The estimation of the number of endogenous PC and PH molecules bound to chromatin in interphase (approximately 2500 to 11000 depending on cell type, Table A.2) suggests that the expression of PRC1 components is coordinated. In the future, similar studies could be performed in different cell types in order to confirm if this correlation holds true or if this regulation is cell type specific. Furthermore, the number of estimated molecules allows the comparison with numbers of PcG target genes estimated from profiling studies (between 400 and 4000 for PH and between 200 and 2000 for PC [79, 96, 132]). If these numbers are true for the cell types studied in this thesis, there are in average 3 to 30 molecules of PH and 1 to 40 molecules of PC per binding site. If two molecules of PC bind each nucleosome (two H3K27me3 tails per nucleosome) and the smaller number of binding sites is taken into account, then, in average, this site is 4000bp long. This size agrees well with the reported size of PREs [255, 256] but is smaller than the average H3K27me3 domain [257].

The number of endogenous molecules of DSP1 and PHO are higher than for PRC1 and PRC2 components, as well as the number of bound molecules. These values correlate well with the larger number of binding sites found in genome-wide mapping efforts for these DNA binding proteins [132]. Additionally the PRC2 component E(Z), which is H3K27, which in its turn is also responsible for the recruitment of PRC1 is bound in lower amounts than the PRC1 components, PH and PC (Table A.2). This result suggests that recruitment of PRC1 components cannot have as a requisite the presence of E(Z), indicating that is probably the activity of E(Z) that is necessary to create the binding sites for PRC1. This result is consistent with the previous report that at the *bxd* PRE, E(Z) methylation activity is required for PC recruitment [173].

The quantification of free and bound numbers and concentrations of endogenous PcG molecules reported in this thesis, shows for the first time the quantitative relationship between these proteins in single cells of live animals. Furthermore, this type of analysis brings new biological meaning to previous descriptive models and allows the elaboration of new, more meaningful, quantitative models of PcG epigenetic action.

4.2 Kinetic properties of PcG proteins

Here I have measured binding parameters and diffusion coefficients of PH::GFP, PC::GFP, GFP::DSP1, GFP::PHO and GFP::E(Z). This analysis allowed the comparison of the behavior of different proteins in single cells, as well as differences in the behavior of the same protein in different cells from different developmental stages and from a well-defined differentiation process. Moreover, I have analyzed the binding parameters of these proteins in interphase to mitosis transitions.

The interphase residence times for both PRC1 proteins measured in this study (0.5–10 sec) are shorter than those previously reported for the same fusion proteins in other tissues (2–6 minutes, [163]). These differences may arise from the different cell types examined, or from the different FRAP analysis models used. Indeed, the residence times measured here are consistent with those measured for several transcription factors, using similar FRAP models [228]. Additionally, the discrepancy between the extracted diffusion coefficients in this study (0.8–1.3$\mu m^2.s^{-1}$ for PH::GFP and 2.4–5.1$\mu m^2.s^{-1}$ for PC::GFP; Table A.2) and the previously described diffusion coefficients for PH::GFP (0.2$\mu m^2.s^{-1}$) and PC::GFP (0.4–0.7$\mu m^2.s^{-1}$) [163] might contribute for the difference in the calculated residence times of these proteins, since the slower diffusion reported previously might occlude part of the binding reaction of PH::GFP or PC::GFP to chromatin. The difference in diffusion coefficients may arise also from the different techniques that were employed. In the previous study the diffusion coefficients were extracted from FRAP experiments performed in early embryos and in salivary gland nucleoplasm, where the authors reason there is no PcG binding to chromatin. Here, I have extracted diffusion coefficients from diffusion/binding reaction FRAP models and compared them to coefficients extracted from FRAP experiments performed in the cytoplasm of cells in metaphase, where no chromatin was visible and therefore no binding is detected, assuring that the measured diffusion coefficients are correct for the cell type of study. In additional experiments not shown in this thesis I have per-

formed FRAP analysis of PC binding to chromatin in interphase of blastoderm nuclei of embryos. A visual inspection of the recovery curves showed a essentially identical curve shape when compared to the previously reported recovery curves of PC FRAP [163]. However, implementation of the FRAP model used in this thesis [228], lead to the extraction of different diffusion and binding parameters ($Df = 6.4\mu m^2.s^{-1}$ and $k_{off} = 1.7s^{-1}$) to the ones previously measured ($Df = 0.7\mu m^2.s^{-1}$ and $k_{off} = 0.03s^{-1}$). This experiment gives a clear insight into the contribution of the FRAP model for the estimation of binding parameters and might elucidate why there is a discrepancy between the results presented here and elsewhere [163].

Comparison of PC::GFP and PH::GFP revealed 2-9 fold longer residence times for PH::GFP than PC::GFP at interphase in all cell types, although the number of bound molecules was similar (Figure 3.12 and Table A.2). This result suggests that PC and PH do not solely operate together, as part of the PRC1 complex, consistent with previous studies [189, 135]. The longer residence times observed for PH::GFP may reflect multimerisation of PH via the SAM domain, which has been shown to be required for PH mediated gene silencing [258]. The cell type specific differences that we observe in the kinetic behaviour of PH::GFP raise the intriguing possibility that some of these may be due to regulation of SAM domain polymerisation and thus, PH silencing properties.

Analysis of binding parameters of the different PcG proteins in neuroblast interphase revealed that PC has a very rapid dissociation rate and that the DNA binding proteins, PHO and DSP1 have the longest residence times (Figure 3.12 and Table A.2). Overall, there is an hierarchical loosening of chromatin binding from DNA-binding proteins, to PRC2 (E(Z)) and finally PRC1 (PC and PH). This result has some analogies to the hierarchical recruitment that has been demonstrated by ChIP studies of PcG proteins to a single PRE [173]. The prediction from this result is that DSP1 and PHO are necessary for recruitment of PRC2 and then PRC1, not just by binding the same sites, but by binding these sites for longer times, increasing the chance of recruitment of these proteins. This is not a general phenomenon that DNA binding proteins bind chromatin with longer residence times than chromatin binding proteins, as a study performed in baby hamster kidney cells showed that chromatin binding proteins HP1β and BRD4 have longer residence times than the DSP1 homolog, HMGB1 and many transcription factors [160]. I have tested the hypothesis of a global hierarchical recruitment of PC in neuroblasts by reducing the levels of DSP1 and PHO separately through a neuroblast-specific RNAi knockdown of these genes in interphase, and subsequent analysis of PC::GFP kinetics (Figure 3.18). Although no difference was detected in the levels of PC binding to chromatin or in its res-

idence time by FRAP analysis, this result does not exclude the possibility that PHO and DSP1 have a role in recruitment or regulation of the kinetic behavior of PC. It has been shown that PHO has an functional homolog in *Drosophila*, PHO-like which can partially replace its silencing activity and that the double mutant for both proteins is still able to recruit PcG proteins to many loci [129]. Moreover, there is evidence that PREs are constituted of a multitude of combinations of binding sites for different proteins [69], which suggests that the absence of any changes in PC::GFP-chromatin binding might be due to redundancy in DNA binding protein recruitment. Nevertheless, it will be essential to address this question again in the future, as the knockdown efficiency has not been determined for each of the genes and possibly a combinatorial downregulation of two or more PcG recruiters might have a stronger phenotype. Alternatively, these DNA-binding proteins might have cell cycle stage-specific recruiting properties as they could be necessary for the binding of PcG proteins to mitotic chromatin or for the initial recruitment of PcG proteins to new chromatin after DNA replication. These hypothesis can be addressed in future by reducing the levels of these proteins and analyzing PRC1 and PRC2 binding properties at different cell cycle stages. In addition, a modeling approach, in which PC recruitment depends on DSP1, PHO or a combination of these and other DNA binding proteins could be used to predict which knockdown efficiencies would be necessary to measure a reduction in PC::GFP binding or residence time *in vivo*.

I document a reduction in mobility of both PC::GFP and PH::GFP upon lineage commitment between neuroblasts and SOPs (Figure 3.12 and Table A.2), consistent with studies showing reduced mobility of these proteins at later developmental stages [163] and a general loss of chromatin plasticity upon ES cell differentiation [161]. Interestingly, a recent study of TFIIH-chromatin binding in developing mammalian tissues, performed in living mice, revealed a differentiation-driven reduction in TFIIH mobility, revealing long lasting but reversible immobilization in post-mitotic cells [162]. It will be of great interest in future to examine PRC2 and DNA-binding proteins in these lineages as well as PcG and TrxG proteins in other cell lineages, to determine the extent to which residence times are modulatable upon changes in cell identity.

I extend these findings to a well defined differentiation process in a live animal. I show that, albeit to a lesser extent, within a single lineage, and upon one cell division, PC shows a reduced mobility. This finding agrees with the common view that differentiation leads to a loss in chromatin plasticity, and shows that this loss can be achieved rapidly.

Furthermore, I identify a fraction of PH, PC, DSP1 and PHO molecules that re-

main bound to mitotic chromatin in both neuroblasts and SOPs. These findings show that these proteins interact dynamically with mitotic chromatin, as well as, interphase chromatin, extending the previous reports that PH, PC and PHO are bound to chromatin during mitosis in larval neuroblasts [188]. The same study also suggests that E(Z) is able to bind mitotic chromatin which does not agree with FRAP and image-based quantification done here. It is unclear if this discrepancy is a result of a very small number of molecules that stays bound to chromatin during mitosis and that is undetectable by the methods used in this thesis, or if they are an artifact from the fixing procedures reported in [188]. If E(Z) does not bind mitotic chromatin, this suggests that neither direct binding of E(Z) to its target site, nor the methylation activity on histones is required during cell division for the transmission of epigenetic memory of transcription. It will be of great interest in the future to dissect the mechanism of how PRC2 components are displaced completely from chromatin and what are the implications of a failure to do so. A possible approach to this question could encompass the generation of mutant versions of E(Z), which lack defined domains or residues that might be important for this regulation, as well as a RNAi screen for regulators of E(Z) identified through a mass spectrometry approach.
The binding of PRC1 proteins to mitotic chromatin that I have measured here is in contrast with reports of complete chromatin dissociation in embryonic cells [189]. It would be essential to perform a careful quantitative analysis of embryonic stages to decipher if PRC1 mitotic binding is a common feature or if it is cell-type specific.
I further analyzed the binding behavior of other PcG proteins during mitosis. The DNA binding proteins DSP1 and PHO maintain their binding parameters upon the transition to mitosis (Figure 3.12 and Table A.2). The reduction of the number of bound molecules observed is most probably caused by dilution upon nuclear envelope breakdown, although it cannot be completely excluded that the interaction of these proteins with DNA is modified and regulated upon cell division, although maintaining the same overall parameters. Interestingly, due to the extracted pseudo association rates (k^*_{on}) not changing significantly, these results suggest that the dramatic chromatin reorganisation upon mitosis, does not occlude the binding sites or changes the affinity for the binding sites of both DSP1 and PHO. Additionally, upon binding, the residence time is also not altered, meaning that in interphase and mitosis, DSP1 and PHO have similar binding behaviours. It will be interesting to address if the binding sites for DSP1 and PHO are maintained or altered from interphase to mitosis, and if these loci that are able to retain these DNA binding proteins during cell division are stronger recruiters due to DNA sequence specificity and if they have

a better ability to epigenetically maintain the expression state of the associated genes. If this behaviour is maintained in cell culture, one could approach this question by synchronizing cells at different cell cycle stages, and, by ChIP analysis, mapping the binding sites of these proteins.
The number of PH and PC molecules bound to chromatin is severely reduced during cell division. However, the residence time measured for these proteins in metaphase can exceed 10 minutes indicating a very strong binding that can be longer than the time that neuroblasts and SOPs spend in metaphase [238, 243]. Regulation of binding properties during mitosis has been reported before for other proteins [185, 187]. Moreover, this type of regulation has been shown to have functional roles [187]. These results suggest that this small fraction of very stably bound molecules (in the range of few hundred) might also have a functional role and be responsible for the transmission of epigenetic memory. It has been shown *in vitro* that PRC1 has a very tight interaction with chromatin during replication, and a model has been put forward, where this tight interaction is responsible for the transmission of epigenetic memory through replication [120, 259]. I show here that a similar tight interaction with chromatin might also be responsible for transmission of epigenetic memory through mitosis. It is not clear how is this tight interaction achieved, as experiments *in vitro* show that PcG proteins directly contact DNA, but not explain how the specific targeting is accomplished. It will be interesting to uncover more about the mechanism of PC binding to mitotic chromatin, perhaps by testing a set of different mutants of PC proteins for loss of tight binding to mitotic chromatin. This type of analysis might be integral to identify what is the interaction partner of PC during mitosis.
The detailed study of PcG protein kinetic properties described here uncovered new insights into how PcG proteins function. In combination with the quantitative measurements of protein concentrations, it allows the comparison of dynamic transitions in different cell types and in different cell cycle stages. In addition it opens a door to the creation of mathematical models, that will allow the identification of which parameters of the system can best explain the observed changes in the plasticity of PcG-chromatin binding upon mitosis and differentiation in stem cells and in more determined lineages.

4.3 Mathematical modeling

The determination of molecule numbers, concentrations and kinetic constants gives insight into the absolute quantities and mobilities of free and bound PcG molecules in specific cell types in the endogenous situation, thus providing *in vivo* quantitation of an epigenetic system. These *in vivo* measurements will be essential for interpretation of models based on *in vitro* findings. Furthermore, this analysis enabled us to use quantitative mathematical modeling to examine the predicted behaviour of the system over time during an entire cell cycle. One of the advantages of cell cycle modeling is that by using known time constraints, one can examine transitions in PC binding in continuous time instead of snapshots that the FRAP analysis can provide. The most important insight provided by the model is the requirement for accelerated PC displacement in SOP cells, and the prediction that this may be provided by a reduction in association rate during prophase. I demonstrate that H3S28 phosphorylation is a good candidate mechanism for PC displacement during prophase and metaphase, in addition to its documented role in PcG displacement during interphase [123, 125]. The observation of accumulation of this double mark in prophase and metaphase is consistent with observations of mitotic accumulation of H3K9me3/S10p [126, 127], but is in contrast to a study [123] that reports only slight changes in levels of H3K27me3/S28p from interphase to metaphase in human fibroblasts. This discrepancy strongly suggests that the extent of mitotic S28 phosphorylation on K27 methylated H3 tails is cell-type specific, consistent with a potential role for this mark in distinguishing the mitotic behaviour of PC in SOPs and neuroblasts.

This model leaves some important questions unanswered. I could not determine the *in vivo* dissociation constant of PC for chromatin, as to do so it is necessary to know the number of binding sites in cells. Because it is virtually impossible to determine this number, I have used 80000 sites as the total number of binding sites. This number is based on the number of H3K27me3 tails in the *Drosophila* diploid genome extrapolated from the $\pm$100 H3K27me3 bands present in polytene chromosomes [13]. Nevertheless this approximation allowed the calculation of a K_d of 7–18μM which agrees with the value determined *in vitro* for the dissociation constant of the PC chromodomain with the H3K27me3 mark [10].

The model presented here allowed new insights into PC regulation in stem cells and differentiated cells. However, due to its simplicity I cannot provide a mechanism for the increased residence time of the small fraction of PC bound in mitosis. Additional experiments to uncover this mechanism, as well as a more

complex model which might include several populations of PC proteins and more PcG and TrxG interactors might provide us a more complete understanding of what is happening to PC-chromatin binding during mitosis.
An additional question pertains to the presence of this tightly bound fraction during interphase. In the mathematical model for PC behavior during cell cycle (Figure 3.16) all PC molecules are treated as belonging to a single population, whose properties change upon entry into mitosis. I note that a model in which a sub-population with long residence time exists during interphase, would also be compatible with the observed data, but such a subpopulation was not discernible from the FRAP recovery data.
Whether or not present in interphase, this small fraction of PC tightly bound in mitosis suggests a different binding modes for PC. Since H3K27me3S28p is associated with ejection of PC from chromatin, and the double mark is highly enriched on mitotic chromatin, additional mechanisms must contribute to the increased residence times of the small bound fraction of PH and PC that we observe in mitosis. These may include post-translational modifications of PC and PH proteins themselves [260], a switch of binding platform (e.g, from histone tails to DNA or RNA) and modification of recruiting or competing molecules (Figure 4.1).
Previous studies have reported that post-translational modifications of CBX proteins can have an effect on protein localisation and specificity for binding of histone marks [145, 156]. Furthermore, recent studies have shown that methylation of CBX2 can change its localisation and specific interaction with ncRNAs [16]. Taken together, these results show that there are precedents for regulation of PcG binding behavior through PTMs and indicate that the identification of mitosis-specific modifications of PcG proteins is of great interest.
I suggest that the accumulation of the H3K27me3S28p mark ejects PC from chromatin, thereby changing its binding partner from histones to other molecules. There are reports that PC and PH homologs can bind RNA [14, 16, 261] and DNA [22]. It is possible that these molecules are used specifically during mitosis to recruit PRC1 proteins and it would be interesting to study these interaction *in vivo* with more detail. If PRC1 binding to mitotic chromatin is similar in cell culture, the reduction of RNA levels by the addition of RNAses [262] could be performed and the kinetic properties of PC binding posteriorly analysed.
Furthermore, an additional layer of regulation could be the recruitment of or mitosis-specific interaction with TrxG or recruiting proteins. It has been shown by ChIP in synchronized mammalian cells that MLL1 is able to bind mitotic chromatin and to change its binding loci from interphase [192]. If similar pro-

cesses are occurring in the cells studied here, it is possible that changes in TrxG protein behavior may uncover new binding sites for PcG proteins, leading to the changes in the kinetic properties of PC and PH measured here. To gain further insight into the regulation of PC upon cell division, I have reduced the levels of JIL-1, a TrxG protein [263], which is the homolog of human MSK1 [264], known to phosphorylate H3S28 [123, 125], and of ASH1, one of the major TrxG proteins known to work antagonistically to PcG proteins [48]. The findings of an increased residence time of PC in interphase for both protein knockdowns indicates that both proteins counteract the binding of PC to its target sites (Figure 3.18). The mechanism for this effect are unknown and will be subject of further study, however one can speculate that JIL-1 phosphorylation of H3S28 reduces the affinity of PC for the neighbor H3K27me3 site, leading to a decrease in the residence time of PC. ASH1 might regulate the residence time of PC throughout two different mechanisms. First, the H3K4/K36 methylation activity on the common binding sites might reduce the affinity of PC and, second, through a direct competition for the binding sites. Interestingly, the number of bound PC molecules was not altered with both RNAi knockdowns suggesting that the amount of bound molecules is subject to further regulation. The analysis of the effect on PC of the knockdown of these proteins in metaphase showed a surprising reverse effect to the one registered in interphase (Figure 3.18). Both knockdowns lead to a decrease of the residence time when compared to wild-type cells and ASH1-RNAi leads to an increase in the bound fraction of PC molecules during metaphase. Interestingly, the reduction of average residence time registered in mitosis leads to maintenance of the binding parameters from interphase. This result suggests that both ASH1 and JIL-1 are essential for the switch in PC binding mode from interphase to metaphase. However it is unclear if this increased retention of PC on mitotic chromatin and faster kinetics are a result of direct interaction between PC and ASH1 or JIL-1 or a more global role of these proteins, since only ASH1 knockdown has a strong phenotype (Figure 3.19). Whether these proposed mechanisms directly contribute to mitotic PcG displacement and retention, and whether they are regulated differently in different lineages, will be key questions for future studies.

The extension of these quantitative studies to TrxG proteins and the inclusion of the PcG proteins studied here, into a more complex mathematical model will be a key extension of the work presented here. By knowing the quantities of ASH1 or JIL-1 and modeling the effects of the knockdown, one can hypothesize what is the role of these proteins: are they competing for the same binding sites or are they modifying the PcG binding sites? Further experiments to measure the levels of histone methylation marks correlated with active sites might be

useful, as well as methylation-dead mutants of ASH1 and kinase-dead mutants of JIL-1, to test the hypotheses generated by mathematical models.
Other models could describe the interaction of PRC1 proteins with chromatin in interphase and how they depend on E(Z), its methylation activity and DNA binding proteins, as well as other factors. Knockdown experiments in live animals, followed by quantitative binding measurements could be intercalated with refinements of the mathematical model. This iterative cycle between modeling and quantitative experiments in genetically tractable and defined systems, will allow for a better understanding of the complex regulation of PcG-chromatin interaction in mitosis and differentiation.

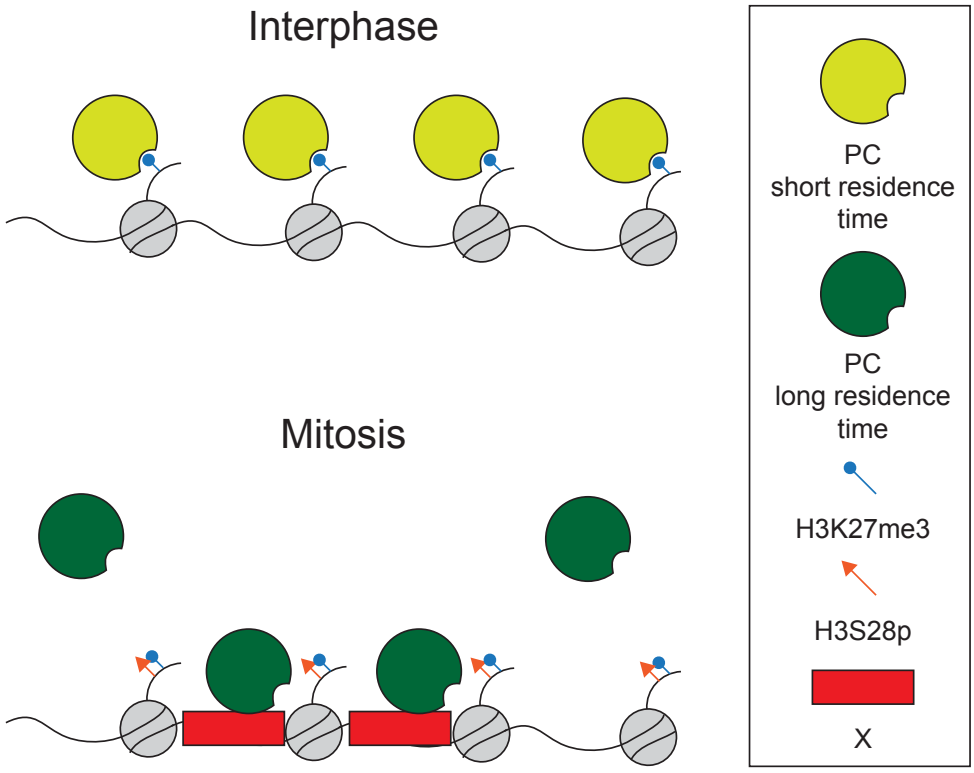

Figure 4.1: Model for interaction of Polycomb (PC) with chromatin during mitosis. During interphase PC binds chromatin through the interaction of its chromodomain with histone H3 trimethylated at serine 27 (H3K27me3). As cells enter mitosis, phosphorylation of H3S28 reduces the available binding sites for PC which, in parallel with the protein dilution at nuclear envelope breakdown, leads to the dispersion of PC from mitotic chromatin. Additional cell type specific processes (X) lead to a change in the overall binding properties of PC at metaphase, so that the remaining binding PC molecules are able to bind longer to chromatin. Such mechanisms may include post- translational modifications (PTM) of PcG proteins themselves, a switch of binding platform (e.g, from histone tails to DNA or RNA) and modification of recruiting or competing molecules.

4.4 Summary

In summary, I demonstrate here that the properties of the PcG proteins are not only different in different lineages, but can also be profoundly altered at mitosis. I propose that this regulation of PcG properties may be essential both to the stability of determined cell identities, and to the flexibility of the stem cell state. The combination of absolute quantification with analysis in living animals that I have used in this study offers three key advances to the study of epigenetic regulation: First, I examine single defined, genetically marked cell lineages as they go through mitosis and differentiation or self-renewal. Only in a living animal can we observe a defined mitotic event and its differentiated or self-renewed daughter cells. Second, only by quantifying absolute numbers of chromatin bound endogenous molecules, in real volumes, can we begin to understand the biological meaning of observed differences, in terms of cellular concentrations and protein abundance. Third, these quantitative measurements enable not only the comparison of dynamic transitions in different cell types but also enable meaningful mathematical models, identifying which parameters of the system can best explain the observed changes in the plasticity of PcG-chromatin binding upon mitosis and differentiation in stem cells and in more determined lineages.

Taken together, the combined use of live imaging and mathematical modeling in genetically tractable, dynamically changing *in vivo* experiments provides quantitative insight into how a system whose components are in constant flux can ensure both stability and flexibility.

5

Bibliography

[1] M. Ptashne, "On the use of the word 'epigenetic'.," *Current biology : CB*, vol. 17, pp. R233–6, Apr. 2007. 11

[2] L. Ringrose and R. Paro, "Epigenetic regulation of cellular memory by the Polycomb and Trithorax group proteins.," *Annual review of genetics*, vol. 38, pp. 413–443, 2004. 11, 12, 25

[3] J. A. Kennison, "The Polycomb and trithorax group proteins of Drosophila: trans-regulators of homeotic gene function.," *Annual review of genetics*, vol. 29, pp. 289–303, 1995. 11, 15

[4] J. A. Kennison, "Introduction to Trx-G and Pc-G genes.," *Methods in enzymology*, vol. 377, pp. 61–70, 2004. 11

[5] B. Schuettengruber, D. Chourrout, M. Vervoort, B. Leblanc, and G. Cavalli, "Genome regulation by polycomb and trithorax proteins," *Cell*, vol. 128, no. 4, pp. 735–745, 2007. 11, 12

[6] Z. Shao, F. Raible, R. Mollaaghababa, J. R. Guyon, C. T. Wu, W. Bender, and R. E. Kingston, "Stabilization of chromatin structure by PRC1, a Polycomb complex.," *Cell*, vol. 98, pp. 37–46, July 1999. 12, 13, 65

[7] S. S. Levine, A. Weiss, H. Erdjument-Bromage, Z. Shao, P. Tempst, and R. E. Kingston, "The core of the polycomb repressive complex is compositionally and functionally conserved in flies and humans.," *Molecular and cellular biology*, vol. 22, pp. 6070–6078, Sept. 2002. 12

[8] A. J. Saurin, Z. Shao, H. Erdjument-Bromage, P. Tempst, and R. E. Kingston, "A Drosophila Polycomb group complex includes Zeste and dTAFII proteins.," *Nature*, vol. 412, pp. 655–660, Aug. 2001. 12, 13, 65

[9] Z. Gao, J. Zhang, R. Bonasio, F. Strino, A. Sawai, F. Parisi, Y. Kluger, and D. Reinberg, "PCGF Homologs, CBX Proteins, and RYBP Define Functionally Distinct PRC1 Family Complexes," *Molecular cell*, vol. 45, pp. 344–356, Feb. 2012. 12, 21

[10] W. Fischle, Y. Wang, S. A. Jacobs, Y. Kim, C. D. Allis, and S. Khorasanizadeh, "Molecular basis for the discrimination of repressive

methyl-lysine marks in histone H3 by Polycomb and HP1 chromodomains.," *Genes & development*, vol. 17, pp. 1870–1881, Aug. 2003. 12, 16, 88

[11] M. D. Biggin, "Animal transcription networks as highly connected, quantitative continua.," *Developmental cell*, vol. 21, pp. 611–626, Oct. 2011. 12, 80

[12] J. S. Platero, T. Hartnett, and J. C. Eissenberg, "Functional analysis of the chromo domain of HP1.," *The EMBO journal*, vol. 14, pp. 3977–3986, Aug. 1995. 12

[13] L. Ringrose, H. Ehret, and R. Paro, "Distinct contributions of histone H3 lysine 9 and 27 methylation to locus-specific stability of polycomb complexes.," *Molecular cell*, vol. 16, pp. 641–653, Nov. 2004. 12, 16, 23, 31, 80, 88

[14] E. Bernstein, E. M. Duncan, O. Masui, J. Gil, E. Heard, and C. D. Allis, "Mouse Polycomb Proteins Bind Differentially to Methylated Histone H3 and RNA and Are Enriched in Facultative Heterochromatin," *Molecular and cellular biology*, vol. 26, pp. 2560–2569, Mar. 2006. 12, 89

[15] L. Morey, G. Pascual, L. Cozzuto, G. Roma, A. Wutz, S. A. Benitah, and L. Di Croce, "Nonoverlapping Functions of the Polycomb Group Cbx Family of Proteins in Embryonic Stem Cells," *Cell stem cell*, vol. 10, pp. 47–62, Jan. 2012. 12, 21

[16] L. Yang, C. Lin, W. Liu, J. Zhang, K. A. Ohgi, J. D. Grinstein, P. C. Dorrestein, and M. G. Rosenfeld, "ncRNA- and Pc2 Methylation-Dependent Gene Relocation between Nuclear Structures Mediates Gene Activation Programs," *Cell*, vol. 147, pp. 773–788, Nov. 2011. 13, 89

[17] J. W. Hodgson, N. N. Cheng, D. A. Sinclair, M. Kyba, N. B. Randsholt, and H. Brock, "The polyhomeotic locus of Drosophila melanogaster is transcriptionally and post-transcriptionally regulated during embryogenesis.," *Mechanisms of development*, vol. 66, pp. 69–81, Aug. 1997. 13

[18] A. J. Peterson, M. Kyba, D. Bornemann, K. Morgan, H. Brock, and J. Simon, "A domain shared by the Polycomb group proteins Scm and ph mediates heterotypic and homotypic interactions.," *Molecular and cellular biology*, vol. 17, pp. 6683–6692, Nov. 1997. 13

[19] C. A. Kim, M. R. Sawaya, D. Cascio, W. Kim, and J. U. Bowie, "Structural organization of a Sex-comb-on-midleg/polyhomeotic copolymer.," *The Journal of biological chemistry*, vol. 280, pp. 27769–27775, July 2005. 13

[20] M. C. Gambetta, K. Oktaba, and J. Müller, "Essential role of the glycosyltransferase sxc/Ogt in polycomb repression.," *Science (New York, N.Y.)*, vol. 325, pp. 93–96, July 2009. 13, 22

[21] D. J. Grau, J. M. Antao, and R. E. Kingston, "Functional dissection of Polycomb repressive complex 1 reveals the importance of a charged domain.," *Cold Spring Harbor symposia on quantitative biology*, vol. 75, pp. 61–70, 2010. 13, 17

[22] N. Francis, R. Kingston, and C. Woodcock, "Chromatin compaction by a polycomb group protein complex," *Science (New York, N.Y.)*, vol. 306, no. 5701, pp. 1574–1577, 2004. 13, 17, 89

[23] S. M. Lo, N. K. Ahuja, and N. J. Francis, "Polycomb group protein Suppressor 2 of zeste is a functional homolog of Posterior Sex Combs.," *Molecular and cellular biology*, vol. 29, pp. 515–525, Jan. 2009. 13, 21

[24] H. Wang, L. Wang, H. Erdjument-Bromage, M. Vidal, P. Tempst, R. Jones, and Y. Zhang, "Role of histone H2A ubiquitination in polycomb silencing," *Nature*, vol. 431, no. 7010, pp. 873–878, 2004. 13

[25] L. Wang, N. Jahren, E. L. Miller, C. S. Ketel, D. R. Mallin, and J. A. Simon, "Comparative analysis of chromatin binding by Sex Comb on Midleg (SCM) and other polycomb group repressors at a Drosophila Hox gene.," *Molecular and cellular biology*, vol. 30, pp. 2584–2593, June 2010. 13

[26] N. M. Mulholland, I. F. G. King, and R. E. Kingston, "Regulation of Polycomb group complexes by the sequence-specific DNA binding proteins Zeste and GAGA.," *Genes & development*, vol. 17, pp. 2741–2746, Nov. 2003. 13

[27] D. Huang, Y. Chang, C. Yang, I. Pan, and B. King, "pipsqueak encodes a factor essential for sequence-specific targeting of a polycomb group protein complex," *Molecular and cellular biology*, vol. 22, no. 17, pp. 6261–6271, 2002. 13

[28] D.-H. Huang and Y.-L. Chang, "Isolation and characterization of CHRASCH, a polycomb-containing silencing complex.," *Methods in enzymology*, vol. 377, pp. 267–282, 2004. 13

[29] F. Tie, T. Furuyama, J. Prasad-Sinha, E. Jane, and P. Harte, "The Drosophila Polycomb Group proteins ESC and E(Z) are present in a complex containing the histone-binding protein p55 and the histone deacetylase RPD3," *Development (Cambridge, England)*, vol. 128, no. 2, pp. 275–286, 2001. 13

[30] B. Czermin, R. Melfi, D. McCabe, V. Seitz, A. Imhof, and V. Pirrotta, "Drosophila enhancer of Zeste/ESC complexes have a histone H3 methyltransferase activity that marks chromosomal polycomb sites," *Cell*, vol. 111, no. 2, pp. 185–196, 2002. 13

[31] J. Müller, C. M. Hart, N. J. Francis, M. L. Vargas, A. Sengupta, B. Wild, E. L. Miller, M. B. O'Connor, R. E. Kingston, and J. A. Simon, "Histone methyltransferase activity of a Drosophila Polycomb group repressor complex.," *Cell*, vol. 111, pp. 197–208, Oct. 2002. 13

[32] R. Cao, L. Wang, H. Wang, L. Xia, H. Erdjument-Bromage, P. Tempst, R. S. Jones, and Y. Zhang, "Role of histone H3 lysine 27 methylation in Polycomb-group silencing.," *Science (New York, N.Y.)*, vol. 298, pp. 1039–1043, Nov. 2002. 13

[33] A. Kuzmichev, "Histone methyltransferase activity associated with a human multiprotein complex containing the Enhancer of Zeste protein," *Genes & development*, vol. 16, pp. 2893–2905, Nov. 2002. 13

[34] F. Tie, J. Prasad-Sinha, A. Birve, A. Rasmuson-Lestander, and P. Harte, "A 1-megadalton ESC/E(Z) complex from Drosophila that contains polycomblike and RPD3," *Molecular and cellular biology*, vol. 23, no. 9, pp. 3352–3362, 2003. 13

[35] A. He, X. Shen, Q. Ma, J. Cao, A. von Gise, P. Zhou, G. Wang, V. E. Marquez, S. H. Orkin, and W. T. Pu, "PRC2 directly methylates GATA4 and represses its transcriptional activity.," *Genes & development*, vol. 26, pp. 37–42, Jan. 2012. 13, 18, 22

[36] F. Tie, T. Furuyama, and P. Harte, "The Drosophila Polycomb Group proteins ESC and E(Z) bind directly to each other and co-localize at multiple chromosomal sites," *Development (Cambridge, England)*, vol. 125, no. 17, pp. 3483–3496, 1998. 13

[37] C. A. Jones, J. Ng, A. J. Peterson, K. Morgan, J. Simon, and R. S. Jones, "The Drosophila esc and E(z) proteins are direct partners in polycomb group-mediated repression.," *Molecular and cellular biology*, vol. 18, pp. 2825–2834, May 1998. 13

[38] D. Pasini, A. P. Bracken, M. R. Jensen, E. Lazzerini Denchi, and K. Helin, "Suz12 is essential for mouse development and for EZH2 histone methyltransferase activity.," *The EMBO journal*, vol. 23, pp. 4061–4071, Oct. 2004. 13

[39] T. Klymenko, B. Papp, W. Fischle, T. Köcher, M. Schelder, C. Fritsch, B. Wild, M. Wilm, and J. Müller, "A Polycomb group protein complex with sequence-specific DNA-binding and selective methyl-lysine-binding activities.," *Genes & development*, vol. 20, pp. 1110–1122, May 2006. 14

[40] K. Oktaba, L. Gutierrez, J. Gagneur, C. Girardot, A. K. Sengupta, E. E. M. Furlong, and J. Mueller, "Dynamic Regulation by Polycomb Group Protein Complexes Controls Pattern Formation and the Cell Cycle in Drosophila," *Developmental cell*, vol. 15, no. 6, pp. 877–889, 2008. 14, 19, 20

[41] S. Wu, R. C. Trievel, and J. C. Rice, "Human SFMBT is a transcriptional repressor protein that selectively binds the N-terminal tail of histone H3.," *FEBS letters*, vol. 581, pp. 3289–3296, July 2007. 14

[42] C. Grimm, R. Matos, N. Ly-Hartig, U. Steuerwald, D. Lindner, V. Rybin, J. Müller, and C. W. Müller, "Molecular recognition of histone lysine methylation by the Polycomb group repressor dSfmbt.," *The EMBO journal*, vol. 28, pp. 1965–1977, July 2009. 14

[43] S. Poux and R. Melfi, "Establishment of Polycomb silencing requires a transient interaction between PC and ESC," *Genes & development*, 2001. 14

[44] A. Mohd-Sarip, F. Venturini, G. E. Chalkley, and C. P. Verrijzer, "Pleiohomeotic can link polycomb to DNA and mediate transcriptional repression.," *Molecular and cellular biology*, vol. 22, pp. 7473–7483, Nov. 2002. 14, 75

[45] A. Lagarou, A. Mohd-Sarip, Y. M. Moshkin, G. E. Chalkley, K. Bezstarosti, J. A. A. Demmers, and C. P. Verrijzer, "dKDM2 couples histone H2A ubiquitylation to histone H3 demethylation during Polycomb group silencing," *Genes & development*, vol. 22, no. 20, pp. 2799–2810, 2008. 14

[46] J. C. Scheuermann, A. G. de Ayala Alonso, K. Oktaba, N. Ly-Hartig, R. K. McGinty, S. Fraterman, M. Wilm, T. W. Muir, and J. Müller, "Histone H2A deubiquitinase activity of the Polycomb repressive complex PR-DUB.," *Nature*, vol. 465, pp. 243–247, May 2010. 14

[47] B. Schuettengruber, A.-M. Martinez, N. Iovino, and G. Cavalli, "Trithorax group proteins: switching genes on and keeping them active.," *Nature reviews. Molecular cell biology*, vol. 12, pp. 799–814, Dec. 2011. 15

[48] T. Klymenko and J. Müller, "The histone methyltransferases Trithorax and Ash1 prevent transcriptional silencing by Polycomb group proteins.," *EMBO reports*, vol. 5, pp. 373–377, Apr. 2004. 15, 25, 75, 90

[49] C. Beisel, A. Imhof, J. Greene, E. Kremmer, and F. Sauer, "Histone methylation by the Drosophila epigenetic transcriptional regulator Ash1.," *Nature*, vol. 419, pp. 857–862, Oct. 2002. 15

[50] T. A. Milne, S. D. Briggs, H. W. Brock, M. E. Martin, D. Gibbs, C. D. Allis, and J. L. Hess, "MLL targets SET domain methyltransferase activity to Hox gene promoters.," *Molecular cell*, vol. 10, pp. 1107–1117, Nov. 2002. 15

[51] T. Nakamura, T. Mori, S. Tada, W. Krajewski, T. Rozovskaia, R. Wassell, G. Dubois, A. Mazo, C. M. Croce, and E. Canaani, "ALL-1 is a histone methyltransferase that assembles a supercomplex of proteins involved in transcriptional regulation.," *Molecular cell*, vol. 10, pp. 1119–1128, Nov. 2002. 15

[52] K. N. Byrd and A. Shearn, "ASH1, a Drosophila trithorax group protein, is required for methylation of lysine 4 residues on histone H3.," *Proceedings of the National Academy of Sciences of the United States of America*, vol. 100, pp. 11535–11540, Sept. 2003. 15

[53] Y. Tanaka, Z.-i. Katagiri, K. Kawahashi, D. Kioussis, and S. Kitajima, "Trithorax-group protein ASH1 methylates histone H3 lysine 36," *Gene*, vol. 397, no. 1-2, pp. 161–168, 2007. 15

[54] S. Beltran, M. Angulo, M. Pignatelli, F. Serras, and M. Corominas, "Functional dissection of the ash2 and ash1 transcriptomes provides insights into the transcriptional basis of wing phenotypes and reveals conserved protein interactions.," *Genome biology*, vol. 8, no. 4, p. R67, 2007. 15

[55] D. Schubert, O. Clarenz, and J. Goodrich, "Epigenetic control of plant development by Polycomb-group proteins," *Current Opinion in Plant Biology*, vol. 8, pp. 553–561, Oct. 2005. 15

[56] A. Sparmann and M. van Lohuizen, "Polycomb silencers control cell fate, development and cancer," *Nature Reviews Cancer*, vol. 6, pp. 846–856, Nov. 2006. 15

[57] B. Bello, N. Holbro, and H. Reichert, "Polycomb group genes are required for neural stem cell survival in postembryonic neurogenesis of Drosophila.," *Development (Cambridge, England)*, vol. 134, pp. 1091–1099, Mar. 2007. 15, 46

[58] R. A. Neumüller, C. Richter, A. Fischer, M. Novatchkova, K. G. Neumüller, and J. A. Knoblich, "Genome-Wide Analysis of Self-Renewal in Drosophila Neural Stem Cells by Transgenic RNAi," *Cell stem cell*, vol. 8, no. 5, pp. 580–593, 2011. 15, 46

[59] J. J. Touma, F. F. Weckerle, and M. D. Cleary, "Drosophila Polycomb complexes restrict neuroblast competence to generate motoneurons.," *Development (Cambridge, England)*, vol. 139, pp. 657–666, Feb. 2012. 15

[60] E. J. Sharp, E. C. Martin, and P. N. Adler, "Directed overexpression of suppressor 2 of zeste and Posterior Sex Combs results in bristle abnormalities in Drosophila melanogaster.," *Developmental biology*, vol. 161, pp. 379–392, Feb. 1994. 15, 46

[61] J. L. Mummery-Widmer, M. Yamazaki, T. Stoeger, M. Novatchkova, S. Bhalerao, D. Chen, G. Dietzl, B. J. Dickson, and J. A. Knoblich, "Genome-wide analysis of Notch signalling in Drosophila by transgenic RNAi," *Nature*, vol. 458, no. 7241, pp. 987–U59, 2009. 15, 46

[62] F. Janody, J. Lee, N. Jahren, D. Hazelett, A. Benlali, G. Miura, I. Draskovic, and J. Treisman, "A mosaic genetic screen reveals distinct roles for trithorax and polycomb group genes in Drosophila eye development," *Genetics*, vol. 166, no. 1, pp. 187–200, 2004. 15

[63] D. Ferres-Marco, I. Gutierrez-Garcia, D. Vallejo, J. Bolivar, F. Gutierrez-Avino, and M. Dominguez, "Epigenetic silencers and Notch collaborate to promote malignant tumours by Rb silencing," *Nature*, vol. 439, no. 7075, pp. 430–436, 2006. 15

[64] A.-M. Martinez, B. Schuettengruber, S. Sakr, A. Janic, C. Gonzalez, and G. Cavalli, "Polyhomeotic has a tumor suppressor activity mediated by repression of Notch signaling.," *Nature genetics*, vol. 41, pp. 1076–1082, Oct. 2009. 15, 21, 46

[65] L. Ringrose and R. Paro, "Polycomb/Trithorax response elements and epigenetic memory of cell identity," *Development (Cambridge, England)*, vol. 134, no. 2, pp. 223–232, 2007. 16, 25

[66] J. Simon, A. Chiang, W. Bender, M. J. Shimell, and M. O'Connor, "Elements of the Drosophila bithorax complex that mediate repression by Polycomb group products.," *Developmental biology*, vol. 158, pp. 131–144, July 1993. 16, 18

[67] C. S. Chan, L. Rastelli, and V. Pirrotta, "A Polycomb response element in the Ubx gene that determines an epigenetically inherited state of repression.," *The EMBO journal*, vol. 13, pp. 2553–2564, June 1994. 16, 18

[68] J. Gindhart and T. Kaufman, "Identification of Polycomb and Trithorax Group Responsive Elements in the Regulatory Region of the Drosophila Homeotic Gene Sex Combs Reduced," *Genetics*, vol. 139, no. 2, pp. 797–814, 1995. 16, 18

[69] L. Ringrose, M. Rehmsmeier, J.-M. Dura, and R. Paro, "Genome-wide prediction of Polycomb/Trithorax response elements in Drosophila melanogaster.," *Developmental cell*, vol. 5, pp. 759–771, Nov. 2003. 16, 18, 85

[70] J. Müller and J. A. Kassis, "Polycomb response elements and targeting of Polycomb group proteins in Drosophila.," *Current Opinion in Genetics & Development*, vol. 16, pp. 476–484, Oct. 2006. 16

[71] N. K. Matharu, T. Hussain, R. Sankaranarayanan, and R. K. Mishra, "Vertebrate homologue of Drosophila GAGA factor.," *Journal of molecular biology*, vol. 400, pp. 434–447, July 2010. 16

[72] C. J. Woo, P. V. Kharchenko, L. Daheron, P. J. Park, and R. E. Kingston, "A Region of the Human HOXD Cluster that Confers Polycomb-Group Responsiveness," *Cell*, vol. 140, no. 1, pp. 99–110, 2010. 16

[73] E. M. Mendenhall, R. P. Koche, T. Truong, V. W. Zhou, B. Issac, A. S. Chi, M. Ku, and B. E. Bernstein, "GC-rich sequence elements recruit PRC2 in mammalian ES cells.," *PLoS genetics*, vol. 6, no. 12, pp. e1001244–, 2010. 16, 17

[74] G. Li, R. Margueron, M. Ku, P. Chambon, B. E. Bernstein, and D. Reinberg, "Jarid2 and PRC2, partners in regulating gene expression," *Genes & development*, vol. 24, no. 4, pp. 368–380, 2010. 16

[75] D. Landeira, S. Sauer, R. Poot, M. Dvorkina, L. Mazzarella, H. F. Jorgensen, C. F. Pereira, M. Leleu, F. M. Piccolo, M. Spivakov, E. Brookes,

A. Pombo, C. Fisher, W. C. Skarnes, T. Snoek, K. Bezstarosti, J. Demmers, R. J. Klose, M. Casanova, L. Tavares, N. Brockdorff, M. Merkenschlager, and A. G. Fisher, "Jarid2 is a PRC2 component in embryonic stem cells required for multi-lineage differentiation and recruitment of PRC1 and RNA Polymerase II to developmental regulators," *Nature cell biology*, vol. 12, no. 6, pp. 618–U214, 2010. 16

[76] D. Pasini, P. A. C. Cloos, J. Walfridsson, L. Olsson, J.-P. Bukowski, J. V. Johansen, M. Bak, N. Tommerup, J. Rappsilber, and K. Helin, "JARID2 regulates binding of the Polycomb repressive complex 2 to target genes in ES cells," *Nature*, vol. 464, no. 7286, pp. 306–U193, 2010. 16

[77] N. Dietrich, M. Lerdrup, E. Landt, S. Agrawal-Singh, M. Bak, N. Tommerup, J. Rappsilber, E. Södersten, and K. Hansen, "REST-Mediated Recruitment of Polycomb Repressor Complexes in Mammalian Cells.," *PLoS genetics*, vol. 8, p. e1002494, Mar. 2012. 16

[78] M. Yu, T. Mazor, H. Huang, H.-T. Huang, K. L. Kathrein, A. J. Woo, C. R. Chouinard, A. Labadorf, T. E. Akie, T. B. Moran, H. Xie, S. Zacharek, I. Taniuchi, R. G. Roeder, C. F. Kim, L. I. Zon, E. Fraenkel, and A. B. Cantor, "Direct recruitment of polycomb repressive complex 1 to chromatin by core binding transcription factors.," *Molecular cell*, vol. 45, pp. 330–343, Feb. 2012. 16, 27

[79] Y. B. Schwartz, T. G. Kahn, D. A. Nix, X.-Y. Li, R. Bourgon, M. Biggin, and V. Pirrotta, "Genome-wide analysis of Polycomb targets in Drosophila melanogaster," *Nature genetics*, vol. 38, pp. 700–705, May 2006. 16, 18, 82

[80] N. Negre, J. Hennetin, L. V. Sun, S. Lavrov, M. Bellis, K. P. White, and G. Cavalli, "Chromosomal distribution of PcG proteins during drosophila development," *Plos Biology*, vol. 4, no. 6, pp. 917–932, 2006. 16, 18, 21

[81] B. Tolhuis, I. Muijrers, E. de Wit, H. Teunissen, W. Talhout, B. van Steensel, and M. van Lohuizen, "Genome-wide profiling of PRC1 and PRC2 polycomb chromatin binding in Drosophila melanogaster," *Nature genetics*, vol. 38, no. 6, pp. 694–699, 2006. 16, 18, 21

[82] K. H. Hansen, A. P. Bracken, D. Pasini, N. Dietrich, S. S. Gehani, A. Monrad, J. Rappsilber, M. Lerdrup, and K. Helin, "A model for transmission of the H3K27me3 epigenetic mark," *Nature cell biology*, vol. 10, no. 11, pp. 1291–U89, 2008. 16, 19

[83] K. H. Hansen and K. Helin, "Epigenetic inheritance through self-recruitment of the polycomb repressive complex 2.," *Epigenetics : official journal of the DNA Methylation Society*, vol. 4, pp. 133–138, Apr. 2009. 16, 19

[84] R. Margueron, N. Justin, K. Ohno, M. L. Sharpe, J. Son, W. J. I. Drury, P. Voigt, S. R. Martin, W. R. Taylor, V. De Marco, V. Pirrotta, D. Reinberg,

and S. J. Gamblin, "Role of the polycomb protein EED in the propagation of repressive histone marks," *Nature*, vol. 461, no. 7265, pp. 762–U11, 2009. 16

[85] B. Hekimoglu and L. Ringrose, "Non-coding RNAs in Polycomb/Trithorax regulation," *RNA biology*, vol. 6, no. 2, pp. 129–137, 2009. 16

[86] T. Sanchez-Elsner, D. Gou, E. Kremmer, and F. Sauer, "Noncoding RNAs of trithorax response elements recruit Drosophila Ash1 to Ultrabithorax.," *Science (New York, N.Y.)*, vol. 311, pp. 1118–1123, Feb. 2006. 17, 25

[87] J. Zhao, T. K. Ohsumi, J. T. Kung, Y. Ogawa, D. J. Grau, K. Sarma, J. J. Song, R. E. Kingston, M. Borowsky, and J. T. Lee, "Genome-wide identification of polycomb-associated RNAs by RIP-seq.," *Molecular cell*, vol. 40, pp. 939–953, Dec. 2010. 17, 25

[88] K. C. Wang, Y. W. Yang, B. Liu, A. Sanyal, R. Corces-Zimmerman, Y. Chen, B. R. Lajoie, A. Protacio, R. A. Flynn, R. A. Gupta, J. Wysocka, M. Lei, J. Dekker, J. A. Helms, and H. Y. Chang, "A long noncoding RNA maintains active chromatin to coordinate homeotic gene expression.," *Nature*, vol. 472, pp. 120–124, Apr. 2011. 17, 25

[89] M. Ku, R. P. Koche, E. Rheinbay, E. M. Mendenhall, M. Endoh, T. S. Mikkelsen, A. Presser, C. Nusbaum, X. Xie, A. S. Chi, M. Adli, S. Kasif, L. M. Ptaszek, C. A. Cowan, E. S. Lander, H. Koseki, and B. E. Bernstein, "Genomewide Analysis of PRC1 and PRC2 Occupancy Identifies Two Classes of Bivalent Domains," *PLoS genetics*, vol. 4, no. 10, pp. –, 2008. 17

[90] J. Zeng, B. D. Kirk, Y. Gou, Q. Wang, and J. Ma, "Genome-wide polycomb target gene prediction in Drosophila melanogaster.," *Nucleic Acids Research*, Mar. 2012. 17

[91] R. Eskeland, M. Leeb, G. R. Grimes, C. Kress, S. Boyle, D. Sproul, N. Gilbert, Y. Fan, A. I. Skoultchi, A. Wutz, and W. A. Bickmore, "Ring1B Compacts Chromatin Structure and Represses Gene Expression Independent of Histone Ubiquitination," *Molecular cell*, vol. 38, no. 3, pp. 452–464, 2010. 17

[92] D. J. Grau, B. A. Chapman, J. D. Garlick, M. Borowsky, N. J. Francis, and R. E. Kingston, "Compaction of chromatin by diverse Polycomb group proteins requires localized regions of high charge.," *Genes & development*, vol. 25, pp. 2210–2221, Oct. 2011. 17

[93] A. Breiling, B. M. Turner, M. E. Bianchi, and V. Orlando, "General transcription factors bind promoters repressed by Polycomb group proteins.," *Nature*, vol. 412, pp. 651–655, Aug. 2001. 17

[94] G. Dellino, Y. Schwartz, G. Farkas, D. McCabe, S. Elgin, and V. Pirrotta, "Polycomb silencing blocks transcription initiation," *Molecular cell*, vol. 13, no. 6, pp. 887–893, 2004. 17

[95] V. Chopra and J. Hong, "Regulation of Hox Gene Activity by Transcriptional Elongation in Drosophila 10.1016/j.cub.2009.02.055 : Current Biology — ScienceDirect.com," *Current biology*, 2009. 17

[96] D. Enderle, C. Beisel, M. B. Stadler, M. Gerstung, P. Athri, and R. Paro, "Polycomb preferentially targets stalled promoters of coding and noncoding transcripts.," *Genome research*, vol. 21, pp. 216–226, Feb. 2011. 17, 25, 82

[97] V. S. Chopra, D. A. Hendrix, L. J. Core, C. Tsui, J. T. Lis, and M. Levine, "The Polycomb Group Mutant esc Leads to Augmented Levels of Paused Pol II in the Drosophila Embryo," *Molecular cell*, vol. 42, pp. 837–844, June 2011. 17

[98] A. Kanhere, K. Viiri, C. C. Araújo, J. Rasaiyaah, R. D. Bouwman, W. A. Whyte, C. F. Pereira, E. Brookes, K. Walker, G. W. Bell, A. Pombo, A. G. Fisher, R. A. Young, and R. G. Jenner, "Short RNAs are transcribed from repressed polycomb target genes and interact with polycomb repressive complex-2.," *Molecular cell*, vol. 38, pp. 675–688, June 2010. 17

[99] J. K. Stock, S. Giadrossi, M. Casanova, E. Brookes, M. Vidal, H. Koseki, N. Brockdorff, A. G. Fisher, and A. Pombo, "Ring1-mediated ubiquitination of H2A restrains poised RNA polymerase II at bivalent genes in mouse ES cells.," *Nature cell biology*, vol. 9, pp. 1428–1435, Dec. 2007. 17

[100] T. Nakagawa, T. Kajitani, S. Togo, N. Masuko, H. Ohdan, Y. Hishikawa, T. Koji, T. Matsuyama, T. Ikura, M. Muramatsu, and T. Ito, "Deubiquitylation of histone H2A activates transcriptional initiation via trans-histone cross-talk with H3K4 di- and trimethylation," *Genes & Development*, vol. 22, pp. 37–49, Jan. 2008. 17

[101] W. Zhou, P. Zhu, J. Wang, G. Pascual, K. A. Ohgi, J. Lozach, C. K. Glass, and M. G. Rosenfeld, "Histione H2A monoubiquitination represses transcription by inhibiting RNA polymerase II transcriptional elongation," *Molecular cell*, vol. 29, no. 1, pp. 69–80, 2008. 17

[102] T. S. Mikkelsen, M. Ku, D. B. Jaffe, B. Issac, E. Lieberman, G. Giannoukos, P. Alvarez, W. Brockman, T.-K. Kim, R. P. Koche, W. Lee, E. Mendenhall, A. O'Donovan, A. Presser, C. Russ, X. Xie, A. Meissner, M. Wernig, R. Jaenisch, C. Nusbaum, E. S. Lander, and B. E. Bernstein, "Genome-wide maps of chromatin state in pluripotent and lineage-committed cells," *Nature*, vol. 448, pp. 553–560, July 2007. 17

[103] R. B. Deal, J. G. Henikoff, and S. Henikoff, "Genome-Wide Kinetics of Nucleosome Turnover Determined by Metabolic Labeling of Histones," *Science (New York, N.Y.)*, vol. 328, no. 5982, pp. 1161–1164, 2010. 18

[104] S. S. Teves and S. Henikoff, "Heat shock reduces stalled RNA polymerase II and nucleosome turnover genome-wide.," *Genes & development*, vol. 25, pp. 2387–2397, Nov. 2011. 18

[105] S. Poux, C. Kostic, and V. Pirrotta, "Hunchback-independent silencing of late Ubx enhancers by a Polycomb Group Response Element.," *The EMBO journal*, vol. 15, pp. 4713–4722, Sept. 1996. 18

[106] G. Cavalli and R. Paro, "The Drosophila Fab-7 chromosomal element conveys epigenetic inheritance during mitosis and meiosis.," *Cell*, vol. 93, pp. 505–518, May 1998. 18, 19

[107] G. Rank, M. Prestel, and R. Paro, "Transcription through intergenic chromosomal memory elements of the Drosophila bithorax complex correlates with an epigenetic switch.," *Molecular and cellular biology*, vol. 22, pp. 8026–8034, Nov. 2002. 18, 19, 25

[108] C. Maurange and R. Paro, "A cellular memory module conveys epigenetic inheritance of hedgehog expression during Drosophila wing imaginal disc development," *Genes & Development*, vol. 16, no. 20, pp. 2672–2683, 2002. 18

[109] S. Schmitt, M. Prestel, and R. Paro, "Intergenic transcription through a polycomb group response element counteracts silencing.," *Genes & Development*, vol. 19, pp. 697–708, Mar. 2005. 18, 25

[110] N. Lee, C. Maurange, L. Ringrose, and R. Paro, "Suppression of Polycomb group proteins by JNK signalling induces transdetermination in Drosophila imaginal discs.," *Nature*, vol. 438, pp. 234–237, Nov. 2005. 18

[111] H. Okulski, B. Druck, S. Bhalerao, and L. Ringrose, "Quantitative analysis of polycomb response elements (PREs) at identical genomic locations distinguishes contributions of PRE sequence and genomic environment," *Epigenetics & Chromatin*, vol. 4, pp. –, 2011. 18

[112] L. Perez, L. Barrio, D. Cano, U. M. Fiuza, M. Muzzopappa, and M. Milan, "Enhancer-PRE communication contributes to the expansion of gene expression domains in proliferating primordia," *Development (Cambridge, England)*, vol. 138, pp. 3125–3134, July 2011. 18

[113] A. P. Bracken, N. Dietrich, D. Pasini, K. H. Hansen, and K. Helin, "Genome-wide mapping of Polycomb target genes unravels their roles in cell fate transitions.," *Genes & development*, vol. 20, pp. 1123–1136, May 2006. 18, 19, 20

[114] T. Lee, R. Jenner, L. Boyer, M. Guenther, S. Levine, R. Kumar, B. Chevalier, S. Johnstone, M. Cole, K. Isono, H. Koseki, T. Fuchikami, K. Abe, H. Murray, J. Zucker, B. Yuan, G. Bell, E. Herbolsheimer, N. Hannett, K. Sun, D. Odom, A. Otte, T. Volkert, D. Bartel, D. Melton, D. Gifford, R. Jaenisch, and R. Young, "Control of developmental regulator's by polycomb in human embryonic stem cells," *Cell*, vol. 125, no. 2, pp. 301–313, 2006. 18, 20

[115] L. Boyer, K. Plath, J. Zeitlinger, T. Brambrink, L. Medeiros, T. Lee, S. Levine, M. Wernig, A. Tajonar, M. Ray, G. Bell, A. Otte, M. Vidal, D. Gifford, R. Young, and R. Jaenisch, "Polycomb complexes repress developmental regulators in murine embryonic stem cells," *Nature*, vol. 441, no. 7091, pp. 349–353, 2006. 18, 20

[116] F. Mohn, M. Weber, M. Rebhan, T. C. Roloff, J. Richter, M. B. Stadler, M. Bibel, and D. Schuebeler, "Lineage-specific polycomb targets and de novo DNA methylation define restriction and potential of neuronal progenitors," *Molecular cell*, vol. 30, no. 6, pp. 755–766, 2008. 19, 20

[117] C. Beisel, A. Buness, I. M. Roustan-Espinosa, B. Koch, S. Schmitt, S. A. Haas, M. Hild, T. Katsuyama, and R. Paro, "Comparing active and repressed expression states of genes controlled by the Polycomb/Trithorax group proteins.," *Proceedings of the National Academy of Sciences of the United States of America*, vol. 104, pp. 16615–16620, Oct. 2007. 19, 20

[118] C. Kwong, B. Adryan, I. Bell, L. Meadows, S. Russell, J. R. Manak, and R. White, "Stability and dynamics of polycomb target sites in Drosophila development," *PLoS genetics*, vol. 4, no. 9, p. e1000178, 2008. 19, 20, 46

[119] Y. B. Schwartz, T. G. Kahn, P. Stenberg, K. Ohno, R. Bourgon, and V. Pirrotta, "Alternative Epigenetic Chromatin States of Polycomb Target Genes," *PLoS genetics*, vol. 6, p. e1000805, Jan. 2010. 19, 20

[120] N. J. Francis, N. E. Follmer, M. D. Simon, G. Aghia, and J. D. Butler, "Polycomb Proteins Remain Bound to Chromatin and DNA during DNA Replication In Vitro," *Cell*, vol. 137, no. 1, pp. 110–122, 2009. 19, 87

[121] C. Lanzuolo, F. Lo Sardo, A. Diamantini, and V. Orlando, "PcG complexes set the stage for epigenetic inheritance of gene silencing in early S phase before replication.," *PLoS genetics*, vol. 7, pp. e1002370–, Nov. 2011. 19

[122] B. Hekimoglu-Balkan, A. Aszodi, R. Heinen, M. Jaritz, and L. Ringrose, "Intergenic Polycomb target sites are dynamically marked by non-coding transcription during lineage commitment.," *RNA biology*, vol. 9, Mar. 2012. 20, 25

[123] S. S. Gehani, S. Agrawal-Singh, N. Dietrich, N. S. Christophersen, K. Helin, and K. Hansen, "Polycomb group protein displacement and gene activation through MSK-dependent H3K27me3S28 phosphorylation.," *Molecular cell*, vol. 39, pp. 886–900, Sept. 2010. 20, 74, 75, 88, 90

[124] L. Stojic, Z. Jasencakova, C. Prezioso, A. Stuetzer, B. Bodega, D. Pasini, R. Klingberg, C. Mozzetta, R. Margueron, P. L. Puri, D. Schwarzer, K. Helin, W. Fischle, and V. Orlando, "Chromatin regulated interchange between polycomb repressive complex 2 (PRC2)-Ezh2 and PRC2-Ezh1 complexes controls myogenin activation in skeletal muscle cells," *Epigenetics & Chromatin*, vol. 4, pp. –, 2011. 20, 21

[125] P. N. I. Lau and P. Cheung, "Histone code pathway involving H3 S28 phosphorylation and K27 acetylation activates transcription and antagonizes polycomb silencing.," *Proceedings of the National Academy of Sciences of the United States of America*, vol. 108, pp. 2801–2806, Feb. 2011. 20, 74, 75, 88, 90

[126] W. Fischle, B. S. Tseng, H. L. Dormann, B. M. Ueberheide, B. A. Garcia, J. Shabanowitz, D. F. Hunt, H. Funabiki, and C. D. Allis, "Regulation of HP1-chromatin binding by histone H3 methylation and phosphorylation.," *Nature*, vol. 438, pp. 1116–1122, Dec. 2005. 20, 74, 88

[127] T. Hirota, J. J. Lipp, B.-H. Toh, and J.-M. Peters, "Histone H3 serine 10 phosphorylation by Aurora B causes HP1 dissociation from heterochromatin.," *Nature*, vol. 438, pp. 1176–1180, Dec. 2005. 20, 74, 88

[128] R. A. Varier, N. S. Outchkourov, P. de Graaf, F. M. A. van Schaik, H. J. L. Ensing, F. Wang, J. M. G. Higgins, G. J. P. L. Kops, and H. T. M. Timmers, "A phospho/methyl switch at histone H3 regulates TFIID association with mitotic chromosomes.," *The EMBO journal*, vol. 29, pp. 3967–3978, Dec. 2010. 20

[129] J. L. Brown, C. Fritsch, J. Mueller, and J. A. Kassis, "The Drosophila pho-like gene encodes a YY1-related DNA binding protein that is redundant with pleiohomeotic in homeotic gene silencing.," *Development (Cambridge, England)*, vol. 130, pp. 285–294, Jan. 2003. 21, 85

[130] R. L. Kurzhals, F. Tie, C. A. Stratton, and P. J. Harte, "Drosophila ESC-like can substitute for ESC and becomes required for Polycomb silencing if ESC is absent," *Developmental biology*, vol. 313, no. 1, pp. 293–306, 2008. 21

[131] H. Strutt and R. Paro, "The polycomb group protein complex of Drosophila melanogaster has different compositions at different target genes.," *Molecular and cellular biology*, vol. 17, pp. 6773–6783, Dec. 1997. 21

[132] B. Schuettengruber, M. Ganapathi, B. Leblanc, M. Portoso, R. Jaschek, B. Tolhuis, M. van Lohuizen, A. Tanay, and G. Cavalli, "Functional Anatomy of Polycomb and Trithorax Chromatin Landscapes in Drosophila Embryos," *Plos Biology*, vol. 7, no. 1, pp. 146–163, 2009. 21, 82

[133] F. Pelegri and R. Lehmann, "A role of polycomb group genes in the regulation of gap gene expression in Drosophila.," *Genetics*, vol. 136, pp. 1341–1353, Apr. 1994. 21

[134] J. Jacobs, K. Kieboom, S. Marino, R. DePinho, and M. van Lohuizen, "The oncogene and Polycomb-group gene bmi-1 regulates cell proliferation and senescence through the ink4a locus," *Nature*, vol. 397, no. 6715, pp. 164–168, 1999. 21

[135] A. Saj, Z. Arziman, D. Stempfle, W. van Belle, U. Sauder, T. Horn, M. Dürrenberger, R. Paro, M. Boutros, and G. Merdes, "A combined ex vivo and in vivo RNAi screen for notch regulators in Drosophila reveals an extensive notch interaction network.," *Developmental cell*, vol. 18, pp. 862–876, May 2010. 21, 84

[136] K. Mousavi, H. Zare, A. H. Wang, and V. Sartorelli, "Polycomb Protein Ezh1 Promotes RNA Polymerase II Elongation.," *Molecular cell*, vol. 45, pp. 255–262, Jan. 2012. 21

[137] R. Margueron, G. Li, K. Sarma, A. Blais, J. Zavadil, C. L. Woodcock, B. D. Dynlacht, and D. Reinberg, "Ezh1 and Ezh2 maintain repressive chromatin through different mechanisms.," *Molecular cell*, vol. 32, pp. 503–518, Nov. 2008. 21

[138] X. Shen, Y. Liu, Y.-J. Hsu, Y. Fujiwara, J. Kim, X. Mao, G.-C. Yuan, and S. H. Orkin, "EZH1 mediates methylation on histone H3 lysine 27 and complements EZH2 in maintaining stem cell identity and executing pluripotency.," *Molecular cell*, vol. 32, pp. 491–502, Nov. 2008. 21

[139] A. Kuzmichev, T. Jenuwein, P. Tempst, and D. Reinberg, "Different EZH2-containing complexes target methylation of histone H1 or nucleosomal histone H3.," *Molecular cell*, vol. 14, pp. 183–193, Apr. 2004. 21

[140] A. Kuzmichev, R. Margueron, A. Vaquero, T. Preissner, M. Scher, A. Kirmizis, X. Ougang, N. Brockdorff, C. Abate-Shen, P. Farnham, and D. Reinberg, "Composition and histone substrates of polycomb repressive group complexes change during cellular differentiation," *Proceedings of the National Academy of Sciences of the United States of America*, vol. 102, no. 6, pp. 1859–1864, 2005. 21

[141] L. Wang, N. Jahren, M. L. Vargas, E. F. Andersen, J. Benes, J. Zhang, E. L. Miller, R. S. Jones, and J. A. Simon, "Alternative ESC and ESC-like subunits of a polycomb group histone methyltransferase complex are differentially deployed during Drosophila development.," *Molecular and cellular biology*, vol. 26, pp. 2637–2647, Apr. 2006. 21

[142] K. Ohno, D. McCabe, B. Czermin, A. Imhof, and V. Pirrotta, "ESC, ESCL and their roles in Polycomb Group mechanisms.," *Mechanisms of development*, vol. 125, pp. 527–541, Apr. 2008. 21

[143] J. Ng, C. Hart, and K. Morgan, "A Drosophila ESC-E(Z) Protein Complex Is Distinct from Other Polycomb Group Complexes and Contains Covalently Modified ESC," *Molecular and Cellular . . .*, 2000. 22

[144] F. Tie, A. Siebold, and P. Harte, "The N-terminus of Drosophila ESC mediates its phosphorylation and dimerization," *Biochemical and Biophysical Research Communications*, vol. 332, no. 2, pp. 622–632, 2005. 22

[145] A. Hatano, M. Matsumoto, T. Higashinakagawa, and K. I. Nakayama, "Phosphorylation of the chromodomain changes the binding specificity

of Cbx2 for methylated histone H3," *Biochemical and Biophysical Research Communications*, vol. 397, no. 1, pp. 93–99, 2010. 22, 89

[146] G. Caretti, D. Palacios, V. Sartorelli, and P. L. Puri, "Phosphoryl-EZH-ion.," *Cell stem cell*, vol. 8, pp. 262–265, Mar. 2011. 22

[147] S. Kaneko, G. Li, J. Son, C.-F. Xu, R. Margueron, T. A. Neubert, and D. Reinberg, "Phosphorylation of the PRC2 component Ezh2 is cell cycle-regulated and up-regulates its binding to ncRNA.," *Genes & development*, vol. 24, pp. 2615–2620, Dec. 2010. 22, 32

[148] S. Chen, L. R. Bohrer, A. N. Rai, Y. Pan, L. Gan, X. Zhou, A. Bagchi, J. A. Simon, and H. Huang, "Cyclin-dependent kinases regulate epigenetic gene silencing through phosphorylation of EZH2.," *Nature*, vol. 12, pp. 1108–1114, Nov. 2010. 22

[149] Y. Wei, Y.-H. Chen, L.-Y. Li, J. Lang, S.-P. Yeh, B. Shi, C.-C. Yang, J.-Y. Yang, C.-Y. Lin, C.-C. Lai, and M.-C. Hung, "CDK1-dependent phosphorylation of EZH2 suppresses methylation of H3K27 and promotes osteogenic differentiation of human mesenchymal stem cells," *Nature*, vol. 13, no. 1, pp. 87–U211, 2011. 22

[150] T.-L. Cha, B. P. Zhou, W. Xia, Y. Wu, C.-C. Yang, C.-T. Chen, B. Ping, A. P. Otte, and M.-C. Hung, "Akt-mediated phosphorylation of EZH2 suppresses methylation of lysine 27 in histone H3.," *Science (New York, N.Y.)*, vol. 310, pp. 306–310, Oct. 2005. 22

[151] D. Palacios, C. Mozzetta, S. Consalvi, G. Caretti, V. Saccone, V. Proserpio, V. E. Marquez, S. Valente, A. Mai, S. V. Forcales, V. Sartorelli, and P. L. Puri, "TNF/p38/polycomb signaling to Pax7 locus in satellite cells links inflammation to the epigenetic control of muscle regeneration.," *Cell stem cell*, vol. 7, pp. 455–469, Oct. 2010. 22

[152] J. Voncken, D. Schweizer, and L. Aagaard, "Chromatin-association of the Polycomb group protein BMI1 is cell cycle-regulated and correlates with its phosphorylation status," *Journal of cell . . .* , 1999. 22, 27

[153] J. Voncken, H. Niessen, B. Neufeld, U. Rennefahrt, V. Dahlmans, N. Kubben, B. Holzer, S. Ludwig, and U. Rapp, "MAPKAP kinase 3pK phosphorylates and regulates chromatin association of the polycomb group protein Bmi1," *The Journal of biological chemistry*, vol. 280, no. 7, pp. 5178–5187, 2005. 22

[154] S. Elderkin, G. N. Maertens, M. Endoh, D. L. Mallery, N. Morrice, H. Koseki, G. Peters, N. Brockdorff, and K. Hiom, "A phosphorylated form of mel-18 targets the Ring1B histone H2A ubliquitin ligase to chromatin," *Molecular cell*, vol. 28, no. 1, pp. 107–120, 2007. 22

[155] L. Palko, H. W. Bass, M. J. Beyrouthy, and M. M. Hurt, "The Yin Yang-1 (YY1) protein undergoes a DNA-replication-associated switch in localization from the cytoplasm to the nucleus at the onset of S phase.," *Journal of cell science*, vol. 117, pp. 465–476, Jan. 2004. 22

[156] K. Noguchi, R. Shiurba, and T. Higashinakagawa, "Nuclear translocation of mouse Polycomb M33 protein in regenerating liver," *Biochemical and Biophysical Research Communications*, vol. 291, no. 3, pp. 508–515, 2002. 23, 89

[157] X. Chen, M. Hiller, Y. Sancak, and M. T. Fuller, "Tissue-specific TAFs counteract Polycomb to turn on terminal differentiation.," *Science (New York, N.Y.)*, vol. 310, pp. 869–872, Nov. 2005. 23

[158] J. Wang, R. M. Kumar, V. J. Biggs, H. Lee, Y. Chen, M. H. Kagey, R. A. Young, and C. Abate-Shen, "The Msx1 Homeoprotein Recruits Polycomb to the Nuclear Periphery during Development.," *Developmental cell*, vol. 21, pp. 575–588, Sept. 2011. 23

[159] R. Phair and T. Misteli, "High mobility of proteins in the mammalian cell nucleus," *Nature*, vol. 404, no. 6778, pp. 604–+, 2000. 23

[160] R. Phair, P. Scaffidi, C. Elbi, J. Vecerova, A. Dey, K. Ozato, D. Brown, G. Hager, M. Bustin, and T. Misteli, "Global nature of dynamic protein-chromatin interactions in vivo: Three-dimensional genome scanning and dynamic interaction networks of chromatin proteins," *Molecular and cellular biology*, vol. 24, no. 14, pp. 6393–6402, 2004. 23, 84

[161] E. Meshorer, D. Yellajoshula, E. George, P. Scambler, D. Brown, and T. Mistell, "Hyperdynamic plasticity in pluripotent embryonic of chromatin proteins stem cells," *Developmental cell*, vol. 10, no. 1, pp. 105–116, 2006. 23, 85

[162] G. Giglia-Mari, A. F. Theil, P.-O. Mari, S. Mourgues, J. Nonnekens, L. O. Andrieux, J. de Wit, C. Miquel, N. Wijgers, A. Maas, M. Fousteri, J. H. J. Hoeijmakers, and W. Vermeulen, "Differentiation Driven Changes in the Dynamic Organization of Basal Transcription Initiation," *Plos Biology*, vol. 7, no. 10, pp. –, 2009. 23, 24, 85

[163] G. Ficz, R. Heintzmann, and D. J. Arndt-Jovin, "Polycomb group protein complexes exchange rapidly in living Drosophila.," *Development (Cambridge, England)*, vol. 132, pp. 3963–3976, Sept. 2005. 23, 39, 45, 46, 50, 69, 80, 81, 83, 84, 85

[164] T. Cheutin and G. Cavalli, "Progressive Polycomb Assembly on H3K27me3 Compartments Generates Polycomb Bodies with Developmentally Regulated Motion.," *PLoS genetics*, vol. 8, p. e1002465, Jan. 2012. 23

[165] I. Hernández-Muñoz, P. Taghavi, C. Kuijl, J. Neefjes, and M. van Lohuizen, "Association of BMI1 with polycomb bodies is dynamic and requires PRC2/EZH2 and the maintenance DNA methyltransferase DNMT1.," *Molecular and cellular biology*, vol. 25, pp. 11047–11058, Dec. 2005. 24

[166] X. Ren, C. Vincenz, and T. K. Kerppola, "Changes in the distributions and dynamics of Polycomb repressive complexes during embryonic stem cell differentiation," *Molecular and cellular biology*, vol. 28, no. 9, pp. 2884–2895, 2008. 24

[167] D. Prescott and M. Bender, "Synthesis of Rna and Protein During Mitosis in Mammalian Tissue Culture Cells," *Experimental Cell Research*, vol. 26, no. 2, pp. 260–&, 1962. 25

[168] M. A. Martínez-Balbás, A. Dey, S. K. Rabindran, K. Ozato, and C. Wu, "Displacement of sequence-specific transcription factors from mitotic chromatin.," *Cell*, vol. 83, pp. 29–38, Oct. 1995. 25

[169] J. Gottesfeld and D. Forbes, "Mitotic repression of the transcriptional machinery," *Trends in Biochemical Sciences*, vol. 22, no. 6, pp. 197–202, 1997. 25

[170] R. Sims, K. Nishioka, and D. Reinberg, "Histone lysine methylation: a signature for chromatin function," *Trends in genetics : TIG*, vol. 19, no. 11, pp. 629–639, 2003. 25

[171] S. Henikoff and A. Shilatifard, "Histone modification: cause or cog?," *Trends in genetics : TIG*, vol. 27, pp. 389–396, Oct. 2011. 25

[172] A. N. D. Scharf, T. K. Barth, and A. Imhof, "Establishment of histone modifications after chromatin assembly.," *Nucleic Acids Research*, vol. 37, pp. 5032–5040, Aug. 2009. 25

[173] L. Wang, J. L. Brown, R. Cao, Y. Zhang, J. A. Kassis, and R. S. Jones, "Hierarchical recruitment of polycomb group silencing complexes.," *Molecular cell*, vol. 14, pp. 637–646, June 2004. 25, 82, 84

[174] J. L. Rinn, M. Kertesz, J. K. Wang, S. L. Squazzo, X. Xu, S. A. Brugmann, L. H. Goodnough, J. A. Helms, P. J. Farnham, E. Segal, and H. Y. Chang, "Functional demarcation of active and silent chromatin domains in human HOX loci by noncoding RNAs.," *Cell*, vol. 129, pp. 1311–1323, June 2007. 25

[175] L. Sessa, A. Breiling, G. Lavorgna, L. Silvestri, G. Casari, and V. Orlando, "Noncoding RNA synthesis and loss of Polycomb group repression accompanies the colinear activation of the human HOXA cluster.," *RNA (New York, N.Y.)*, vol. 13, pp. 223–239, Feb. 2007. 25

[176] W. A. Krajewski, T. Nakamura, A. Mazo, and E. Canaani, "A motif within SET-domain proteins binds single-stranded nucleic acids and transcribed and supercoiled DNAs and can interfere with assembly of nucleosomes.," *Molecular and cellular biology*, vol. 25, pp. 1891–1899, Mar. 2005. 25

[177] A. K. Sengupta, A. Kuhrs, and J. Müller, "General transcriptional silencing by a Polycomb response element in Drosophila.," *Development (Cambridge, England)*, vol. 131, pp. 1959–1965, May 2004. 25

[178] Y. Mito, J. G. Henikoff, and S. Henikoff, "Genome-scale profiling of histone H3.3 replacement patterns.," *Nature genetics*, vol. 37, pp. 1090–1097, Oct. 2005. 25

[179] R. K. Ng and J. B. Gurdon, "Epigenetic memory of an active gene state depends on histone H3.3 incorporation into chromatin in the absence of transcription," *Nature cell biology*, vol. 10, pp. 102–109, Dec. 2007. 25

[180] T. A. Milne, J. Kim, G. G. Wang, S. C. Stadler, V. Basrur, S. J. Whitcomb, Z. Wang, A. J. Ruthenburg, K. S. J. Elenitoba-Johnson, R. G. Roeder, and C. D. Allis, "Multiple interactions recruit MLL1 and MLL1 fusion proteins to the HOXA9 locus in leukemogenesis.," *Molecular cell*, vol. 38, pp. 853–863, June 2010. 26

[181] R. Zhao, T. Nakamura, Y. Fu, Z. Lazar, and D. L. Spector, "Gene bookmarking accelerates the kinetics of post-mitotic transcriptional reactivation," *Nature cell biology*, vol. 13, pp. 1295–1304, Oct. 2011. 26

[182] D. Chen, C. Hinkley, and R. Henry, "TBP Dynamics in Living Human Cells: Constitutive Association of TBP with Mitotic Chromosomes," *Molecular biology of the . . .*, 2002. 26

[183] D. Chen, M. Dundr, C. Wang, A. Leung, A. Lamond, T. Misteli, and S. Huang, "Condensed mitotic chromatin is accessible to transcription factors and chromatin structural proteins.," *The Journal of cell biology*, vol. 168, pp. 41–54, Jan. 2005. 26

[184] A. Green, A. Lonn, K. H. Peterson, K. Ollinger, and I. Rundquist, "Translocation of Histone H1 Subtypes Between Chromatin and Cytoplasm During Mitosis in Normal Human Fibroblasts," in *Cytometry Part A*, pp. 478–484, Linkoping Univ, Div Cell Biol, Dept Clin & Expt Med, Fac Hlth Sci, SE-58185 Linkoping, Sweden, 2010. 26

[185] S. P. Hergeth, M. Dundr, P. Tropberger, B. M. Zee, B. A. Garcia, S. Daujat, and R. Schneider, "Isoform-specific phosphorylation of human linker histone H1.4 in mitosis by the kinase Aurora B," *Journal of cell science*, vol. 124, no. 10, pp. 1623–1628, 2011. 26, 87

[186] M. Harrer, H. Lührs, M. Bustin, U. Scheer, and R. Hock, "Dynamic interaction of HMGA1a proteins with chromatin.," *Journal of cell science*, vol. 117, pp. 3459–3471, July 2004. 27

[187] J. Hutchins, W. Moore, F. Hood, and J. Wilson, "Phosphorylation Regulates the Dynamic Interaction of RCC1 with Chromosomes during Mitosis 10.1016/j.cub.2004.05.021 : Current Biology — ScienceDirect.com," *Current biology*, 2004. 27, 87

[188] L. Fanti, B. Perrini, L. Piacentini, M. Berloco, E. Marchetti, G. Palumbo, and S. Pimpinelli, "The trithorax group and Pc group proteins are differentially involved in heterochromatin formation in Drosophila.," *Chromosoma*, vol. 117, pp. 25–39, Feb. 2008. 27, 86

[189] P. Buchenau, J. Hodgson, H. Strutt, and D. J. Arndt-Jovin, "The distribution of polycomb-group proteins during cell division and development in Drosophila embryos: impact on models for silencing.," *The Journal of cell biology*, vol. 141, no. 2, pp. 469–481, 1998. 27, 46, 84, 86

[190] H. Miyagishima, K. Isono, Y. Fujimura, M. Iyo, Y. Takihara, H. Masumoto, M. Vidal, and H. Koseki, "Dissociation of mammalian Polycomb-group proteins, Ring1B and Rae28/Ph1, from the chromatin correlates with configuration changes of the chromatin in mitotic and meiotic prophase.," *Histochemistry and cell biology*, vol. 120, pp. 111–119, Aug. 2003. 27

[191] C. Vincenz and T. K. Kerppola, "Different polycomb group CBX family proteins associate with distinct regions of chromatin using nonhomologous protein sequences," *Proceedings of the National Academy of Sciences of the United States of America*, vol. 105, no. 43, pp. 16572–16577, 2008. 27

[192] G. A. Blobel, S. Kadauke, E. Wang, A. W. Lau, J. Zuber, M. M. Chou, and C. R. Vakoc, "A Reconfigured Pattern of MLL Occupancy within Mitotic Chromatin Promotes Rapid Transcriptional Reactivation Following Mitotic Exit," *Molecular cell*, vol. 36, no. 6, pp. 970–983, 2009. 27, 89

[193] S. Dietzel, H. Niemann, B. Brückner, C. Maurange, and R. Paro, "The nuclear distribution of Polycomb during Drosophila melanogaster development shown with a GFP fusion protein," *Chromosoma*, vol. 108, no. 2, pp. 83–94, 1999. 27, 45, 46

[194] A. Schwendemann and M. Lehmann, "Pipsqueak and GAGA factor act in concert as partners at homeotic and many other loci.," *Proceedings of the National Academy of Sciences of the United States of America*, vol. 99, pp. 12883–12888, Oct. 2002. 27

[195] D. W. Young, M. Q. Hassan, X.-Q. Yang, M. Galindo, A. Javed, S. K. Zaidi, P. Furcinitti, D. Lapointe, M. Montecino, J. B. Lian, J. L. Stein, A. J. van Wijnen, and G. S. Stein, "Mitotic retention of gene expression patterns by the cell fate-determining transcription factor Runx2.," *Proceedings of the National Academy of Sciences of the United States of America*, vol. 104, pp. 3189–3194, Feb. 2007. 27

[196] A. Mogilner, R. Wollman, and W. F. Marshall, "Quantitative modeling in cell biology: what is it good for?," *Developmental cell*, vol. 11, pp. 279–287, Sept. 2006. 29

[197] C. C. Fowlkes, C. L. L. Hendriks, S. V. E. Keränen, G. H. Weber, O. Rübel, M.-Y. Huang, S. Chatoor, A. H. DePace, L. Simirenko, C. Henriquez, A. Beaton, R. Weiszmann, S. Celniker, B. Hamann, D. W. Knowles, M. D. Biggin, M. B. Eisen, and J. Malik, "A quantitative spatiotemporal atlas of gene expression in the Drosophila blastoderm.," *Cell*, vol. 133, pp. 364–374, Apr. 2008. 29, 32

[198] The modENCODE Consortium, S. Roy, J. Ernst, P. V. Kharchenko, P. Kheradpour, N. Negre, M. L. Eaton, J. M. Landolin, C. A. Bristow, L. Ma,

M. F. Lin, S. Washietl, B. I. Arshinoff, F. Ay, P. E. Meyer, N. Robine, N. L. Washington, L. Di Stefano, E. Berezikov, C. D. Brown, R. Candeias, J. W. Carlson, A. Carr, I. Jungreis, D. Marbach, R. Sealfon, M. Y. Tolstorukov, S. Will, A. A. Alekseyenko, C. Artieri, B. W. Booth, A. N. Brooks, Q. Dai, C. A. Davis, M. O. Duff, X. Feng, A. A. Gorchakov, T. Gu, J. G. Henikoff, P. Kapranov, R. Li, H. K. MacAlpine, J. Malone, A. Minoda, J. Nordman, K. Okamura, M. Perry, S. K. Powell, N. C. Riddle, A. Sakai, A. Samsonova, J. E. Sandler, Y. B. Schwartz, N. Sher, R. Spokony, D. Sturgill, M. van Baren, K. H. Wan, L. Yang, C. Yu, E. Feingold, P. Good, M. Guyer, R. Lowdon, K. Ahmad, J. Andrews, B. Berger, S. E. Brenner, M. R. Brent, L. Cherbas, S. C. R. Elgin, T. R. Gingeras, R. Grossman, R. A. Hoskins, T. C. Kaufman, W. Kent, M. I. Kuroda, T. Orr-Weaver, N. Perrimon, V. Pirrotta, J. W. Posakony, B. Ren, S. Russell, P. Cherbas, B. R. Graveley, S. Lewis, G. Micklem, B. Oliver, P. J. Park, S. E. Celniker, S. Henikoff, G. H. Karpen, E. C. Lai, D. M. MacAlpine, L. D. Stein, K. P. White, M. Kellis, D. Acevedo, R. Auburn, G. Barber, H. J. Bellen, E. P. Bishop, T. D. Bryson, A. Chateigner, J. Chen, H. Clawson, C. L. G. Comstock, S. Contrino, L. C. DeNapoli, Q. Ding, A. Dobin, M. H. Domanus, J. Drenkow, S. Dudoit, J. Dumais, T. Eng, D. Fagegaltier, S. E. Gadel, S. Ghosh, F. Guillier, D. Hanley, G. J. Hannon, K. D. Hansen, E. Heinz, A. S. Hinrichs, M. Hirst, S. Jha, L. Jiang, Y. L. Jung, H. Kashevsky, C. D. Kennedy, E. T. Kephart, L. Langton, O. K. Lee, S. Li, Z. Li, W. Lin, D. Linder-Basso, P. Lloyd, R. Lyne, S. E. Marchetti, M. Marra, N. R. Mattiuzzo, S. McKay, F. Meyer, D. Miller, S. W. Miller, R. A. Moore, C. A. Morrison, J. A. Prinz, M. Rooks, R. Moore, K. M. Rutherford, P. Ruzanov, D. A. Scheftner, L. Senderowicz, P. K. Shah, G. Shanower, R. Smith, E. O. Stinson, S. Suchy, A. E. Tenney, F. Tian, K. J. T. Venken, H. Wang, R. White, J. Wilkening, A. T. Willingham, C. Zaleski, Z. Zha, D. Zhang, Y. Zhao, and J. Zieba, "Identification of Functional Elements and Regulatory Circuits by Drosophila modENCODE," *Science (New York, N.Y.)*, vol. 330, pp. 1787–1797, Dec. 2010. 29

[199] M. B. Gerstein, Z. J. Lu, E. L. Van Nostrand, C. Cheng, B. I. Arshinoff, T. Liu, K. Y. Yip, R. Robilotto, A. Rechtsteiner, K. Ikegami, P. Alves, A. Chateigner, M. Perry, M. Morris, R. K. Auerbach, X. Feng, J. Leng, A. Vielle, W. Niu, K. Rhrissorrakrai, A. Agarwal, R. P. Alexander, G. Barber, C. M. Brdlik, J. Brennan, J. J. Brouillet, A. Carr, M. S. Cheung, H. Clawson, S. Contrino, L. O. Dannenberg, A. F. Dernburg, A. Desai, L. Dick, A. C. Dose, J. Du, T. Egelhofer, S. Ercan, G. Euskirchen, B. Ewing, E. A. Feingold, R. Gassmann, P. J. Good, P. Green, F. Gullier, M. Gutwein, M. S. Guyer, L. Habegger, T. Han, J. G. Henikoff, S. R. Henz, A. Hinrichs, H. Holster, T. Hyman, A. L. Iniguez, J. Janette, M. Jensen, M. Kato, W. J. Kent, E. Kephart, V. Khivansara, E. Khurana, J. K. Kim, P. Kolasinska-Zwierz, E. C. Lai, I. Latorre, A. Leahey, S. Lewis, P. Lloyd, L. Lochovsky, R. F. Lowdon, Y. Lubling, R. Lyne, M. MacCoss, S. D. Mackowiak, M. Mangone, S. McKay, D. Mecenas, G. Merrihew, D. M. Miller, A. Muroyama, J. I. Murray, S. L. Ooi, H. Pham, T. Phippen, E. A. Preston, N. Rajewsky, G. Ratsch, H. Rosenbaum, J. Rozowsky, K. Rutherford, P. Ruzanov, M. Sarov, R. Sasidharan, A. Sboner, P. Scheid, E. Se-

gal, H. Shin, C. Shou, F. J. Slack, C. Slightam, R. Smith, W. C. Spencer, E. O. Stinson, S. Taing, T. Takasaki, D. Vafeados, K. Voronina, G. Wang, N. L. Washington, C. M. Whittle, B. Wu, K. K. Yan, G. Zeller, Z. Zha, M. Zhong, X. Zhou, modENCODE Consortium, J. Ahringer, S. Strome, K. C. Gunsalus, G. Micklem, X. S. Liu, V. Reinke, S. K. Kim, L. W. Hillier, S. Henikoff, F. Piano, M. Snyder, L. Stein, J. D. Lieb, and R. H. Waterston, "Integrative Analysis of the Caenorhabditis elegans Genome by the modENCODE Project," *Science (New York, N.Y.)*, vol. 330, pp. 1775–1787, Dec. 2010. 29

[200] E. A. Sobie, Y.-S. Lee, S. L. Jenkins, and R. Iyengar, "Systems biology–biomedical modeling.," *Science signaling*, vol. 4, p. tr2, Sept. 2011. 29

[201] T. Cheutin, S. A. Gorski, K. M. May, P. B. Singh, and T. Misteli, "In vivo dynamics of Swi6 in yeast: evidence for a stochastic model of heterochromatin.," *Molecular and cellular biology*, vol. 24, pp. 3157–3167, Apr. 2004. 29, 30

[202] D. Canzio, E. Y. Chang, S. Shankar, K. M. Kuchenbecker, M. D. Simon, H. D. Madhani, G. J. Narlikar, and B. Al-Sady, "Chromodomain-mediated oligomerization of HP1 suggests a nucleosome-bridging mechanism for heterochromatin assembly.," *Molecular cell*, vol. 41, pp. 67–81, Jan. 2011. 29

[203] I. B. Dodd, M. A. Micheelsen, K. Sneppen, and G. Thon, "Theoretical analysis of epigenetic cell memory by nucleosome modification.," *Cell*, vol. 129, pp. 813–822, May 2007. 30

[204] M. A. Micheelsen, N. Mitarai, K. Sneppen, and I. B. Dodd, "Theory for the stability and regulation of epigenetic landscapes.," *Physical biology*, vol. 7, no. 2, pp. 026010–, 2010. 30

[205] D. De Vos, F. Frederiks, M. Terweij, T. van Welsem, K. F. Verzijlbergen, E. Iachina, E. L. de Graaf, A. F. M. Altelaar, G. Oudgenoeg, A. J. R. Heck, J. Krijgsveld, B. M. Bakker, and F. van Leeuwen, "Progressive methylation of ageing histones by Dot1 functions as a timer.," *EMBO reports*, vol. 12, pp. 956–962, Sept. 2011. 30, 31

[206] A. Angel, J. Song, C. Dean, and M. Howard, "A Polycomb-based switch underlying quantitative epigenetic memory.," *Nature*, vol. 476, pp. 105–108, Aug. 2011. 30

[207] L. K. Nguyen, J. Munoz-Garcia, H. Maccario, A. Ciechanover, W. Kolch, and B. N. Kholodenko, "Switches, Excitable Responses and Oscillations in the Ring1B/Bmi1 Ubiquitination System," *Plos Computational Biology*, vol. 7, no. 12, pp. –, 2011. 30, 31

[208] H. Binder, L. Steiner, T. Rohlf, S. Prohaska, and J. Galle, "Transcriptional memory emerges from cooperative histone modifications," *Nature Precedings*, 2011. 31

[209] M. M. Harrison, M. R. Botchan, and T. W. Cline, "Grainyhead and Zelda compete for binding to the promoters of the earliest-expressed Drosophila genes.," *Developmental biology*, vol. 345, pp. 248–255, Sept. 2010. 32

[210] V. Raia, M. Schilling, M. Boehm, B. Hahn, A. Kowarsch, A. Raue, C. Sticht, S. Bohl, M. Saile, P. Moeller, N. Gretz, J. Timmer, F. Theis, W.-D. Lehmann, P. Lichter, and U. Klingmueller, "Dynamic Mathematical Modeling of IL13-Induced Signaling in Hodgkin and Primary Mediastinal B-Cell Lymphoma Allows Prediction of Therapeutic Targets," *Cancer Research*, vol. 71, no. 3, pp. 693–704, 2011. 32

[211] D. G. Spiller, C. D. Wood, D. A. Rand, and M. R. H. White, "Measurement of single-cell dynamics.," *Nature*, vol. 465, pp. 736–745, June 2010. 32, 33, 35

[212] M. Bantscheff, M. Schirle, G. Sweetman, J. Rick, and B. Kuster, "Quantitative mass spectrometry in proteomics: a critical review," *Analytical and Bioanalytical Chemistry*, vol. 389, no. 4, pp. 1017–1031, 2007. 32

[213] H. G. Stunnenberg and M. Vermeulen, "Towards cracking the epigenetic code using a combination of high-throughput epigenomics and quantitative mass spectrometry-based proteomics.," *BioEssays : news and reviews in molecular, cellular and developmental biology*, vol. 33, pp. 547–551, July 2011. 32

[214] J.-Q. Wu and T. D. Pollard, "Counting cytokinesis proteins globally and locally in fission yeast.," *Science (New York, N.Y.)*, vol. 310, pp. 310–314, Oct. 2005. 32

[215] A. Charpilienne, M. Nejmeddine, M. Berois, N. Parez, E. Neumann, E. Hewat, G. Trugnan, and J. Cohen, "Individual rotavirus-like particles containing 120 molecules of fluorescent protein are visible in living cells.," *The Journal of biological chemistry*, vol. 276, pp. 29361–29367, Aug. 2001. 32, 56

[216] M. Dundr, J. G. McNally, J. Cohen, and T. Misteli, "Quantitation of GFP-fusion proteins in single living cells," *Journal of structural biology*, vol. 140, no. 1-3, pp. 92–99, 2002. 32, 56, 57, 80

[217] G. Rabut, V. Doye, and J. Ellenberg, "Mapping the dynamic organization of the nuclear pore complex inside single living cells," *Nature cell biology*, vol. 6, no. 11, pp. 1114–1121, 2004. 32, 57, 80

[218] E. L. Elson, "Fluorescence correlation spectroscopy: past, present, future.," *Biophysical journal*, vol. 101, pp. 2855–2870, Dec. 2011. 32

[219] A. Abu-Arish, A. Porcher, A. Czerwonka, N. Dostatni, and C. Fradin, "High mobility of bicoid captured by fluorescence correlation spectroscopy: implication for the rapid establishment of its gradient.," *Biophysical journal*, vol. 99, pp. L33–5, Aug. 2010. 32

[220] J. G. McNally, "Quantitative FRAP in analysis of molecular binding dynamics in vivo.," *Methods in cell biology*, vol. 85, pp. 329–351, 2008. 32, 43, 60, 61, 64, 65, 81

[221] N. Plachta, T. Bollenbach, S. Pease, S. E. Fraser, and P. Pantazis, "Oct4 kinetics predict cell lineage patterning in the early mammalian embryo.," *Nature cell biology*, vol. 13, pp. 117–123, Feb. 2011. 34

[222] T. K. Kerppola, "Bimolecular fluorescence complementatlon: Visualization of molecular interactions in living cells," *Fluorescent Proteins, Second Edition*, vol. 85, pp. 431–+, 2008. 34

[223] D. Mazza, T. J. Stasevich, T. S. Karpova, and J. G. McNally, "Monitoring dynamic binding of chromatin proteins in vivo by fluorescence correlation spectroscopy and temporal image correlation spectroscopy.," *Methods in molecular biology (Clifton, N.J.)*, vol. 833, pp. 177–200, 2012. 34

[224] D. W. Piston and G.-J. Kremers, "Fluorescent protein FRET: the good, the bad and the ugly," *Trends in Biochemical Sciences*, vol. 32, pp. 407–414, Sept. 2007. 34

[225] F. Mueller, T. S. Karpova, D. Mazza, and J. G. McNally, "Monitoring dynamic binding of chromatin proteins in vivo by fluorescence recovery after photobleaching.," *Methods in molecular biology (Clifton, N.J.)*, vol. 833, pp. 153–176, 2012. 34

[226] B. L. Sprague, F. Müller, R. L. Pego, P. M. Bungay, D. A. Stavreva, and J. G. McNally, "Analysis of binding at a single spatially localized cluster of binding sites by fluorescence recovery after photobleaching.," *Biophysical journal*, vol. 91, pp. 1169–1191, Aug. 2006. 34, 42, 60, 81, 133

[227] J. Beaudouin, F. Mora-Bermúdez, T. Klee, N. Daigle, and J. Ellenberg, "Dissecting the contribution of diffusion and interactions to the mobility of nuclear proteins.," *Biophysical journal*, vol. 90, pp. 1878–1894, Mar. 2006. 34, 42, 60, 61, 66, 68, 81, 119, 131, 133, 134

[228] F. Mueller, P. Wach, and J. G. McNally, "Evidence for a common mode of transcription factor interaction with chromatin as revealed by improved quantitative fluorescence recovery after photobleaching.," *Biophysical journal*, vol. 94, no. 8, pp. 3323–3339, 2008. 34, 42, 61, 64, 65, 68, 81, 83, 84, 127, 131, 132, 133, 134

[229] S. K. Bowman, V. Rolland, J. Betschinger, K. A. Kinsey, G. Emery, and J. A. Knoblich, "The tumor suppressors Brat and Numb regulate transit-amplifying neuroblast lineages in Drosophila.," *Developmental cell*, vol. 14, pp. 535–546, Apr. 2008. 35, 77

[230] F. Roegiers, S. Younger-Shepherd, L. Y. Jan, and Y. N. Jan, "Two types of asymmetric divisions in the Drosophila sensory organ precursor cell lineage.," *Nature cell biology*, vol. 3, pp. 58–67, Jan. 2001. 35

[231] T. Hermle, D. Saltukoglu, J. Grünewald, G. Walz, and M. Simons, "Regulation of Frizzled-dependent planar polarity signaling by a V-ATPase subunit.," *Current biology : CB*, vol. 20, pp. 1269–1276, July 2010. 35

[232] C. Q. Doe, "Neural stem cells: balancing self-renewal with differentiation.," *Development (Cambridge, England)*, vol. 135, pp. 1575–1587, May 2008. 36

[233] R. A. Neumueller and J. A. Knoblich, "Dividing cellular asymmetry: asymmetric cell division and its implications for stem cells and cancer," *Genes & development*, vol. 23, no. 23, pp. 2675–2699, 2009. 36

[234] J. Betschinger, K. Mechtler, and J. A. Knoblich, "Asymmetric segregation of the tumor suppressor brat regulates self-renewal in Drosophila neural stem cells.," *Cell*, vol. 124, pp. 1241–1253, Mar. 2006. 40

[235] J. P. Fonseca, P. A. Steffen, S. Müller, J. Lu, A. Sawicka, C. Seiser, and L. Ringrose, "In vivo polycomb kinetics and mitotic chromatin binding distinguish stem cells from differentiated cells," *Genes & Development*, vol. 26, pp. –, Apr. 2012. 40, 41, 119

[236] C. Gänger, *Quantitative Analysis and Live Imaging of Polycomb Group Proteins in Drosophila melanogaster*. PhD thesis, University of Vienna, 2010. 45, 46, 81, 82

[237] E. Dworschak, "Generation and characterisation of ash-1-egfp transgenic fly lines for live imaging of ash1," Master's thesis, Fachhochschule Campus Wien, 2009. 46

[238] C.-Y. Lee, R. O. Andersen, C. Cabernard, L. Manning, K. D. Tran, M. J. Lanskey, A. Bashirullah, and C. Q. Doe, "Drosophila Aurora-A kinase inhibits neuroblast self-renewal by regulating aPKC/Numb cortical polarity and spindle orientation," *Genes & development*, vol. 20, no. 24, pp. 3464–3474, 2006. 47, 71, 87

[239] S. R. Wheeler, J. B. Kearney, A. R. Guardiola, and S. T. Crews, "Single-cell mapping of neural and glial gene expression in the developing Drosophila CNS midline cells.," *Developmental biology*, vol. 294, no. 2, pp. 509–524, 2006. 47

[240] Y. Bellaïche, M. Gho, J. A. Kaltschmidt, A. H. Brand, and F. Schweisguth, "Frizzled regulates localization of cell-fate determinants and mitotic spindle rotation during asymmetric cell division," *Nature cell biology*, vol. 3, no. 1, pp. 50–57, 2001. 41, 47

[241] E. Bier, H. Vaessin, S. Younger-Shepherd, L. Jan, and Y. Jan, "deadpan, an essential pan-neural gene in Drosophila, encodes a helix-loop-helix protein similar to the hairy gene product.," *Genes & development*, vol. 6, no. 11, p. 2137, 1992. 49

[242] F. Mueller, D. Mazza, T. J. Stasevich, and J. G. McNally, "FRAP and kinetic modeling in the analysis of nuclear protein dynamics: what do we really know?," *Current opinion in cell biology*, vol. 22, pp. 403–411, June 2010. 61

[243] B. Mayer, G. Emery, D. Berdnik, F. Wirtz-Peitz, and J. A. Knoblich, "Quantitative analysis of protein dynamics during asymmetric cell division.," *Current biology : CB*, vol. 15, pp. 1847–1854, Oct. 2005. 71, 87

[244] S. J. Nowak and V. G. Corces, "Phosphorylation of histone H3: a balancing act between chromosome condensation and transcriptional activation.," *Trends in genetics : TIG*, vol. 20, pp. 214–220, Apr. 2004. 73

[245] R. Giet and D. M. Glover, "Drosophila aurora B kinase is required for histone H3 phosphorylation and condensin recruitment during chromosome condensation and to organize the central spindle during cytokinesis.," *The Journal of cell biology*, vol. 152, pp. 669–682, Feb. 2001. 74

[246] H. Goto, Y. Tomono, K. Ajiro, H. Kosako, M. Fujita, M. Sakurai, K. Okawa, A. Iwamatsu, T. Okigaki, T. Takahashi, and M. Inagaki, "Identification of a novel phosphorylation site on histone H3 coupled with mitotic chromosome condensation.," *The Journal of biological chemistry*, vol. 274, pp. 25543–25549, Sept. 1999. 74

[247] J. Déjardin, A. Rappailles, O. Cuvier, C. Grimaud, M. Decoville, D. Locker, and G. Cavalli, "Recruitment of Drosophila Polycomb group proteins to chromatin by DSP1.," *Nature*, vol. 434, pp. 533–538, Mar. 2005. 75

[248] S. Netter, M. Faucheux, and L. Theodore, "Developmental dynamics of a polyhomeotic-EGFP fusion in vivo," *Dna and Cell Biology*, vol. 20, no. 8, pp. 483–492, 2001. 79

[249] G. Ficz, *Protein dynamics in the nucleus: Implications for gene expression*. PhD thesis, Georg-August-Universitä t, Göttingen, Germany, 2005. 79

[250] I. Solovei, M. Kreysing, C. Lanctôt, S. Kösem, L. Peichl, T. Cremer, J. Guck, and B. Joffe, "Nuclear architecture of rod photoreceptor cells adapts to vision in mammalian evolution.," *Cell*, vol. 137, pp. 356–368, Apr. 2009. 80

[251] H. M. Krause, R. Klemenz, and W. J. Gehring, "Expression, modification, and localization of the fushi tarazu protein in Drosophila embryos.," *Genes & Development*, vol. 2, pp. 1021–1036, Aug. 1988. 80

[252] J. Yao, K. M. Munson, W. W. Webb, and J. T. Lis, "Dynamics of heat shock factor association with native gene loci in living cells.," *Nature*, vol. 442, pp. 1050–1053, Aug. 2006. 80

[253] T. J. Stasevich, F. Mueller, A. Michelman-Ribeiro, T. Rosales, J. R. Knutson, and J. G. McNally, "Cross-Validating FRAP and FCS to Quantify the Impact of Photobleaching on In Vivo Binding Estimates," *Biophysical journal*, vol. 99, no. 9, pp. 3093–3101, 2010. 81

[254] C. Pallier, P. Scaffidi, S. Chopineau-Proust, A. Agresti, P. Nordmann, M. E. Bianchi, and V. Marechal, "Association of chromatin proteins high mobility group box (HMGB) 1 and HMGB2 with mitotic chromosomes.," *Molecular biology of the cell*, vol. 14, pp. 3414–3426, Aug. 2003. 82

[255] D. Zink and R. Paro, "Drosophila Polycomb-group regulated chromatin inhibits the accessibility of a trans-activator to its target DNA.," *The EMBO journal*, vol. 14, pp. 5660–5671, Nov. 1995. 82

[256] J. Hodgson, B. Argiropoulos, and H. Brock, "Site-specific recognition of a 70-base-pair element containing d(GA)(n) repeats mediates bithoraxoid polycomb group response element-dependent silencing," *Molecular and cellular biology*, vol. 21, no. 14, pp. 4528–4543, 2001. 82

[257] N. Negre, C. D. Brown, L. Ma, C. A. Bristow, S. W. Miller, U. Wagner, P. Kheradpour, M. L. Eaton, P. Loriaux, R. Sealfon, Z. Li, H. Ishii, R. F. Spokony, J. Chen, L. Hwang, C. Cheng, R. P. Auburn, M. B. Davis, M. Domanus, P. K. Shah, C. A. Morrison, J. Zieba, S. Suchy, L. Senderowicz, A. Victorsen, N. A. Bild, A. J. Grundstad, D. Hanley, D. M. MacAlpine, M. Mannervik, K. Venken, H. Bellen, R. White, M. Gerstein, S. Russell, R. L. Grossman, B. Ren, J. W. Posakony, M. Kellis, and K. P. White, "A cis-regulatory map of the Drosophila genome.," *Nature*, vol. 471, pp. 527–531, Mar. 2011. 82

[258] A. K. Robinson, B. Z. Leal, L. V. Chadwell, R. Wang, U. Ilangovan, Y. Kaur, S. E. Junco, V. Schirf, P. A. Osmulski, M. Gaczynska, A. P. Hinck, B. Demeler, D. G. McEwen, and C. A. Kim, "The growth-suppressive function of the Polycomb group protein Polyhomeotic is mediated by polymerization of its sterile alpha motif (SAM) domain.," *Journal of Biological Chemistry*, Jan. 2012. 84

[259] N. Francis, "Mechanisms of epigenetic inheritance Copying of polycomb repressed chromatin," *Cell Cycle*, 2009. 87

[260] H. E. C. Niessen, J. A. Demmers, and J. W. Voncken, "Talking to chromatin: post-translational modulation of polycomb group function.," *Epigenetics & Chromatin*, vol. 2, no. 1, pp. 10–, 2009. 89

[261] H. Zhang, A. Christoforou, L. Aravind, S. W. Emmons, S. van den Heuvel, and D. A. Haber, "The C. elegans Polycomb gene SOP-2 encodes an RNA binding protein.," *Molecular cell*, vol. 14, pp. 841–847, June 2004. 89

[262] C. Muchardt, M. Guilleme, J.-S. Seeler, D. Trouche, A. Dejean, and M. Yaniv, "Coordinated methyl and RNA binding is required for heterochromatin localization of mammalian HP1alpha.," *EMBO reports*, vol. 3, pp. 975–981, Oct. 2002. 89

[263] W. Zhang, Y. Jin, Y. Ji, J. Girton, J. Johansen, and K. M. Johansen, "Genetic and phenotypic analysis of alleles of the Drosophila chromosomal JIL-1 kinase reveals a functional requirement at multiple developmental stages.," *Genetics*, vol. 165, pp. 1341–1354, Nov. 2003. 90

[264] Y. Jin, Y. Wang, D. L. Walker, H. Dong, C. Conley, J. Johansen, and K. M. Johansen, "JIL-1: a novel chromosomal tandem kinase implicated in transcriptional regulation in Drosophila.," *Molecular cell*, vol. 4, pp. 129–135, July 1999. 90

6

Contributions

The experimental work in this study was designed and performed by João Pedro Fonseca under the supervision of Dr. Leonie Ringrose, unless noted below.

Philipp Steffen performed ELISA experiments, wrote MATLAB scripts, and was fundamental in discussion of FRAP and modeling experiments.

Dr. Stefan Müller collaborated in the implementation of mathematical models and wrote Appendix C.

Dr. James Lu wrote the Mathematica adaptation of the FRAP model described in [227].

Parts of this thesis have been merged into a manuscript, which has been accepted for publication [235]. The manuscript was jointly written by João Pedro Fonseca and Dr. Leonie Ringrose, and is shown in Appendix E as a galley proof.

7

Acknowledgments

In the end of this thesis I would like to thank Leonie for all her constant support and encouragement, and the contagious energy that she brings to work everyday. Her mentoring and leadership made my time in the lab very enjoyable and I cannot fully express how I am grateful for that. Additionally, I would like to apologize for ruining your eyesight.
I would also like to thank my thesis committee, Juergen Knoblich and Carrie Cowan, for their help and advice in our meetings. I am grateful towards Juergen Knoblich, Wendy Bickmore and Florian Raible for accepting to review my thesis and be my examiners. In addition, I want to thank Pawel Pasierbek for help in setting up the live imaging procedure, Didier Poncet and Annie Charpilienne for supplying GFP-VLPs, Florian Mueller for Matlab files and advice on FRAP, Jennifer Mummery-Widmer, Federico Mauri, Anja Fischer, Catarina Homem, Spyros Goulas, Elif Eroglu, Ilka Reichardt and others from the Knoblich lab for reagents, fly stocks, advice with dissection techniques and many helpful discussions and good fun in the shared fly room.
Special thanks to my lab mates, present and past. They provided the best work environment that I can only hope to find again. I would like to thank Philipp for sharing extremely interesting and long discussions and the frustration with the ever changing numbers. I would like to express my gratitude towards Betül, Robert, Frank, Helena and Philipp for being so much more than colleagues. Thank you for cigarrete breaks, table soccer, and any chance that you gave me to have a nice chat. You are the best!
Finally I would like to thank Catarina, Flávia, Nuno, António and Branka for sharing great moments (such good food!) and always being there for the last 5 years. I am grateful to my family for all their encouragement in starting this adventure, and their constant care and love. I wish to express my love and gratitude to Marisa for all her support, understanding and confidence in me. This would not be possible without you.

8

Curriculum Vitae

JOÃO PEDRO FONSECA

address
Högelmüllergasse 6/23
1050, Vienna, Austria

mail joao.fonseca@imba.oeaw.ac.at
mail joaopfonseca@gmail.com
tel +43 1 79044 - 4653

Profile

Nationality: Portuguese

Birthdate: 30th March, 1984

Birthplace: Barreiro, Portugal

Experience

PhD, IMBA Vienna, Austria, 2007-2012
PhD thesis project on "Kinetic properties of Polycomb Group Proteins during differentation and mitosis of live *Drosophila"* performed in Dr. Leonie Ringrose's laboratory

Internship, IMBA Vienna, Austria, 2007
Analysis of DNA methylation changes upon stem cell differentiation, performed in Dr. Leonie Ringrose's laboratory

Internship, ITQB Oeiras, Portugal, 2007
SOS response in *S. aureus*, performed in Dr. Mariana Pinho's laboratory

Internship, IMM Lisboa, Portugal, 2006-2007
Roles of actin in gene regulation, performed in J. Ferreira's laboratory

Internship, KCL London, UK, 2006
Undergrad thesis project on "Integration-defective lentiviral vectors for muscle gene therapy", performed in M. Antoniou's laboratory

Monitor, UNL Lisbon, Portugal, 2005-2006
Autonomous Section of Biotechnology, Faculty of Science and Tecnology, New University of Lisbon

Education

New University of Lisbon, Lisbon, Portugal — Degree in Cell and Molecular Biology, 2002-2006

University of Vienna, Vienna, Austria — PhD in Molecular Biology, 2007-2012

Additional Education

Joint EMBL-EBI-Wellcome Trust Course: In silico Systems Biology, Hinxton, UK, 2012

13th Annual Live Cell Microscopy Course, Vancouver, Canada, 2008

4th Course on Epigenetics, Paris, France, 2008

Presentations

1st Epigenesys Annual Meeting, Vienna, Austria, 2011

Focus on Microscopy 2009, Krakow, Poland, 2009

Publications

Fonseca, JP., *et al*. *In vivo* Polycomb kinetics and mitotic chromatin binding distinguish stem cells from differentiated cells. 2012. Genes & Development. *In press*

Appendix A

Supplementary tables

Table A.1: Quantification parameters of PH::GFP, PC::GFP, GFP::DSP1, GFP::PHO and GFP::nls in Neuroblast interphase (NB) and metaphase (NBmet), SOP interphase (SOP) and metaphase (SOPmet), pIIa interphase (pIIa) and pIIb interphase (pIIb). Volume measurements in cubic micrometers, determined by GFP fluorescence (Blue masks in Figure 3.6 and Figure 3.7), are shown (A), as well as number and micromolar concentrations of GFP-fused (B,C), total endogenous + GFP-fused (D,E) and endogenous in *yw* flies (F, G) molecules of PH, PC, DSP1, PHO and E(Z).

	Variable ID	Volume (μm^3) A	# GFP B	μM GFP C	# end + GFP D	μM end + GFP E	# end yw F	μM end yw G
PH:GFP	NB	239.55 ± 26.43	139409 ± 16220	0.98 ± 0.06	153169 ± 17821	1.06 ± 0.17	37189 ± 4327	0.26 ± 0.04
	NBmet	682.99 ± 97.67	74930 ± 8811	0.19 ± 0.03	82326 ± 9681	0.20 ± 0.04	19988 ± 2350	0.05 ± 0.01
	SOP	149.26 ± 12.12	119147 ± 25089	1.36 ± 0.39				
	SOPmet	752.52 ± 31.53	133038 ± 22613	0.29 ± 0.04				
	pIIa	72.71 ± 2.65	37372 ± 2367	0.86 ± 0.02				
	pIIb	53.86 ± 4.40	25656 ± 2059	0.80 ± 0.01				
PC::GFP	NB	176.33 ± 9.56	73350 ± 8201	0.70 ± 0.08	97698 ± 10923	0.69 ± 0.09	40615 ± 9306	0.38 ± 0.09
	NBmet	726.72 ± 74.88	118877 ± 12065	0.27 ± 0.02	158337 ± 16070	0.27 ± 0.04	65823 ± 14762	0.15 ± 0.03
	SOP	171.60 ± 5.94	37461± 3090	0.36 ± 0.02	57850 ± 4772	0.36 ± 0.03	48474 ± 13310	0.48 ± 0.13
	SOPmet	590.66 ± 37.02	39228 ± 3145	0.11 ± 0.01	600578 ± 4857	0.11 ± 0.01	50762 ± 13904	0.14 ± 0.04
	pIIa	97.15 ± 11.59	20902 ± 2222	0.36 ± 0.03	32278 ± 3431	0.36 ± 0.06	27048 ± 7646	0.48 ± 0.13
	pIIb	68.62 ± 9.76	14749 ± 1484	0.36 ± 0.03	22776 ± 2292	0.36 ± 0.06	19083 ± 5355	0.48 ± 0.13
GFP::DSP1	NB	247.88 ± 17.58	112143 ± 12026	0.75 ± 0.10	415276 ± 44536	2.78 ± 0.36	285983 ± 30670	1.92 ± 0.25
	NBmet	440.73 ± 49.39	92874 ± 22600	0.35 ± 0.09	343948 ± 83697	1.30 ± 0.35	236863 ± 57638	0.89 ± 0.24
GFP::PHO	NB	130.41 ± 5.45	14004 ± 1122	0.18 ± 0.02	121423 ± 9725	1.55 ± 0.14	118081 ± 9457	1.50 ± 0.14
	NBmet	529.18 ± 94.37	17729 ± 4538	0.06 ± 0.02	153720 ± 39345	0.48 ± 0.15	149940 ± 38262	0.47 ± 0.15
GFP::E(Z)	NB	176.37 ± 15.40	61506 ± 8291	0.58 ± 0.09	83101 ± 11202	0.78 ± 0.13	29111 ± 3924	0.27 ± 0.04
	NBmet	535.88 39.49	47561 ± 5521	0.15 ± 0.02	64260 ± 7459	0.20 ± 0.03	22511 ± 2613	0.07 ± 0.01

Table A.2: Kinetic parameters of PH::GFP, PC::GFP, GFP::DSP1, GFP::PHO, GFP::E(Z) and GFP::nls in Neuroblast interphase (NB) and metaphase (NBmet), SOP interphase (SOP) and metaphase (SOPmet), pIIa interphase (pIIa) and pIIb interphase (pIIb), extracted using the methods described in [228]. The radius used for the parameter extraction is shown in μm (H). (I) represents the extracted diffusion from the full model (3 parameter fit) for PcG proteins and from the pure diffusion model (single parameter fit) for GFPnls. (J) represents the extracted diffusion from the pure diffusion model in regions outside chromatin in NBmet and SOPmet, and the estimated PcG protein diffusions in interphase of all other cell types through the comparison with GFPnls diffusions (Figure 3.13). Residence time (M) was calculated as (1/K). The fraction of bound molecules in the chromatin region (N) was calculated by the following equation: 100*(L)/(L+M). The total fraction of bound molecules (O) was calculated with the following equation: (N)*(T)/(B). (T) represents the number of GFP-fused proteins that are localised in the region determined by H2A::RFP fluorescence (Yellow masks in Figure 3.6 and Figure 3.7). Number of bound GFP-fused (P), GFP-fused and endogenous (Q) and endogenous in *yw* flies (R) molecules are shown.

	Variable ID	Radius (μm) H	$D_f(1)$ ($\mu m^2.s^{-1}$) I	$D_f(2)$ ($\mu m^2.s^{-1}$) J	k_{off} (s^{-1}) K	k^*_{on} (s^{-1}) L	Rtime (s) M	Fbound chr (%) N	Fbound total (%) O	# GFP bound P	#GFP + end bound Q	# end bound *yw* R
PH:GFP	NB	2.27	1.05 ± 0.17	1.14 ± 0.07	0.23 ± 0.05	0.10 ± 0.04	4.26 ± 0.86	29.67	29.67	41363 ± 4812	45445 ± 5287	11034 ± 1284
	NBmet	4.38	1.26 ± 0.15	1.05 ± 0.06	0.002 ± 0.0007	0.0001 ± 0.00005	607.72 ± 248.49	7.78	0.41	307 ± 36	338 ± 40	82 ± 10
	SOP	2.86	0.76 ± 0.23	0.68 ± 0.05	0.10 ± 0.01	0.13 ± 0.04	9.77 ± 1.00	56.59	56.59	67421 ± 14197		
	SOPmet	3.43	1.52 ± 0.56	0.77 ± 0.06	0.24 ± 0.06	0.15 ± 0.08	4.17 ± 1.00	37.87	1.81	2410 ± 410		
	pIIa	2.28	1.12 ± 0.31	0.57 ± 0.04	0.15 ± 0.01	0.29 ± 0.05	7.78 ± 0.55	65.74	65.74	24569 ± 1556		
	pIIb	2.28	1.11 ± 0.43	0.48 ± 0.04	0.13 ± 0.01	0.27 ± 0.06	4.26 ± 0.86	67.82	67.82	17399 ± 1396		
PC::GFP	NB	2.99	5.10 ± 0.92	3.41 ± 0.41	2.19 ± 0.75	0.51 ± 0.38	0.46 ± 0.16	18.93	18.93	13885 ± 1552	18498 ± 2068	7688 ± 860
	NBmet	3.45	2.17 ± 0.45	3.13 ± 0.38	0.30 ± 0.18	0.06 ± 0.06	3.35 ± 2.00	17.60	0.53	627 ± 64	835 ± 85	347 ± 35
	SOP	2.91	3.00 ± 0.34	2.80 ± 0.17	0.72 ± 0.40	0.08 ± 0.08	1.39 ± 0.78	10.44	10.44	3912 ± 321	6038 ± 496	5062 ± 416
	SOPmet	6.36	2.43 ± 0.30	2.53 ± 0.15	0.002 ± 0.0007	0.0003 ± 0.00003	431.33 ± 128.96	9.78	0.94	367 ± 29	566 ± 45	475 ± 38
	pIIa	2.37	2.42 ± 0.38	2.33 ± 0.14	0.24 ± 0.11	0.07 ± 0.04	4.09 ± 1.81	21.92	21.92	4581 ± 487	7070 ± 752	5928 ± 630
	pIIb	2.19	2.90 ± 0.35	1.97 ± 0.12	0.27 ± 0.14	0.04 ± 0.03	3.72 ± 1.94	13.29	13.29	1960 ± 197	3026 ± 304	2537 ± 255
GFP::DSP1	NB	3.55	5.52 ± 0.48	2.90 ± 0.76	0.24 ± 0.12	0.02 ± 0.02	4.24 ± 2.12	8.52	8.52	9554 ± 1025	35382 ± 3794	24366 ± 2613
	NBmet	4.30	7.32 ± 2.52	2.66 ± 0.70	0.21 ± 0.09	0.06 ± 0.04	4.80 ± 2.02	22.68	2.29	2129 ± 518	7883 ± 1918	5429 ± 1321
GFP::PHO	NB	2.55	1.52 ± 0.17	2.04 ± 0.62	0.19 ± 0.08	0.04 ± 0.02	5.22 ± 2.11	17.67	17.67	2474 ± 198	21454 ± 1718	20864 ± 1671
	NBmet	3.80	1.95 ± 0.58	1.87 ± 0.57	0.10 ± 0.07	0.06 ± 0.05	9.60 ± 6.04	35.55	1.18	209 ± 54	1814 ± 464	1764 ± 452
GFP::E(Z)	NB	3.40	4.08 ± 0.76	$1,79 \pm 0.13$	0.48 ± 0.28	0.08 ± 0.08	2.10 ± 1.26	14.33	14.33	8816 ± 1188	11912 ± 1606	4173 ± 562
	NBmet	4.02	1.15 ± 0.19	1.65 ± 0.23								
GFPnls	NB	4.19	11.43 ± 0.96									
	NBmet	8.18	10.50 ± 0.45									
	SOP	2.91	8.17 ± 0.64									
	SOPmet	5.52	9.15 ± 0.50									
	pIIa	2.78	6.82 ± 0.72									
	pIIb	2.80	5.77 ± 0.61									

Table A.3: Image based parameters of PH::GFP, PC::GFP, GFP::DSP1, GFP::PHO, and GFP::E(Z) in neuroblast metaphase (NBmet) and SOP metaphase (SOPmet). In this table are listed the volume in cubic micrometers occupied by chromatin (S) and the number of GFP proteins that are in this volume (T). As (T), (S) was determined by H2A::RFP fluorescence. The calculated fraction of bound molecules in the chromatin region, without the assumption of equilibrium, according to equation 18 of Appendix C, is listed as (U). The number of GFP-fused proteins bound to chromatin is listed as (W). The total fraction of bound molecules (V) was calculated with the ratio (W)/(Table A.1 B).

	Variable ID	Volume chr (μm^3) S	# GFP chr T	Fbound chr (%) U	Fbound total (%) V	# GFP chr bound W
PH:GFP	NBmet	33.24	3977	8.725169726	0.46	347
	SOPmet	31.58	6365	12.8358209	0.61	817
PC:GFP	NBmet	14.15	3562	35.73834924	1.07	1273
	SOPmet	30.59	3750	48.32	4.62	1812
GFP::DSP1	NBmet	20.54	9387	56.52	5.71	5305
	SOPmet	20.51	4537a	30.86	2.35	1400
GFP::PHO	NBmet	24.02	827	2.84	0.13	23
	SOPmet	27.70	749	54.99	5.89	412
GFP::E(Z)	NBmet	30.00	2391	-12.01	-0.60	-287
	SOPmet	19.98	845	0.46	0.02	4

Table A.4: Parameters used for modeling of Polycomb (PC) interaction with chromatin during cell cycle progression in in neuroblast interphase (NB) and metaphase (NBmet), SOP interphase (SOP) and metaphase (SOPmet), pIIa interphase (pIIa) and pIIb interphase (pIIb) (Figure 3.16) are listed: pseudo-first order association rate (X), the dissociation rate (Y) the number of endogenous Polycomb proteins (Z), as well as the cell (AA) and chromatin (AB) volumes. These parameters were selected from the experimentally determined values listed in Table A.1, Table A.2 and Table A.3 ((L), (K), (F), (A) and (S)). Also shown are the assumed number of binding sites (AC), representing the maximum possible number of H3K27 methylated tails in the diploid genome based on H3K27 distributions in polytene chromosomes and genome-wide ChIP profiles, assuming methylation of all H3 tails within a region of H3K27me3 signal. Based on this number of binding sites, the calculated micromolar dissociation constant (AD) is shown.

	Variable	k^*_{on} (s^{-1})	k_{off} (s^{-1})	# PC	Volume Cell (μm^3)	Volume Chr (μm^3)	# chromatin sites	Kd (μM)
	ID	X	Y	Z	AA	AB	AC	AD
PC	NB	0.51	2.19	40615	176.33	176.33	80000	11.23
	NBmet	0.06	0.3	1216	14.15	14.15	80000	35.04
	SOP	0.08	0.71689	48474	171.6026	171.6026	80000	18.28
	SOPmet	0.00	0.0023184	4633	30.59475	30.59475	80000	36.67
	pIIa	0.07	0.24429	27048	97.15	97.15	80000	7.71
	pIIb	0.04	0.26871	19083	68.62	68.62	80000	14.13

Appendix B

FRAP modeling

B.1 Contribution of Diffusion to the recovery curves

In order to confirm the contribution of diffusion to the FRAP recovery curves of PcG::GFP proteins (Figure 3.10) I performed curve smoothing tests for these recovery curves and compared them to GFPnls (diffusion dependent) and H2A::RFP (diffusion independent) recovery curves confirming a contribution of diffusion to recovery for all PcG::GFP data sets Figure 3.11.
Diffusion test was performed using an adaptation of the method of curve smoothing [227], where gaussian photobleaching profiles of FRAP experiments [228] were acquired at four different time points after photobleaching and the slope region was fitted using linear regression. Comparison of the extracted slopes was performed using ANCOVA.
Matlab scripts for gaussian profile determination were written with Philipp Steffen and are available on request.

B.2 Extraction of kinetic parameters from FRAP data

The FRAP recovery data were analysed by fitting kinetic models [228] to averaged FRAP recovery data shown in Figure 3.10. This fitting procedure enables the extraction of values for diffusion coefficient (k^*_{on}), the pseudo first order association rate k^*_{on} and the dissociation rate k_{off}. For FRAP modeling of recovery curves shown in Figure 3.18, Df was fixed to the previously estimated Df parameter of PC::GFP in neuroblast interphase or metaphase Table A.2, and k^*_{on} and k_{off} were extracted using the procedure described in [228].

B.2.1 Adaptation of model for optimal parameter combination

An additional step was performed to optimise extracted kinetic parameters. After the calculation of the radius of the model nucleus (RM) [228] an additional set of radii was defined, composed of radii -10 pixels from RM to +20 pixels. These 30 radii were used as input values for the reaction-diffusion or pure-difusion model fit to the experimental data. The resulting set of individual extracted kinetic parameters and their confidence intervals as well as the goodness of fit was used to select the optimal radius for the experiment. This selection consisted of a weighted search with 1/3 of the weight being given to the goodness of the confidence intervals of association and dissociation constants, 1/3 to the goodness of the extracted diffusion constant confidence interval, 1/6 to the size of the squared sum of residuals and 1/6 to the distance from the initial RM, with smaller distances being favoured.
MATLAB files for parameter extraction were written with Philipp Steffen and are available on request.

B.2.2 Contribution of binding to FRAP recovery curves

To evaluate the role of binding in the recovery kinetics we compared reaction-diffusion (3 extracted parameters: Df, k^*_{on} and k_{off}) and pure-difusion model fits (single extracted parameter: Df) as described in [228] to our experimental data. In all cases shown in Figure 3.10, except GFP::E(Z) in NB metaphase, the best fit was given by the full reaction-diffusion model, indicating the presence of a bound fraction, and giving extracted values for Df, k^*_{on} and k_{off}.

B.2.3 Cross-validation of extracted Df

In addition to the extracted values for Df from fitting the reaction-diffusion model, the Df for each protein in each cell type was measured independently. This was achieved by performing FRAP on the region of the metaphase cell that is outside chromatin and fitting the pure diffusion model [228] to the recovery data, giving an independent and direct measure of Df. Interphase values were calculated by conversion via diffusion coefficients measured for GFP by fitting the pure diffusion model to FRAP recovery curves measured in both interphase and metaphase, Table A.2. The values of Df thus measured showed excellent agreement with those extracted from fitting the full model (Figure 3.13).

B.2.4 Robustness of extracted k^*_{on} and k_{off}

The robustness of the extracted k^*_{on} and k_{off} values was examined by simulations performed at the value of Df that was extracted from the reaction-diffusion model fit, and in which k^*_{on} and k_{off} were varied, and the fit to experimental data was evaluated (Figure 3.14). This analysis showed that for most data sets, a limited range of k^*_{on} and k_{off} values gave optimal fits to the data (Figure 3.14).
Matlab scripts used to generate FRAP simulations and plot the best fit regions were written with Philipp Steffen and are available in request.

B.2.5 Other models

Localised binding sites: metaphase

The effect of localised binding sites in metaphase was examined using the local binding site model described in [226] showing that both the improved global binding [228] and the localised binding [226] models give essentially identical results in conditions of low binding, as is the case for the metaphase data shown here (data not shown). Unlike the Müller model [228] the Sprague model [226] does not include consideration of the radial bleach profile. Thus in order to achieve consistency of analysis, the Müller Model [228] was used for analysis of all data sets.

Non homogeneous distribution of proteins: interphase

To test for the effect of non-homogeneity in protein distribution observed in interphase (Figure 3.6 and Figure 3.7) on extracted kinetic parameters, we adapted the model described in [227] from its original application to redistribution of photoactivatable GFP, to render it applicable to the analysis of FRAP recovery curves, described here. Fitting this model to interphase data for individual nuclei gave similar values for the three extracted parameters whether initial distribution was assumed to be heterogenous or homogeneous (Figure 3.15).

Generation of images of single nuclei In order to construct input protein distribution images for parameter extraction, all prebleach images of a single nucleus (250) were averaged and used to threshold the region of the nucleus in the total image. This region was selected to define the nucleus within the average image of 2s before photobleaching. To reconstruct the entire nucleus, this image was tiled twice vertically and horizontally. On the resulting image a circle of radius RM (model nucleus radius calculated as described in [228] with

adaptation as described in subsection B.2.1 above) was defined with the bleach region centered. This image was used to give the initial distribution of binding sites in the nucleus. In order to produce the first postbleach image, a bleach pattern with parameters describing the bleach spot profile was calculated from the experimental data [228] and was superimposed on the prebleach image.
Matlab files for image processing were written with Philipp Steffen and are available on request.

Extraction of kinetic parameters from FRAP data, taking non homogeneous protein distribution into account The intensity distribution images generated as described above were used as input for fitting the spatial model described below to the individual FRAP recovery curve for each nucleus, and extraction of parameters.
The reaction-diffusion system is simulated on a 2D circular domain, with a Neumann no-flux condition imposed on the boundary. The method-of-lines is used to numerically solve the resulting partial-differential equation, where a second-order finite difference method is used to discretize the diffusion operator on a uniform mesh. The spatial discretization gives rise to a coupled system of ordinary differential equations for the free and bound concentrations at each mesh point, which is then numerically integrated using an implicit solution scheme. The unknown parameters in the model consist of: the diffusion constant Df, the off-rate of the reaction k_{off}, and the ratio of the total amount of free molecules to bound molecules, *Free*. Given a value for the free fraction, *Free*, the initial conditions for the free and bound proteins are obtained from the smoothed, pre-bleached images. Given the values of k_{off} and *Free*, the spatially varying $k_{on}\ [C]$ is computed from the intensity distribution of the averaged chromatin images, following the methodology of [227]. In order to ensure the positivity of $k_{on}\ [C]$ in the model, a lower bound on the free fraction is imposed, whose value is required to be greater than the minimum chromatin intensity over its average for the circular domain. The unknown parameters (Df, k_{off}, *Free*) are estimated from the measured fluorescence recovery curve for each individual nucleus by solving the inequality constrained optimization problem using the interior point method. As starting values for these three parameters, the extracted values from averaged data were used (Table A.2).
The spatial model was implemented in Mathematica (Wolfram) by Dr. James Lu and scripts are shown in Appendix D.

Appendix C

Mathematical modeling

Supplementary Information

1 Mathematical model

In the following, we consider a variable volume V_{chr} (the chromatin region) inside a fixed volume V_{cell} (the whole cell). Let there be a total number of N_S^{tot} binding sites (located in V_{chr}) and a total number of N_P^{tot} proteins (diffusing in V_{cell}). The proteins can form complexes with the binding sites:

$$\mathbf{S} + \mathbf{P} \rightleftharpoons \mathbf{C} \tag{1}$$

There are N_S^{free} free binding sites, N_P^{free} free proteins, and N_C complexes; the rate constants for binding and unbinding are k_{on} and k_{off}. We make the following simplifying assumptions: (i) diffusion is fast compared to chemical binding (and hence all molecular species are homogeneously distributed in their respective volumes); (ii) the number of complexes is much smaller than the total number of binding sites, that is $N_C \ll N_S^{\mathrm{tot}}$ or $N_S^{\mathrm{free}} \approx N_S^{\mathrm{tot}}$. The validity of the assumptions is discussed below.

In order to derive the ODE which determines the dynamics of this system, we will formulate the relation for the conservation of proteins. Before that, we recall the definitions of amount of substance (in mol) and concentration (in M=mol/L): Given N molecules, the corresponding amount s is defined as

$$s = \frac{N}{N_A}\,, \tag{2}$$

where $N_A \approx 6 \times 10^{23}\ \mathrm{mol}^{-1}$ is the Avogadro constant, and given an amount s in a volume V, the corresponding concentration c is defined as

$$c = \frac{s}{V}\,. \tag{3}$$

In the following, we will use this equation mostly in the form $s = c\,V$.

For the system described above, the total amount of proteins s_P^{tot} is constant over time:

$$\begin{aligned} s_P^{\mathrm{tot}} &= c_C(t)\,V_{\mathrm{chr}}(t) + c_P^{\mathrm{free}}(t)\,V_{\mathrm{cell}} \\ &= s_C(t) + c_P^{\mathrm{free}}(t)\,V_{\mathrm{cell}}\,, \end{aligned} \tag{4}$$

where c_C is the concentration of the complexes and c_P^{free} is the concentration of the free proteins. Since both c_C and V_{chr} vary over time, we will derive an ODE for the amount of complexes $s_C = c_C\,V_{\mathrm{chr}}$. By differentiating the conservation relation with respect to time, we obtain:

$$0 = \frac{\mathrm{d}s_C(t)}{\mathrm{d}t} + \frac{\mathrm{d}c_P^{\mathrm{free}}(t)}{\mathrm{d}t}\,V_{\mathrm{cell}} \tag{5}$$

Since we assume fast diffusion, any change in protein concentration due to chemical reactions in V_{chr} is immediately diluted over V_{cell}. Hence, the ODE for the free protein concentration c_P^{free} amounts to:

$$\frac{\mathrm{d}c_P^{\mathrm{free}}}{\mathrm{d}t} = \left(-k_{\mathrm{on}}\,c_S^{\mathrm{free}}\,c_P^{\mathrm{free}} + k_{\mathrm{off}}\,c_C\right)\frac{V_{\mathrm{chr}}}{V_{\mathrm{cell}}}\,, \tag{6}$$

where c_S^{free} is the concentration of free binding sites. Since we assume $c_S^{\text{free}} \approx c_S^{\text{tot}}$, we can derive a linear ODE for the amount of bound protein:

$$\begin{aligned}\frac{\mathrm{d}s_C}{\mathrm{d}t} &= -\frac{\mathrm{d}c_P^{\text{free}}}{\mathrm{d}t}\, V_{\text{cell}} \\ &= \left(k_{\text{on}}\, c_S^{\text{tot}}\, c_P^{\text{free}} - k_{\text{off}}\, c_C\right) V_{\text{chr}} \\ &= k_{\text{on}}\, s_S^{\text{tot}}\, c_P^{\text{free}} - k_{\text{off}}\, s_C \\ &= k_{\text{on}}\, s_S^{\text{tot}}\, \frac{s_P^{\text{tot}} - s_C}{V_{\text{cell}}} - k_{\text{off}}\, s_C\,,\end{aligned} \tag{7}$$

where s_S^{tot} is the total amount of binding sites, and where we used the conservation relation for the proteins in the last step. We have obtained a linear ODE with constant coefficients, which can be written as

$$\begin{aligned}\frac{\mathrm{d}s_C}{\mathrm{d}t} &= -\left(k_{\text{on}}\, \frac{s_S^{\text{tot}}}{V_{\text{cell}}} + k_{\text{off}}\right) s_C + k_{\text{on}}\, \frac{s_S^{\text{tot}}}{V_{\text{cell}}}\, s_P^{\text{tot}} \\ &= -k\,(s_C - s_C^{\infty})\end{aligned} \tag{8}$$

with

$$k = k_{\text{on}}\, \frac{s_S^{\text{tot}}}{V_{\text{cell}}} + k_{\text{off}}\,, \tag{9a}$$

$$s_C^{\infty} = \frac{s_P^{\text{tot}}}{1 + \frac{k_{\text{off}}}{k_{\text{on}}}\, \frac{V_{\text{cell}}}{s_S^{\text{tot}}}}\,. \tag{9b}$$

The solution of the ODE amounts to:

$$s_C(t) = (s_C(0) - s_C^{\infty})\, e^{-k\,t} + s_C^{\infty} \tag{10}$$

It is remarkable that the dynamics of the amount of complexes s_C does not depend on the variable volume $V_{\text{chr}}(t)$.

In FRAP experiments, k_{on} is derived from a measured $k_{\text{on}}^* = k_{\text{on}}\, c_S^{\text{free}}$. If we use the assumption $c_S^{\text{free}} \approx c_S^{\text{tot}}$ again, we obtain $k_{\text{on}}^* = k_{\text{on}}\, c_S^{\text{tot}}$ and

$$k_{\text{on}} = \frac{k_{\text{on}}^*}{c_S^{\text{tot}}} = k_{\text{on}}^*\, \frac{V_{\text{chr}}^*}{s_S^{\text{tot}}}\,, \tag{11}$$

where V_{chr}^* is the volume for which k_{on}^* was measured. Hence, we can fully specify the constants in the solution of the ODE by measured quantities:

$$k = k_{\text{on}}^*\, \frac{V_{\text{chr}}^*}{V_{\text{cell}}} + k_{\text{off}} \tag{12a}$$

$$s_C^{\infty} = \frac{s_P^{\text{tot}}}{1 + \frac{k_{\text{off}}}{k_{\text{on}}^*}\, \frac{V_{\text{cell}}}{V_{\text{chr}}^*}} \tag{12b}$$

2 Comparison of model predictions with experimental data

In FRAP experiments, the amount of complexes cannot be measured directly. It has to be determined from the total amount of protein in the chromatin region. If the system is in equilibrium, one has

$$k_{\text{on}}\, c_S^{\text{free}}\, c_P^{\text{free}} = k_{\text{on}}^*\, c_P^{\text{free}} = k_{\text{off}}\, c_C\,. \tag{13}$$

Additionally, the conservation relation for proteins can be written as

$$c_P^{\mathrm{free}} + c_C = c_P^{\mathrm{chr}}\,, \tag{14}$$

where c_P^{chr} is the total concentration of protein in the chromatin region. From the last two equations, one can determine the fraction of bound protein,

$$\frac{c_C}{c_P^{\mathrm{chr}}} = \frac{1}{1+\frac{k_{\mathrm{off}}}{k_{\mathrm{on}}^*}}\,, \tag{15}$$

and hence the total amount of complexes,

$$s_C = s_P^{\mathrm{chr}} \frac{1}{1+\frac{k_{\mathrm{off}}}{k_{\mathrm{on}}^*}}\,, \tag{16}$$

where s_P^{chr} is the total amount of protein in the chromatin region.

If the system is not in equilibrium, one has

$$\begin{aligned} s_P^{\mathrm{chr}}(t) &= s_C(t) + c_P^{\mathrm{free}}(t)\, V_{\mathrm{chr}}(t) \\ &= s_C(t) + \frac{s_P^{\mathrm{tot}} - s_C(t)}{V_{\mathrm{cell}}}\, V_{\mathrm{chr}}(t) \\ &= s_C(t)\left(1 - \frac{V_{\mathrm{chr}}(t)}{V_{\mathrm{cell}}}\right) + s_P^{\mathrm{tot}}\,\frac{V_{\mathrm{chr}}(t)}{V_{\mathrm{cell}}}\,, \end{aligned} \tag{17}$$

where the conservation relation for the proteins has been used. Obviously, the dynamics of s_P^{chr} does depend on the variable volume $V_{\mathrm{chr}}(t)$. The above relation can be easily inverted, in order to infer s_C from the measurement of s_P^{chr} and V_{chr}:

$$s_C(t) = \frac{s_P^{\mathrm{chr}}(t) - s_P^{\mathrm{tot}}\,\frac{V_{\mathrm{chr}}(t)}{V_{\mathrm{cell}}}}{1-\frac{V_{\mathrm{chr}}(t)}{V_{\mathrm{cell}}}} \tag{18}$$

Now, one can compare the values inferred from experimental data via Eqns. (16) and (18) with the value predicted by the model (10). The values for s_C inferred from experimental data are listed in Supplementary Table 1.

3 The assumption of fast diffusion

The diffusion length Δx provides a measure for the propagation of diffusion during the time Δt. It is given by

$$\Delta x = 2\sqrt{D\,\Delta t}\,, \tag{19}$$

where D is the diffusion constant.

The assumption that diffusion is fast compared to chemical binding means that the diffusion length during the characteristic time of the chemical reaction is large compared to the radius of the respective volume. Let k be the characteristic rate of the chemical reaction (and hence $\Delta t = 1/k$ the characteristic time), and let r be the radius of the volume under consideration. Then we have to ensure that

$$r \ll \Delta x = 2\sqrt{\frac{D}{k}}\,. \tag{20}$$

Since unbinding is much faster than binding, we have to ensure this inequality for $k = k_{\mathrm{off}}$. Clearly, r is the radius of the chromatin region in interphase, whereas it

is the cell radius in metaphase. We find the following experimental values for D, k, r, and the resulting diffusion length Δx:

	$D\,[m^2\,s^{-1}]$	$k\,[s^{-1}]$	$r\,[m]$	$\Delta x\,[m]$
interphase	3.0×10^{-12}	0.7	3.5×10^{-6}	4.1×10^{-6}
metaphase	2.4×10^{-12}	2.0×10^{-3}	5.2×10^{-6}	69×10^{-6}

In metaphase, the assumption of fast diffusion is very well justified, whereas in interphase, the diffusion length is in the range of the cell radius. However, since the transition of interest starts at the onset of metaphase, it can be reasoned that the situation in interphase has little impact on the dynamics.

4 The assumption $c_C \ll c_S^{\text{tot}}$ (or $c_S^{\text{free}} \approx c_S^{\text{tot}}$)

In order to linearize the ODE system for the binding reaction, one often assumes that $c_C \ll c_S^{\text{tot}}$ (or equivalently $c_S^{\text{free}} \approx c_S^{\text{tot}}$). The relative error of this assumption amounts to:

$$\epsilon = \frac{c_C}{c_S^{\text{tot}}} = \frac{s_C}{s_S^{\text{tot}}} \tag{21}$$

For a given error ϵ_0, we will derive a condition (depending on s_S^{tot} and s_P^{tot}) such that

$$\epsilon < \epsilon_0 \tag{22}$$

is fulfilled for the equilibrium value $s_C = s_C(s_S^{\text{tot}}, s_P^{\text{tot}})$.

Using the conservation relations for binding sites and proteins

$$s_S^{\text{free}} + s_C = s_S^{\text{tot}} \tag{23a}$$

$$s_P^{\text{free}} + s_C = s_P^{\text{tot}} \tag{23b}$$

in the equilibrium condition

$$c_S^{\text{free}}\, c_P^{\text{free}} = K_D\, c_C\,, \tag{24}$$

where

$$K_D = \frac{k_{\text{off}}}{k_{\text{on}}}\,, \tag{25}$$

we obtain:

$$\frac{s_S^{\text{tot}} - s_C}{V_{\text{chr}}}\,\frac{s_P^{\text{tot}} - s_C}{V_{\text{cell}}} = K_D \frac{s_C}{V_{\text{chr}}}\,. \tag{26}$$

By using

$$s_C = \epsilon\, s_S^{\text{tot}}\,, \tag{27}$$

we can rewrite this relation as

$$\frac{s_P^{\text{tot}}}{K_D V_{\text{cell}}} = \frac{\epsilon}{1-\epsilon} + \epsilon\,\frac{s_S^{\text{tot}}}{K_D V_{\text{cell}}}\,. \tag{28}$$

For a given error ϵ_0, we have $\epsilon < \epsilon_0$ whenever

$$\frac{s_P^{\text{tot}}}{K_D V_{\text{cell}}} < \frac{\epsilon_0}{1-\epsilon_0} + \epsilon_0\,\frac{s_S^{\text{tot}}}{K_D V_{\text{cell}}}\,. \tag{29}$$

In order to ensure a small relative error, i.e. $\epsilon < \epsilon_0 \ll 1$, one may require either $s_P^{\mathrm{tot}}/s_S^{\mathrm{tot}} \ll 1$ or $s_P^{\mathrm{tot}}/(K_D V_{\mathrm{cell}}) \ll 1$. The former case can be called "abundance of binding sites", whereas the latter case can be called "weak binding".

It should be noted that the condition $s_P^{\mathrm{tot}}/s_S^{\mathrm{tot}} \ll 1$ does not depend on the volume involved, whereas the condition $s_P^{\mathrm{tot}}/(K_D V_{\mathrm{cell}}) \ll 1$ might me satisfied for a certain volume, but not for a decreased volume.

By using

$$K_D = \frac{k_{\mathrm{off}}}{k_{\mathrm{on}}} = \frac{k_{\mathrm{off}}}{k_{\mathrm{on}}^* \frac{V_{\mathrm{chr}}^*}{s_S^{\mathrm{tot}}}} = \frac{k_{\mathrm{off}}}{k_{\mathrm{on}}^*} \frac{s_S^{\mathrm{tot}}}{V_{\mathrm{chr}}^*} \tag{30}$$

we can further rewrite the condition for weak binding:

$$\frac{s_P^{\mathrm{tot}}}{K_D V_{\mathrm{cell}}} = \frac{s_P^{\mathrm{tot}}}{s_S^{\mathrm{tot}}} \frac{k_{\mathrm{on}}^*}{k_{\mathrm{off}}} \frac{V_{\mathrm{chr}}^*}{V_{\mathrm{cell}}} \ll 1 \tag{31}$$

We find the following experimental values for $s_P^{\mathrm{tot}}/s_S^{\mathrm{tot}}$, $k_{\mathrm{on}}^*/k_{\mathrm{off}}$, and $V_{\mathrm{chr}}^*/V_{\mathrm{cell}}$:

	$s_P^{\mathrm{tot}}/s_S^{\mathrm{tot}}$	$k_{\mathrm{on}}^*/k_{\mathrm{off}}$	$V_{\mathrm{chr}}^*/V_{\mathrm{cell}}$
interphase	0.5	0.1	0.9
metaphase	0.5	0.15	0.05

The condition for weak binding, $s_P^{\mathrm{tot}}/(K_D V_{\mathrm{cell}}) \ll 1$, is satisfied to a high degree both in interphase and metaphase. As a consequence, the assumption of interest, $c_C \ll c_S^{\mathrm{tot}}$ (or $c_S^{\mathrm{free}} \approx c_S^{\mathrm{tot}}$), is fully justified.

Appendix D

Mathematica scripts

D.1 MathFRAP Algorithm

MathFRAP

The *Mathematica* solution to FRAP analysis

Optimized for Mathematica 7.0 on multi-core machines

Prelude

```
SetOptions[ListPlot, Frame → True, ImageSize → {300, Automatic}];
myLabelStyle[label_] := Style[label, Bold, Brown, 15];
$cutOffVal = 0;

BeginPackage["MathFRAP`"]

getNucleusRegion::usage =
  "Obtains an estimate of nucleus boundary from averged
    image intensity in the horizontal direction.";
triplicateDomain::usage = "Create an image that is triplicate tiled
    in the vertical direction and center cropped if so desired.";
getBleachedProfile::usage = "Get Gaussian shaped bleach
    profile from input parameters.";
solveSystem::usage = "Solve the discretized diffusion reaction system.";
getRecoveryProfile::usage =
  "Obtain the FRAP recovery curve from computed solution.";
getChromatinFunctionOnDisk::usage =
  "Get the interpolation of chromatin distribution onto the domain disk";
getNormalizedProteinOnDisk::usage =
  "Get the interpolation function of a given image for
    the inten protein distribution onto the domain disk";
fitCutOffFunction::usage = "Estimate circular cutoff
    boundary function from image data.";
fitCutOffFunctionOnDisk::usage =
  "Estimate cutoff function on the disk from image data.";
getEqnSystem::usage =
  "Get the system of equations obtained from discretization.";
imageToInitCondition::usage = "Take the intensity data
    in an image and use it as an initial condition.";
makePlots::usage = "Plot solution, as either contour or 3D plots.";
computeRecoveryCurve::usage =
  "Given parameter and problem input, computes the
    solution and the recovery curve.";
computeMismatch::usage = "Given parameter and problem input,
    computes mismatch to the input recovery curve.";
logBinData::usage = "Bins the data according to given bin size.";
```

Private Functions

```
Begin["`Private`"]
```

```
photoBleachProfile[x_, y_, center_List, {theta_, rC_, sigma_}] :=
  Module[{rInMicron = 0.045 * Sqrt[(x - center[[1]])^2 + (y - center[[2]])^2]},
```

```
    If[rInMicron ≤ rC, theta,
     1 - (1 - theta) Exp[- (rInMicron - rC)^2 / (2 sigma^2)]]
   ];

fitFunc_Cutoff[plateauWidth_, totalWidth_, height_, basal_] := Piecewise[{
    {basal + x / ((totalWidth - plateauWidth) / 2) * height,
     0 ≤ x ≤ (totalWidth - plateauWidth) / 2}, {basal + height,
     (totalWidth - plateauWidth) / 2 ≤ x ≤ totalWidth / 2 + plateauWidth / 2},
    {basal + height - (x - (totalWidth / 2 + plateauWidth / 2)) /
        ((totalWidth - plateauWidth) / 2) * height,
     totalWidth / 2 + plateauWidth / 2 ≤ x ≤ totalWidth}},
   0(*basal*)];

findInteriorNeighbour[inputIndex_, domainCenter_, interiorCellIndices_] :=
  Module[{pointingVec, pickCellQ, pickedIndex, interiorCellIntervals},

   interiorCellIntervals =
    Function[index, Interval[{# - 1, #}] & /@ index] /@ interiorCellIndices;

   (*Print["interiorCellIntervals = ",interiorCellIntervals[[1;;5]]];*)

   pointingVec = # / Norm@# &@((inputIndex - 1 / 2) - domainCenter);

   (*Print["pointingVec = ", pointingVec];*)

   pickCellQ = Function[intervals,
      (And @@ MapThread[IntervalMemberQ[#1, #2] &, {intervals,
          (inputIndex - 1 / 2) - pointingVec}])] /@ interiorCellIntervals;
   pickedIndex = Pick[interiorCellIndices, pickCellQ, True];

   (*If[Length@pickedIndex> 1, Print[
      "More than 1 neighbor cell found! picking the first one..."]];*)
   If[Length@pickedIndex == 0,

    (*Print["No neighboring interior
        element found...try extend search vector."];*)

    pointingVec = 2 * # / Norm@# &@((inputIndex - 1 / 2) - domainCenter);
    pickCellQ = Function[intervals,
       (And @@ MapThread[IntervalMemberQ[#1, #2] &, {intervals,
           (inputIndex - 1 / 2) - pointingVec}])] /@ interiorCellIntervals;
    pickedIndex = Pick[interiorCellIndices, pickCellQ, True];
   ];
   If[Length@pickedIndex == 0,
    Print["Failed upon extension..aborting!"]; Abort[]];

   Return@pickedIndex[[1]]
  ];

laplacianOperator[values_, {xgrid_, ygrid_}] :=
  NDSolve`FiniteDifferenceDerivative[{2, 0},
    {xgrid, ygrid}, values, DifferenceOrder → 2] +
   NDSolve`FiniteDifferenceDerivative[{0, 2},
    {xgrid, ygrid}, values, DifferenceOrder → 2];
```

```
laplacianOperatorMatrix[{xgrid_, ygrid_}] := Module[{flap},
   flap = Function[Evaluate[
      NDSolve`FiniteDifferenceDerivative[{2, 0}, {xgrid, ygrid},
        DifferenceOrder → 2][#] + NDSolve`FiniteDifferenceDerivative[
        {0, 2}, {xgrid, ygrid}, DifferenceOrder → 2][#]]];
   Return[Total@Map[(Head[#]["DifferentiationMatrix"]) &,
      List @@ First[flap]]]];

neumannFluxOperator[values_, {xgrid_, ygrid_}, directionVector_] :=
  {First@#, Last@#} &@
   (If[directionVector == {1, 0}, #, Transpose@#] &@
     ((NDSolve`FiniteDifferenceDerivative[directionVector,
          {xgrid, ygrid}, #, DifferenceOrder → 2]) &@values));

compileEqnSys[eqnSys_, var_] := Module[{allVar},
   allVar = List[#, Blank[Real]] & /@ var;
   Return[Compile[Evaluate@allVar, Evaluate@eqnSys]];
  ];

obsHoleFunction[inputX_, inputY_, discretDim_List,
   imgDim_List, {pixelNuclLeft_, pixelNuclRight_}] :=
  Module[{origImgWidth = 512, observeRadius = 20, x, y, offSet, center},
   offSet = {(pixelNuclLeft + pixelNuclRight) / 2 - origImgWidth / 2, 0};
   center = imgDim / 2;
    x = inputX / (discretDim[[1]]) * imgDim[[1]];
   y = inputY / (discretDim[[2]]) * imgDim[[2]] ;
   If[(x - (center[[1]] + offSet[[1]]))^2 +
      (y - (center[[2]] + offSet[[2]]))^2 ≤ observeRadius^2, 1, 0]
  ];
```

Public Functions

- Image & Data Processing

```
Options[getNucleusRegion] = {Global`ReturnIntensity → False};
getNucleusRegion[nucleusThreshHold_?NumericQ,
  {imgList__}, selectedInterval_: {}, opt___Rule] :=
 Module[{intensityHoriz, maxIntensity, minIntensity,
   numPixLeftNucleusList, numPixRightNucleusList},

  intensityHoriz =
   Function[image, ((Plus @@ Flatten@#) & /@ Transpose[ImageData[image]])] /@
    Flatten@{imgList};


  minIntensity = Min /@ intensityHoriz;
  intensityHoriz = intensityHoriz - minIntensity;
  maxIntensity = Max /@ intensityHoriz;

  If[selectedInterval == {},
   numPixLeftNucleusList = MapIndexed[Function[{intensity, index},
       Length@TakeWhile[intensity, # < nucleusThreshHold *
            maxIntensity[[index[[1]]]] &]], intensityHoriz];
   ,
   numPixLeftNucleusList = MapIndexed[Function[{intensity, index},
       Length@TakeWhile[intensity[[First@selectedInterval ;;]],
          # < nucleusThreshHold * maxIntensity[[index[[1]]]] &]
        +First@selectedInterval ], intensityHoriz];
  ];

  If[selectedInterval == {},
   numPixRightNucleusList = MapIndexed[Function[{intensity, index},
       Length@TakeWhile[Reverse@intensity, # < nucleusThreshHold *
            maxIntensity[[index[[1]]]] &]], intensityHoriz];
   ,
   numPixRightNucleusList = MapIndexed[Function[{intensity, index},
       Length@TakeWhile[Reverse@(intensity[[ ;; Last@selectedInterval]]),
          # < nucleusThreshHold * maxIntensity[[index[[1]]]] &] +
        (Length@intensity - Last@selectedInterval) ], intensityHoriz ];
  ];

  If[Global`ReturnIntensity /. List@opt /. Options[getNucleusRegion],
   Return[
    {{numPixLeftNucleusList, -numPixRightNucleusList}, intensityHoriz}]
   ,
   Return[{numPixLeftNucleusList, -numPixRightNucleusList}]
  ]]
```

```
triplicateDomain[img_Image, size_: 0] := Module[{imgList},
   If[(ImageDimensions@img)[[1]] ≥ (ImageDimensions@img)[[2]] * 3,

    Print["Image long in horizontal direction (length = " <>
      ToString[(ImageDimensions@img)[[1]]] <>
      " pixels): tiling it 5 time vertically."];

    imgList = List[ List@img, List@ImageReflect@img,
      List@img, List@ImageReflect@img, List@img];
    ,
    imgList =
      List[ List@ImageReflect@img, List@img, List@ImageReflect@img];
   ];

   Return@ImageCrop[ImageAssemble@imgList, If[size == 0,
      {1, 1} * (ImageDimensions@img)[[1]], {size, size}] , {Center, Center}]
  ];
```

```
getBleachedProfile[{pixelLeft_, pixelRight_}, nucleusSize_,
  {theta_, rC_, sigma_}] := Module[{centerX = 512 / 2, initGaussProfile},
  initGaussProfile = MapIndexed[photoBleachProfile[#2[[1]], #2[[2]],
      {centerX - pixelLeft, nucleusSize / 2}, {theta, rC, sigma}] &,
    IdentityMatrix[nucleusSize], {2}];

  Return@initGaussProfile
 ]
```

```
Options[fitCutOffFunction] =
  {Global`DoFit → True, Global`UseSliceData → True};
fitCutOffFunction[img_Image, opt___Rule] :=
  Module[{imgHorizAvg, imgHorizAvgData, basalInit,
    heightInit, platWidthInit, nlm, platWidth, height, basal},

   If[Global`UseSliceData /. {opt} /. Options[fitCutOffFunction],
    imgHorizAvg = (ImageData@img)[[Round[ImageDimensions[img][[2]] / 2]]];
    ,
    imgHorizAvg = (Mean[#] & /@ Transpose@ImageData@img);
   ];

   imgHorizAvgData = MapIndexed[{#2[[1]], #1} &, imgHorizAvg];

   basalInit = Min@imgHorizAvg;
   heightInit = 0.9 * Max@imgHorizAvg;
   platWidthInit = 0.9 * Length@imgHorizAvg;

   If[Global`DoFit /. {opt} /. Options[fitCutOffFunction],
    nlm = NonlinearModelFit[imgHorizAvgData, fitFunc_Cutoff[platWidth,
       Length@imgHorizAvgData, height, basal], {{platWidth, platWidthInit},
       {height, heightInit}, {basal, basalInit}}, x];

    Print@Plot[nlm[x], {x, 0 - 1, Length@imgHorizAvgData + 1}, Axes → None,
      Frame → True, Filling → 0, ImageSize → {350, Automatic} ,
      FrameLabel → (Style[#, Bold, Brown, 14] & /@ {"Pixel (horizontal)",
          "Mean intensity\n&fit by piece-wise function"}), Epilog :→
       {Blue, Point[imgHorizAvgData]}, PlotStyle → {Red, Dashed, Thick},
      PlotRange → {All, {0, 1.05 * Max@imgHorizAvg}}];
    ,
    nlm[x_] := If[0 ≤ x ≤ Length@imgHorizAvgData, 1, 0];

    (*Print@Plot[nlm[x],{x,0-1,Length@imgHorizAvgData+1},
       Axes→ None,Frame→ True,Filling→ 0,ImageSize→{350,Automatic} ,
       FrameLabel→ (Style[#,Bold,Brown,14]&/@{"Pixel (horizontal)",
           "Mean intensity\n&fit by piece-wise function"}),
       PlotStyle→{Red,Dashed,Thick}];*)

   ];


   cutOffFunc[x_?NumericQ, y_?NumericQ] :=
    (halfDim = (ImageDimensions@img)[[1]] / 2;
     nlm[halfDim + Sqrt[(x - halfDim)^2 + (y - halfDim)^2]] / nlm[halfDim]);

   Return[cutOffFunc]
  ];
```

```
Options[fitCutOffFunctionOnDisk] = {Global`UseSliceData → True};
fitCutOffFunctionOnDisk[img_Image , opt___Rule] :=
  Module[{imgHorizAvg, imgHorizAvgData, basalInit,
    heightInit, platWidthInit, nlm, platWidth, height, basal},

   If[Global`UseSliceData /. {opt} /. Options[fitCutOffFunctionOnDisk],
    imgHorizAvg = (ImageData@img)[[Round[ImageDimensions[img][[2]] / 2]]];
    Print["imgHorizAvg = ", imgHorizAvg];
    ,
    imgHorizAvg = (Mean[#] & /@ Transpose@ImageData@img);
   ];

   imgHorizAvgData = MapIndexed[{#2[[1]], #1} &, imgHorizAvg];

   basalInit = Min@imgHorizAvg;
   heightInit = 0.9 * Max@imgHorizAvg;
   platWidthInit = 0.9 * Length@imgHorizAvg;

   nlm = NonlinearModelFit[imgHorizAvgData, fitFunc_Cutoff[platWidth,
      Length@imgHorizAvgData, height, basal], {{platWidth, platWidthInit},
      {height, heightInit}, {basal, basalInit}}, x];

   Print@Plot[nlm[x], {x, 0 - 1, Length@imgHorizAvgData + 1}, Axes → None,
     Frame → True, Filling → 0, ImageSize → {350, Automatic} ,
     FrameLabel → (Style[#, Bold, Brown, 14] & /@ {"Pixel (horizontal)",
         "Mean intensity\n&fit by piece-wise function"}), Epilog :→
      {Blue, Point[imgHorizAvgData]}, PlotStyle → {Red, Dashed, Thick},
     PlotRange → {All, {0, 1.05 * Max@imgHorizAvg}}];

   cutOffFunc[x_?NumericQ, y_?NumericQ] :=
    (halfDim = (ImageDimensions@img)[[1]] / 2;
     nlm[halfDim + Sqrt[(x - halfDim) ^ 2 + (y - halfDim) ^ 2]] / nlm[halfDim]);

   Return[cutOffFunc]
  ];
```

```
getChromatinFunctionOnDisk[img_, cutOffFunc_: (# &)] :=
  Module[{pixDim = 0.045, chromInterpFunc, avgIntensity,
    imgDim = ImageDimensions@img, normChromInterpFunc,
    imgWithCutoffList, imageDataList},
   Off[NIntegrate::"slwcon"];

   imageDataList = Transpose@ImageData@ImageReflect@img;

   imgWithCutoffList =
    MapIndexed[#1 * cutOffFunc[Sequence @@ #2] &, imageDataList, {2}];

   Print["Processed image: ",
    ImageAdjust[#] &@( Image@Reverse@Transpose@imgWithCutoffList)];

   chromInterpFunc = ListInterpolation[
     imgWithCutoffList, {0, #} & /@ imgDim, InterpolationOrder → 1];
   avgIntensity = NIntegrate[chromInterpFunc[x, y], {x, 0, imgDim[[1]]},
      {y, 0, imgDim[[2]]}, AccuracyGoal → 3, PrecisionGoal → 3] /
     ((*pixDim^2**)Times @@ imgDim);
   On[NIntegrate::"slwcon"];
   normChromInterpFunc =
    Compile[ {{x, _Real}, {y, _Real}}, chromInterpFunc[x, y] / avgIntensity];
   Return@normChromInterpFunc
  ];
```

```
getNormalizedProteinOnDisk[img_, outputDim_, cutOffFunc_: (# &)] :=
  Module[{pixDim = 0.045, intensityInterpFunc, avgIntensity,
    imgDim = ImageDimensions@img, normIntensityInterpFunc,
    imgWithCutoffList, imgDataList, normIntensityList, minNormIntensity},
   Off[NIntegrate::"slwcon"];

   imgDataList = Transpose@ImageData@ImageReflect@img;
   imgWithCutoffList =
    MapIndexed[#1 * cutOffFunc[Sequence @@ #2] &, imgDataList, {2}];

   (*Print["Processed image: ",
     Image[ImageAdjust[#],ImageSize→ {100,Automatic}]&@
      ( Image@Reverse@Transpose@imgWithCutoffList)];*)

   intensityInterpFunc = ListInterpolation[imgWithCutoffList,
     {0, #} & /@ imgDim, InterpolationOrder → 0(*0*)];

   avgIntensity = NIntegrate[intensityInterpFunc[x, y],
      {x, 1, imgDim[[1]]}, {y, 1, imgDim[[2]]},
      Method → "LocalAdaptive", MaxPoints → 10^5,
      AccuracyGoal → (3 + 2), PrecisionGoal → (3 + 2)] / (Times @@ imgDim);

   On[NIntegrate::"slwcon"];
   normIntensityInterpFunc = Compile[
     {{x, _Real}, {y, _Real}}, intensityInterpFunc[x, y] / avgIntensity];

   (*multFactor=1;*)

   normIntensityList = Table[
     (*cutOffFunc[
      multFactor*(1+(i-1)/(outputDim-1)*(imgDim[[1]]-1)),
      multFactor*(1+(j-1)/(outputDim-1)*(imgDim[[2]]-1))]
     **)normIntensityInterpFunc[
      1 + (i - 1) / (outputDim - 1) * (imgDim[[1]] - 1),
      1 + (j - 1) / (outputDim - 1) * (imgDim[[2]] - 1)],
     {i, 1, outputDim}, {j, 1, outputDim}];

   minNormIntensity =
    Min@(Complement[Flatten@#, {0., 0}] &@normIntensityList);

   Return@{normIntensityInterpFunc, normIntensityList, minNormIntensity,
     Image[ImageAdjust[#], ImageSize → {150, Automatic}] &@
      ( Image@Reverse@Transpose@imgWithCutoffList)}
  ];
```

```
imageToInitCondition[img_Image, iC_List, componentToSet_Integer] :=
 Module[{iCRange, interpImageData , indices = {i, j}, newIC, eqnSysJac},
  iCRange = {1, #} & /@ Reverse[Dimensions[iC[[componentToSet]]]];
  interpImageData = ListInterpolation[Transpose@ImageData@img, iCRange];
  newIC = ReplacePart[iC,
      componentToSet → MapThread[Thread[#1 == #2] &,
        {iC[[componentToSet]], Transpose@#}]] &@(Map[Max[#, 0] &,
      Table[interpImageData @@ indices, Evaluate[Sequence @@ #]] &@
       MapIndexed[Prepend[#1, indices[[#2[[1]]]]] &, iCRange], {2}]);
  Return@
   newIC]
```

```
logBinData[data_List, interval_List] :=
 Module[{intervalSize, bin, xTime, jList, logtimex = {}, xxTime, xAvg},

  intervalSize = #[[2]] - #[[1]] + 1 & /@ interval;
  bin = #[[3]] & /@ interval;
  xTime = data[[#[[1]] ;; #[[2]]]] & /@ interval;
  jList = MapThread[Table[i, {i, 1, #1 / #2}] &, {intervalSize, bin}];

  xxTime = MapIndexed[
    Function[{binInput, index}, xTime[[index[[1]]]][[(1 + (# - 1) * binInput) ;;
          ((# - 1) * binInput + binInput)]] & /@ jList[[index[[1]]]], bin];

  xAvg = Function[timeList, N[Mean /@ timeList]] /@ xxTime;
  AppendTo[logtimex, #] & /@ xAvg;

  Return@Flatten@logtimex
 ]
```

Discretization

```
Options[getEqnSystem] = {Global`DoPlots → False};

getEqnSystem[imgDim_Integer,
   {numMeshPtsX_?NumericQ, numMeshPtsY_?NumericQ}, speciesNames_List,
   diffusingSpecies_, AssumeSpatial_: False , chromatinDistribution_: None,
   nominalParamList_List: {}, AssumeCircleGeometry_: False, opts___Rule] :=
  getEqnSystem[Image@IdentityMatrix[imgDim], {numMeshPtsX, numMeshPtsY},
   speciesNames, diffusingSpecies, AssumeSpatial,
   chromatinDistribution, nominalParamList, AssumeCircleGeometry, opts] ;

getEqnSystem[img_Image, {numMeshPtsX_?NumericQ, numMeshPtsY_?NumericQ},
   speciesNames_List, diffusingSpecies_, AssumeSpatial_: False,
   chromatinDistribution_: None, nominalParamList_List: {},
   AssumeCircleGeometry_: False, opts___Rule] :=
  Module[{pSize, hGrid, vGrid, locToMeshIndexRule, speciesList,
    neumannFluxTerms, lapTerm, varList, interiorLapTerm,
    interiorEqnSys, interiorVarList, varToTimeDepRule, varDimX, bC,
    iC, diffEqnSysJac, varListDeriv, diffEqnSys, selInteriorResCrit,
    diffVarList, diffVarListDeriv, interiorDiffVarList, boundEqnSys,
    paramList, spatialVarList, spatialIndexList, domainCenter,
    domainSelectMat, interiorDomainSelectMat, boundarySelectMat,
```

```
 selectedSpeciesList, boundarySpeciesList, boundaryNeumannFluxX,
 boundaryNeumannFluxY, NeumannFluxXIndices, NeumannFluxYIndices,
 neumannFluxPieces, neumannFluxXRule, neumannFluxYRule,
 partitionedVarList, bCRewrittenForm, oldneumannFluxTerms,
 interiorDomainSpeciesList, interiorCellIndices, boundaryCellIndices},

If[! MemberQ[speciesNames, diffusingSpecies], Print[
  "Error: diffusingspecies must be a member of Species"]; Abort[]];
If[! Equal @@ (ImageDimensions@img),
 Print["Image should have height = width, exiting."]; Abort[]];
If[! Equal @@ {numMeshPtsX, numMeshPtsY},
 Print["Image should have height = width, exiting."]; Abort[]];

{hGrid, vGrid} =  (ImageDimensions@img) *
  (Range[0, 1, 1 / (# - 1)] & /@ {numMeshPtsX, numMeshPtsY});

locToMeshIndexRule = Flatten@(Function[species, Flatten@
      Outer[species @@ {#1[[1]], #2[[1]]} → species @@ {#1[[2]], #2[[2]]} &,
       Thread[hGrid → Range[Length@hGrid]],
       Thread[vGrid → Range[Length@vGrid]]]] /@ speciesNames);
speciesList = (Transpose@Outer[#, hGrid, vGrid]) & /@ speciesNames;

If[AssumeCircleGeometry,
 domainCenter = {numMeshPtsX, numMeshPtsY} / 2;
 domainSelectMat = DiskMatrix[All, numMeshPtsX];
 interiorDomainSelectMat = ArrayPad[DiskMatrix[All, numMeshPtsX - 2], 1];
 interiorDomainSpeciesList =
  Flatten@Pick[speciesList[[1]], interiorDomainSelectMat, 1] /.
   locToMeshIndexRule;
 interiorCellIndices = interiorDomainSpeciesList /.
   Global`freeProtein[x__] :> List@x;
 boundarySelectMat = MapThread[#2 * (1 - #1) &,
   {interiorDomainSelectMat, domainSelectMat}];

 If[Global`DoPlots /. {opts} /. Options[getEqnSystem],
  Print[Style[#, Bold, Brown, 15] &@"Domain & boundary elements:\n",
    List@{ArrayPlot[boundarySelectMat, Mesh → All,
        MeshStyle → Cyan, ImageSize → {200, Automatic}],
       ArrayPlot[domainSelectMat, Mesh → All, MeshStyle → Cyan,
        ImageSize → {200, Automatic}]} // Grid];
 ];

 selectedSpeciesList =
  Pick[speciesList[[1]], domainSelectMat, 1] /. locToMeshIndexRule;
 boundarySpeciesList = Flatten@Pick[speciesList[[1]],
     boundarySelectMat, 1] /. locToMeshIndexRule;
 boundaryCellIndices = boundarySpeciesList /.
   Global`freeProtein[x__] :> List@x;

 neumannFluxTerms = ((Global`freeProtein @@ #) ==
      Global`freeProtein @@ (findInteriorNeighbour[#, domainCenter,
         interiorCellIndices]) & /@ boundaryCellIndices);

 ,
 neumannFluxTerms = Function[species, Flatten@({Drop[Drop[#, 1], -1] & /@
```

```
            (neumannFluxOperator@(Sequence@@Append[#, {1, 0}])),
           neumannFluxOperator@(Sequence@@Append[#, {0, 1}])} &@
         {Transpose@species, {hGrid, vGrid}}) /.
       locToMeshIndexRule] /@ ({speciesList[[1]]});
];

spatialVarList =
 Function[species, #[Global`t] & /@ (Flatten@species)] /@ speciesList;
varList = spatialVarList /. locToMeshIndexRule;
varDimX = numMeshPtsX;

If[! AssumeSpatial,

 (*Print[Style[#,Bold,Red]&@"NOT ASSUMING SPATIAL!"];*)

 reactionEqnSys = {
   MapThread[-Global`kOn #1 + Global`kOff #2 & , varList] // Flatten,
   MapThread[Global`kOn #1 - Global`kOff #2 & , varList] // Flatten};
 paramList = {Global`𝒟, Global`kOn, Global`kOff};
 ,
 spatialIndexList =
  Map[(# /. name_[position__?NumericQ][Global`t] :> List@position) & ,
   Flatten@
    (Reverse@Partition[varList[[1]], varDimX, varDimX, 1, {}])  ];

 reactionEqnSys = {
   MapThread[- Global`kOff / Global`freeFraction * Max[0,
         (chromatinDistribution@@{hGrid[[#3[[1]]]], vGrid[[#3[[2]]]]} -
           Global`freeFraction)] * #1 + Global`kOff #2 & ,
     Join[varList, List@spatialIndexList]] // Flatten,
   MapThread[  Global`kOff / Global`freeFraction *
        Max[0, (chromatinDistribution@@{hGrid[[#3[[1]]]], vGrid[[
              #3[[2]]]]} - Global`freeFraction)] * #1 - Global`kOff #2 & ,
     Join[varList, List@spatialIndexList]] // Flatten};

 kOnValues =
  Map[Max[0, Global`kOff / Global`freeFraction * (chromatinDistribution@@
          {hGrid[[#[[1]]]], vGrid[[#[[2]]]]} - Global`freeFraction)] &,
    Partition[spatialIndexList, varDimX, varDimX, 1, {}],
    {2}] /. nominalParamList;

 If[Global`DoPlots /. {opts} /. Options[getEqnSystem],
  Print[ListPlot3D[ArrayPad[#, 1] &@(Reverse@kOnValues), Boxed → False,
    PlotRange → {All, All, All}, InterpolationOrder → 1, Mesh → None,
    ImageSize → {250, Automatic}, AspectRatio → Automatic,
    AxesLabel → (Style[#, Bold, 14, Purple] & /@ {"x", "y"}), PlotLabel →
     Style["kOn[C(r)] over\nthe complete domain", Bold, Brown, 14]]];

  If[AssumeCircleGeometry,
   Print[ListPlot3D[ArrayPad[#, 1] &@
       MapThread[#1 * #2 &, {Reverse@kOnValues, domainSelectMat}, 2],
     Boxed → False, PlotRange → {All, All, All}, InterpolationOrder → 1,
     Mesh → None, ImageSize → {250, Automatic}, AspectRatio → Automatic,
     AxesLabel → (Style[#, Bold, 14, Purple] & /@ {"x", "y"}), PlotLabel →
      Style["kOn[C(r)] over\nthe disk domain", Bold, Brown, 14]]];
```

```
    ];
   ];

   paramList = {Global`𝒟, Global`kOff, Global`freeFraction};
  ];

  diffVarList = Function[species,
     #[Global`t] & /@ (Flatten@species /. locToMeshIndexRule)]@
    speciesList[[Position[speciesNames, diffusingSpecies][[1, 1]]]];
  varToTimeDepRule =  # → #[Global`t] & /@
    (Flatten@speciesList /. locToMeshIndexRule);
  varDimX = numMeshPtsX;

  interiorDiffVarList = Function[speciesVar,
     Flatten@(Drop[Drop[#, -1], 1] & /@ (Drop[Drop[#, -1], 1] &@
          Partition[speciesVar, varDimX, varDimX, 1, {}]))]@diffVarList;

  diffEqnSysJac = laplacianOperatorMatrix[{vGrid, hGrid}];

  If[! AssumeCircleGeometry,
   bC = Thread[Flatten@(neumannFluxTerms /. varToTimeDepRule) == 0];
   ,
   bC = (neumannFluxTerms /. varToTimeDepRule);
  ];

  varListDeriv =
   Function[var, Head@#'[Global`t] & /@ (Flatten@var)] /@ varList;
  diffVarListDeriv = (Head@#'[Global`t] & /@ (Flatten@diffVarList));

  If[AssumeCircleGeometry,
   selInteriorResCrit = Flatten@interiorDomainSelectMat;
   partitionedVarList = Pick[#, domainSelectMat, 1] & /@
     (Partition[#, varDimX, varDimX, 1, {}] & /@ varList);
   boundEqnSys = Pick[#, Flatten@domainSelectMat, 1] &@
     Thread[varListDeriv[[2]] == reactionEqnSys[[2]]];
   iC = Partition[# /. Global`t → 0, varDimX, varDimX, 1, {}] & /@ varList;
   ,
   selInteriorResCrit =
    If[MemberQ[Flatten@interiorDiffVarList, #], 1, 0] & /@
     (Flatten@ diffVarList );
   partitionedVarList = Partition[#, varDimX, varDimX, 1, {}] & /@ varList;
   boundEqnSys = Thread[varListDeriv[[2]] == reactionEqnSys[[2]]];
   iC = Partition[# /. Global`t → 0, varDimX, varDimX, 1, {}] & /@ varList;
  ];

  diffEqnSys =
   Pick[#, selInteriorResCrit, 1] &@Thread[diffVarListDeriv ==  (Global`𝒟
         diffEqnSysJac.(Flatten@diffVarList ) + reactionEqnSys[[1]])];

  Return[
   {Join[diffEqnSys, boundEqnSys], bC, iC, partitionedVarList, paramList}]
 ];
```

- **Solver**

```
solveSystem[paramList_List, tEnd_,
    {EqnSys_, bC_, iC_, varList_}, setIC_: {}, useCircleDomain_: False] :=
  Module[{nsol, varListDeriv, useIC, cutOff,
    domainSelectMat, iCLength, origUseIC},
   useIC = Global`pickIC /. setIC /. Global`pickIC → iC;

   If[useCircleDomain,
    origUseIC = useIC;
    iCLength = Length[iC[[1]]];
    domainSelectMat = DiskMatrix[All, iCLength];
    (*useIC= Pick[#,domainSelectMat,1]&/@useIC;*)
    useIC = Map[First@# == If[Last@# ≤ 0, 0, Last@#] &,
      (Pick[#, domainSelectMat, 1] & /@ useIC), {3}];
   ];

   (*Print[Length@useIC];
   Print[Dimensions@useIC];
   Print[Flatten@useIC//Length];
   Print[Length@bC];
   Print[Length@EqnSys];
   Print[Length@(Flatten@varList)];
   Abort[];*)

   (*
   Print[Length@(Flatten@EqnSys),(Flatten@EqnSys)[[1;;2]]/.paramList];
   Print[Length@(Flatten@useIC), (Flatten@useIC)[[1;;10]]];
   Print[Length@(Flatten@bC), (Flatten@bC)];
   Print[Length@(Flatten@varList), (Flatten@varList)[[1;;10]]];

   Print[Length@(Union@Flatten@varList),
    (Union@Flatten@varList)[[1;;10]]];
   Abort[];(**)*)

   nsol = NDSolve[Join[EqnSys /. paramList, Flatten@bC, Flatten@useIC],
     Flatten@varList, {Global`t, 0, tEnd}, Method → Automatic,
     AccuracyGoal → 4, PrecisionGoal → 4]
  ];
```

Plotting

```
Options[computeRecoveryCurve] =
  {Global`Binning → {{1, 20, 1}, {21, 40, 2}, {41, 58, 3},
     {59, 78, 4}, {79, 98, 5}, {99, 116, 6}, {117, 137, 7},
     {138, 153, 8}, {154, 171, 9}, {172 , 191 , 10}, {192, 200, 9}}};

computeRecoveryCurve[paramRule_List, solverStructure_List,
   setGaussIC_, { normProteinDistribList_, minNormProteinDistribList_},
   {pixelLeft_, pixelRight_}, imgDim_, recoveryData_List,
   discretizationDim_, tMax_, opts___Rule] :=
  Module[{eqnSys, bC, iC, varList, freeFracVal, gaussProfAsFreePIC,
    gaussProfAsBoundPIC, spatial_nsol, sumProteinRecoveryList,
    sumProteinRecoveryPlot, recoveryDataTimePoints,
    misMatchObj, doPlot, numPlotPoints = 500, myBin
```

```
 (*myBin={{1,20,1},{21,34,2},{35,43,3},{44,51,4},{52,56,5},
   {57,62,6},{63,69,7},{70,77,8},{78,86,9},{87,496,10}}*)
 (*myBin={{1,20,1},{21,40,2},{41,58,3},{59,78,4},{79,98,5},
   {99,116,6},{117,137,7},{138,153,8},{154,171,9},{172 ,191 ,10},
   {192,213,11},{214,237 ,12},{238 ,250 ,13},{251, 278, 14},
   {279 ,293 ,15},{294 ,309, 16},{310 ,326 ,17},{327 ,344 ,18},
   {345, 363 ,19},{364 ,383 ,20},{384 ,404 ,21},{405 ,426 ,22},
   {427 ,449 ,23},{450, 473, 24},{474 ,498 ,25},{499, 525 ,27}}*)

 (*={{1,20,1},{21,40,2},{41,58,3},{59,78,4},{79,98,5},{99,116,6},
   {117,137,7},{138,153,8},{154,171,9},{172 ,191 ,10},{192,200,9}}*)
},


(*myBin=Global`Binning/.{opts}/.Options[computeRecoveryCurve];*)
(*Print["mybin = ",myBin];*)

{eqnSys, bC, iC, varList} = solverStructure;
freeFracVal = Global`freeFraction /. paramRule;

(*If[(!NumericQ[freeFracVal])||(freeFracVal≤ 0),
  Print["Error: freeFracVal should be a positive value."];
  Abort[]
 ];*)

(*gaussProfAsFreePIC=
 MapThread[First@#1==If[#2==0,0,Last@#1*1/(#2/freeFracVal)]&,
  {setGaussIC[[1]], normProteinDistribList},2];
guassProfAsBoundPIC=MapThread[First@#1==
    Max[0,If[#2==0,0,Last@#1*(#2/freeFracVal-1)/(#2/freeFracVal)]]&,
  {setGaussIC[[2]], normProteinDistribList},2];*)

(*If[freeFracVal== 1,
  gaussProfAsFreePIC=MapThread[(First@#1==Last@#1)&,
    {setGaussIC[[1]], normProteinDistribList},2];
  guassProfAsBoundPIC=MapThread[(First@#1==0)&,
    {setGaussIC[[2]], normProteinDistribList},2];
  ,
  gaussProfAsFreePIC=
   MapThread[First@#1==If[#2==0,0,Last@#1*1/(#2/freeFracVal)]&,
    {setGaussIC[[1]], normProteinDistribList},2];
  guassProfAsBoundPIC=MapThread[First@#1==
      Max[0,If[#2==0,0,Last@#1*(#2/freeFracVal-1)/(#2/freeFracVal)]]&,
    {setGaussIC[[2]], normProteinDistribList},2];
 ];*)

If[freeFracVal === 1,
 gaussProfAsFreePIC = MapThread[(First@#1 == Last@#1) &,
   {setGaussIC[[1]], normProteinDistribList}, 2];
 gaussProfAsBoundPIC = MapThread[(First@#1 == 0) &,
   {setGaussIC[[2]], normProteinDistribList}, 2];
 ,
 (*Print["myBin = ",myBin];*)
 gaussProfAsFreePIC =
  MapThread[((First@#1) == (Last@#1) * Min[freeFracVal, #2]) &,
```

```
    {setGaussIC[[1]], normProteinDistribList}, 2];
  gaussProfAsBoundPIC =
   MapThread[((First@#1) == (Last@#1) * Max[(#2 - freeFracVal), 0]) &,
    {setGaussIC[[2]], normProteinDistribList}, 2];
  (*Print["gaussProfAsFreePIC[[1,1]] = ", gaussProfAsFreePIC[[1,1]]];*)
 ];

 (*Print[tMax];*)
 If[! NumericQ[tMax], Print["tMax not numerical!"]; Abort[]];

 spatial…nsol = solveSystem[paramRule, tMax, solverStructure,
   Global`pickIC → {gaussProfAsFreePIC, gaussProfAsBoundPIC}, True];

 recoveryDataTimePoints = First /@ recoveryData;

 Print["recoveryDataTimePoints[[1;;5]] = ",
  recoveryDataTimePoints[[1 ;; 5]]];

 (*Print["last time point =",
   Last[logBinData[Range[0,tMax,tMax/numPlotPoints],myBin]]];*)

 {sumProteinRecoveryList, sumProteinRecoveryPlot} =
  getRecoveryProfile[varList, spatial…nsol, {pixelLeft, pixelRight},
   imgDim, {#, #} &@discretizationDim, recoveryDataTimePoints
   (*logBinData[recoveryDataTimePoints,myBin]*), Global`getPlot → True];

 Return@sumProteinRecoveryPlot
];
```

```
Options[makePlots] = {Global`plotType → "3D"};
makePlots[varList_List, component_Integer, nsol_,
  tList_List, opt___Rule] := Module[{(**)paddedVarList(**)},

  paddedVarList =
   Function[var, ArrayPad[#, (Max@(Length@varList[[1]]) - Length@#) / 2] & /@
      var] /@ varList;


    (* DistributeDefinitions[paddedVarList,nsol];*)

  (*parMapResult=ParallelMap[Dimensions@#&,paddedVarList];
  Print[parMapResult];
  parMapResult=ParallelMap[Dimensions@#&,paddedVarList[[1]]];
  Print[parMapResult];*)

  If[(Global`plotType /. {opt} /. Options[makePlots]) == "Contour",

   (*Print["tList = ", tList];
   Print["dim = ",ParallelMap[
     Dimensions[Reverse@(paddedVarList[[component]])/.nsol/.Global`t→#]&,
     tList]];*)

   myPlot = (*Parallel*)Map[
        ListContourPlot[
          Reverse@(paddedVarList[[component]]) /. nsol /. Global`t → #,
          PlotLabel → Style["t = " <> ToString@#, Bold, Brown],
          ImageSize → {150, Automatic}, AspectRatio → 1, FrameTicks → None] &,
        tList] // Partition[#, 4, 4, 1, {}] & // Grid;
   ,
   myPlot = (*Parallel*)
     Map[ListPlot3D[Evaluate[(ArrayPad[#, 1] &@Reverse@(paddedVarList[[
                   component]])) /. nsol /. Global`t → #], PlotRange → All,
          PlotLabel → Style["t = " <> ToString@#, Bold, Brown],
          ImageSize → {150, Automatic}, AspectRatio → 1, Mesh → None] &,
        tList] // Partition[#, 4, 4, 1, {}] & // Grid;
  ];
  Return@myPlot
 ]
```

Parameter Optimization

```
Options[computeMismatch] = {Global`DisplayPrint → None};
computeMismatch[paramVal__?NumericQ,
   paramVar_List, solverStructure_List, setGaussIC_,
   {normProteinDistribList_, minNormProteinDistribList_},
   {pixelLeft_, pixelRight_}, imgDim_, recoveryData_,
   discretizationDim_?NumericQ, tMax_, opts___Rule] :=
  Module[{eqnSys, bC, iC, varList, freeFracVal,
    gaussProfAsFreePIC, gaussProfAsBoundPIC, spatial_nsol,
    sumProteinRecoveryList, sumProteinRecoveryPlot,
    recoveryDataTimePoints, misMatchObj, doPlot, paramRule},
```

```
paramRule = Thread[paramVar → {paramVal}];

{eqnSys, bC, iC, varList} = solverStructure;
freeFracVal = Global`freeFraction /. paramRule;

(*If[freeFracVal== 1,
  gaussProfAsFreePIC=MapThread[(First@#1==Last@#1)&,
    {setGaussIC[[1]], normProteinDistribList},2];
  guassProfAsBoundPIC=MapThread[(First@#1==0)&,
    {setGaussIC[[2]], normProteinDistribList},2];
  ,
  gaussProfAsFreePIC=
   MapThread[First@#1==If[#2==0,0,Last@#1*1/(#2/freeFracVal)]&,
    {setGaussIC[[1]], normProteinDistribList},2];
  guassProfAsBoundPIC=MapThread[First@#1==
      Max[0,If[#2==0,0,Last@#1*(#2/freeFracVal-1)/(#2/freeFracVal)]]&,
    {setGaussIC[[2]], normProteinDistribList},2];
 ];*)

(*If[(!NumericQ[freeFracVal])||(freeFracVal≤ 0),
  Print["Error: freeFracVal should be a positive value."];
  Abort[]
 ];*)

If[freeFracVal === 1,
 gaussProfAsFreePIC = MapThread[(First@#1 == Last@#1) &,
   {setGaussIC[[1]], normProteinDistribList}, 2];
 gaussProfAsBoundPIC = MapThread[(First@#1 == 0) &,
   {setGaussIC[[2]], normProteinDistribList}, 2];
 ,
 gaussProfAsFreePIC =
  MapThread[((First@#1) == (Last@#1) * Min[freeFracVal, #2]) &,
   {setGaussIC[[1]], normProteinDistribList}, 2];
 gaussProfAsBoundPIC =
  MapThread[(First@#1 == (Last@#1) * Max[(#2 - freeFracVal), 0]) &,
   {setGaussIC[[2]], normProteinDistribList}, 2];
];

spatial_nsol = solveSystem[paramRule, tMax, solverStructure,
  Global`pickIC → {gaussProfAsFreePIC, gaussProfAsBoundPIC}, True];

(*Print[Last/@recoveryData];*)
recoveryDataTimePoints = Select[First /@ recoveryData, 0 ≤ # ≤ tMax &];

(*Print["last time pt = ",Last@recoveryDataTimePoints];*)

sumProteinRecoveryList = getRecoveryProfile[varList, spatial_nsol,
  {pixelLeft, pixelRight}, imgDim, {#, #} &@discretizationDim,
  recoveryDataTimePoints, Global`getPlot → False];

misMatchObj = (*1/Length@sumProteinRecoveryList**)
 (Norm[#, 2] &@MapThread[(#1[[2]] - #2[[2]]) &, {sumProteinRecoveryList,
     Select[recoveryData[[2 ;;]], 0 ≤ First@# ≤ tMax &]}]);

(*Print[{ListPlot[#,PlotRange→ {All,{-0.5,1}}]&@
```

```
      MapThread[(#1[[2]]-#2[[2]])&,{sumProteinRecoveryList, Select[
         recoveryData[[2;;]],0≤  First@#≤ tMax&]}], misMatchObj}];*)

  (*If[(Global`DisplayPrint/.{opts}/.Options[computeMismatch]),*)
  If[NumericQ[Global`DisplayPrint /. {opts} /. Options[computeMismatch]],
   If[NumericQ[misMatchObj],
    Print["Problem " <> ToString[Global`DisplayPrint /. {opts}],
      ", param: ", paramRule, " obj: ", misMatchObj];
    ,
    Print["Problem " <> ToString[Global`DisplayPrint /. {opts}],
      ", param: ", paramRule, " obj NOT A NUMBER! "];
   ]
  ];

  If[NumericQ[misMatchObj],
   Return@misMatchObj,
   Return@1000
  ];
 ];
```

Post-Process

```
Options[getRecoveryProfile] = {Global`getPlot → True};
getRecoveryProfile[varList_List, nsol_,
   {pixelNuclLeft_?NumericQ, pixelNuclRight_?NumericQ},
   imgDim_List, discretDim_List, timeList_List, opts___Rule] :=
  Module[{intensityNormFactor, varOfInterest,
    (*discretDim={#,#}&@@Global`$discretizationDim,*)
    recoveryList, recoveryPlot, paddedVarList},

   (*Print["discretDim = ", discretDim];
   Print["timeList = ",timeList];*)

   paddedVarList =
    Function[var, ArrayPad[#, (Max@(Length@varList[[1]]) - Length@#) / 2] & /@
       var] /@ varList;



   (*Print["getRecoveryProfile: {pixelNuclLeft,pixelNuclRight} = ",
     {pixelNuclLeft,pixelNuclRight}];*)

   intensityNormFactor = Plus @@ Flatten@MapIndexed[
       obsHoleFunction[Sequence @@ (Reverse@
            {#2[[1]], discretDim[[2]] + 1 - #2[[2]]}), discretDim, imgDim,
         {pixelNuclLeft, pixelNuclRight}] &, paddedVarList[[1]], {2}];

   (*Print["intensityNormFactor = ",intensityNormFactor];*)

   (*Print["var of interest = ",
     MapIndexed[#1*obsHoleFunction[Sequence@@Reverse@{#2[[1]],discretDim[[
                2]]+1-#2[[2]]}, discretDim,imgDim, {pixelNuclLeft,
           pixelNuclRight}]&,Plus@@paddedVarList,{2}]/.x_[t]:→ 1
```

```
      //ArrayPlot];*)

  varOfInterest =
   Plus @@ (Flatten@MapIndexed[#1 * obsHoleFunction[Sequence @@ Reverse@
              {#2[[1]], discretDim[[2]] + 1 - #2[[2]]},
            discretDim, imgDim, {pixelNuclLeft, pixelNuclRight}] &,
        Plus @@ paddedVarList, {2}]) /. nsol;

  (*DistributeDefinitions[intensityNormFactor, varOfInterest];
  Return@ParallelMap[
    Flatten@{#,1/intensityNormFactor*varOfInterest/.t→ #}&, timeList]*)

  (*Print["timeList = ", timeList];*)

  recoveryList = Prepend[#, {timeList[[1]], 1}] &@Map[
     Flatten@{#, 1 / intensityNormFactor * varOfInterest /. Global`t → #} &,
     timeList[[2 ;;]]];

  (*Print["recoveryList[[1;;5]] = ",recoveryList[[1;;5]]];*)

  If[Global`getPlot /. {opts} /. Options[getRecoveryProfile],
   (*Print["doing getPlot..."];*)

   recoveryPlot = ListPlot[Prepend[#, {timeList[[1]], 1}] &@ recoveryList,
     Frame → True, ImageSize → {400, Automatic}, Filling → 0,
     FillingStyle → Opacity[0.3, LightPink], FrameLabel →
      (Style[#, Bold, 12, Brown] & /@ {"Time (s)", "Normalized intensity"}) ,
     Joined → True, PlotRange → {All, {0, All}},
     PlotStyle → Directive[ Thick, Orange], Axes → None, Mesh → All];
   Return[{recoveryList, recoveryPlot}]
   ,
   Return@recoveryList]
 ];
```

```
End[]
```

```
EndPackage[]
```

D.2 MathFRAP Sample

FRAP Analysis Results

Initialization

```
myWorkingDirectory = "~/Documents/IMBA/MathFolder/";
SetDirectory[%];
<< MathFRAP_Algorithm.m
SetOptions[ListPlot, Frame → True, ImageSize → {300, Automatic}];
DistributeDefinitions["MathFRAP`*"];
DistributeDefinitions["MathFRAP`Private`*"];
```

Code

```
holeFunction[x_, y_] :=
  Module[{radius = 40}, If[(x - 256)^2 + (y - 31)^2 ≤ 20^2, 1, 0]];
photoBleachProfile[x_, y_, center_List, {theta_, rC_, sigma_}] := Module[
   {rInMicron = 0.045 * Sqrt[(x - center[[1]])^2 + (y - center[[2]])^2]},
   If[rInMicron ≤ rC, theta,
    1 - (1 - theta) Exp[-(rInMicron - rC)^2 / (2 sigma^2)]]
  ];

getMyBleachProfile[{centerHoriz_, centerVert_}, nucleusSize_,
  {theta_, rC_, sigma_}] := Module[{centerX = 512 / 2, initGaussProfile},
  initGaussProfile = MapIndexed[photoBleachProfile[#2[[1]], #2[[2]],
      {centerHoriz, centerVert}, {theta, rC, sigma}] &,
    IdentityMatrix[nucleusSize], {2}];

  Return@initGaussProfile
 ]
```

```
myObsHole[inputX_, inputY_,
   discretDim_List, imgDim_List, {centerX_, centerY_}] :=
  Module[{origImgWidth = 512, observeRadius = 20, x, y, bleachSpot},
   bleachSpot = {centerX, centerY};
    x = inputX / (discretDim[[1]]) * imgDim[[1]];
   y = inputY / (discretDim[[2]]) * imgDim[[2]] ;
   If[
    (x - bleachSpot[[1]])^2 + (y - bleachSpot[[2]])^2 ≤ observeRadius^2, 1, 0]
  ];
```

```
Options[myGetRecoveryProfile] = {Global`getPlot → True};
myGetRecoveryProfile[varList_List, nsol_,
    {centerX_?NumericQ, centerY_?NumericQ}, imgDim_List,
    discretDim_List, timeList_List, prebleachImgIC_List, opts___Rule] :=
  Module[{intensityNormFactor, varOfInterest,
    recoveryList, recoveryPlot, paddedVarList},

   paddedVarList =
    Function[var, ArrayPad[#, (Max@(Length@varList[[1]]) - Length@#) / 2] & /@
       var] /@ varList;


   paddedVarListToPrebleachedIC =
    paddedVarList[[1]] /. t → 0 /. (Flatten@prebleachImgIC /. Equal → Rule);

   intensityNormFactor = Plus @@ Flatten@MapIndexed[
       #1 * myObsHole[Sequence @@ ((*Reverse@*)
             {#2[[1]], discretDim[[2]] + 1 - #2[[2]]}), discretDim, imgDim,
          {centerX, centerY}] &, paddedVarListToPrebleachedIC, {2}];


   varOfInterest =
    Plus @@ (Flatten@MapIndexed[#1 * myObsHole[Sequence @@ (*Reverse@*)
              {#2[[1]], discretDim[[2]] + 1 - #2[[2]]}, discretDim, imgDim,
            {centerX, centerY}] &, Plus @@ paddedVarList, {2}]) /. nsol;

   recoveryList = Map[
     Flatten@{#, 1 / intensityNormFactor * varOfInterest /. Global`t → #} &,
     timeList];

   Return@recoveryList
  ];
```

```
myComputeRecoveryCurve[paramRule_List, solverStructure_List,
    setGaussIC_, { normProteinDistribList_, minNormProteinDistribList_},
    {centerX_, centerY_}, imgDim_, recoveryData_List,
    prebleachImgIC_, discretizationDim_, tMax_] :=
  Module[{eqnSys, bC, iC, varList, freeFracVal, gaussProfAsFreePIC,
     gaussProfAsBoundPIC, spatial…nsol, sumProteinRecoveryList,
     sumProteinRecoveryPlot, recoveryDataTimePoints,
     misMatchObj, doPlot, numPlotPoints = 500, myBin},

    {eqnSys, bC, iC, varList} = solverStructure;
    freeFracVal = Global`freeFraction /. paramRule;

    If[freeFracVal === 1,
     gaussProfAsFreePIC = MapThread[(First@#1 == Last@#1) &,
       {setGaussIC[[1]], normProteinDistribList}, 2];
     gaussProfAsBoundPIC = MapThread[(First@#1 == 0) &,
       {setGaussIC[[2]], normProteinDistribList}, 2];
     ,
     gaussProfAsFreePIC = MapThread[((First@#1) == (Last@#1) * freeFracVal) &,
       {setGaussIC[[1]], normProteinDistribList}, 2];
     gaussProfAsBoundPIC =
      MapThread[((First@#1) == (Last@#1) * (1 - freeFracVal)) &,
       {setGaussIC[[2]], normProteinDistribList}, 2];
    ];

    If[! NumericQ[tMax],
     Print["tMax = ", tMax, ": not numerical!"]; Abort[]];

    spatial…nsol = solveSystem[paramRule, tMax, solverStructure,
      Global`pickIC → {gaussProfAsFreePIC, gaussProfAsBoundPIC}, True];
    recoveryDataTimePoints = First /@ recoveryData;


    sumProteinRecoveryList = myGetRecoveryProfile[
      varList,  spatial…nsol, {centerX, centerY} , imgDim,
      {#, #} &@discretizationDim, recoveryDataTimePoints, prebleachImgIC ];

    Return@sumProteinRecoveryList
   ];
```

```
myComputeMismatch[paramRule_List, solverStructure_List, setGaussIC_,
    {normProteinDistribList_, minNormProteinDistribList_},
    {centerX_, centerY_}, imgDim_, recoveryData_List,
    prebleachImgIC_, discretizationDim_, tMax_] :=
  Module[{eqnSys, bC, iC, varList, freeFracVal, gaussProfAsFreePIC,
    gaussProfAsBoundPIC, spatial…nsol, sumProteinRecoveryList,
    sumProteinRecoveryPlot, recoveryDataTimePoints,
    misMatchObj, doPlot, numPlotPoints = 500, myBin},

   {eqnSys, bC, iC, varList} = solverStructure;
   freeFracVal = Global`freeFraction /. paramRule;

   If[freeFracVal === 1,
    gaussProfAsFreePIC = MapThread[(First@#1 == Last@#1) &,
      {setGaussIC[[1]], normProteinDistribList}, 2];
    gaussProfAsBoundPIC = MapThread[(First@#1 == 0) &,
      {setGaussIC[[2]], normProteinDistribList}, 2];
    ,
    gaussProfAsFreePIC = MapThread[((First@#1) == (Last@#1) * freeFracVal) &,
      {setGaussIC[[1]], normProteinDistribList}, 2];
    gaussProfAsBoundPIC =
     MapThread[((First@#1) == (Last@#1) * (1 - freeFracVal)) &,
      {setGaussIC[[2]], normProteinDistribList}, 2];
   ];

   If[! NumericQ[tMax],
    Print["tMax = ", tMax, ": not numerical!"]; Abort[]];

   spatial…nsol = solveSystem[paramRule, tMax, solverStructure,
     Global`pickIC → {gaussProfAsFreePIC, gaussProfAsBoundPIC}, True];
   recoveryDataTimePoints = First /@ recoveryData;

   sumProteinRecoveryList = myGetRecoveryProfile[
     varList,  spatial…nsol, {centerX, centerY} , imgDim,
     {#, #} &@discretizationDim, recoveryDataTimePoints, prebleachImgIC ];

   misMatchObj = (Norm[#, 2] &@MapThread[
        (#1[[2]] - #2[[2]]) &, {sumProteinRecoveryList, recoveryData }]);
   Return@misMatchObj
  ];
```

Upload Data

PC

```
directoryPrefix = "~/Documents/IMBA/MathFolder/PCGFP 101215/";
directoryNames = {"images"}
```

```
imageNames[pre] =
 (FileNames[directoryPrefix <> # <> "/*_pre.png"] & /@ directoryNames) //
  Flatten
image[pre] = Import[#] & /@ %;
ImageAdjust /@ %
```

```
imageNames[post] =
 (FileNames[directoryPrefix <> # <> "/*_post.png"] & /@ directoryNames) //
  Flatten
image[post] = Import[#] & /@ %;
ImageAdjust /@ %
```

```
recoveryDataNames =
 (FileNames[directoryPrefix <> # <> "/*_FRAPdata.mat"] & /@ directoryNames) //
  Flatten
recoveryData = Import /@ %;
```

```
imageDataNames = (FileNames[directoryPrefix <> # <> "/*_parameters.mat"] & /@
    directoryNames) // Flatten
imageData = Import /@
  %
```

Parameter Identification

PC

Initial Recovery Curve

```
discretizationDim = 40;
myCodeDirectory = myWorkingDirectory;
SetDirectory[%];
```

```
DistributeDefinitions[getNormalizedProteinOnDisk,
 discretizationDim, fitCutOffFunction]
chromatinStructure["GFP"] =
  Map[getNormalizedProteinOnDisk[#, discretizationDim,
     fitCutOffFunction[#, Global`DoFit → False]] &, image[pre]];
(*Nintegrate errors are fine at this position*)
```

```
nomParamList = { kOn → #[[7]], kOff → #[[8]] ,
    freeFraction → Min[( #[[8]] / ( #[[7]] + #[[8]])), 1],
    𝒟 → #[[6]] / 0.045^2} & /@ Flatten[imageData, 2]
```

```
DistributeDefinitions[discretizationDim];
DistributeDefinitions["MathFRAP`*"];
DistributeDefinitions["MathFRAP`Private`*"];

equationStructure["GFP"] =
  ParallelMap[getEqnSystem[#[[1]], {discretizationDim, discretizationDim} ,
     {freeProtein, boundProtein}, freeProtein,
     True, #[[2]], #[[3, 2]], True, DoPlots → True] &,
   getEqnSysInput["GFP"], Method → "CoarsestGrained"];
```

```
gaussICInput["GFP"] = MapThread[{#1, #2} &,
   {ImageData[#] & /@ image[post], #[[3]] & /@ equationStructure["GFP"] }];
gaussIC["GFP"] = Map[Function[{input},
    imageToInitCondition[Image@(input[[1]]), input[[2]], #][[#]] & /@
     {1, 2}], gaussICInput["GFP"]];
```

```
prebleachImageInput["GFP"] = MapThread[{#1, #2} &,
   {ImageData /@ image[pre], #[[3]] & /@ equationStructure["GFP"] }];
prebleachImgToIC["GFP"] = Map[Function[{input},
    imageToInitCondition[Image@(input[[1]]), input[[2]], #][[#]] & /@
     {1, 2}], prebleachImageInput["GFP"]];
```

```
freeFracMax = #[[3]] & /@ chromatinStructure["GFP"]
```

```
getRecoveryCurveInput["GFP"] = {
    MapIndexed[ #2[[1]] → #1 &, nomParamList],
    #[[1 ;; 4]] & /@ equationStructure["GFP"],
    gaussIC["GFP"],
    #[[2 ;; 3]] & /@ chromatinStructure["GFP"],
    #[[1 ;; 2]] & /@ Flatten[imageData, 2],
    ImageDimensions /@ image[pre],
    Flatten[recoveryData, 1],
    prebleachImgToIC["GFP"]
    } // Transpose;
```

```
tEnd = Max[First /@ (Last[#] & /@ Flatten[recoveryData, 1])];
DistributeDefinitions[holeFunction, getMyBleachProfile,
  myObsHole, myGetRecoveryProfile, myComputeRecoveryCurve,
  myComputeMismatch, tEnd, discretizationDim, tEnd];

recoveryCurves["GFP"] = ParallelMap[
   myComputeRecoveryCurve[#[[1, 2]], #[[2]], #[[3]], #[[4]],
     #[[5]], #[[6]], #[[7]], #[[8]], discretizationDim, tEnd] &,
   getRecoveryCurveInput["GFP"]];
```

```
recoveryCurves["GFP"][[2]]
```

```
MapThread[
 ({ListPlot[#1, Joined → True, PlotStyle → {Thick, Blue}, Filling → 0,
      Axes → None, PlotRange → {All, {0, All}}, Background → White],
    ListPlot[(#2), Joined → True, PlotStyle → {Thick, Orange}, Filling → 0,
      Axes → None, PlotRange → {All, {0, All}}, Background → White]} //
   Show)  &, {recoveryCurves["GFP"], recoveryData}]
```

InteriorPoint

```
myObjFunc[𝒟val_?NumericQ, kOffval_?NumericQ,
   freeFractionval_?NumericQ, regParam_, recoveryCurveInput_] :=
  Module[{nominalParamVector = recoveryCurveInput[[1, 2]]},

   inputParamRule =
    Thread[{𝒟, kOff, freeFraction} → {𝒟val, kOffval, freeFractionval}];
   Print[inputParamRule];

   misMatchValue =
    Map[myComputeMismatch[inputParamRule, #[[2]], #[[3]], #[[4]],
        #[[5]], #[[6]], #[[7]], #[[8]], discretizationDim, tEnd] &,
      {recoveryCurveInput}][[1]];

   regularizationValue = +regParam * Sqrt@(Plus @@
        (#^2 & /@ {(𝒟val - 𝒟 /. nominalParamVector) / (𝒟 /. nominalParamVector)
            , kOffval - kOff /. nominalParamVector,
           freeFractionval - freeFraction /. nominalParamVector}));

   Print["prob ", recoveryCurveInput[[1, 1]], " mis-match = ",
    misMatchValue, " regularization = ", regularizationValue];
   Return[misMatchValue + regularizationValue]];
```

```
mu = 0.1;
(*the larger the more fixed at the starting value*)
DistributeDefinitions[mu, myObjFunc];
DistributeDefinitions[holeFunction,
  getMyBleachProfile, myObsHole, myGetRecoveryProfile,
  myComputeRecoveryCurve, myComputeMismatch, discretizationDim];

findMinSol["GFP"] = ParallelMap[FindMinimum[
     {myObjFunc[𝒟val, kOffval, freeFractionval, mu, #],
      𝒟val ≥ 0, kOffval ≥ 0, 0 ≤ freeFractionval ≤ #[[4, 2]] },
     {{𝒟val, 𝒟 /. #[[1, 2]]}, {kOffval, kOff /. #[[1, 2]]},
      { freeFractionval, freeFraction /. #[[1, 2]]}},
     Method → "InteriorPoint", MaxIterations → (30 + 20), AccuracyGoal →
      (2 + 1), PrecisionGoal → (2 + 1)] &, getRecoveryCurveInput["GFP"] ];
```

```
findMinSol["GFP"]
params = Flatten /@ findMinSol["GFP"]
```

```
MapIndexed[StringReplace[ imageNames[pre][[#2[[1]]]],
        {y__ ~~ "/" ~~ x__ :> x, "_pre.png" → "", "SOP_*" → ""}] →
       (Thread[{misMatch, 𝒟, kOff, freeFraction} →
          Join[{First@#1}, (Last /@ Last@#1)]]) &,
    # & /@ findMinSol["GFP"]] /. HoldPattern[𝒟 → x_] :> 𝒟 → x * 0.045^2 //
  TableForm // Style[#, Bold, 15, Background → LightBlue] &
```

```
getRecoveryCurveInput["GFP_result"] = {
    MapIndexed[
     #2[[1]] → (Thread[{𝒟, kOff, freeFraction} → (Join[Last /@ #1, {}])]) &,
     (Last@# & /@ findMinSol["GFP"])],
    #[[1 ;; 4]] & /@ equationStructure["GFP"],
    gaussIC["GFP"],
    #[[2 ;; 3]] & /@ chromatinStructure["GFP"],
    #[[1 ;; 2]] & /@ Flatten[imageData, 2],
    ImageDimensions /@ image[pre],
    Flatten[recoveryData, 1],
    prebleachImgToIC["GFP"]
    } // Transpose;
```

```
recoveryCurves["GFP_result"] = ParallelMap[
   myComputeRecoveryCurve[#[[1, 2]], #[[2]], #[[3]], #[[4]],
     #[[5]], #[[6]], #[[7]], #[[8]], discretizationDim, tEnd] &,
   getRecoveryCurveInput["GFP_result"]];
```

```
MapThread[
  {#3, ({ListPlot[#1, Joined → True, PlotStyle → {Thick, Blue}, Filling → 0,
       Axes → None, PlotRange → {All, {0, All}}, Background → White],
      ListPlot[Flatten[(#2), 1], Joined → True,
       PlotStyle → {Thick, Orange}, Filling → 0, Axes → None,
       PlotRange → {All, {0, All}}, Background → White]} // Show)}  &,
  {recoveryCurves["GFP_result"], recoveryData, Style[
     StringReplace[#, {"_pre.png" → "", "SOP_" → "", y__ ~~ "/" ~~ x__ :> x}],
     Bold, Blue] & /@ imageNames[pre]}] // TableForm
```

```
SetDirectory[directoryPrefix ]
```

```
fitparameters = MapIndexed[StringReplace[
       imageNames[pre][[#2[[1]]]], {y__ ~~ "Binary" ~~ x__ :> x}] →
      (Thread[Join[{First@#1}, (Last /@ Last@#1)]]) &,
   # & /@ findMinSol["GFP"]];

test = Last /@ fitparameters;
test2 = ReplacePart[# , 2 → #[[2]] * 0.045^2] & /@ test;

(*names=MapIndexed[
     StringReplace[ imageNames[pre][[#2[[1]]]],{y__~~"Binary"~~x__:> x}] &,
     #&/@ findMinSol["GFP"]]

   fitparameters=MapIndexed[
   StringReplace[ imageNames[pre][[#2[[1]]]],{y__~~"Binary"~~x__:> x}] →
     (Thread[ReplacePart[# , 2→ #[[2]]*0.045^2]&/@test) &,
   #&/@ findMinSol["GFP"]];

fitparameters=MapIndexed[
  StringReplace[ imageNames[pre][[#2[[1]]]],{y__~~"Binary"~~x__:> x}] →
    (Thread[Last[#]])&,#&/@ findMinSol["GFP"]];

fitparameters=MapIndexed[
   StringReplace[ imageNames[pre][[#2[[1]]]],{y__~~"Binary"~~x__:> x}] →
     (test2[#2])&,#&/@ findMinSol["GFP"]]

  test2,1*)

Export["fitparameters.xls", test2]
```

```
parameters = MapIndexed[
   StringReplace[ imageNames[pre][[#2[[1]]]], {y__ ~~ "Binary" ~~ x__ :> x}] →
     First@#1 &, # & /@ Flatten[imageData, 1]];
Export["parameters.xls", parameters]
```

```
fitcurves = MapIndexed[
   StringReplace[ imageNames[pre][[#2[[1]]]], {y__ ~~ "Binary" ~~ x__ :> x}] →
     #1 &, # & /@ recoveryCurves["GFP_result"]];
Export["fitcurves.xls", fitcurves]
```

```
recoveryDataFRAP = MapIndexed[
   StringReplace[ imageNames[pre][[#2[[1]]]], {y__ ~~ "Binary" ~~ x__ :> x}] →
     #1 &, # & /@ Flatten[recoveryData, 1]];
Export["recoveryData.xls", recoveryDataFRAP]
```

Appendix E

Publications

RESOURCE/METHODOLOGY

In vivo Polycomb kinetics and mitotic chromatin binding distinguish stem cells from differentiated cells

João Pedro Fonseca,[1] Philipp A. Steffen,[1] Stefan Müller,[2,5] James Lu,[3,5] Anna Sawicka,[4] Christian Seiser,[4] and Leonie Ringrose[1,6]

[1]Institute of Molecular Biotechnology (IMBA), 1030 Vienna, Austria; [2]Johann Radon Institute for Computational and Applied Mathematics (RICAM), 1030 Vienna, Austria; [3]Biomolecular Signaling and Control Group, Automatic Control Laboratory, Swiss Federal Institute of Technology (ETH Zurich), 9082 Zurich, Switzerland; [4]Max F. Perutz Laboratories (MFPL), Medical University of Vienna, 1030 Vienna, Austria

Epigenetic memory mediated by Polycomb group (PcG) proteins must be maintained during cell division, but must also be flexible to allow cell fate transitions. Here we quantify dynamic chromatin-binding properties of PH::GFP and PC::GFP in living *Drosophila* in two cell types that undergo defined differentiation and mitosis events. Quantitative fluorescence recovery after photobleaching (FRAP) analysis demonstrates that PcG binding has a higher plasticity in stem cells than in more determined cells and identifies a fraction of PcG proteins that binds mitotic chromatin with up to 300-fold longer residence times than in interphase. Mathematical modeling examines which parameters best distinguish stem cells from differentiated cells. We identify phosphorylation of histone H3 at Ser 28 as a potential mechanism governing the extent and rate of mitotic PC dissociation in different lineages. We propose that regulation of the kinetic properties of PcG–chromatin binding is an essential factor in the choice between stability and flexibility in the establishment of cell identities.

[*Keywords*: Polycomb; Polyhomeotic; *Drosophila*; mitosis; kinetics; stem cell]

Supplemental material is available for this article.

Received December 22, 2011; revised version accepted March 6, 2012.

Polycomb group (PcG) proteins play a crucial role in maintaining the repressed transcriptional states of their target genes in stem cells and differentiated cells (Sawarkar and Paro 2010). Cell division is a vital moment for the action of PcG proteins. The vast majority of chromatin-binding proteins dissociate from mitotic chromatin, and there is a global transcriptional shutdown (Prescott and Bender 1962; Martinez-Balbas et al. 1995; Gottesfeld and Forbes 1997). However, for the PcG target genes, it is through mitosis that the memory of transcriptional status must be maintained, and it is also during mitosis that an opportunity for flexibility in PcG target status exists, enabling changes of cell identity during differentiation. Thus, to better understand memory and flexibility, it is essential to study the behavior of PcG proteins during mitosis and differentiation.

Genome-wide profiling indicates that fly and vertebrate PcG proteins change their targets dynamically upon differentiation (Mohn et al. 2008; Schuettengruber and Cavalli 2009). Consistent with this, live imaging studies have documented changes in subcellular localization and PcG protein mobility upon differentiation (Chen et al. 2005; Ren et al. 2008) or at different stages of development (Ficz et al. 2005). However, a detailed quantitative analysis of the behavior of PcG proteins in living animals in a single-cell system with defined differentiation processes and mitotic activity is lacking. Binding of fly and vertebrate PcG proteins to mitotic chromatin has been observed in some cell types (Fanti et al. 2008; Vincenz and Kerppola 2008), while other studies report substantial dissociation (Buchenau et al. 1998; Dietzel et al. 1999). These differences may arise from the use of different techniques or may be species-specific or cell type-specific. Thus, whether there are quantitative changes in the nature

[5]These authors contributed equally to this work.
[6]Corresponding author.
E-mail leonie.ringrose@imba.oeaw.ac.at.
Article is online at http://www.genesdev.org/cgi/doi/10.1101/gad.184648.111.

of PcG binding to mitotic chromatin in different cell types of a single animal is not clear.

Here we investigate the behavior of GFP-fused Polycomb (PC::GFP) and Polyhomeotic (PH::GFP) in living *Drosophila* larval neuroblasts and pupal sensory organ precursor cells (SOPs). Neuroblasts are stem cell neuronal progenitors that divide asymmetrically to give origin to another neuroblast and a ganglion mother cell (GMC) (Doe 2008). SOPs are more determined cells that arise later in fly development and divide asymmetrically to give two well-defined daughter cells, pIIa and pIIb (Neumuller and Knoblich 2009). We use a combination of quantitative live imaging and mathematical modeling to query the interaction of PcG proteins with chromatin in the neuroblast and SOP lineages both in interphase and on metaphase chromosomes. We show that PcG protein mobility is decreased in more differentiated cells. In addition, we identify and quantify a fraction of mitotically bound PcG proteins whose chromatin-binding properties are profoundly different from those measured in interphase, showing up to 300-fold longer residence times. We identify mitotic phosphorylation of histone H3 at Ser 28 as a potential mechanism governing the extent and rate of mitotic PC dissociation. These findings suggest that mitosis provides a unique time frame in the cell cycle where the PcG system chooses between stability and flexibility during the establishment of cell identities.

Results

Transgenic PC::GFP and PH::GFP fulfill the functions of the endogenous proteins

To investigate the behavior of the Polycomb-repressive complex 1 (PRC1) proteins PC and PH during cell division and differentiation, we studied previously characterized EGFP fusions of these proteins (Dietzel et al. 1999; Ficz et al. 2005). (EGFP is henceforth referred to as GFP.) The PH::GFP fusion protein rescues homozygous *ph*-null alleles (Ficz 2005; Ficz et al. 2005) and thus can replace the endogenous protein. The PC::GFP fusion protein has been reported to rescue homozygous alleles carrying mutations in the PC chromodomain, such as Pc^{XL5}, but not homozygous null alleles, such as Pc^{3}, or those that produce C-terminally truncated protein (Dietzel et al. 1999). Thus the PC::GFP fusion can partially fulfill the functions of the endogenous protein in a *Pc* homozygous mutant context. The suitability of this fusion protein for live imaging studies had been addressed by several investigators, demonstrating that the PC::GFP fusion protein binds chromatin and participates in the PRC1 complex. This is supported by the banding pattern of PC::GFP on polytene chromosomes in both intact salivary gland nuclei (Dietzel et al. 1999; Ficz et al. 2005) and fixed preparations (Ficz et al. 2005). In addition, the genome-wide distribution of PC::GFP shows good agreement with that of endogenous PC (Kwong et al. 2008). Further supporting evidence for the correct chromatin-binding behavior of PC::GFP is the timing of mitotic dissociation and reassociation (Dietzel et al. 1999), which is identical to the distribution of PC measured for the endogenous PC protein determined by immunofluorescence (Buchenau et al. 1998).

Nevertheless, to further characterize the PC::GFP fusion protein, we re-examined its ability to rescue transheterozygous *Pc* mutants. Previous rescue experiments have been performed in homozygous mutant backgrounds (Dietzel et al. 1999). Since chromosomes carrying lethal mutations are maintained as heterozygote stocks over balancer chromosomes, they may accumulate second site mutations that lead to lethality when the chromosome is brought into the homozygous state in the rescue experiment. We did not observe rescue of transheterozygous combinations of null alleles; however, this analysis showed that the transheterozygous lethal combination of Pc^{3}/Pc^{XL5} was rescued to adulthood by the PC::GFP transgene (Fig. 1A). Thus, the PC::GFP transgene can rescue lethality in a more severely compromised genetic background than previously shown. F1

In the following experiments, we examine the behavior of PH::GFP and PC::GFP in neuroblasts of third instar larval brains and in SOPs of pupae. PcG expression is essential for neuroblast survival (Bello et al. 2007; Neumuller et al. 2011) and for normal development of SOPs and sensory organs (Sharp et al. 1994; Mummery-Widmer et al. 2009). We therefore asked whether the expression of an additional transgenic copy of PC or PH would adversely affect development in these lineages. PC::GFP was expressed under the control of the ubiquitous PC promoter (Dietzel et al. 1999), whereas PH::GFP was expressed from a UAS transgene (Ficz et al. 2005). In addition to the UAS sequence, the *ph::gfp* construct contains the *Pc* promoter; however, this promoter gives expression of PH::GFP only in salivary glands (Ficz et al. 2005). To drive expression of PH::GFP specifically in the neuroblast and SOP lineages, we used the *worniu* and *neuralized* GAL4 drivers. *worniu* is active in all neuroblasts of the larval brain but not in neuroblast progeny (Lee et al. 2006), in addition to expression in the embryonic CNS (Wheeler et al. 2006). *neuralized* is expressed in the SOP and its progeny cells (Bellaiche et al. 2001). It has been demonstrated that overexpression of PH transgenes leads to cell death and tissue abnormalities (Ficz 2005; Martinez et al. 2009). The UAS-GAL4 expression strategy for PH::GFP was intended to circumvent this problem by expressing the transgene during a limited developmental window.

In order to test whether even this limited expression strategy would nevertheless disrupt the lineages of interest, we examined the morphology and number of neuroblasts in larval brains and the morphology of sensory organs in adult flies. This analysis was performed for both PH::GFP and PC::GFP transgenes. Despite readily visible GFP signals, transgenic animals expressing either PH::GFP or PC::GFP showed normal larval brain morphology (Fig. 1B–D) and no detectable change in the number or morphology of neuroblasts (Fig. 1E–G). Likewise, in adults, no change in the number or morphology of sensory organs was detected in transgenic animals (Fig. 1H–J). We therefore conclude that the additional

transgenic copy of PH or PC does not adversely affect the development of the neuroblast and SOP lineages.

To determine expression levels of transgenes, we used quantitative Western blotting. Quantification of transgenic PH::GFP by Western blot was not possible due to the driver-inducible neuroblast- and SOP-specific expression of PH::GFP, which would require isolation of cell type-specific protein extracts. However, since PC::GFP is expressed under the control of the ubiquitous PC promoter, we reasoned that whole-tissue extracts of larval brains (Fig. 1K,L) and whole pupae (Fig. 1M,N) would be informative. Interestingly, the endogenous PC protein was substantially down-regulated in the presence of the transgene in both tissues, leading to a total PC overexpression of twofold in brains (Fig. 1L) and 1.2-fold in pupae (Fig. 1N). Similar down-regulation of the endogenous proteins in the presence of PH::GFP or PC::GFP transgenes in wing discs and embryos has been reported previously (Ficz et al. 2005). Thus, despite the presence of the additional transgenic copy, the total protein levels are near to endogenous levels. In addition, since they rescue mutants and do not adversely affect development, we conclude that both the PH::GFP and PC::GFP transgenes are useful reporters of endogenous protein behavior.

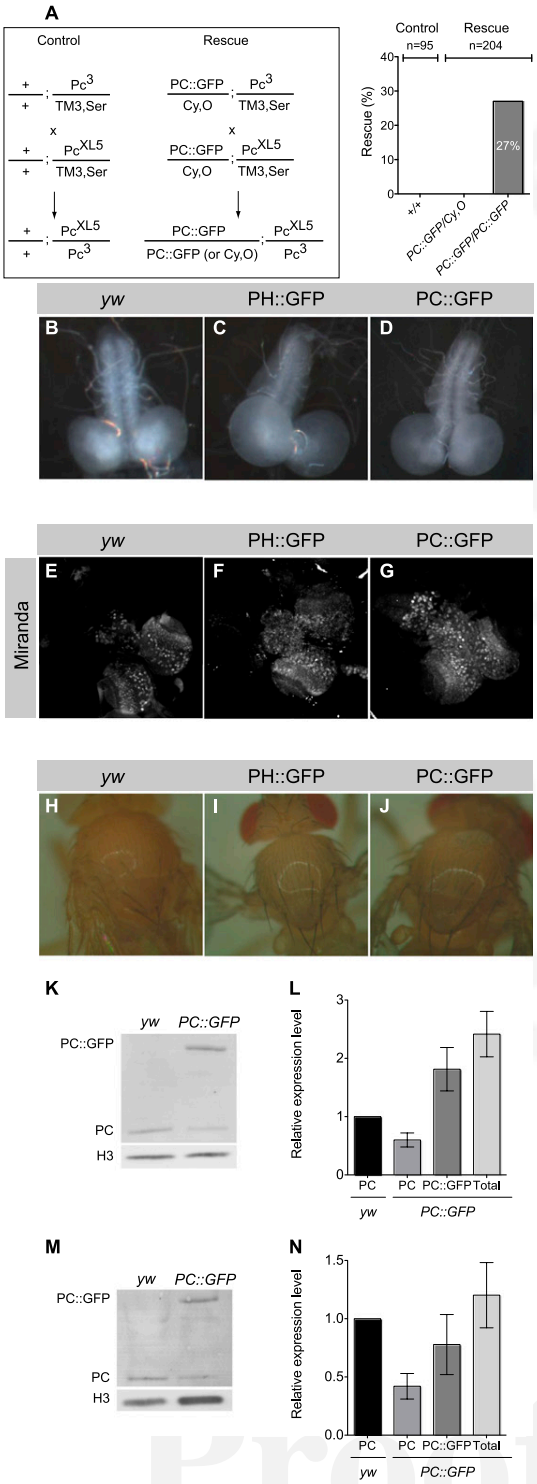

Quantitative live imaging of PcG proteins in single defined cell lineages reveals transitions in protein concentration upon entry into mitosis

To examine the behavior of PC::GFP and PH::GFP during mitotic division in neuroblasts and SOPs, we performed live-cell imaging on neuroblasts in whole larval brains (Fig. 2; Supplemental Movies S1, S2) and the SOP lineage in pupal notum (Fig. 3; Supplemental Movies S3, S4). To quantify GFP signal intensities, a three-dimensional (3D)

Figure 1. Analysis of PC and PH transgenes. (*A*) Rescue of Pc^{XL5}/Pc^{3} mutants by PC::GFP expression. Progeny of the crosses between +;Pc^{XL5}/*TM3,Sb* and +; Pc^{3}/*TM3,Sb* and between *Pc::GFP/CyO*; Pc^{XL5}/*TM3,Sb* and *Pc::GFP/CyO*; Pc^{3}/*TM3,Sb* were scored for the number of adult flies for which the third chromosome was Pc^{XL5}/Pc^{3}, and the proportion of these for which the second chromosome was heterozygous for the transgene (*PC::GFP*/+) or homozygous for the transgene (*PC::GFP/PC::GFP*) was calculated. The expected number of flies of each genotype in the event of a full rescue was calculated. (% rescue) The percentage of this expected number that was represented by flies of that genotype. *Above* the plot are shown the total number of flies counted in each experiment. (*B–J*) Transgenic PH::GFP and PC::GFP do not adversely affect the neuroblast and SOP lineages. (*B–D*) Third instar larval brains showing normal morphology in the presence of either PH::GFP (*C*) or PC::GFP (*D*) in comparison with control *yw* brains (*B*). (*E–G*) Third instar larval brains were stained with αMiranda antibody (see the Materials and Methods) to visualize neuroblasts, showing no detectable change in neuroblast number and localization in the presence of either transgene. (*H–J*) Adult nota of *yw* (*H*), *PH::GFP* (*I*), and *PC::GFP* (*J*) flies are shown, showing no detectable change in sensory organ number and morphology in transgenic flies. (*K,M*) Western blot using αPC antibody to detect endogenous and GFP-fused PC in extracts of third instar larval brains (*K*) and whole pupae (*M*) of *yw* and *PC::GFP* flies. Histone H3 was used as loading control. (*L,N*) Quantification of Western blots in *K* and *M*, performed as described in the Materials and Methods. Data show the mean and standard error of three independent Western blots.

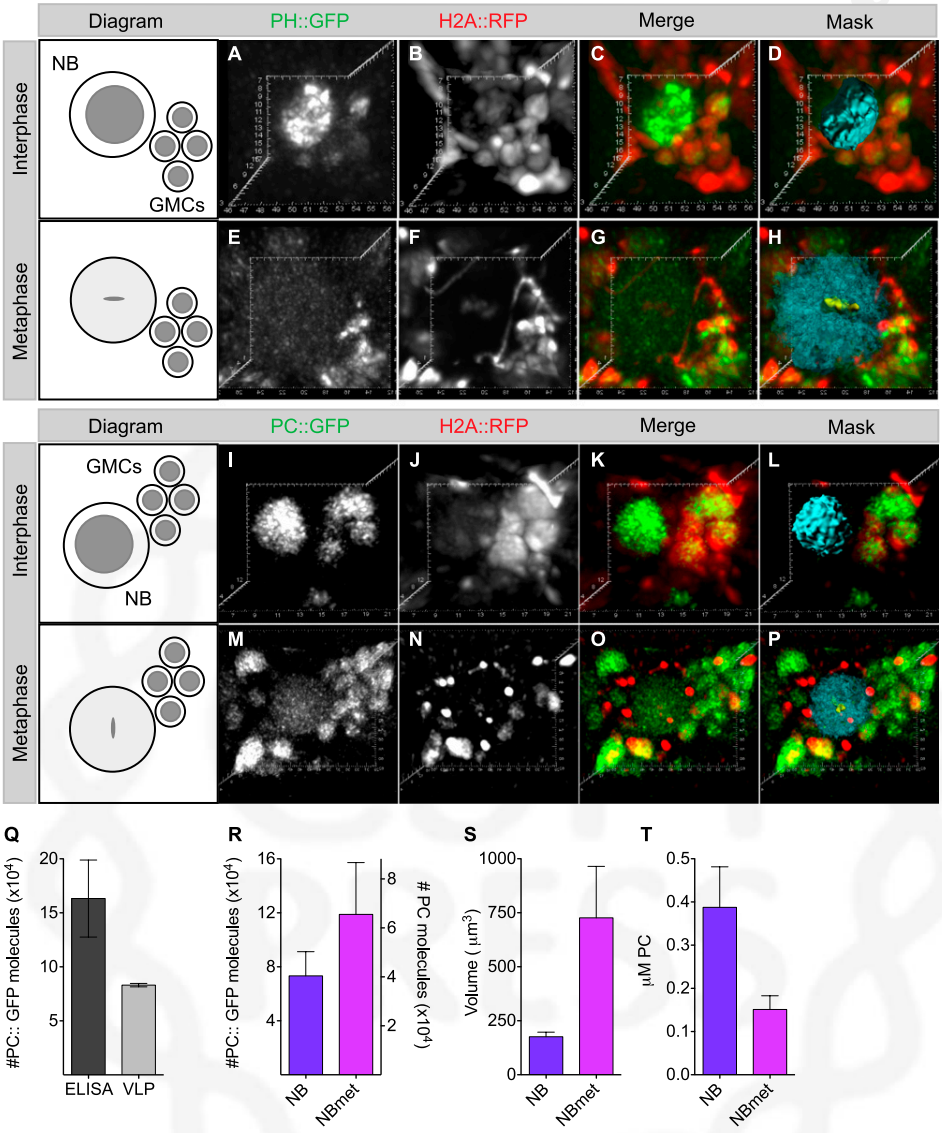

Figure 2. Quantification of PH::GFP and PC::GFP in neuroblast lineage. (*A–P*) Deconvolved confocal laser scanning images of PH::GFP (*A,E*), PC::GFP (*I,M*), and H2A::RFP (*B,F,J,N*) in neuroblast interphase (*A–D,I–L*) and metaphase (*E–H,M–P*). (*Left*) Diagrams identify neuroblast (NB) and GMCs in images. (*C,G,K,O*) Merge panels show PH::GFP (*C,G*) or PC::GFP (*K,O*) in green and H2A::RFP in red. (*D,H,L,P*) Mask panels show the volumes occupied by PH::GFP (*D,H*) and PC::GFP (*L,P*) in blue and the volume occupied by H2A::RFP in yellow. Neuroblast lineage-specific expression of PH::GFP and H2A::RFP was obtained by using a *worniu*-GAL4 driver. For PC::GFP imaging, PC::GFP was expressed under the endogenous *Pc* promoter, and H2A RFP was expressed from the ubiquitin promoter (see the Materials and Methods for genotypes). (*Q*) Estimated number per nucleus of PC::GFP molecules in blastoderm embryos (2–3 h) using GFP detection by ELISA (Cell Biolabs) or by GFP-VLP calibration, as described in the Materials and Methods. Data show the mean and 95% confidence intervals of 10 cells for GFP-VLP measurements and 10 independent ELISA assays. (*R*) Estimated number per cell of PC::GFP molecules (*left Y*-axis) and endogenous PC molecules (*right Y*-axis) in *yw* flies by GFP-VLP calibration in neuroblast interphase (NB) and metaphase (NBmet). Data show the mean and 95% confidence interval of at least four independent measurements. (*S*) Measured cell volume of neuroblasts in interphase (NB) and metaphase (NBmet). Data show the mean and 95% confidence intervals of at least four cells. (*T*) Estimated micromolar concentrations of endogenous PC in *yw* flies in neuroblast interphase (NB) and metaphase (NBmet).

mask of the volume occupied by the GFP fusion protein in the cell of interest was applied, and signal intensities were calculated (Figs. 2D,H,L,P, 3D,H,L,P,T,X). In order to convert signal intensities to absolute concentrations of GFP fusion proteins in single cells, we performed calibration using GFP-containing virus-like particles (GFP-VLPs) (Figs. 2Q,R, 3Y; Supplemental Table S1; Dundr et al. 2002; Rabut et al. 2004). To evaluate the accuracy of GFP-VLP calibration for live GFP quantification, we compared this technique with GFP ELISA (enzyme-linked

Fig(s). 2 live 4/C

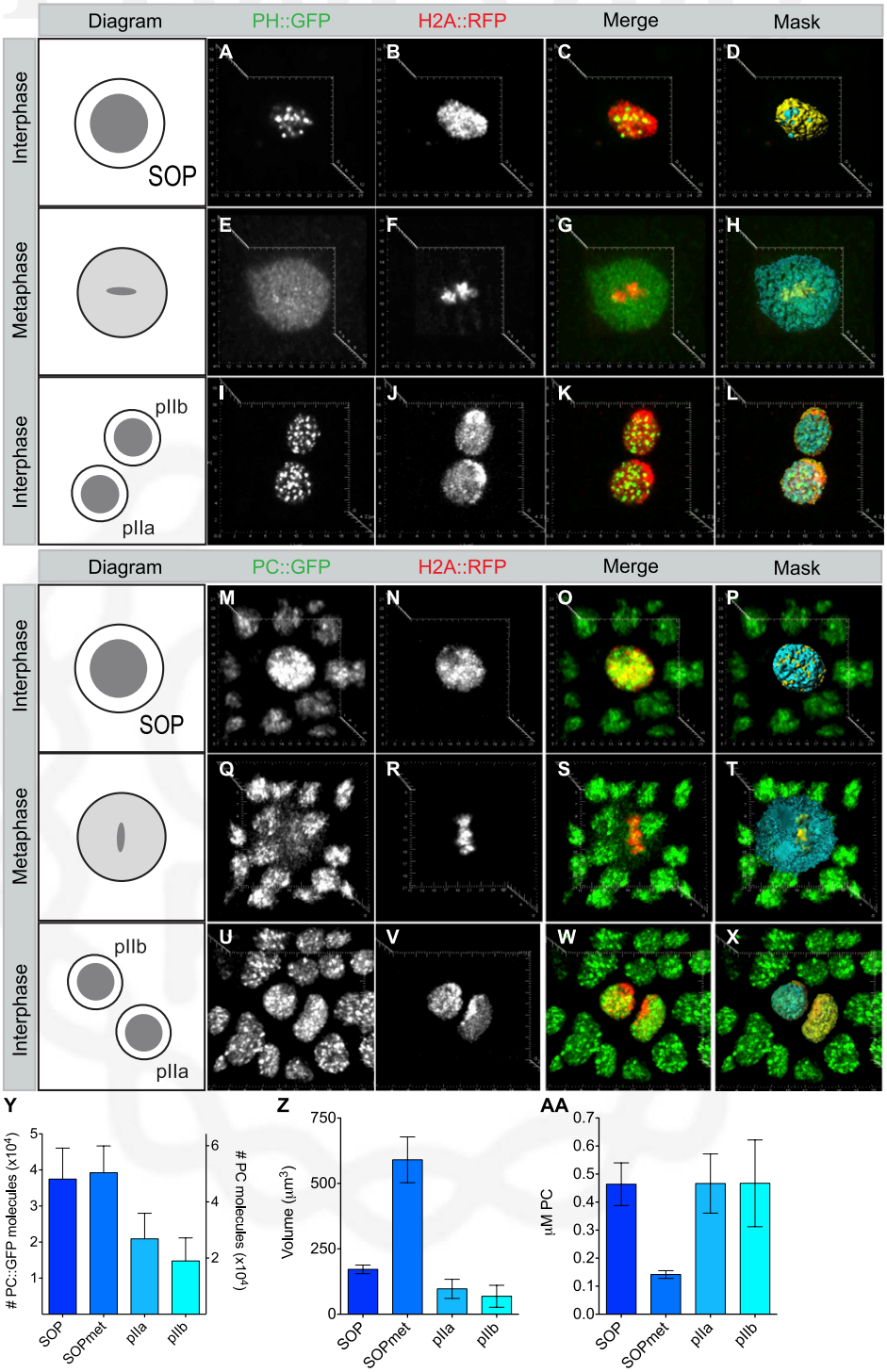

Figure 3. Quantification of PH::GFP and PC::GFP in SOP lineage. (*A–X*) Deconvolved confocal laser scanning images of PH::GFP (*A,E,I*), PC::GFP (*M,Q,U*), and H2A::RFP (*B,F,J,N,R,V*) in SOP interphase (*A–D,M–P*) and metaphase (*E–H,Q–T*) and pIIa and pIIb interphase (*I–L,U–X*). (*Left*) Diagrams identify SOPs and their daughter cells in images. (*C,G,K,O,S,W*) Merge panels show PH::GFP (*C,G,K*) or PC::GFP (*O,S,W*) in green and H2A::RFP in red. (*D,H,L,P,T,X*) Mask panels show the volumes occupied by PH::GFP (*D,H,L*) and PC::GFP (*P,T,X*) in blue and the volume occupied by H2A::RFP in yellow. SOP lineage-specific expression of PH::GFP and H2A::RFP was obtained by using a *neuralized*-GAL4 driver. For PC::GFP imaging, PC::GFP was expressed under the endogenous PC promoter.(see the Materials and Methods for genotypes). (*Y*) Estimated number per nucleus or metaphase cell of PC::GFP molecules (*left Y*-axis) and endogenous PC molecules (*right Y*-axis) in *yw* flies measured by GFP-VLP calibration in SOP interphase (SOP) and metaphase (SOPmet) and pIIa and pIIb interphase. Data show the mean and 95% confidence intervals of at least three cells. (*Z*) Measured cell volumes of different cells in SOP lineage. Data show the mean and 95% confidence intervals of at least three cells. (*AA*) Estimated micromolar concentrations of endogenous PC in *yw* flies, per nucleus or metaphase cell in different cells of SOP lineage.

immunosorbent assay) by applying both quantification methods to blastoderm embryos (Fig. 2Q; see the Materials and Methods; Supplemental Material). This analysis showed an approximately twofold difference between the ELISA and VLP measurements, probably due to diffraction of the GFP signal caused by the thickness of the embryo. We conclude that live GFP quantification by GFP-VLP calibration gives a meaningful readout of protein concentrations for single-cell experiments.

By performing live GFP quantification and GFP-VLP calibration for PH::GFP and PC::GFP in each cell lineage at interphase and metaphase (Figs. 2, 3), we calculated the number of GFP fusion protein molecules in each cell type (Figs. 2, 3; Supplemental Table S1). Conversion to micromolar concentrations via the measured volume occupied by GFP in each cell type revealed that both GFP fusion proteins undergo a substantial dilution (between 2.6-fold and 5.2-fold) (see Supplemental Table S1) upon the interphase-to-metaphase transition in both cell lineages due to the increase in volume upon nuclear envelope breakdown (NEBD) (Figs. 2S, 3Z; Supplemental Table S1). Since the PC::GFP expression strategy allowed estimation of endogenous PC protein levels (Fig. 1), we were able to use measured PC::GFP molecule numbers and concentrations to calculate the expected values for the endogenous PC protein in the wild-type situation (Figs. 2R,T, 3Y,AA). This analysis revealed different absolute numbers of endogenous PC molecules calculated in interphase for the neuroblast (Fig. 2R), the SOP, and the SOP daughter cells pIIa and pIIb (Fig. 3Y). Remarkably, however, due to the different nuclear volumes of these four different cell types (Figs. 2S, 3Z), the calculated micromolar concentration of endogenous PC was essentially identical in all four cell types, at ~0.4 μM (Figs. 2T, 3AA). In summary, this quantitative analysis of single defined cell lineages reveals substantial dilution of PC and PH upon entry into mitosis, but a remarkably similar endogenous concentration of PC at interphase in both lineages.

PC shows more dynamic interaction with chromatin than PH

Previous studies have determined similar dissociation rates for PH::GFP and PC::GFP from interphase chromatin in wing discs (Ficz 2005; Ficz et al. 2005). However, studies of mitotic dissociation showed distinct behavior for the two proteins upon reassociation to chromatin after mitosis (Buchenau et al. 1998). We thus asked whether PC and PH interact differently with chromatin in neuroblasts and SOPs and whether different cell cycle stages are distinguished by different chromatin-binding properties of either protein. To this end, we performed fluorescence recovery after photobleaching (FRAP) on both GFP fusion proteins in each cell type at interphase and metaphase (Fig. 4). Histone H2A fused to RFP (H2A::RFP) was used to mark chromatin in both lineages (Figs. 2, 3) and served as a guide for bleach spot placement on metaphase chromatin.

The recovery data were analyzed by fitting kinetic models (McNally 2008; Mueller et al. 2008, 2010). Comparison of different fitting procedures showed contributions of both diffusion and binding to the recovery kinetics (Supplemental Fig. S1). Thus the reaction–diffusion model of Mueller et al. (2008) was used for all data sets, enabling values to be extracted for the diffusion coefficient (Df), the pseudo-first-order association rate ($k_{on}{}^{\star}$), and the dissociation rate (k_{off}) (Fig. 4). To evaluate the robustness of the extracted values, these parameters were cross-validated by several independent means (see Supplemental Material [FRAP Data Analysis]). This cross-validation analysis confirmed that a homogeneous global binding model is sufficient to describe both the interphase and metaphase data (Supplemental Fig. S2; Beaudouin et al. 2006; Sprague et al. 2006), provided independent measures for Df that are in excellent agreement with those extracted from fitting (Supplemental Fig. S3), and defined limits for the extracted values of $k_{on}{}^{\star}$ and k_{off} for each data set (Supplemental Fig. S4).

Comparison of the recovery kinetics and measured parameters for PC::GFP and PH::GFP revealed striking differences between the two proteins. PH::GFP typically showed far slower recovery than PC::GFP (Fig. 4A–F). This was due in part to a slower Df determined for PH::GFP than for PC::GFP (Supplemental Fig. S3; Supplemental Table S1). Further differences between PC::GFP and PH::GFP were observed upon comparison of the bound fractions and kinetic rate constants. Calculation of the percentage of total protein bound at interphase in different cell types showed 30%–70% of total PH::GFP bound, in contrast to 10%–20% of total PC::GFP bound (Fig. 4G; Supplemental Table S1). We note that one caveat of these comparisons is that the percentage of total PH protein represented by PH::GFP is unknown. Nevertheless, the comparison of residence times—which reflect an inherent, concentration-independent property of protein–chromatin binding—revealed twofold to ninefold longer residence times for PH::GFP than PC::GFP at interphase in all cell types (Fig. 4I; Supplemental Table S1). Taken together, these results demonstrate inherently different behaviors of PC::GFP and PH::GFP in terms of both diffusion and chromatin interaction, with PC::GFP showing faster diffusion and more dynamic interaction with chromatin than PH::GFP.

PcG proteins show decreased mobility upon lineage commitment

Previous studies of the kinetics of PH::GFP chromatin binding in *Drosophila* at different developmental stages have documented an approximately twofold lower average dissociation rate in larval wing imaginal discs than in embryos, indicating longer residence times and thus suggesting more stable chromatin association as development proceeds (Ficz et al. 2005).

To evaluate whether PcG proteins interact differently with chromatin in different cell lineages and in the progressive commitment of a single lineage, we compared kinetic parameters at interphase in neuroblasts and the SOP lineage (Fig. 4G–I). For PH::GFP, we measured an approximately twofold lower dissociation rate constant, giving a twofold longer residence time in SOP interphase

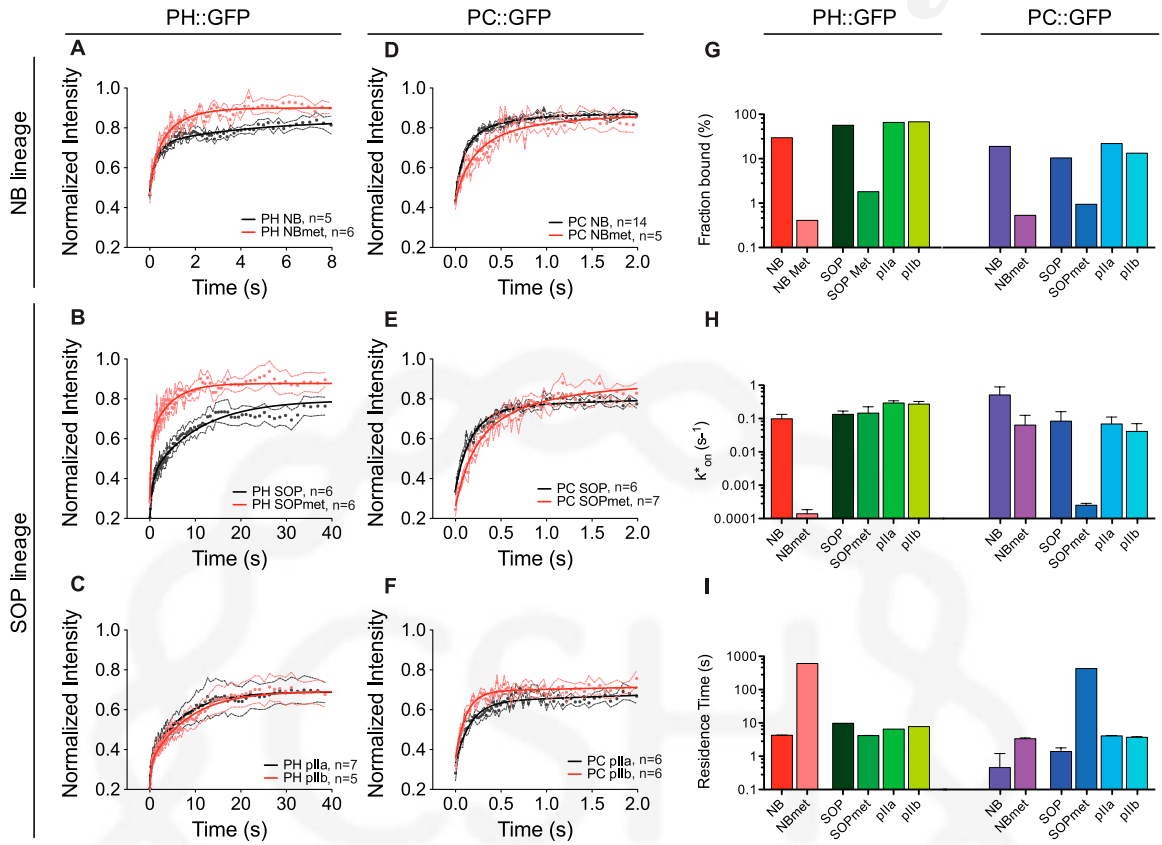

Figure 4. FRAP analysis of PH::GFP and PC::GFP in neuroblast (NB) and SOP lineages. (*A–F*) FRAP recovery curves of PH::GFP (*A–C*) and PC::GFP (*D–F*) in the neuroblast (NB) (*A*,*D*) and SOP (*B*,*C*,*E*,*F*) lineages. Interphase bleach spots were placed to cover several PC::GFP or PH::GFP foci (see Figs. 2, 3). Metaphase bleach spots were placed in the region of the RFP signal (see Figs. 2, 3). Symbols represent the mean of experimental values and are accompanied by the standard error of the mean, represented by a dashed line of the same color. The solid darker line shows fit of FRAP model to the experimental data (see the Materials Methods; Supplementary Material [FRAP Data Analysis], for full description of model and fitting procedures). NB and SOP (black on *A*,*B*,*D*,*E*) indicate neuroblast and SOP interphase, and NBmet and SOPmet (red on *A*,*B*,*D*,*E*) indicate neuroblast and SOP metaphase. pIIa (black in *C*,*F*) and pIIb (red in *C*,*F*) indicate the interphase of the respective SOP daughter cells. (*G–I*) Extracted total fraction bound (*G*), pseudo-first-order association rate k_{on}^* (*H*), and residence time (*I*) of PH::GFP and PC::GFP in neuroblast and SOP lineages from FRAP model fit. The fraction bound in the chromatin region was calculated as $k_{on}^*/(k_{off} + k_{on}^*)$. For metaphase measurements, the fraction bound in the chromatin region was used in combination with the quantity of free protein outside the chromatin volume to calculate the fraction of total protein bound, shown on the plots (see also Supplemental Table S1). Residence time was calculated as $1/k_{off}$. Error bars show 95% confidence intervals.

compared with neuroblast interphase (Fig. 4I; Supplemental Table S1). In the more determined daughters of the SOP (pIIa and pIIb), no further increase in residence time was detected. However, the association rate constant was approximately twofold higher in these daughter cells, contributing to a substantial increase in the calculated bound fraction from 57% in SOPs to 66%–68% in the daughters (Fig. 4G; Supplemental Table S1). For PC::GFP, a similar trend was observed. We measured a threefold longer residence time at interphase in SOPs than in neuroblasts and a further threefold increase in residence time in pIIa and pIIb (Fig. 4I; Supplemental Table S1). Taken together, these results indicate not only that the interaction of both PC and PH with chromatin is more dynamic in the stem cell neuroblast than in the SOPs, but also that the mobility of both proteins decreases upon increasing cell fate commitment within the SOP lineage.

A fraction of PcG proteins remains strongly bound to mitotic chromatin

To determine whether the nature of PcG–chromatin interactions changes during the cell cycle, we examined metaphase binding. Calculation of bound fractions of PH::GFP and PC::GFP from FRAP analysis of metaphase chromatin showed a clear reduction in binding, with 0.4%–2% of total protein remaining bound to metaphase chromosomes in both cell lineages (Fig. 4G; Supplemental Table S1). Independent calculation of metaphase-bound fractions based on image quantification gave consistent results (Supplemental Table S1). Thus,

a small fraction of PcG proteins remains bound to mitotic chromatin.

To assess the kinetic properties of this fraction, we examined association rates and residence times (Fig. 4H,I; Supplemental Table S1). Remarkably, in most cases, this metaphase-bound population showed properties profoundly different from that bound in interphase, in terms of both a slower association rate (Fig. 4H) and a longer residence time (Fig. 4I). For each protein, the extent of kinetic changes was different in different lineages. For example, PH::GFP showed no significant change in behavior between interphase and metaphase in SOPs, but a profound change in neuroblasts (Fig. 4H,I; Supplemental Table S1). For PC::GFP, the residence time in neuroblasts increased 7.3-fold, from 0.46 sec in interphase to 3.35 sec in metaphase. In contrast, in SOPs for the same protein, the increase in residence time at metaphase was >300-fold, from 1.39 sec in interphase to >5 min in metaphase (Supplemental Table S1). To determine the robustness of the extracted parameters, we performed simulations of FRAP recovery for a range of k_{on}* and k_{off} values and evaluated the fit to the experimental data (Supplemental Fig. S4). In both lineages and for both proteins, the k_{on}* and k_{off} combinations giving the best fits to the metaphase and interphase data occupied distinct parameter spaces (Supplemental Fig. S4), indicating robust differences between the measured data sets between interphase and metaphase. These protein- and lineage-specific differences in kinetic behavior suggest that the changes in binding properties at metaphase are not a general effect of chromatin condensation at mitosis but are specific to each protein in each cell type.

Mathematical modeling predicts a slower time scale for mitotic dissociation of PC in SOPs than in neuroblasts

In the above experiments, we measured different chromatin-binding properties of PcG proteins at specific points during the cell cycle; namely, interphase and metaphase. We next asked whether the changes in kinetic properties that we measured are sufficient to account for the observed reduction in binding at metaphase within the known time frame of cell division in SOPs and neuroblasts (Mayer et al. 2005; Lee et al. 2006). To this end, we used mathematical modeling to simulate a time course of protein–chromatin interactions upon cell cycle transitions. The PcG–chromatin interaction was modeled using ordinary differential equations (Fig. 5A; Supplemental Material [Mathematical Modeling]). As inputs, we used the calculated numbers of endogenous PC molecules in SOPs and neuroblasts, the association and dissociation rates measured in FRAP at interphase and metaphase in each cell lineage, and the corresponding nuclear or cell volumes (Supplemental Table S1).

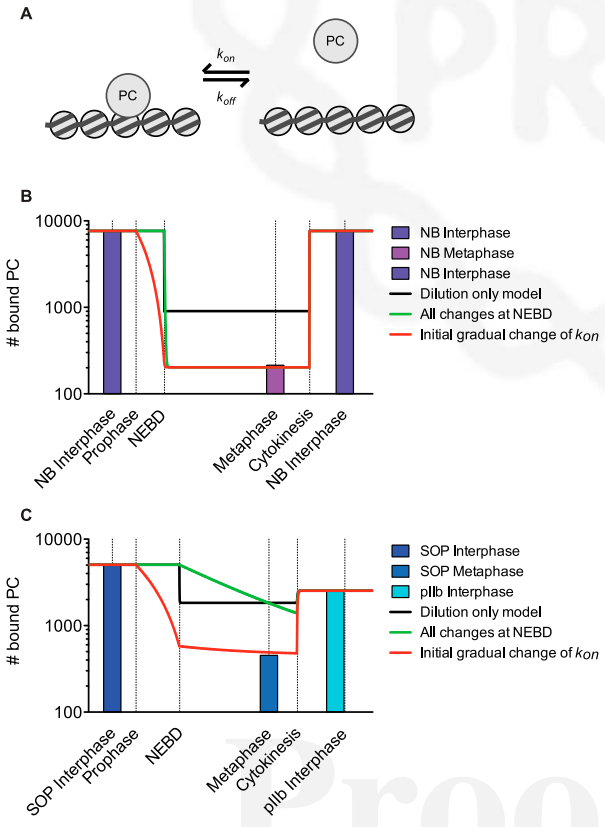

Figure 5. Mathematical modeling of mitotic dissociation of PC from chromatin. (*A*) Model for interaction of PC protein with chromatin targets. PC interacts with chromatin with the association rates k_{on} and dissociation rates k_{off}. The model describes three species: chromatin-bound PC, free PC, and free chromatin. Implementation of the model is described in the Supplemental Material, (Mathematical Modeling). (*B*,*C*) Modeling of endogenous PC in neuroblast (*B*) and SOP (*C*) lineages of *yw* flies. Time is scaled in real time according to Mayer et al. (2005) and Lee et al. (2006). Solid bars represent calculated numbers of bound PC molecules extracted from FRAP experiments at interphase or metaphase in each cell type as indicated. Solid lines represent bound numbers of PC molecules predicted by simulation using the model shown in *A* under different assumptions as follows: (Black line) Dilution only model: Dilution of PC as measured (Figs. 2T, 3AA) occurs at NEBD, but changes in binding rates are not included in the simulation to evaluate the contribution of dilution alone to the chromatin-binding properties of the system. This model predicts a substantial dissociation of PC caused by dilution alone in both cell types (shown in *B*,*C*), which nevertheless fails to reach the measured levels of dissociation. (Green) All changes at NEBD. The measured dilution (Figs. 2T, 3AA) and extracted changes in binding parameters (Fig. 4H,I) are included in the model, with all changes occurring simultaneously at NEBD. For neuroblasts (*A*), this model predicts a rapid dissociation to measured levels, whereas for SOPs (*B*), the same model using SOP parameters predicts a gradual dissociation, which does not reach measured levels of dissociation by the onset of cytokinesis. (Red) Initial gradual change of k_{on}. The model assumes dilution as measured (Figs. 2T, 3AA) at NEBD and change in k_{off} as measured (Fig 4I) at NEBD, but the association rate changes gradually from extracted interphase to metaphase values (Fig 4H) from prophase to NEBD. This model predicts dissociation of PC in SOPs that is close to measured levels (shown in *B*).

Fig(s). 5 live 4/C

We first asked whether a change in the kinetic properties of PC is actually required for protein dissociation at metaphase or whether the simple effects of protein dilution at NEBD would be sufficient (Fig. 5B,C, black lines). These simulations predicted that although dilution alone would achieve a substantial degree of dissociation, the measured levels of metaphase binding are an order of magnitude lower still. We next asked whether the changes in kinetic rate constants that we measured would be sufficient to remove this additional protein from mitotic chromosomes within the time frame imposed by the cell cycle (Fig. 5B,C, green lines). For this simulation, the dilution and changes in binding properties were all effected concomitantly upon NEBD. This simulation predicted a rapid dissociation to the observed levels within seconds of NEBD in neuroblasts. However, the predicted dissociation in SOPs was very slow, such that the observed levels were not reached before the cell entered cytokinesis at the end of metaphase (Fig. 5C). In the simulation, the system reached equilibrium after ~33 min, predicting 385 bound molecules (data not shown). Further inspection of parameters revealed that this difference between the cell types was independent of diffusion (Supplemental Material [Mathematical Modeling]) and was due mainly to the faster exchange of PC in neuroblast interphase and the very slow dissociation of PC in SOP metaphase.

The assumption made above—that all parameters change at the same moment upon NEBD—is sufficient to explain dissociation in neuroblasts but proved to be invalid for SOPs (Fig 5C). We thus evaluated whether a changed order of events could accelerate mitotic dissociation. The moment of NEBD is well defined in our experiments (visible as dispersal of GFP fusion proteins in Figs. 2, 3; Supplemental Movies S1–S4). Simulations, including diffusion (data not shown), predicted that protein dilution occurs within seconds after NEBD, thus the assumption that protein dilution occurs effectively instantaneously upon NEBD is valid. However, the condensation and modification of chromatin begin at prophase, well before NEBD (Nowak and Corces 2004). To simulate this gradual change in the nature of the chromatin template, we introduced a gradual change in the association rate k_{on}, starting at prophase (Fig. 5C, red line). In both neuroblasts and SOPs, this resulted in rapid dissociation of PC before NEBD and full dissociation to the measured levels at metaphase. In summary, this analysis predicts a slower dissociation kinetic for PC in SOPs than in neuroblasts, which can be accelerated by modeling a reduction in the association rate during prophase.

H3S28 phosphorylation during prophase may accelerate PC mitotic dissociation

We next asked what molecular mechanisms could account for a change in the association rate of PC to chromatin during prophase. We reasoned that phosphorylation of Ser 28 on histone H3 (H3S28p) may be a good candidate. H3S28 phosphorylation is present during interphase and increases during mitosis (Goto et al. 1999; Giet and Glover 2001). PcG proteins have a reduced ability to bind to the H3 tail trimethylated at Lys 27 (H3K27me3) if the adjacent H3S28 site is phosphorylated (Gehani et al. 2010; Lau and Cheung 2011). We reasoned that an accumulation of H3K27me3/S28p during prophase could effectively reduce the association rate of PC to chromatin by reducing the number of sites available for binding in a manner analogous to that reported for heterochromatin protein 1 (HP1) (Fischle et al. 2005; Hirota et al. 2005). To determine whether H3K27me3/S28p accumulates during prophase in neuroblasts and SOPs, we generated an antibody that specifically recognizes the double modification (see the Materials and Methods; Supplemental Fig. S5). Figure 6 shows that robust accumulation of H3K27me3/S28P was indeed detectable in prophase in both neuroblasts and SOPs before the onset of NEBD. These results are consistent with a role of this double modification in ejecting PC from chromatin during prophase.

To further examine a functional role for the H3K27me3S28p double mark in regulating PC binding, we performed RNAi-mediated knockdown of the *JIL-1* kinase in neuroblasts. *JIL-1* is a homolog of the MSK kinase, which phosphorylates both H3S10 and H3S28 in interphase (Jin et al. 1999; Gehani et al. 2010; Lau and Cheung 2011). *JIL-1* knockdown had no effect on the expression levels of PC::GFP (data not shown). Remarkably, knockdown of *JIL-1* led to an increase in the residence time of PC::GFP on interphase chromatin (Fig. 6S), consistent with a role for H3S28p in ejecting PC from chromatin. We conclude that this modification may contribute to the active reduction in PC binding that we predicted by mathematical modeling to be required before NEBD, thus accelerating mitotic dissociation of PC.

Discussion

We used a combination of quantitative live imaging and mathematical modeling to investigate changes in the dynamic behavior of PcG proteins upon mitosis and cell fate transitions in living *Drosophila*, giving quantitative insight into the properties of the PcG system.

For the PH::GFP fusion protein, the use of limited tissue-specific expression strategies was necessary to avoid cell death associated with PH overexpression. This, in turn, precluded the quantification of endogenous PH molecule numbers, since protocols for the isolation of GFP-marked SOPs and neuroblasts are not currently available. A goal of future studies will be to isolate the PH::GFP-expressing cell types of interest in order to enable relative quantification of PH::GFP and endogenous PH. For the PC::GFP fusion protein, the transgene was expressed under the endogenous *Pc* promoter, enabling quantification of relative amounts of transgenic and endogenous protein from whole tissues. It is important to consider to what extent the partial rescue of *Pc* mutants by the PC::GFP transgene will affect the quantitative conclusions we draw here. By quantitative comparison with PH::GFP behavior, it has been proposed that

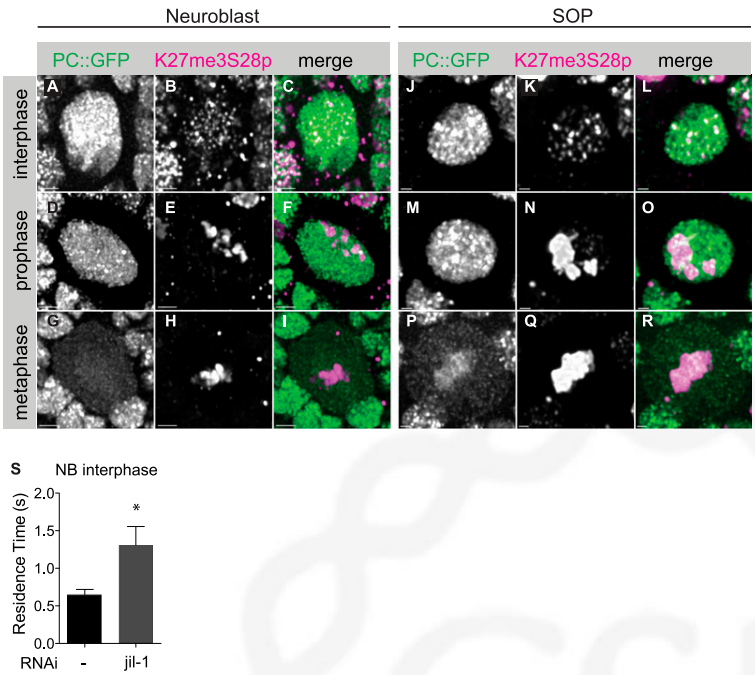

Figure 6. The H3K27me3/S28p double mark accumulates during prophase in neuroblasts and SOPs. Neuroblasts (*A–I*) and SOPs (*J–R*) of larvae and pupae expressing PC::GFP were fixed and stained with αH3K27me3/S28p (see the Materials and Methods). (*A*,*D*,*G*,*J*,*M*,*P*) The GFP signal reveals PC::GFP distribution and identifies cells that have not yet undergone NEBD, visible as distinct nuclear and cytoplasmic regions in *A*, *D*, *J*, and *M*. (*G*,*P*) After NEBD, the PC::GFP signal is dispersed throughout the cell volume. Detection of H3K27me3/S28p reveals that the double mark is present in interphase (*B*,*K*) and accumulates during prophase, prior to NEBD (*E*,*N*). (*H*,Q) Maximum levels of double mark are detected at metaphase. Bars: *A–I*, 2 μm; *J–R*, 1 μm. (*S*) *JIL-1* knockdown modulates PC::GFP kinetics in neuroblasts. The residence time of PC::GFP in neuroblast interphase upon no RNAi (–) and knockdown of *JIL-1*. Transient expression of a UAS -*JIL-1* RNAi construct (Dietzl et al. 2007) (obtained from the Vienna *Drosophila* RNAi Center [VDRC], http://stockcenter.vdrc.at/control/main) was achieved using an *inscuteable* GAL4 driver line for expression in neuroblasts (Kraut and Campos- Ortega 1996) in combination with GAL80ts (see the Materials and Methods) to achieve transient expression of the RNAi construct in third instar larvae. Data show the mean and SEM of at least three experiments. (*) *P*-value < 0.05 (two-tailed *t*-test). Residence times were extracted from FRAP experiments as shown in Figure 4. Fitting was performed with fixed *Df* [*Df*(1)] (Supplemental Table S1).

the PC::GFP fusion is less favored by fourfold to fivefold in the PRC1 complex than the endogenous protein (Ficz et al. 2005). Ficz et al. (2005) concluded that the population of PRC1 is marked with PC::GFP, but the bound fraction of PC::GFP may be an underestimation of the bound fraction of endogenous PC. This effect may lead to the lower bound fraction that we measure for PC::GFP in comparison with PH::GFP. It also follows from this that second-order kinetic processes (on rates) will be prone to inaccuracies, but first-order processes (off rates and therefore residence times) will be unaffected. We note that the accurate determination of the true on rate (k_{on}) from the pseudo-first-order association rate (k_{on}*), extracted from FRAP experiments such as these, is also limited by the unknown quantity of free binding sites (McNally 2008); thus, at best, one can extract relative k_{on} values that allow comparisons between different cell types. This in itself allows meaningful comparisons. In summary, we conclude that the PC::GFP fusion protein is a useful reporter of specific aspects of endogenous protein behavior: It enables the accurate determination of residence times, absolute protein quantities (which do not rely on protein activity), and relative differences between on rates in different cell types and at different cell cycle stages.

Comparison of PC::GFP and PH::GFP revealed twofold to ninefold longer residence times for PH::GFP than PC::GFP at interphase in all cell types. This result suggests that PC and PH do not solely operate as part of the PRC1 complex, consistent with previous studies (Buchenau et al. 1998). The longer residence times observed for PH::GFP may reflect multimerization of PH via the SAM domain, which has been shown to be required for PH-mediated gene silencing (Robinson et al. 2012). The cell type-specific differences that we observe in the kinetic behavior of PH::GFP raise the intriguing possibility that some of these may be due to regulation of sterile α motif (SAM) domain polymerization and thus PH silencing properties.

The estimation of the number of endogenous PC molecules bound to chromatin in interphase (~2500–7500 depending on cell type) (Supplemental Table S1) allows comparison with numbers of PcG target genes estimated from profiling studies (between 400 and 2000) (Martinez et al. 2009; Enderle et al. 2011). We note that the interphase residence times for both proteins measured in this study (0.5–10 sec) (Supplemental Table S1) are shorter than those previously reported for the same fusion proteins in other tissues (2–6 min) (Ficz et al. 2005). These differences may arise from the different cell types examined or from the different FRAP analysis models used. Indeed, the residence times measured here are consistent with those measured for several transcription factors using similar FRAP models (Mueller et al. 2008). These findings suggest that in interphase, several PC molecules are bound to a given target gene and exchange within a matter of seconds on a time scale similar to transcription factor-binding events. The fact that we measured shorter residence times in neuroblasts than in SOPs suggests that the mode of PcG binding, and thus the extent of silencing, may be differently regulated in stem cells and differentiated cells.

Fig(s). 6 live 4/C

The analysis of different cell lineages and of interphase-to-mitotic transitions led to two key findings. First, we document a progressive reduction in mobility of both PC::GFP and PH::GFP upon lineage commitment both between cell types and within a single lineage, consistent with and extending previous studies showing reduced mobility of these proteins at later developmental stages (Ficz et al. 2005) and a general loss of chromatin plasticity upon embryonic stem (ES) cell differentiation (Meshorer et al. 2006). Interestingly, a recent study of TFIIH binding in developing mammalian tissues, performed in living mice, revealed a differentiation-driven reduction in TFIIH mobility, revealing long-lasting but reversible immobilization in post-mitotic cells (Giglia-Mari et al. 2009). It will be of great interest in the future to examine PC, PH, and other PcG and TrxG (Trithorax group) proteins in other cell lineages to determine the extent to which residence times are modulatable upon changes in cell identity. In particular, it will be interesting to examine the kinetics of the DNA-binding proteins that recruit the PcG and TrxG proteins to their sites of action.

Second, we identify a fraction of PcG molecules that remain strongly bound to mitotic chromatin in both neuroblasts and SOPs. The long residence times (up to several minutes) of this bound fraction raise the important question of whether these molecules are carriers of mitotic memory. Thus, how the mitotic chromatin-binding properties of the PcG are differently regulated in SOPs and neuroblasts will be a key question for future studies. Does a strongly bound subpopulation exist in interphase? In the mathematical model for PC dissociation (Fig. 5), all PC molecules are treated as belonging to a single population whose properties change upon entry into mitosis. We note that a model in which a subpopulation with long residence time exists during interphase would also be compatible with the observed data, but such a subpopulation was not discernible from the FRAP recovery data.

The determination of molecule numbers, concentrations, and kinetic constants gives insight into the absolute quantities and mobilities of free and bound PC molecules in specific cell types in the endogenous situation, thus providing in vivo quantitation of an epigenetic system. These in vivo measurements will be essential for interpretation of models based on in vitro findings. Furthermore, this analysis enabled us to use quantitative mathematical modeling to examine the predicted behavior of the system over time during an entire cell cycle. The most important insight provided by the model is the requirement for accelerated PC displacement in SOPs and the prediction that this may be provided by a reduction in association rate during prophase. We demonstrate that H3S28 phosphorylation is a good candidate mechanism for PC displacement during prophase and metaphase, in addition to its documented role in PcG displacement during interphase (Gehani et al. 2010; Lau and Cheung 2011). The increased residence time that we observed for PC::GFP upon RNAi-mediated knockdown of *JIL-1* is consistent with a role of H3S28P in ejecting PC from H3K27me3 sites on chromatin. Our observation of accumulation of this double mark in prophase and metaphase is consistent with observations of mitotic accumulation of H3K9me3/S10p (Fischle et al. 2005; Hirota et al. 2005) but is in contrast to the study of Gehani et al. (2010), who report only slight changes in levels of H3K27me3/S28p from interphase to metaphase in human fibroblasts. This discrepancy strongly suggests that the extent of mitotic S28 phosphorylation on K27-methylated H3 tails is cell type-specific, consistent with a potential role for this mark in distinguishing the mitotic behavior of PC in SOPs and neuroblasts.

Since H3K27me3/S28p is associated with ejection of PC from chromatin, and the double mark is highly enriched on mitotic chromatin, additional mechanisms must contribute to the increased residence times of the small bound fraction of PC::GFP that we observed in mitosis. These may include post-translational modifications of PC and PH proteins themselves (Niessen et al. 2009), a switch of binding platform (e.g., from histone tails to DNA or RNA), and modification of recruiting or competing molecules (Fig. 7). Whether these proposed mechanisms contribute to mitotic PcG displacement and retention and whether they are regulated differently in different lineages will be key questions for future studies.

In summary, we demonstrate here that the properties of the PcG proteins are not only different in different lineages, but also profoundly altered at mitosis. We propose that this regulation of PcG properties may be essential to both the stability of determined cell identities and the flexibility of the stem cell state.

The combination of absolute quantification with analysis in living animals that we used in this study offers

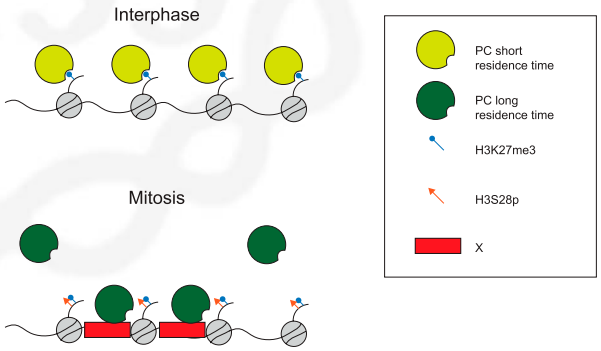

Figure 7. Model for interaction of PC with chromatin during mitosis. During interphase, PC binds chromatin through the interaction of its chromodomain with histone H3 trimethylated at Ser 27 (H3K27me3). As cells enter mitosis, phosphorylation of H3S28 reduces the available binding sites for PC, which, in parallel with the protein dilution at NEBD, leads to the dispersion of PC from mitotic chromatin. Additional cell type-specific processes (X) lead to a change in the overall binding properties of PC at metaphase, so that the remaining binding PC molecules are able to bind longer to chromatin. Such mechanisms may include post-translational modifications of PcG proteins themselves, a switch of binding platform (e.g., from histone tails to DNA or RNA), and modification of recruiting or competing molecules.

three key advances to the study of epigenetic regulation: First, we examine single, defined, genetically marked cell lineages as they go through mitosis and differentiation or self-renewal. Only in a living animal can we observe a defined mitotic event and its differentiated or self-renewed daughter cells. Second, only by quantifying absolute numbers of chromatin-bound endogenous molecules in real volumes can we begin to understand the biological meaning of observed differences in terms of cellular concentrations and protein abundance. Third, these quantitative measurements enable not only the comparison of dynamic transitions in different cell types, but also meaningful mathematical models, identifying which parameters of the system can best explain the observed changes in the plasticity of PcG–chromatin binding upon mitosis and differentiation in stem cells and in more determined lineages. In summary, the combined use of live imaging and mathematical modeling in genetically tractable, dynamically changing in vivo experiments provides quantitative insight into how a system whose components are in constant flux can ensure both stability and flexibility.

Materials and methods

Fly strains, husbandry, and rescue experiments

The strains used in this study are shown in Table 1. Both PC and PH were used as EGFP fusion proteins (designated PC::GFP and PH::GFP).

Flies were maintained in standard medium at 18°C. Rescue experiments were performed at 25°C, according to the scheme shown in Figure 1. For SOP lineage imaging of PH::GFP, PC::GFP, and GFPnls, crosses were made between the *neuralized* (*neur*)-GAL4 driver and *PH::GFP, PC::GFP,* and *GFPnls* flies to obtain the following respective progenies: w^{1118}; *P{Tub-GAL80^{ts},w$^+$}/P{UAS,pPc-PH::GFP,w$^+$}; P{neur-GAL4,w$^+$}, P{UAS-H2A::mRFP, w$^+$}/+.* w^{1118}; *P{Tub-GAL80^{ts},w$^+$}/+; P{neur-GAL4,w$^+$}, P{UAS-H2A::mRFP, w$^+$}/P{pPc-PC::GFP,w$^+$}.* w^{1118}; *P{Tub-GAL80^{ts},w$^+$}/P{UAS-GFPnls,w$^+$}; P{neur-GAL4,w$^+$},P{UAS-H2A::mRFP, w$^+$}/+.* These flies were switched to 25°C 15 h before SOP imaging and FRAP to allow for GAL4-driven expression. For neuroblast lineage imaging of PH::GFP, *PH::GFP,H2A::RFP* third instar larvae were collected and imaged without further crossing. For neuroblast lineage imaging of PC::GFP, a cross between *H2A::RFP* and *PC::GFP,H2A::RFP* flies was conducted to obtain the following genotype: w^{1118};+; *P{pPc-PC::GFP,w$^+$}, P{Ubi-H2A::mRFP,w$^+$}/P{Ubi-H2A::mRFP,w$^+$}* For neuroblast imaging of GFPnls, a cross between *GFPnls* and *H2A::RFP* flies was conducted to obtain the following genotype: w^{1118}; *P{UAS-GFPnls,w$^+$}/+; P{Ubi-H2A::mRFP,w$^+$}/+.* For RNAi knockdown of *JIL-1*, Insc-driver female flies were crossed to *JIL-1* RNAi males and raised at 18°C. Upon appearance of third instar larvae, the progeny was transferred for 24–48 h to 29°C. H2A::RFP-expressing neuroblasts were then used for subsequent experiments.

Quantitative Western blotting

Fly extracts and Western blots were performed as described in Ficz et al. (2005) with minimal changes. Proteins were separated in NuPAGE 4%–12% Bis-Tris, and PC was probed with a primary polyclonal α-PC antibody (d-220, Santa Cruz Biotechnology) and histone H3 with a primary polyclonal α-H3 antibody (Abcam). HRP-conjugated antibodies were used for secondary detection. ECL-Plus (Amersham) detection was used to generate chemofluorescence detected and quantified using a Typhoon scanner (GE Healthcare). All values were normalized to a loading control.

H3K27me3S28ph antibody production

A rabbit polyclonal H3K27me3S28ph antibody was generated in collaboration with Eurogentec. Animals were immunized with the KLH-conjugated synthetic peptide QLATKAARK(me3)S(ph)APATGGVKKC corresponding to amino acids 19–37 of histone H3. Positive sera were purified by the manufacturer in a two-step procedure. Antibodies specific to the dual modification were captured on the AF-Amino TOYOPEARL 650 M matrix coupled with the peptide used for immunization: QLATKAARK(me3)S(ph)APATGGVKKC. Following elution with 100 mM glycine (pH 2.5), antibodies recognizing the peptide in the absence of modifications were removed with a matrix coupled with the unmodified peptide QLATKAARKSAPATGGVKKC. After the purification, antibody specificity was tested by dot blotting.

Table 1. *Strains used in this study*

Name	Genotype	Source
PC::GFP	w^{1118};+; *P{pPc-PC::GFP,w$^+$}*	R. Paro
PH::GFP	w^{1118}; *P{UAS,pPc-PH::GFP,w$^+$};+*	D. Arndt-Jovin
GFPnls	w^{1118}; *P{UAS-GFPnls,w$^+$;+}*	B. Dickson
neur driver	w^{1118}; *P{Tub-GAL80^{ts},w$^+$}; P{neur-GAL4,w$^+$},P{UAS-H2A::mRFP, w$^+$}*	J. Knoblich
H2A::RFP	w^{1118};+; *P{Ubi-H2A::mRFP,w$^+$}*	J. Knoblich
PC::GFP, H2A::RFP	w^{1118};+; *P{pPc-PC::GFP,w$^+$}, P{Ubi-H2A::mRFP,w$^+$*	
PH::GFP, H2A::RFP	w^{1118}; *P{UAS,pPc-PH::GFP,w$^+$}, P{worn-GAL4,w$^+$}/Cy,O; P{Ubi-H2A::mRFP,w$^+$}.*	
GFPnls, H2A::RFP	w^{1118}; *P{UAS-GFPnls,w$^+$}, P{worn-GAL4,w$^+$}/Cy,O; P{Ubi-H2A::mRFP,w$^+$}*	
Pc^{XL5}	w^{1118};+; *Pc^{XL5}/TM3,Ser*	
Pc^3	*In(3R)P(Pc^3), $Pc^{3/}$TM1*	*Drosophila* Genomics Resource Center no. 106475
PC::GFP (II)	w^{1118}; *P{pPc-PC::GFP,w$^+$};+*	R. Paro
Insc driver	w^{1118}; *P{neur-GAL4,w$^+$}/Cy,O;P{Tub-GAL80^{ts},w$^+$}*	J. Knoblich
JIL-1 RNAi	*w1118; {UAS-JIL-1 RNAi (VDRC #107001KK)}, w$^+$; P{pPc-PC::GFP,w+}, P{Ubi-H2A::mRFP,w+}*	VDRC no. 107001KK

Dot blot

Synthetic peptides corresponding to the N-terminal sequence of histone H3 (amino acids 19–37), with different S28 phosphorylation and K27 methylation status, were spotted on a PVDF membrane and probed with the a-H3K27me3S28ph antibody (dilution 1:20,000). For detection, a secondary anti-rabbit horseradish peroxidase-conjugated antibody and the Enhanced Chemiluminescence (ECL) detection system were used. To ensure equal peptide loading, a duplicate membrane was stained with Ponceau S (Supplemental Fig. S5).

Immunocytochemistry in larval brains and pupal nota

Immunocytochemistry experiments in larval brains were performed as described (Betschinger et al. 2006). Immunocytochemistry experiments in pupal nota were performed by dissecting the pupae in 5% paraformaldehyde in phosphate-buffered saline (PBS). The total time of fixation was 20 min, and the subsequent procedure was identical to that described for larval brains. The primary antibodies used were rabbit α-Miranda (1:250) (Betschinger et al. 2006) and rabbit α-H3K27me3S28ph (1:2000) (this study). The secondary antibody was AlexaFluor 647 goat α-rabbit (1:500) (Invitrogen A-21245). For the images shown in Figure 6, GFP was imaged directly without staining.

Quantification of GFP fusion proteins using GFP-VLPs

For quantification of EGFP-fused proteins, EGFP-VLPs (100 ng/μL) were spread on a #1.5 coverslip and imaged under the same settings as the GFP fusion protein of interest. Images of GFP-VLPs were deconvolved with the CMLE method of the software Huygens Pro (SVI), and a total intensity of at least 80 particles was determined using Imaris (Bitplane). After binning of intensities, the mode of the distribution was selected as the intensity of 120 GFP molecules. Comparison of GFP fusion intensities calculated with Imaris (Bitplane) with this value allowed the estimation of GFP fusion protein quantities.

Quantification of GFP fusion proteins using ELISA

ELISA was performed using a GFP ELISA kit (Cell Biolabs), according to the manufacturer's instructions. Total protein was extracted from 20 hand-collected, dechorionated, 2:15- to 2:45-h-old embryos by sonification in 100 μL of DLB buffer (20 mM HEPES-KOH at pH 7.5, 100 mM KCl, 2 mM EDTA, 0.5% Triton X-100, 5 mM DTT, 1 mM $MgAc_2$, Roche Complete protease inhibitors). Extracts were cleared by centrifugation and diluted 20-fold using assay diluent (GFP ELISA kit). Samples were measured in duplicates. The number of GFP molecules per nucleus was calculated based on the observation that each embryo contains 6000 nuclei (Foe and Alberts 1983) and that 100 μL of diluted extract corresponds to the protein from one embryo. The number of PC::EGFP molecules per nucleus was calculated using the following equation: molecules = (mass of PC::GFP[g]/MW GFP) × (6.022×10^{-23})/6000 nuclei.

Preparation of specimens for microscopy and imaging

For SOP imaging, pupae were prepared as described in Bellaiche et al. (2001). Imaging was performed at room temperature on a Zeiss LSM710 with a 63× 1.4 NA oil immersion objective using an Argon laser at 488 nm for GFP imaging (collection between 485 and 563 nm) and a DPSS 561-10 laser at 561 nm for mRFP imaging (collection between 563 and 728 nm) and a pinhole equivalent to 2.45 Airy units. The voxel size was 51 × 51 × 150 nm.

For neuroblast imaging, larval brains were dissected in a Lab-Tek II Chamber #1.5 German Coverglass (Nalgene Nunc International) containing 200 μL of PBS. Imaging was performed at room temperature on a Zeiss LSM710 with a 63× 1.2 NA water immersion objective using an Argon laser at 488 nm for GFP imaging (collection between 485 and 563 nm) and a DPSS 561-10 laser at 561 nm for mRFP imaging (collection between 563 and 728 nm) and a pinhole equivalent to 2.07 Airy units. The voxel size was 51 × 51 × 150 nm.

Image processing

All images acquired were deconvolved using measured PSFs with the CMLE method of the software Huygens Pro (SVI). The measurement of the volumes occupied and the total fluorescence intensity of GFP and mRFP were performed with Imaris (Bitplane). Background was subtracted from intensity measurements.

FRAP

FRAP experiments were performed as described in Mueller et al. (2008) with minimal changes. FRAP was performed in a Zeiss LSM710 with the confocal pinhole set to 3 Airy units. The image size was 512 × 62 pixels, with a pixel size of 45 nm. Images were acquired every 20 msec for GFPnls and PC::GFP experiments and 50 msec and 100 msec for PH::GFP using 1% AOTF of the 488 line of an Argon laser. The circle bleach region had a diameter of 40 pixels; it was centered on the image field and overlapped with expression of H2A::RFP. The bleach iteration number was set to 2 and 100% AOTF of the 488 line in an Argon laser. Background was measured within a region with no cells of the image and subtracted from data. All intensity measurements were performed with MatLab (Mathworks).

FRAP model fitting

FRAP modeling of recovery curves was performed according to Mueller et al. (2008) in MatLab (Mathworks) with minimal changes, described in detail in the Supplemental Material (FRAP Data Analysis). An adaptation of the model described in Beaudouin et al. (2006) for evaluation of the effect of nonhomogeneous protein distribution on extracted parameters was implemented in Mathematica (Wolfram). Cross-validation was also performed on FRAP recovery curves measured in metaphase according to Sprague et al. (2006) using Matlab (Mathworks). The above methods are described in detail in the Supplemental Material (FRAP Data Analysis).

Mathematical model of PC interaction with chromatin

A linearized ordinary differential equation system was used to model the interaction of endogenous PC proteins with chromatin. A full description of the equations and parameters of this model are given in the Supplemental Material (Mathematical Modeling) and Supplemental Table S1. Simulations were performed using MatLab (Mathworks).

Acknowledgments

We are grateful to P. Pasierbek of the IMP/IMBA biooptics facility for advice and assistance on live imaging. We are grateful to D.A.-Jovin and G. Ficz for discussions and advice on imaging. We thank F. Müller for MatLab files and advice on FRAP, and D. Poncet and A. Charpilienne for providing VLPs. We thank J. Knoblich, R. Paro, D.A.-Jovin, and B. Dickson for fly stocks. We

thank J. Mummery-Widmer, F. Mauri, A. Fischer, and C. Homem for advice and assistance on imaging of SOP and neuroblast lineages. We are grateful to M. Baffoe-Bonnie Owusu and C. Ehrhardt for technical assistance, and to M. Rehmsmeier and Ringrose laboratory members for stimulating discussions. This work was funded by the Austrian Academy of Sciences (http://www.oeaw.ac.at) (to L.R., J.L., and S.M.), by the EU FP6 Network of Excellence, "The Epigenome" (http://www.epigenome-noe.net) (to P.S), and the EU FP7 Network of Excellence, "Epigenesys" (http://www.epigenesys.eu/) (to P.S). J.P.F. is supported by the Portuguese Foundation for Science and Technology [http://www.fct.pt (SFRH/BD/40389/2007)]. A.S. is a fellow of the International PhD program "Molecular Mechanism of Cell Signaling" (http://www.phd-cellular-signaling.at), supported by the Austrian Science Fund (http://www.fwf.ac.at/en). Research in the Seiser laboratory was supported by the Austrian Science Fund (FWF P22340).

References

Beaudouin J, Mora-Bermudez F, Klee T, Daigle N, Ellenberg J. 2006. Dissecting the contribution of diffusion and interactions to the mobility of nuclear proteins. *Biophys J* **90:** 1878–1894.

Bellaiche Y, Gho M, Kaltschmidt JA, Brand AH, Schweisguth F. 2001. Frizzled regulates localization of cell-fate determinants and mitotic spindle rotation during asymmetric cell division. *Nat Cell Biol* **3:** 50–57.

Bello B, Holbro N, Reichert H. 2007. Polycomb group genes are required for neural stem cell survival in postembryonic neurogenesis of *Drosophila*. *Development* **134:** 1091–1099.

Betschinger J, Mechtler K, Knoblich JA. 2006. Asymmetric segregation of the tumor suppressor brat regulates self-renewal in *Drosophila* neural stem cells. *Cell* **124:** 1241–1253.

Buchenau P, Hodgson J, Strutt H, Arndt-Jovin DJ. 1998. The distribution of polycomb-group proteins during cell division and development in *Drosophila* embryos: Impact on models for silencing. *J Cell Biol* **141:** 469–481.

Chen X, Hiller M, Sancak Y, Fuller MT. 2005. Tissue-specific TAFs counteract Polycomb to turn on terminal differentiation. *Science* **310:** 869–872.

Dietzel S, Niemann H, Bruckner B, Maurange C, Paro R. 1999. The nuclear distribution of Polycomb during *Drosophila melanogaster* development shown with a GFP fusion protein. *Chromosoma* **108:** 83–94.

Dietzl G, Chen D, Schnorrer F, Su KC, Barinova Y, Fellner M, Gasser B, Kinsey K, Oppel S, Scheiblauer S, et al. 2007. A genome-wide transgenic RNAi library for conditional gene inactivation in *Drosophila*. *Nature* **448:** 151–156.

Doe CQ. 2008. Neural stem cells: Balancing self-renewal with differentiation. *Development* **135:** 1575–1587.

Dundr M, McNally JG, Cohen J, Misteli T. 2002. Quantitation of GFP-fusion proteins in single living cells. *J Struct Biol* **140:** 92–99.

Enderle D, Beisel C, Stadler MB, Gerstung M, Athri P, Paro R. 2011. Polycomb preferentially targets stalled promoters of coding and noncoding transcripts. *Genome Res* **21:** 216–226.

Fanti L, Perrini B, Piacentini L, Berloco M, Marchetti E, Palumbo G, Pimpinelli S. 2008. The trithorax group and Pc group proteins are differentially involved in heterochromatin formation in *Drosophila*. *Chromosoma* **117:** 25–39.

Ficz G. 2005. "Protein dynamics in the nucleus: Implications for gene expression." PhD thesis. Georg-August-Universität, Göttingen, Germany.

Ficz G, Heintzmann R, Arndt-Jovin DJ. 2005. Polycomb group protein complexes exchange rapidly in living *Drosophila*. *Development* **132:** 3963–3976.

Fischle W, Tseng BS, Dormann HL, Ueberheide BM, Garcia BA, Shabanowitz J, Hunt DF, Funabiki H, Allis CD. 2005. Regulation of HP1-chromatin binding by histone H3 methylation and phosphorylation. *Nature* **438:** 1116–1122.

Foe VE, Alberts BM. 1983. Studies of nuclear and cytoplasmic behaviour during the five mitotic cycles that precede gastrulation in *Drosophila* embryogenesis. *J Cell Sci* **61:** 31–70.

Gehani SS, Agrawal-Singh S, Dietrich N, Christophersen NS, Helin K, Hansen K. 2010. Polycomb group protein displacement and gene activation through MSK-dependent H3K27me3S28 phosphorylation. *Mol Cell* **39:** 886–900.

Giet R, Glover DM. 2001. *Drosophila* aurora B kinase is required for histone H3 phosphorylation and condensin recruitment during chromosome condensation and to organize the central spindle during cytokinesis. *J Cell Biol* **152:** 669–682.

Giglia-Mari G, Theil AF, Mari PO, Mourgues S, Nonnekens J, Andrieux LO, de Wit J, Miquel C, Wijgers N, Maas A, et al. 2009. Differentiation driven changes in the dynamic organization of Basal transcription initiation. *PLoS Biol* **7:** e1000220. doi: 10.1371/journal.pbio.1000220.

Goto H, Tomono Y, Ajiro K, Kosako H, Fujita M, Sakurai M, Okawa K, Iwamatsu A, Okigaki T, Takahashi T, et al. 1999. Identification of a novel phosphorylation site on histone H3 coupled with mitotic chromosome condensation. *J Biol Chem* **274:** 25543–25549.

Gottesfeld JM, Forbes DJ. 1997. Mitotic repression of the transcriptional machinery. *Trends Biochem Sci* **22:** 197–202.

Hirota T, Lipp JJ, Toh BH, Peters JM. 2005. Histone H3 serine 10 phosphorylation by Aurora B causes HP1 dissociation from heterochromatin. *Nature* **438:** 1176–1180.

Jin Y, Wang Y, Walker DL, Conley C, Johansen J, Johansen KM. 1999. *JIL-1*: A novel chromosomal tandem kinase implicated in transcriptional regulation in *Drosophila*. *Mol Cell* **4:** 129–135.

Kraut R, Campos-Ortega JA. 1996. inscuteable, a neural precursor gene of *Drosophila*, encodes a candidate for a cytoskeleton adaptor protein. *Dev Biol* **174:** 65–81.

Kwong C, Adryan B, Bell I, Meadows L, Russell S, Manak JR, White R. 2008. Stability and dynamics of Polycomb target sites in *Drosophila* development. *PLoS Genet* **4:** e1000178. doi: 10.1371/journal.pgen.1000178.

Lau PN, Cheung P. 2011. Histone code pathway involving H3 S28 phosphorylation and K27 acetylation activates transcription and antagonizes polycomb silencing. *Proc Natl Acad Sci* **108:** 2801–2806.

Lee CY, Andersen RO, Cabernard C, Manning L, Tran KD, Lanskey MJ, Bashirullah A, Doe CQ. 2006. *Drosophila* Aurora-A kinase inhibits neuroblast self-renewal by regulating aPKC/Numb cortical polarity and spindle orientation. *Genes Dev* **20:** 3464–3474.

Martinez AM, Schuettengruber B, Sakr S, Janic A, Gonzalez C, Cavalli G. 2009. Polyhomeotic has a tumor suppressor activity mediated by repression of Notch signaling. *Nat Genet* **41:** 1076–1082.

Martinez-Balbas MA, Dey A, Rabindran SK, Ozato K, Wu C. 1995. Displacement of sequence-specific transcription factors from mitotic chromatin. *Cell* **83:** 29–38.

Mayer B, Emery G, Berdnik D, Wirtz-Peitz F, Knoblich JA. 2005. Quantitative analysis of protein dynamics during asymmetric cell division. *Curr Biol* **15:** 1847–1854.

McNally JG. 2008. Quantitative FRAP in analysis of molecular binding dynamics in vivo. *Methods Cell Biol* **85:** 329–351.

Meshorer E, Yellajoshula D, George E, Scambler PJ, Brown DT, Misteli T. 2006. Hyperdynamic plasticity of chromatin proteins in pluripotent embryonic stem cells. *Dev Cell* **10:** 105–116.

Mohn F, Weber M, Rebhan M, Roloff TC, Richter J, Stadler MB, Bibel M, Schubeler D. 2008. Lineage-specific polycomb targets and de novo DNA methylation define restriction and potential of neuronal progenitors. *Mol Cell* **30:** 755–766.

Mueller F, Wach P, McNally JG. 2008. Evidence for a common mode of transcription factor interaction with chromatin as revealed by improved quantitative fluorescence recovery after photobleaching. *Biophys J* **94:** 3323–3339.

Mueller F, Mazza D, Stasevich TJ, McNally JG. 2010. FRAP and kinetic modeling in the analysis of nuclear protein dynamics: What do we really know? *Curr Opin Cell Biol* **22:** 403–411.

Mummery-Widmer JL, Yamazaki M, Stoeger T, Novatchkova M, Bhalerao S, Chen D, Dietzl G, Dickson BJ, Knoblich JA. 2009. Genome-wide analysis of Notch signalling in *Drosophila* by transgenic RNAi. *Nature* **458:** 987–992.

Neumuller RA, Knoblich JA. 2009. Dividing cellular asymmetry: Asymmetric cell division and its implications for stem cells and cancer. *Genes Dev* **23:** 2675–2699.

Neumuller RA, Richter C, Fischer A, Novatchkova M, Neumuller KG, Knoblich JA. 2011. Genome-wide analysis of self-renewal in *Drosophila* neural stem cells by transgenic RNAi. *Cell Stem Cell* **8:** 580–593.

Niessen HE, Demmers JA, Voncken JW. 2009. Talking to chromatin: Post-translational modulation of Polycomb group function. *Epigenetics Chromatin* **2:** 10. doi: 10.1186/1756-8935-2-10.

Nowak SJ, Corces VG. 2004. Phosphorylation of histone H3: A balancing act between chromosome condensation and transcriptional activation. *Trends Genet* **20:** 214–220.

Prescott DM, Bender MA. 1962. Synthesis of RNA and protein during mitosis in mammalian tissue culture cells. *Exp Cell Res* **26:** 260–268.

Rabut G, Doye V, Ellenberg J. 2004. Mapping the dynamic organization of the nuclear pore complex inside single living cells. *Nat Cell Biol* **6:** 1114–1121.

Ren X, Vincenz C, Kerppola TK. 2008. Changes in the distributions and dynamics of polycomb repressive complexes during embryonic stem cell differentiation. *Mol Cell Biol* **28:** 2884–2895.

Robinson AK, Leal BZ, Chadwell LV, Wang R, Ilangovan U, Kaur Y, Junco SE, Schirf V, Osmulski PA, Gaczynska M, et al. 2012. The growth-suppressive function of the Polycomb group protein Polyhomeotic is mediated by polymerization of its sterile α motif (SAM) domain. *J Biol Chem* doi: 10.1074/jbc.M111.336115.

Sawarkar R, Paro R. 2010. Interpretation of developmental signaling at chromatin: The Polycomb perspective. *Dev Cell* **19:** 651–661.

Schuettengruber B, Cavalli G. 2009. Recruitment of Polycomb group complexes and their role in the dynamic regulation of cell fate choice. *Development* **136:** 3531–3542.

Sharp EJ, Martin EC, Adler PN. 1994. Directed overexpression of Suppressor 2 of zeste and Posterior Sex Combs results in bristle abnormalities in *Drosophila melanogaster*. *Dev Biol* **161:** 379–392.

Sprague BL, Muller F, Pego RL, Bungay PM, Stavreva DA, McNally JG. 2006. Analysis of binding at a single spatially localized cluster of binding sites by fluorescence recovery after photobleaching. *Biophys J* **91:** 1169–1191.

Vincenz C, Kerppola TK. 2008. Different polycomb group CBX family proteins associate with distinct regions of chromatin using nonhomologous protein sequences. *Proc Natl Acad Sci* **105:** 16572–16577.

Wheeler SR, Kearney JB, Guardiola AR, Crews ST. 2006. Single-cell mapping of neural and glial gene expression in the developing *Drosophila* CNS midline cells. *Dev Biol* **294:** 509–524.